Terms and Conditions of Use of Digitised Theses from Trinity College Library Dublin

Copyright statement

All material supplied by Trinity College Library is protected by copyright (under the Copyright and Related Rights Act, 2000 as amended) and other relevant Intellectual Property Rights. By accessing and using a Digitised Thesis from Trinity College Library you acknowledge that all Intellectual Property Rights in any Works supplied are the sole and exclusive property of the copyright and/or other IPR holder. Specific copyright holders may not be explicitly identified. Use of materials from other sources within a thesis should not be construed as a claim over them.

A non-exclusive, non-transferable licence is hereby granted to those using or reproducing, in whole or in part, the material for valid purposes, providing the copyright owners are acknowledged using the normal conventions. Where specific permission to use material is required, this is identified and such permission must be sought from the copyright holder or agency cited.

Liability statement

By using a Digitised Thesis, I accept that Trinity College Dublin bears no legal responsibility for the accuracy, legality or comprehensiveness of materials contained within the thesis, and that Trinity College Dublin accepts no liability for indirect, consequential, or incidental, damages or losses arising from use of the thesis for whatever reason. Information located in a thesis may be subject to specific use constraints, details of which may not be explicitly described. It is the responsibility of potential and actual users to be aware of such constraints and to abide by them. By making use of material from a digitised thesis, you accept these copyright and disclaimer provisions. Where it is brought to the attention of Trinity College Library that there may be a breach of copyright or other restraint, it is the policy to withdraw or take down access to a thesis while the issue is being resolved.

Access Agreement

By using a Digitised Thesis from Trinity College Library you are bound by the following Terms & Conditions. Please read them carefully.

I have read and I understand the following statement: All material supplied via a Digitised Thesis from Trinity College Library is protected by copyright and other intellectual property rights, and duplication or sale of all or part of any of a thesis is not permitted, except that material may be duplicated by you for your research use or for educational purposes in electronic or print form providing the copyright owners are acknowledged using the normal conventions. You must obtain permission for any other use. Electronic or print copies may not be offered, whether for sale or otherwise to anyone. This copy has been supplied on the understanding that it is copyright material and that no quotation from the thesis may be published without proper acknowledgement.

Application of Capacitive Sensors to Inverse Problems in Electrostatics

Maksym Prybytko

Department of Electronic and Electrical Engineering

University of Dublin

Trinity College

Submitted for the Degree of

Doctor of Philosophy

October, 2002

DECLARATION

This thesis has not been submitted as an exercise for a degree at any other University. Except where otherwise stated, the work described herein has been carried out by the author alone. This thesis may be borrowed or copied upon request with the permission of the Librarian, University of Dublin, Trinity College. The copyright belongs to the University of Dublin and Maksym Prybytko.

Signature of Author

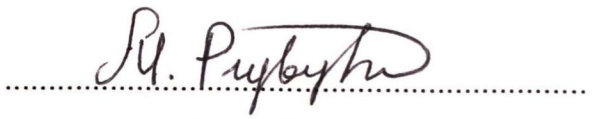

Maksym Prybytko October, 2002

SUMMARY

The electrostatic imaging problem is an inverse electrostatic problem involving the reconstruction of an inhomogeneous dielectric medium from a set of remote electrostatic field measurements. In this thesis we propose and explore a novel application of a capacitive sensor array to the electrostatic imaging problem. The capacitive sensor array that we investigate is composed of planar conducting electrodes located on and insulated from a wider ground plane. The analytical model of the planar capacitive sensor array is proposed to be a doublesided boundary.

Inverse problems occur in various areas of physics, yet the corresponding solution uniqueness theorems are often unproven or have only been recently proven. We found in literature that an inhomogeneous dielectric medium is uniquely determined by the Dirichlet-to-Neumann map on the open subset of the boundary covering the unknown dielectric [99]. The measurement methodology employing the planar capacitive sensor array that complies with this uniqueness theorem is proposed and incorporated into numerical algorithms.

The 2D electrostatic imaging problem is solved using the distorted Born iterative method (DBIM). Unlike existing approaches to the imaging problem where the measurement tools are assumed to have a small dimension such that there are no probing errors, the finite (physical) size of the planar electrodes is incorporated in the DBIM. The forward path in the DBIM, which is a set of the Dirichlet boundary electrostatic problems with a doublesided boundary, is shown to be ill-posed. This ill-conditioning is circumvented by introducing a novel technique employing a conformal mapping which can also be considered as a pre-conditioner. The ill-conditioning of the inverse path of the DBIM, common to all inverse problems, is overcome using a novel optimised Tikhonov regularization technique. The imaging algorithm is proved to be stable for a variety of simulated dielectric profiles. Also the operation of the imaging algorithm is successfully tested using the laboratory capacitive sensor array and experimental PC operated hardware.

ACKNOWLEDGEMENTS

I owe a special debt of gratitude to Dr. Peter Cullen, the supervisor of this project, who went through multiple revisions of the thesis and made many valuable comments throughout the project. Grateful acknowledgements are due to Dr. Conor Brennan and Eamonn Kenny, who assisted in technical questions during the project. It is also a pleasure to acknowledge the generous attitude of Dr. Ronan Bradley for his patience in assisting me improving my language style throughout the project. I would also like to thank the Communications Laboratory team and the Department of Electrical and Electronic engineering for co-operation.

It is to our sponsors Hotron Co. Ltd. and Xilinx Ireland that I owe my involvement into an interesting assignment with many exciting challenges and applications.

I express my sincere gratitude and respect to my wife Svetlana Khramtsova for her patience and support to whom I dedicate my work.

CONTENTS

LIST OF FIGURES

INTRODUCTION INTO INVERSE PROBLEM

Remote sensing is a rapidly developing industry nowdays. The demand for novel remote sensing techniques encourages industrial companies to invest more and more into development and research. Capacitive sensor techniques are attractive with many applications which we now discuss.

Capacitive sensor techniques are very low power and short range[1] techniques which are well suited to many indoor human oriented applications. Max Mathews, Stanford, California suggested the use of a capacitive sensor technique in the electronic drum where the location of a baton (or several batons) on the drum surface is determined from measurements made at several planar electrodes [87]. The baton is equipped with an embedded radio transmitter[2] while the flat capacitor plates of a predefined shape are embedded into the drum support surface.

Neil Gershenfeld, Cambridge, Massachusetts suggested to use a capacitive sensor for measuring the position of a point with respect to at least one axis [88]. This application is particularly suitable for the electronic violin. The radio transmit electrode embedded into the bow has such a property that the transmit signal intensity is monotonically attenuated along the bow. The at least one string of the electronic violin, which is a capacitor electrode, operates as a receiver producing a response signal proportional to the transmitter intensity allowing to detect the exact position of the bow with regard to the string.

[1] Although the law of physics does not limit the range of sensitivity for the capacitive sensors, in practical applications the sensitivity range is usually not greater than several meters. Hence the capacitive sensors are often referred as proximity sensors.

[2] Here, the radio transmitter is a capacitive sensor plate and the electric field is quasi-static (section 2.8). The term *radio transmitter* is used in the original document [87] as well as other patent definitions and therefore is preserved in the text.

The capacitive sensor techniques have found application in safety equipment. John Vranish and Robert McConnel suggested an extended-range capacitive sensor application for robot arm safety control in an industrial environment [86]. In this application a transmit capacitive electrode is placed on the mobile robot arm while the receive electrodes are represented by all grounded objects in the vicinity including the humans. The signal in the transmit electrode is continuously monitored triggering the safety mechanism to prevent the undesired collisions or injury.

The application of capacitive sensors to the determination of the position in space of the human limbs is explained, for example, in [1]. The human body in [1] is either a transmit electrode with a given electrostatic potential or a floating electrode with an unknown electrostatic potential. An application of the capacitive sensor to the three dimensional mouse for computer interface is explored in [2].

The capacitive sensor applications presented above are empirical and intuitive and do not require complicated numerical calculations. In the course of this thesis we develop a novel application of the capacitive sensors to the problem of reconstruction of the unknown dielectric permittivity distribution. We use a capacitive sensor array to generate the field and collect the data. The methods that we develop deal with non-linear electrostatic integral equations and require precise electrostatic field calculation. The problem of recovering the unknown dielectric permittivity from the remote electrostatic field measurements is called the inverse electrostatic problem.

During our early study we adopted the terminology and ideas proposed in [1],[2]. In particular we widely used the term of "Electric Field Sensing" (EFS) which refers to any sensing process involving the measurement of the electric field. After conducting a careful investigation we concluded that EFS is rather an alternative, yet less informative, term for the sensing using capacitive sensor techniques governed by (2.9). Moreover we concluded that the terms "shunt mode", "transmit mode" and "loading mode" introduced in [1] and used later in [3], [2] to describe intuitively the interaction of the human and electric fields are not sufficiently precise for our study which is concerned with exact electrostatic problem formulations.

1.1 Problem That Motivated Our Study

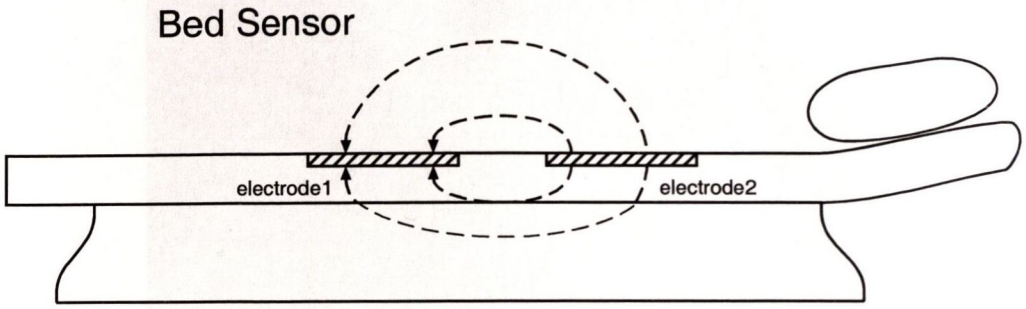

Figure 1.1: Two electrodes embedded into a hospital bench illustrate an application of the basic capacitive bed sensor.

Our industrial sponsor, the Hotron Co. Ltd. sought to collaborate with us in the investigation of a capacitive bed sensor for detecting the position of a person in a bed. A simple capacitive twin electrode bed sensor is illustrated in figure 1.1. Two electrodes are placed either beneath or above the mattress. A low frequency electric potential is applied to one electrode to establish an electric field that interacts with a person lying on the bed. The bed sensor detects the person on the bed by measuring the signal at the other electrode and activates or deactivates the alarm on the remote terminal.

The following requirements are typically imposed on the bed sensor:

1. its installation must be simple
2. it should not produce any discomfort to the patient
3. it should be insensitive to the objects underneath the sensor surface (to avoid calibration routines)

The latest bed sensors that we demonstrated to Hotron are flat and flexible having 1mm thickness, 5-30cm of sensitivity above the sensor surface and negligible sensitivity beneath the sensor. One such sensor is illustrated in figure 1.2. It is composed of two foil electrodes on the upper side of the sensor, a dielectric substrate and a ground plane electrode underneath of the sensor. The purpose of the ground plane electrode is to achieve spatial

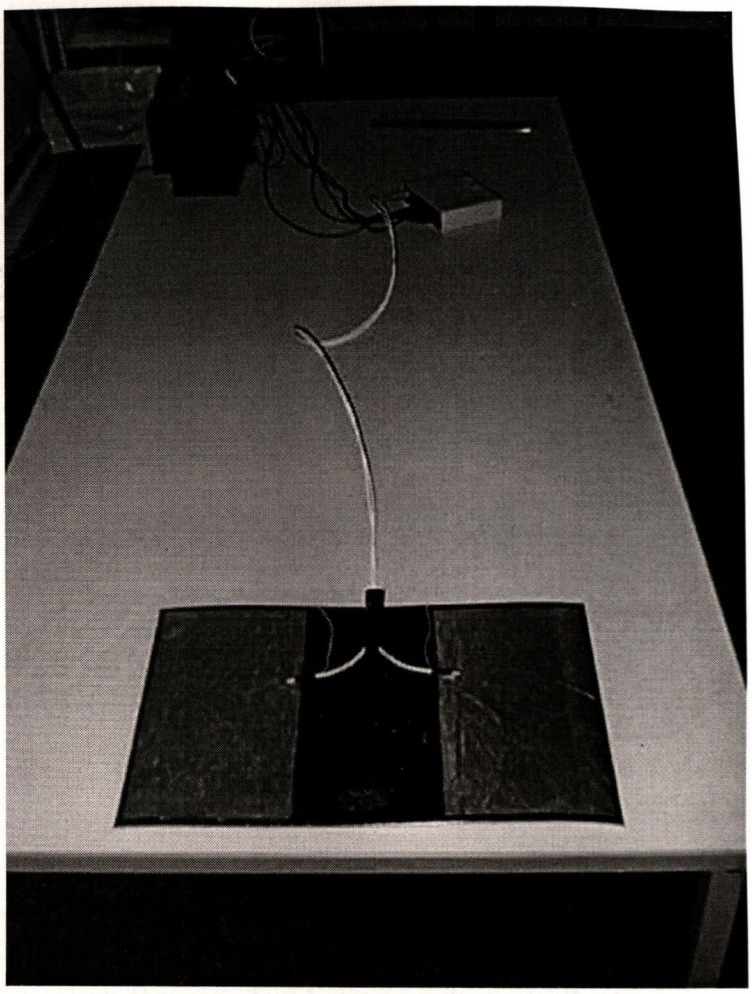

Figure 1.2: A simple capacitive sensor designed and constructed in the Communications Laboratory, Trinity College, Dublin.

selectivity of the sensor. To maximise performance the ground plane covers the entire area of the flat capacitive sensor.

The bed sensor in figure 1.2 can be seen as a simple imaging application. It takes only one measurement and converts it into a binary single pixel image. Hotron asked us to develop a sophisticated multi-electrode bed sensor capable of reconstructing a more elaborate image of a person occupying a bed. Optical quality resolution was not required for the bed sensor application. It was agreed that the bed sensor would be planar to facilitate installation under the mattress. We suggested several configurations for the capacitive sensor array shown in figure 1.3. In particular, the 2D and 3D capacitive sensor arrays that comply with the bed sensor application are shown in figures 1.3 (a) and (c). For faster prototyping

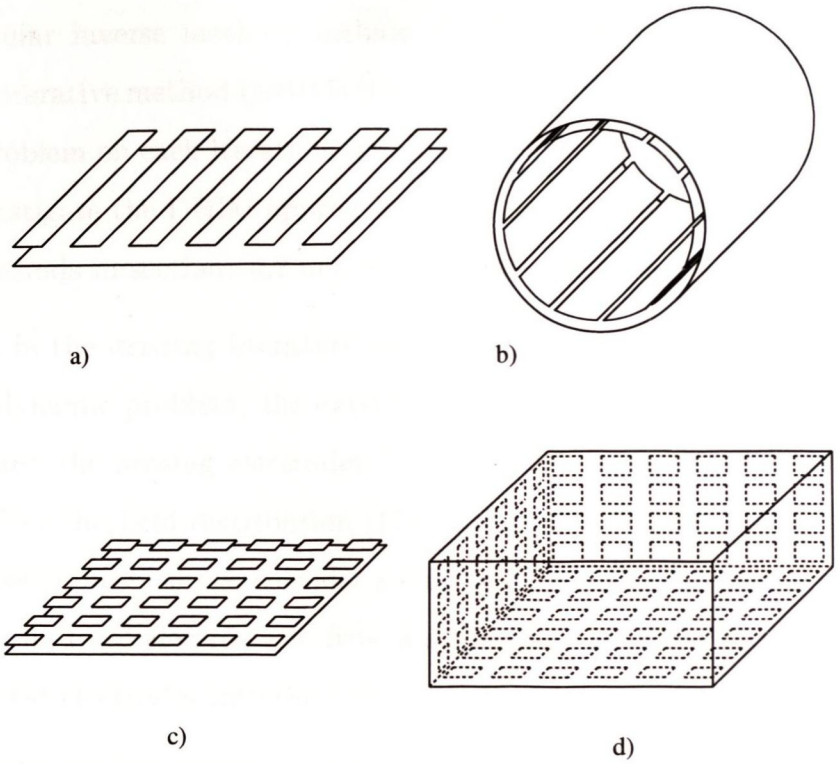

Figure 1.3: Open and closed capacitive sensor workbenchs in the 2D and and 3D respectively.

and numerical implementation we decided to analyse the bed sensor arrangement in the 2D although our techniques are applicable in the 3D. The methods that we develop in this thesis are also applicable to a wide class of inverse electrostatic problems and, in particular, to the problems formulated for enclosed areas as shown in figures 1.3 (b) and (d).

The source free governing equation of electrostatics is fundamental to our study

$$\nabla \epsilon \nabla \phi = 0 \ , \tag{1.1}$$

where ϵ is the dielectric permittivity and ϕ is the electrostatic potential. Both the forward[3] and inverse electrostatic problems are governed by the same equation (1.1). In the next Chapter we consider more governing equations of electrostatics.

[3]We use word 'forward' in order to distinguish an electrostatic problem, which is to obtain an electrostatic field in the given dielectric medium, from the inverse electrostatic problem, which is to reconstruct dielectric medium from the electrostatic field measurements.

Iterative methods provide an efficient framework for the solution of the inverse electrostatic problem. Popular inverse methods include the Born iterative method (BIM) and the distorted Born iterative method (DBIM) [18], [19]. The BIM and DBIM calculate a forward electrostatic problem on each iteration and largely depend on the efficiency of the forward solver. We investigate the DBIM approach in electrostatics and present both the forward and inverse methods in sections 4.2 and 5.2 respectively.

We found that in the existing literature on inverse problems (primarily dealing with the inverse electrodynamic problem) the external field is measured at finite number of observation points and the sensing electrodes (or antennas) are assumed to be so small that they do not affect the field distribution [17],[18],[19],[28],[30],[33]. In our analysis of the electrostatic inverse problem we consider spatially extended electrodes that have a significant effect on the total electrostatic field distribution. We incorporate the effect of the spatially extended electrodes into the DBIM (section 6.2).

In order to model the bed sensor application we introduce a doublesided boundary. We found that an electrostatic problem employing doublesided Dirichlet boundary conditions which arises as a part on the DBIM, for example, is ill-posed. To overcome the ill-conditioning we propose a set of basis functions that put the electrostatic problem in the well posed form. These basis functions can be analytically expressed through a conformal mapping in 2D (section 4.3).

We have found that in the strongly inhomogeneous fields that arise near the boundary containing the measurement electrodes, a Tikhonov regularization method [5] leads to an offset-type distortion. In order to eliminate that distortion we derive an optimised Tikhonov regularization method (section 6.2.3).

The electrodynamic imaging problem is similar to the electrostatic imaging problem. However while the inverse electrodynamic problem is frequently encountered in the current literature, the electrostatic inverse problem has not been investigated. This is explained by the fact that the electrodynamic field has found many applications in geophysics and other areas where long distance sensing is required as opposed to the proximity sensing.

We have illustrated that many existing methods developed for the inverse electrodynamic problem can also be employed in the static case. The convergence rate and precision of the inverse methods in the static case yet need to be investigated. The final quality of the recovered image is different for the electrostatic and electrodynamic inverse problems, for example, because of the time dependency of the electrodynamic field and its ability to transfer energy. In section 5.2 we present inverse methods that have been successfully applied to the electrodynamic inverse problem and formulate them for the electrostatic inverse problem. This is a novel contribution to the inverse electrostatic problem.

ELECTROSTATIC THEORY

This chapter lays the foundation for the analysis of the forward and inverse electrostatic problems that are studied in chapters 4, 5 and 6. The basics of electrostatic theory namely the mathematical formulation of the electrostatics are the foundation for both forward and inverse electrostatic problems. Therefore we do not formulate any particular problem in this chapter but rather systematically introduce the minimum background information required for understanding the research material presented in the thesis. The material presented in this chapter is primarily based on the author's college background.

The equations of many physical problems can be put in either differential or integral form. The differential and integral representations are equivalent from the mathematical perspective. The integral representation can be obtained from the differential one and *vice versa.* In electrostatics which is a particular case of electrodynamics the governing equation can be expressed in either differential or integral form.

From the numerical perspective the integral and differential representations of the governing equations lead to different methods with different computational complexity and different convergence properties. This is because the differential equations express the physical phenomena in terms of *local* field interactions whereas the integral representation primarily deals with *global* field interactions. A typical numerical approach based on the differential governing equations is the Finite Difference Method (FDM) discussed in section 4.2.1. The Finite Element Method (FEM) introduced in section 4.2.2 is based on the electrostatic integral equation.

In the next section we introduce the differential equations of electrostatics and then in section 2.4 we present the corresponding integral representations. In section 2.7.1 we derive simple expressions that relate the boundary conditions arising on the metal electrodes to the electrode measurements. In particular section 2.7.1 explains how the measurements

obtained using spatially extended electrodes are interpreted and employed in the numerical solvers which are central to our research. In section 2.7.2 we discuss the capacitive sensor array and relate the electrode potentials to the accumulated charges. A set of linear equations presented in this section is a starting point for the hardware design. Section 2.7.2 also explains the practical limitations of imaging techniques based on capacitive sensor arrays. Section 2.8 is a continuation of section 2.7 explaining how the currents and voltages (that we measure in our experiments) relate to the static charges and potentials that are simulated numerically.

2.1 Differential Governing Equations

In this section we briefly introduce the electrostatic theory using differential equations and provide necessary definitions that are used widely in the thesis.

The governing equations for the electrostatic theory can easily be obtained from Maxwell's equations by assuming that $\frac{d}{dt}(\cdot) = 0$

$$\nabla \cdot \vec{D} = 4\pi\rho \,, \tag{2.1}$$

$$\nabla \wedge \vec{E} = 0 \,, \tag{2.2}$$

where $\vec{D}$ is an electric flux density, $\vec{E}$ is an electric field intensity and ρ is the electric charge density. Note that equation (2.1) is valid in the 3D and its 2D version should read $\nabla \cdot \vec{D} = 2\pi\rho$. The difference in scaling of the electric field sources by a factor of 2 does not impact those numerical implementations where these sources are represented as unknown functions. In the course of this thesis we deal with cases having unknown source distributions and therefore we derive and use analytical expressions in 3D.

By definition the electric flux density $\vec{D}$ in a linear isotropic medium is proportional to the electric field intensity $\vec{E}$

$$\vec{D} = \epsilon\vec{E} \,, \tag{2.3}$$

where ϵ is a dielectric permittivity. In a non-linear medium the dielectric permittivity ϵ is a function of local material properties and electric field intensity $\vec{E}$

$$\vec{D} = \epsilon(\vec{E})\vec{E} \,. \tag{2.4}$$

Non-linearity of the medium is usually observed only for very large electric fields $\vec{E}$. In our work we deal with very weak electric fields of the order of 1V/cm. In such low intensity fields most known materials behave linearly.

Contrary to (2.3) where the dielectric permittivity ϵ is a scalar many solid materials with a non-symmetric crystalline lattice have a tensor dielectric permittivity

$$\vec{D} = \begin{pmatrix} \epsilon_x & 0 & 0 \\ 0 & \epsilon_y & 0 \\ 0 & 0 & \epsilon_z \end{pmatrix} \vec{E} \,. \tag{2.5}$$

This tensor dielectric permittivity does not reduce to a scalar even in the low intensity fields. Reconstructing a tensor ϵ is not a novel inverse problem. For example, the tensor dielectric permittivity has been successfully reconstructed in the 2D inverse electrodynamic case [4]. For many materials the three tensor components ϵ_x,ϵ_y and ϵ_z in (2.5) are approximately equal. For the methods considered in this thesis the resolution of the recovered ϵ values are relatively low[1] (Chapter 6) when compared to electrodynamic inverse problems [95], [32]. Consideration of the non-isotropic effects is an unnecessary complication because the materials that we investigate satisfy (2.3). Hereafter we assume that ϵ is a scalar.

The electrostatic field is a conservative field; this is a direct consequence of (2.2). Along with the vector field $\vec{E}$ we also use the electrostatic potential ϕ which is related to $\vec{E}$ as follows

$$\vec{E} = -\nabla\phi \,. \tag{2.6}$$

[1] We solve the inverse electrostatic problem using a moment method (Chapters 5 and 6). Even when the resultant mean squared error (5.29) for the moment method is small (down to 0.05%) the reconstructed dielectric distribution may significantly differ from the original dielectric distribution which is inherent to the problems we solve.

Substituting (2.3) and (2.6) into (2.1) gives

$$-\nabla \cdot \epsilon \nabla \phi = 4\pi\rho \,. \tag{2.7}$$

Equation (2.7) is the governing differential equation of electrostatic theory. In homogeneous isotropic media ϵ is constant and (2.7) becomes the Poisson equation. The homogeneous Poisson equation is called the Laplace equation. We now define two operators

$$\hat{L} = -\nabla^2 \,, \tag{2.8}$$

$$\hat{L}_\epsilon = -\nabla \cdot \epsilon \nabla \,. \tag{2.9}$$

We rewrite (2.7) using (2.9)

$$\hat{L}_\epsilon \phi = 4\pi\rho \,, \tag{2.10}$$

or in the absence of charges $\rho = 0$ (2.10) gives

$$\hat{L}_\epsilon \phi = 0 \,. \tag{2.11}$$

If the electrostatic potential ϕ is considered in some domain with boundary Γ (see for example figure 2.6) the values of ϕ and $d\phi/d\vec{n}$ on Γ must satisfy boundary conditions. Otherwise the electrostatic problem may not possess a unique solution. The Dirichlet and mixed boundary conditions are defined as follows

$$\phi|_\Gamma = a \,, \tag{2.12}$$

$$\frac{d\phi}{d\vec{n}} + \gamma\phi\Big|_\Gamma = b \,, \tag{2.13}$$

where γ, a and b are arbitrary functions on Γ, $\vec{n}$ is a normal to Γ. When $\gamma = 0$ (2.13) becomes a Neumann boundary condition.

In infinite domains an additional (to (2.12) and (2.13)) condition is usually imposed on the electrostatic field ϕ

$$\phi(\vec{r}) = -2A\log(|\vec{r}|) + o(\log(|\vec{r}|)) = O\left(\log(|\vec{r}|)\right) \ , |\vec{r}| \to \infty, \tag{2.14}$$

for 2D and

$$\phi(\vec{r}) = A\frac{1}{|\vec{r}|} + o(\frac{1}{|\vec{r}|}) = O(\frac{1}{|\vec{r}|}) \ , |\vec{r}| \to \infty, \tag{2.15}$$

for 3D domains, where A is an arbitrary constant. This condition assumes that all field sources such as charges and higher order multi-poles have a finite support and that the total electrostatic charge Q_{total} is given by

$$Q_{total} = A \ . \tag{2.16}$$

In (2.14) and (2.15) we use conventional symbolic representations $o(.)$ and $O(.)$ that are defined as follows

$$\lim_{\vec{r}\to\infty} \frac{O(f(\vec{r}))}{f(\vec{r})} = const, \tag{2.17}$$

$$\lim_{\vec{r}\to\infty} \frac{o(f(\vec{r}))}{f(\vec{r})} = 0 \ . \tag{2.18}$$

2.2 Green's Function and the Reciprocity Theorem

The Green's function $G(\vec{r_1}, \vec{r_2})$ for the Laplacian operator $\hat{L}$ (2.8) is defined as a solution of the equation

$$\hat{L}\, G(\vec{r_1}, \vec{r_2}) = \delta(\vec{r_1} - \vec{r_2}) \tag{2.19}$$

satisfying conditions (2.14),(2.15) in 2D and 3D respectively

$$G(\vec{r_1}, \vec{r_2}) = O(\log|\vec{r_1} - \vec{r_2}|) \ , \ |\vec{r_1} - \vec{r_2}| \to \infty, \tag{2.20}$$

$$G(\vec{r_1}, \vec{r_2}) = O(\frac{1}{|\vec{r_1} - \vec{r_2}|}) \ , \ |\vec{r_1} - \vec{r_2}| \to \infty, \tag{2.21}$$

where $\delta(\vec{r_1} - \vec{r_2})$ is a Dirac delta function.

The solution of (2.19) is well known and given by

$$G(\vec{r_1}, \vec{r_2}) = -\frac{1}{2\pi} \log(|\vec{r_1} - \vec{r_2}|) \tag{2.22}$$

and

$$G(\vec{r_1}, \vec{r_2}) = \frac{1}{4\pi} \frac{1}{|\vec{r_1} - \vec{r_2}|} \tag{2.23}$$

in 2D and 3D respectively.

The Green's function $G(\vec{r_1}, \vec{r_2})$ is also called a free space Green's function as it is associated with the operator $\hat{L}$ in the Laplace equation ($\epsilon = 1$). The Green's function $G_\epsilon(\vec{r_1}, \vec{r_2})$ for operator $\hat{L}_\epsilon$ (2.9) is defined as a solution to the following equation

$$\hat{L}_\epsilon \, G_\epsilon(\vec{r_1}, \vec{r_2}) = \delta(\vec{r_1} - \vec{r_2}) \ . \tag{2.24}$$

In the case of infinite domain the same conditions at infinity are imposed on $G_\epsilon(\vec{r_1}, \vec{r_2})$

$$G_\epsilon(\vec{r_1}, \vec{r_2}) = O(\log |\vec{r_1} - \vec{r_2}|) \ , \ |\vec{r_1} - \vec{r_2}| \to \infty, \tag{2.25}$$

$$G_\epsilon(\vec{r_1}, \vec{r_2}) = O(\frac{1}{|\vec{r_1} - \vec{r_2}|}) \ , \ |\vec{r_1} - \vec{r_2}| \to \infty, \tag{2.26}$$

in 2D and 3D respectively. In the case of boundary electrostatic problems the Green's function for an inhomogeneous dielectric is stipulated to the corresponding homogenized boundary conditions ((2.12) or (2.13)). In general $G_\epsilon(\vec{r_1}, \vec{r_2})$ does not have a simple analytical representation. However there is a general property of any Green' functions regardless of ϵ which is expressed in the reciprocity theorem. The reciprocity theorem states that if we have two charges q_1 and q_2 located at $\vec{r_1}$ and $\vec{r_2}$ having potentials $\phi_1(\vec{r})$ and $\phi_2(\vec{r})$ respectively, then $q_1\phi_2(\vec{r_1}) = q_2\phi_1(\vec{r_2})$ or

$$G_\epsilon(\vec{r_1}, \vec{r_2}) = G_\epsilon(\vec{r_2}, \vec{r_1}) \ . \tag{2.27}$$

Differentiating (2.27) with $\vec{r_1}$ and $\vec{r_2}$ in the arbitrary direction $\vec{l_1}$ and $\vec{l_2}$ respectively gives

$$\frac{d^2G_\epsilon(\vec{r_1},\vec{r_2})}{d\vec{r_1}d\vec{r_2}} = \frac{d^2G_\epsilon(\vec{r_2},\vec{r_1})}{d\vec{r_1}d\vec{r_2}} \ . \tag{2.28}$$

Equation (2.28) is another representation of the reciprocity theorem which means that if we have two dipoles $\vec{p_1}$ and $\vec{p_2}$ located at $\vec{r_1}$ and $\vec{r_2}$ and having electric fields $\vec{E}_1(\vec{r})$ and $\vec{E}_2(\vec{r})$ respectively then $\vec{E}_1(\vec{r_2})\vec{p_2} = \vec{E}_2(\vec{r_1})\vec{p_1}$.

2.3 Conformal Mapping and Its Application to Electrostatic Problem in Inhomogeneous Dielectric

A conformal mapping is an application of complex variable calculus. Conformal mapping is a powerful tool which can be used to map the potential ϕ_1 of one 2D electrostatic problem onto the potential ϕ_2 of another 2D electrostatic problem

$$\hat{L}\phi_1 = 0 \ , \tag{2.29}$$

$$\hat{L}\phi_2 = 0 \ , \tag{2.30}$$

where operator $\hat{L}$ is the Laplacian operator (2.8). It is less well known that conformal mapping is also suitable for mapping an electrostatic problem formulated for inhomogeneous dielectric ϵ (2.11). In section 2.3.1 we outline the properties of conformal mapping which are important to our study. In section 2.3.2 we show how conformal mapping can be applied to (2.11). Examples of the conformal mappings which we employ in our numerical algorithms are presented in section 2.3.3.

2.3.1 Introduction in Conformal Mapping

We define two simply connected 2D open domains Z and $\tilde{Z}$ in Cartesian planes $z = x + iy$ and $\tilde{z} = \tilde{x} + i\tilde{y}$. In figure 2.1 domains Z and $\tilde{Z}$ are presented as finite domains for illustration purposes only; we do not impose any finiteness restrictions on these domains.

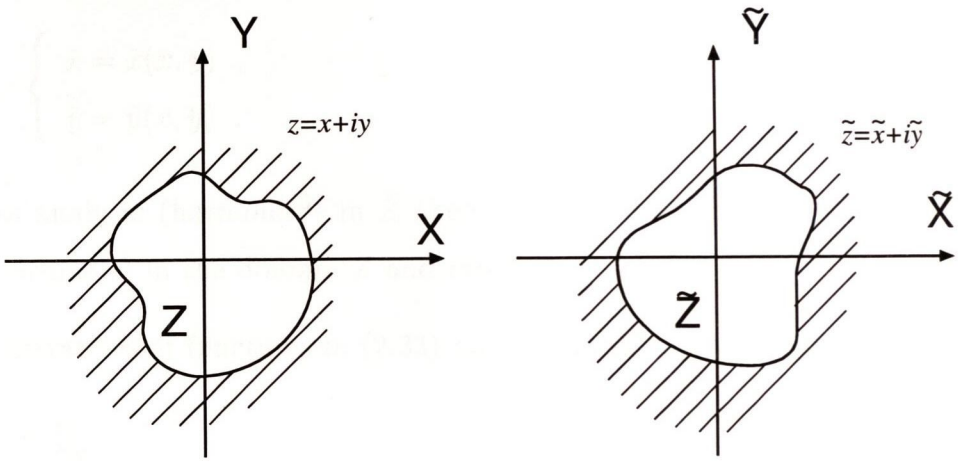

Figure 2.1: Z and $\tilde{Z}$ domains.

Consider the analytic function[2]

$$z(\tilde{z}) = x(\tilde{z}) + iy(\tilde{z}) \ , \tag{2.31}$$

where $\tilde{z} = \tilde{x} + i\tilde{y}$, which establishes a one-to-one mapping between Z and $\tilde{Z}$. The function $z(\tilde{z})$ also establishes a conformal mapping between the domains and there exists an analytic function

$$\tilde{z}(z) = \tilde{x}(z) + i\tilde{y}(z) \tag{2.32}$$

[2] An analytic function is a complex function in a complex plane that has a derivative. The function can be analytic at a point or in a domain. In this thesis whenever we refer to an analytic function we imply that it is analytic at all points where it is defined.

which is an inverse mapping [9]. The conformal mapping (2.31) and the corresponding inverse mapping (2.32) have an alternative representation in the form of real functions

$$z(\tilde{z}) : \begin{cases} x = x(\tilde{x}, \tilde{y}) \ , \\ y = y(\tilde{x}, \tilde{y}) \ . \end{cases} \tag{2.33}$$

$$\tilde{z}(z) : \begin{cases} \tilde{x} = \tilde{x}(x, y) \ , \\ \tilde{y} = \tilde{y}(x, y) \ . \end{cases} \tag{2.34}$$

If $u(\tilde{x}, \tilde{y})$ is analytic (harmonic[3]) in $\tilde{Z}$ then $u(x, y)$ obtained according to (2.34) is also analytic (harmonic) in the domain Z and *vice versa.*

The first derivatives of functions in (2.33) and (2.34) satisfy a fundamental relationship

$$\begin{aligned} \frac{\partial \tilde{x}}{\partial x} &= \frac{\partial \tilde{y}}{\partial y} \ , \\ \frac{\partial \tilde{x}}{\partial y} &= -\frac{\partial \tilde{y}}{\partial x} \end{aligned} \tag{2.35}$$

$$\begin{aligned} \frac{\partial x}{\partial \tilde{x}} &= \frac{\partial y}{\partial \tilde{y}} \ , \\ \frac{\partial x}{\partial \tilde{y}} &= -\frac{\partial y}{\partial \tilde{x}} \ . \end{aligned} \tag{2.36}$$

We now derive a transformation procedure for the gradient of an arbitrary function ϕ which can also be an electrostatic potential. We assume that the gradient of ϕ is given in $(\tilde{x}, \tilde{y}) \in \tilde{Z}$ and that mapping (2.34) is differentiable but not necessarily conformal. The expression for $\nabla\phi$ in $(x, y) \in Z$ can then be obtained as follows

$$\frac{\partial\, \phi(\tilde{x}(x,y), \tilde{y}(x,y))}{\partial\, x} = \frac{\partial\, \phi(\tilde{x}, \tilde{y})}{\partial\, \tilde{x}} \frac{\partial\, \tilde{x}(x,y)}{\partial\, x} + \frac{\partial\, \phi(\tilde{x}, \tilde{y})}{\partial\, \tilde{y}} \frac{\partial\, \tilde{y}(x,y)}{\partial\, x} \ , \tag{2.37}$$

$$\frac{\partial\, \phi(\tilde{x}(x,y), \tilde{y}(x,y))}{\partial\, y} = \frac{\partial\, \phi(\tilde{x}, \tilde{y})}{\partial\, \tilde{x}} \frac{\partial\, \tilde{x}(x,y)}{\partial\, y} + \frac{\partial\, \phi(\tilde{x}, \tilde{y})}{\partial\, \tilde{y}} \frac{\partial\, \tilde{y}(x,y)}{\partial\, y} \ . \tag{2.38}$$

We write (2.37) and (2.38) in a matrix form

$$\begin{pmatrix} \frac{\partial\, \phi}{\partial\, x} \\ \frac{\partial\, \phi}{\partial\, y} \end{pmatrix} = J \begin{pmatrix} \frac{\partial\, \phi}{\partial\, \tilde{x}} \\ \frac{\partial\, \phi}{\partial\, \tilde{y}} \end{pmatrix} \ , \tag{2.39}$$

[3] A harmonic function is a real function satisfying Laplace's equation (2.29), (2.30)

where J is a Jacobi matrix of transformation (2.34)

$$J = \begin{pmatrix} \frac{\partial \tilde{x}}{\partial x} & \frac{\partial \tilde{y}}{\partial x} \\ \frac{\partial \tilde{x}}{\partial y} & \frac{\partial \tilde{y}}{\partial y} \end{pmatrix} . \tag{2.40}$$

Equations (2.39) and (2.40) are obtained for an arbitrary differentiable transformation. We now assume that the transformation (2.34) is conformal and for illustration purposes we denote

$$\begin{aligned} \frac{\partial \tilde{x}}{\partial x} &= a \ , \\ \frac{\partial \tilde{y}}{\partial x} &= b \ . \end{aligned} \tag{2.41}$$

According to (2.35) we rewrite (2.40)

$$J = \begin{pmatrix} a & b \\ -b & a \end{pmatrix} . \tag{2.42}$$

We now demonstrate that (2.42) can be seen as two subsequent operations: a rotation by an angle α and a multiplication by a scaling factor K. Indeed denoting

$$\begin{aligned} \cos\alpha &= \tfrac{a}{\sqrt{a^2+b^2}} \ , \\ \sin\alpha &= \tfrac{b}{\sqrt{a^2+b^2}} \ , \\ K &= \sqrt{a^2+b^2} \end{aligned} \tag{2.43}$$

we rewrite the Jacobi matrix (2.42) as follows

$$J = K \begin{pmatrix} \cos\alpha & \sin\alpha \\ \sin -\alpha & \cos\alpha \end{pmatrix} . \tag{2.44}$$

The matrix in (2.44) is a rotation matrix that rotates the vector by an angle $\alpha = \operatorname{atan} \frac{b}{a}$ counterclockwise. After being rotated by α the vector is then multiplied by a factor K which is a square root of the determinant of the Jacobi matrix (2.42)

$$K = \sqrt{\det|J|} \tag{2.45}$$

Summarizing the conformal mapping transforms the vicinity of any point by rotating and scaling. An important conclusion for us is that the conformal mapping does not change the angle between any two vectors at the point. If the electric field is normal to the boundary and has been conformally mapped into another domain then the right angle will be preserved in the new domain.

2.3.2 Application of Conformal Mapping to the 2D Electrostatic Problem Involving an Inhomogeneous Dielectric Medium

In this section we illustrate how a conformal mapping can be applied to electrostatic problem (2.10). To start with we define the gradient operators in the Z and $\tilde{Z}$ domains (see previous section, figure 2.1) in a vector form

$$\nabla_{xy} = \begin{pmatrix} \frac{\partial}{\partial x} \\ \frac{\partial}{\partial y} \end{pmatrix} , \tag{2.46}$$

$$\nabla_{\tilde{x}\tilde{y}} = \begin{pmatrix} \frac{\partial}{\partial \tilde{x}} \\ \frac{\partial}{\partial \tilde{y}} \end{pmatrix} . \tag{2.47}$$

In the previous section we presented a rule for transforming a gradient of a function from $\tilde{Z}$ domain into Z or alternatively a rule for transforming a gradient operator. Indeed using (2.46),(2.47) and (2.40) we may rewrite that rule as follows

$$\nabla_{xy} = J\nabla_{\tilde{x}\tilde{y}} . \tag{2.48}$$

Let ϕ be an electrostatic potential satisfying (2.10) in Z

$$-\nabla_{xy}^T \epsilon \nabla_{xy} \phi = 4\pi\rho , \tag{2.49}$$

where $\nabla_{xy}^T = (\frac{\partial}{\partial x}, \frac{\partial}{\partial y})$ is the transpose of the operator in (2.46). We now transform equation (2.49) into the $\tilde{Z}$ domain. In order to do so we manipulate with operators. Using (2.48) gives

$$-\nabla_{xy}^T \epsilon J \nabla_{\tilde{x}\tilde{y}} \phi = 4\pi\rho . \tag{2.50}$$

The transposed gradient operator in (2.50) can be rewritten as follows (2.48)

$$\nabla_{xy}^T = (J\nabla_{\tilde{x}\tilde{y}})^T = \nabla_{\tilde{x}\tilde{y}}^T J^T \ . \tag{2.51}$$

Substituting (2.51) into (2.50) gives

$$-\nabla_{\tilde{x}\tilde{y}}^T J^T \epsilon J \nabla_{\tilde{x}\tilde{y}} \phi = 4\pi\rho \ . \tag{2.52}$$

The dielectric permittivity ϵ in (2.52) is a scalar factor that can be placed in front of the Jacobi matrix J. Note that we can also consider ϵ in (2.52) as a diagonal matrix $\begin{pmatrix} \epsilon & 0 \\ 0 & \epsilon \end{pmatrix}$. Of course the alternative representations for ϵ do not change the equation and we can write

$$-\nabla_{\tilde{x}\tilde{y}}^T J^T J \epsilon \nabla_{\tilde{x}\tilde{y}} \phi = 4\pi\rho \ . \tag{2.53}$$

Expression (2.53) is valid for any differentiable transformation between Z and $\tilde{Z}$. We now show that in a case of conformal mapping a product $J^T J$ has a form of a scalar function i.e. it can be represented as const $*$ I, where I is a unity diagonal matrix. Multiplying $J^T J$ gives

$$J^T J = \begin{pmatrix} \left(\frac{\partial \tilde{x}}{\partial x}\right)^2 + \left(\frac{\partial \tilde{x}}{\partial y}\right)^2 & \frac{\partial \tilde{y}}{\partial x}\frac{\partial \tilde{x}}{\partial x} + \frac{\partial \tilde{y}}{\partial y}\frac{\partial \tilde{x}}{\partial y} \\ \frac{\partial \tilde{y}}{\partial x}\frac{\partial \tilde{x}}{\partial x} + \frac{\partial \tilde{y}}{\partial y}\frac{\partial \tilde{x}}{\partial y} & \left(\frac{\partial \tilde{y}}{\partial x}\right)^2 + \left(\frac{\partial \tilde{y}}{\partial y}\right)^2 \end{pmatrix} \ . \tag{2.54}$$

According to (2.35) the non-diagonal components in (2.54) are zero: $\frac{\partial \tilde{y}}{\partial x}\frac{\partial \tilde{x}}{\partial x} + \frac{\partial \tilde{y}}{\partial y}\frac{\partial \tilde{x}}{\partial y} = 0$. The diagonal components in (2.54) are equal to the determinant of the Jacobi matrix (2.40) (a Jacobian)

$$\det|J| = \frac{\partial \tilde{x}}{\partial x}\frac{\partial \tilde{y}}{\partial y} - \frac{\partial \tilde{x}}{\partial y}\frac{\partial \tilde{y}}{\partial x} \ , \tag{2.55}$$

$$J^T J = \det|J| \begin{pmatrix} 1 & 0 \\ 0 & 1 \end{pmatrix} \ . \tag{2.56}$$

Substituting (2.56) into (2.53) gives

$$-\nabla^T_{\tilde{x}\tilde{y}} \det|J|\, \epsilon \nabla_{\tilde{x}\tilde{y}} \phi = 4\pi\rho \,. \tag{2.57}$$

The operator $\nabla^T_{\tilde{x}\tilde{y}}$ on the left in (2.57) acts on each factor on its right as follows

$$-\nabla^T_{\tilde{x}\tilde{y}} \det|J|\, \epsilon \nabla_{\tilde{x}\tilde{y}} \phi = -\epsilon \nabla^T_{\tilde{x}\tilde{y}} (\breve{\det}|J|) \nabla_{\tilde{x}\tilde{y}} \phi - \det|J|\, \nabla^T_{\tilde{x}\tilde{y}} (\epsilon \breve{\nabla}_{\tilde{x}\tilde{y}} \phi) \,. \tag{2.58}$$

It can be shown that

$$\nabla^T_{\tilde{x}\tilde{y}} (\breve{\det}|J|) \nabla_{\tilde{x}\tilde{y}} \phi = 0 \tag{2.59}$$

and ultimately combining (2.57),(2.58) and (2.59) gives

$$-\nabla^T_{\tilde{x}\tilde{y}} \epsilon \nabla_{\tilde{x}\tilde{y}} \phi = 4\pi \frac{\rho}{\det|J|} \,. \tag{2.60}$$

Equation (2.60) describes an electrostatic field in $\tilde{Z}$. Comparing (2.60) and (2.49) we formulate a translation procedure for mapping an inhomogeneous electrostatic problem involving an inhomogeneous dielectric medium: *in order to transform the electrostatic problem from one domain into another using a conformal mapping we map potential ϕ and dielectric distribution ϵ without any changes while the field source function ρ has to be scaled by a reciprocal of the determinant of the Jacobi matrix (2.55).* If an electrostatic charge ρ in the original equation (2.49) is zero then (2.60) is homogeneous

$$-\nabla^T_{\tilde{x}\tilde{y}} \epsilon \nabla_{\tilde{x}\tilde{y}} \phi = 0 \,. \tag{2.61}$$

Note that symbolic representation (2.61) is not affected by the conformal mapping.

2.3.3 Conformal Mapping Examples

In section 2.3.1 we introduced arbitrary domains Z and $\tilde{Z}$ (figure 2.1) and defined a conformal mapping for Z and $\tilde{Z}$. There is a theorem saying that a conformal mapping exists between arbitrary simply connected 2D domains Z and $\tilde{Z}$. However that conformal mapping usually does not have a simple analytical representation and is, therefore, unsuited for practical applications.

Before tackling an electrostatic problem using conformal mapping we have to study the shape of the boundary of the problem. If the boundary of the original electrostatic problem is, for example, a circle, a line segment or a semi-infinite strip then there exists a conformal mapping having a simple analytical representation that maps that original problem onto another electrostatic problem with a boundary also given by a circle, a line segment, a semi-infinite strip etc.

Let the previously introduced Z and $\tilde{Z}$ domains be associated with a real physical space and a virtual space respectively. Recall from section 1.1 that the sensor workbench is flat. Therefore we assume that the workbench sensor array lies on a line segment. In this case define Z to be an infinite domain with a segment boundary $[-1, 1]$. We have an option to choose the $\tilde{Z}$ domain such that it changes the condition number (section 4.1.2) of a numerical implementation of the electrostatic problem.

2.3.4 Conformal mapping example 1

In this example the $\tilde{Z}$ domain is an inner circle domain with unit radius. Both Z and $\tilde{Z}$ domains are illustrated in figure 2.2. We denote the boundaries for Z and $\tilde{Z}$ by Γ and $\tilde{\Gamma}$ respectively. The following conformal mapping transforms Z into $\tilde{Z}$

$$\tilde{z} = z - \sqrt{z^2 - 1} \ . \tag{2.62}$$

The inverse mapping which is also conformal is given by

$$z = \frac{1}{2}\left(\tilde{z} + \frac{1}{\tilde{z}}\right) \ . \tag{2.63}$$

The complex numbers z and $\tilde{z}$ are often represented in a polar co-ordinate system (r, α). If point z_0 has polar co-ordinates (r_0, α_0) then it is also referred to by $(r_0, \alpha_0 + n2\pi)$, where n is an arbitrary integer. To avoid the multiplicity we add plane cuts as shown in figure 2.2. If we now select any point in Z or $\tilde{Z}$ and draw a closed curve starting at that point then the phase angle will never experience a change of a multiple of 2π at the return. The plane cuts do not arise in the physical problem and therefore are artificial. In our study a continuity condition for the electrostatic potential and its derivative is prescribed on the plane cuts.

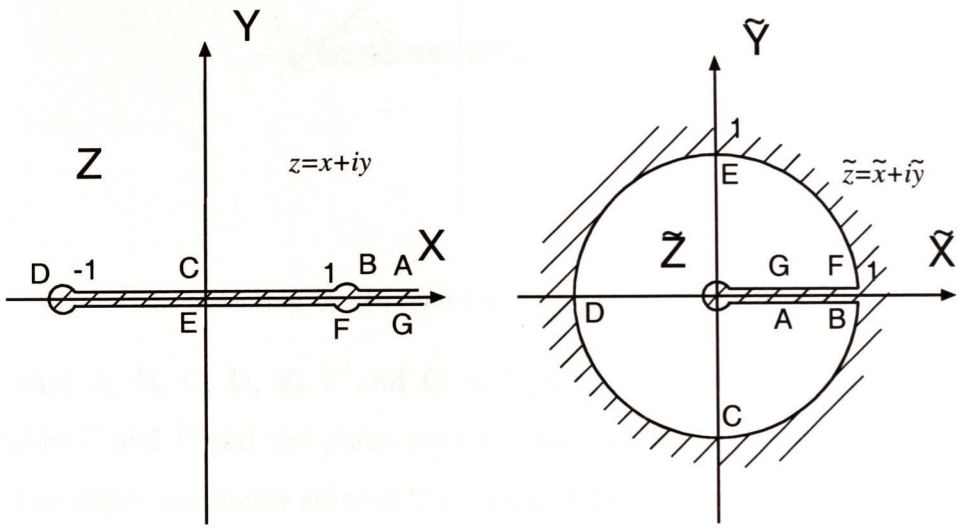

Figure 2.2: Example 1: Outer segment and inner circle domains.

This continuity condition is always satisfied because we do not prescribe field sources on the plane cuts. Another advantage of using the plane cuts is to isolate the branches of multi-valued functions such as squareroot or logarithm functions. In particular we select a branch for the squareroot function in (2.62) such that the phase for that squareroot function is given by $\frac{\alpha_1+\alpha_2}{2}$, where angles α_1 and α_2 are defined in figure 2.3.

An understanding of how conformal mapping works is needed to explain the efficiency of the numerical methods employing conformal mapping. For this reason we now present a comprehensive yet concise analysis of the mapping (2.62). We first illustrate how the boundary is mapped by (2.62). Then we analyse how the electrostatic field intensity is mapped. Mapping of the boundary values of the electrostatic field intensity is given special attention as these values are required for the sensor response computation.

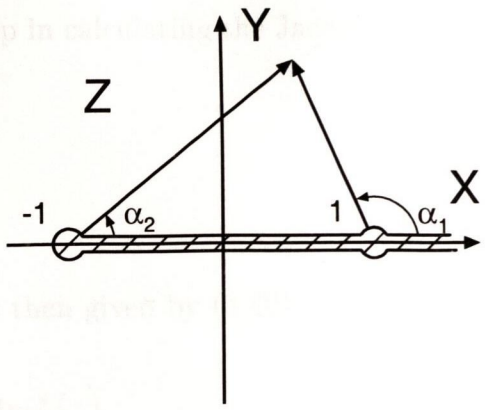

Figure 2.3: Selecting the branch for the squareroot function in (2.62)

Points (marks) A, B, C, D, E, F and G in figure 2.2 are introduced to illustrate how the boundaries Γ and $\tilde{\Gamma}$ and the plane cuts are mapped onto each other in the conformal mapping. The upper and lower sides of Γ are mapped onto the lower and upper semicircles of $\tilde{\Gamma}$ respectively. According to (2.62) the infinity $z \to \infty$ is mapped onto $\tilde{z} = 0$.

We now derive an expression mapping $\tilde{\Gamma}$ onto Γ (figure 2.2). Mapping Γ onto $\tilde{\Gamma}$ is more difficult to present because of the doublesided boundary. Mapping $\tilde{\Gamma}$ onto Γ does not involve such complication. Of course both ways are just alternative aspects of the same problem because the conformal mapping is a one-to-one mapping.

Let $\tilde{z}_0 = \tilde{x}_0 + i\tilde{y}_0$ be an arbitrary point on $\tilde{\Gamma}$ with z_0 being a corresponding image on Γ. We recall that $\tilde{\Gamma}$ is a unit circle and hence

$$|\tilde{z}_0| = 1 \ . \tag{2.64}$$

We substitute $\tilde{z}_0$ into (2.63) to give

$$z_0 = \frac{1}{2}\left(\tilde{z}_0 + \frac{1}{\tilde{z}_0}\right) = \frac{1}{2}(\tilde{z}_0 + \bar{\tilde{z}}_0) = \frac{1}{2}\, 2\,\mathrm{Re}\tilde{z} = \tilde{x} \ , \tag{2.65}$$

where the bar denotes a complex conjugate. According to (2.65) any point $\tilde{z}_0$ on $\tilde{\Gamma}$ has a corresponding image z_0 on Γ and that image can be obtained by projecting $\tilde{z}_0$ onto the X axis of the Cartesian co-ordinates. Thus z_0 can be obtained graphically as shown in figure 2.4. This figure can also be used to map z_0 onto $\tilde{z}_0$.

To map a gradient operator (2.48) we need to know the Jacobi matrix (2.40) of transformation (2.62). The first step in calculating the Jacobi matrix is to calculate the derivative of (2.62)

$$\frac{\partial\,\tilde{z}}{\partial\,z} = 1 - \frac{z}{\sqrt{z^2-1}} \ . \tag{2.66}$$

The Jacobi matrix $J_{Z\to\tilde{Z}}$ is then given by (2.40)

$$J_{Z\to\tilde{Z}} = \begin{pmatrix} \mathrm{Re}\frac{\partial\,\tilde{z}}{\partial\,z} & \mathrm{Im}\frac{\partial\,\tilde{z}}{\partial\,z} \\ -\mathrm{Im}\frac{\partial\,\tilde{z}}{\partial\,z} & \mathrm{Re}\frac{\partial\,\tilde{z}}{\partial\,z} \end{pmatrix} \ . \tag{2.67}$$

We implement the general form expression of (2.67) numerically but do not present it in this section because it is bulky. At the same time the Jacobi matrix (2.67) has an explicit form on the boundary $\tilde{\Gamma}$ which we now derive.

We recall that in our analysis $z_0 \in \Gamma$ ($z_0 = x_0 \in [-1,1]$) is an image of an arbitrary point $\tilde{z}_0 \in \tilde{\Gamma}$ and is obtained by projecting $\tilde{z}_0$ onto X. We substitute x_0 into (2.66) to give

$$\frac{\partial\,\tilde{z}}{\partial\,z} = 1 - \frac{x_0}{\sqrt{x_0^2-1}} \ , \ x_0 \in [-1,1] \ . \tag{2.68}$$

To find the value of the squareroot function in (2.68) we need to know whether we approach Γ from the upper half space $y_0 \to +0$ or from the lower half space $y_0 \to -0$. If $\tilde{z}_0$ is on the lower semicircle of $\tilde{Z}$ then $y_0 \to +0$ and $\alpha_1 = \pi$ and $\alpha_2 = 0$ (figure 2.3). If $\tilde{z}_0$ is on the upper semicircle of $\tilde{Z}$ then $y_0 \to -0$ and $\alpha_1 = \pi$ and $\alpha_2 = 2\pi$. Making either assumption we obtain

$$\frac{\partial\,\tilde{z}}{\partial\,z} = 1 \pm i\frac{x_0}{\sqrt{1-x_0^2}} \ , \ x_0 \in [-1,1], \ \ y_0 \to \mp 0 \ . \tag{2.69}$$

The Jacobi matrix (2.67) is then given by

$$J_{Z\to\tilde{Z}} = \begin{pmatrix} 1 & \pm\frac{x_0}{\sqrt{1-x_0^2}} \\ \mp\frac{x_0}{\sqrt{1-x_0^2}} & 1 \end{pmatrix} \ , \ x_0 \in [-1,1], \ \ y_0 \to \mp 0 \ . \tag{2.70}$$

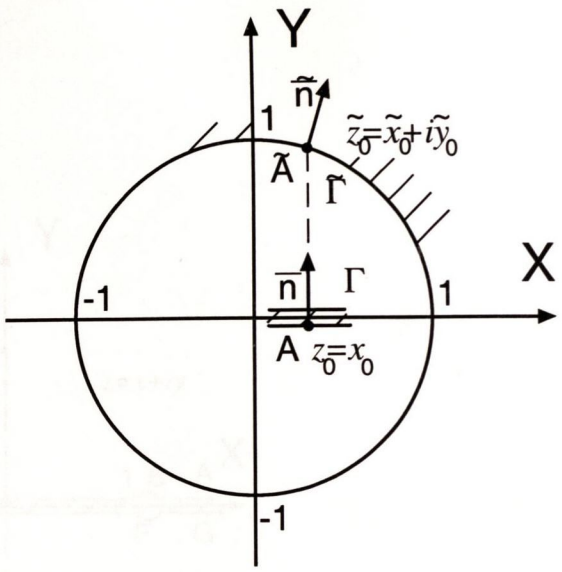

Figure 2.4: Mapping boundaries Γ and $\tilde{\Gamma}$.

According to section 2.3.1 the Jacobi matrix (2.70) contains information about the rotation angle and a scaling factor. We can learn about the rotation angle by looking at figure 2.4: the gradient of the potential is rotated by the same angle as the normal to the boundary. The scaling factor (2.45),(2.70) is given by

$$K = \sqrt{\det|J_{Z\to\tilde{z}}|} = \frac{1}{\sqrt{1-x^2}} \quad , x \in [-1,1] \ . \tag{2.71}$$

According to (2.71) the scaling factor is unity for $x = 0$ and tends to infinity as x approaches the end points of the segment $K \to \infty$, $x \to \pm 1$.

2.3.5 Conformal mapping example 2

In this section we present a conformal mapping similar to the previous example. The Z and $\tilde{Z}$ domains for this example are shown in figure 2.5. Due to similarity we omit the details for this example. The analytical expressions for the conformal mapping and the inverse conformal mapping in figure 2.5 are given by

$$\tilde{z} = z + \sqrt{z^2-1} \ , \tag{2.72}$$

$$z = \frac{1}{2}\left(\tilde{z} + \frac{1}{\tilde{z}}\right) \tag{2.73}$$

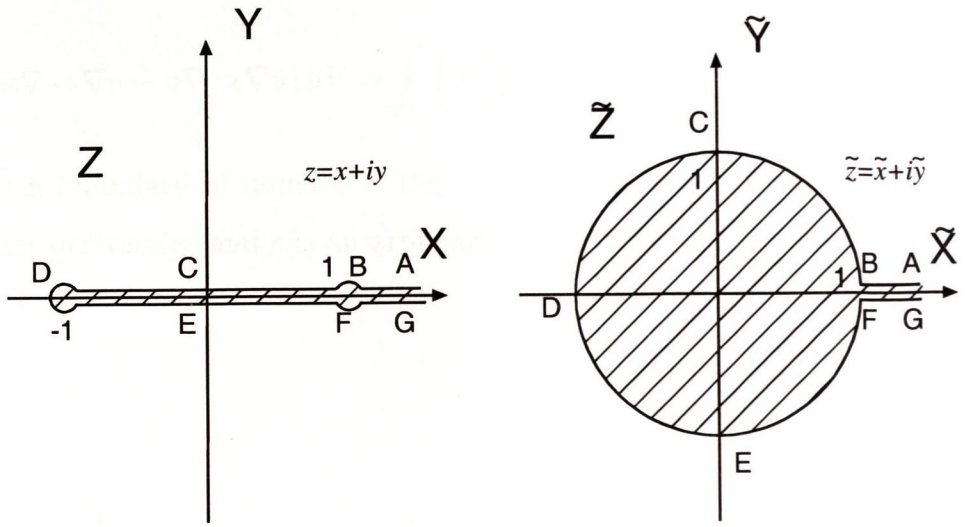

Figure 2.5: Example2: Outer segment and outer circle domains.

respectively. The inverse conformal mapping (2.73) has the same form as (2.63). The difference is that (2.73) and (2.63) are defined for different $\tilde{Z}$ domains. The $\tilde{Z}$ domain in the previous example is a finite domain while $\tilde{Z}$ in figure 2.5 is infinite. When solving an electrostatic problem in the infinite domain we impose an additional condition on the electrostatic field at infinity while for the finite domain we need not. This affects the implementations of the relevant numerical methods. It is worth mentioning that according to (2.72) the point at infinity $z \to \infty$ is now mapped onto the point in the infinity $\tilde{z} \to \infty$.

2.4 Integral Governing Equations

In this section we derive two integral equations which are fundamental in electrostatic theory. The first integral equation (2.78) is based on the Green's function of free space

introduced in section 2.2. The second equation (2.80) employs the Green's function for an inhomogeneous dielectric medium. Both integral equations are further discussed in section 2.5.

We begin with the generalized second Green's formula:

$$\int_V (u\nabla \cdot \epsilon\nabla v - v\nabla \cdot \epsilon\nabla u)\, dV = \int_\Gamma \left(\epsilon u \frac{dv}{d\vec{n}} - \epsilon v \frac{du}{d\vec{n}}\right) d\Gamma \ , \tag{2.74}$$

where Γ is a boundary of domain V (fig. 2.6), v and u are arbitrary functions having second order derivatives and ϵ is an arbitrary function having a first order derivative.

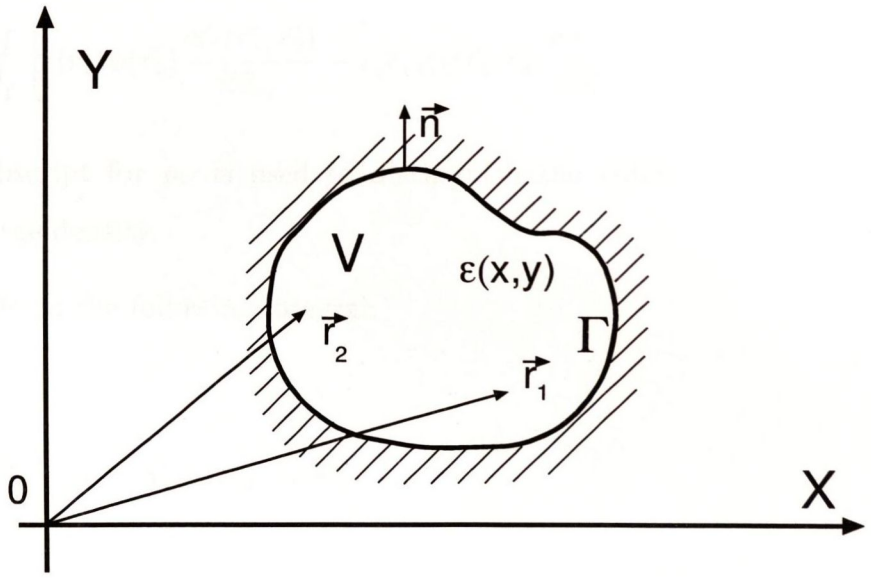

Figure 2.6: Domain V where equation (2.74) holds

Substituting $\phi(\vec{r_1})$ (2.7) and $G(\vec{r_1}, \vec{r_2})$ for u and v in (2.74) respectively gives

$$\int_V (\phi(\vec{r_1})\nabla_{r_1} \cdot \epsilon(r_1)\nabla_{r_1} G(\vec{r_1}, \vec{r_2}) - G(\vec{r_1}, \vec{r_2})\nabla_{r_1} \cdot \epsilon(r_1)\nabla_{r_1}\phi(\vec{r_1}))\, dr_1$$

$$= \int_\Gamma \left(\epsilon(r_1)\phi(\vec{r_1}) \frac{dG(\vec{r_1}, \vec{r_2})}{d\vec{n}_{r_1}} - \epsilon(r_1) G(\vec{r_1}, \vec{r_2}) \frac{d\phi(\vec{r_1})}{d\vec{n}_{r_1}} \right) dr_1 \ , \tag{2.75}$$

where dr_1 is either a volume or boundary differential (according to the type of the integral in (2.75)).

We substitute (2.7) into (2.75) to give

$$\int_V [\phi(\vec{r_1})\nabla_{r_1} \cdot \epsilon(r_1)\nabla_{r_1} G(\vec{r_1}, \vec{r_2}) + 4\pi G(\vec{r_1}, \vec{r_2})\rho_V(\vec{r_1})]\, dr_1$$

$$= \int_\Gamma \left[\epsilon(r_1)\phi(\vec{r_1}) \frac{dG(\vec{r_1}, \vec{r_2})}{d\vec{n}_{r_1}} - \epsilon(r_1) G(\vec{r_1}, \vec{r_2}) \frac{d\phi(\vec{r_1})}{d\vec{n}_{r_1}} \right] dr_1 \ , \tag{2.76}$$

where the subscript for ρ_V is used to distinguish the volume charge density from the boundary charge density.

Now we transform the following integral:

$$\int_V \phi(\vec{r_1})\nabla_{r_1} \cdot \epsilon(r_1)\nabla_{r_1} G(\vec{r_1}, \vec{r_2}) dr_1$$

$$= \int_V \phi(\vec{r_1})\nabla_{r_1} \cdot (\epsilon(r_1) - 1 + 1)\nabla_{r_1} G(\vec{r_1}, \vec{r_2}) dr_1$$

$$= \int_V \phi(\vec{r_1})\nabla^2_{r_1} G(\vec{r_1}, \vec{r_2}) dr_1 + \int_V \phi(\vec{r_1})\nabla_{r_1} \cdot (\epsilon(r_1) - 1)\nabla_{r_1} G(\vec{r_1}, \vec{r_2}) dr_1$$

(see (2.19), we assume that $\vec{r_2} \in V$)

$$= -\phi(\vec{r_2}) + \int_V \phi(\vec{r_1})\nabla_{r_1} \cdot (\epsilon(r_1) - 1)\nabla_{r_1} G(\vec{r_1}, \vec{r_2}) dr_1$$

$$= -\phi(\vec{r_2}) + \int_V \nabla_{r_1} \cdot \{\phi(\vec{r_1})(\epsilon(r_1) - 1)\nabla_{r_1} G(\vec{r_1}, \vec{r_2})\} dr_1$$

$$- \int_V (\epsilon(r_1) - 1)\nabla_{r_1}\phi(\vec{r_1})\nabla_{r_1} G(\vec{r_1}, \vec{r_2}) dr_1$$

(applying the divergence theorem to the first integral)

$$= -\phi(\vec{r_2}) + \int_\Gamma \phi(\vec{r_1})(\epsilon(r_1) - 1)\frac{dG(\vec{r_1}, \vec{r_2})}{d\vec{n}_{r_1}} dr_1$$

$$- \int_V (\epsilon(r_1) - 1)\nabla_{r_1}\phi(\vec{r_1})\nabla_{r_1} G(\vec{r_1}, \vec{r_2}) dr_1 \tag{2.77}$$

We now combine (2.76) and (2.77) to give:

$$-\phi(\vec{r_2}) + \int_\Gamma \{\epsilon(r_1) G(\vec{r_1}, \vec{r_2})\frac{d\phi(\vec{r_1})}{d\vec{n}_{r_1}} - \phi(\vec{r_1})\frac{dG(\vec{r_1}, \vec{r_2})}{d\vec{n}_{r_1}}\} dr_1$$

$$+4\pi \int_V G(\vec{r_1}, \vec{r_2})\rho_V(\vec{r_1}) dr_1 - \int_V (\epsilon(r_1) - 1)\nabla_{r_1}\phi(\vec{r_1})\nabla_{r_1} G(\vec{r_1}, \vec{r_2}) dr_1 = 0 \tag{2.78}$$

The above representation of the electrostatic integral equation is general. It will be used later as the starting point for deriving a particular form of the electrostatic integral equation for a particular electrostatic problem.

We now derive another general electrostatic integral equation which is based on the Green's function for a non-uniform dielectric $G_\epsilon(\vec{r_1}, \vec{r_2})$. Substituting $\phi(\vec{r_1})$ (2.7) and $G_\epsilon(\vec{r_1}, \vec{r_2})$ (2.19) for u and v in (2.74) respectively gives

$$\int_V (\phi(\vec{r_1})\nabla_{r_1} \cdot \epsilon(r_1)\nabla_{r_1} G_\epsilon(\vec{r_1}, \vec{r_2}) - G_\epsilon(\vec{r_1}, \vec{r_2})\nabla_{r_1} \cdot \epsilon(r_1)\nabla_{r_1}\phi(\vec{r_1}))\, dr_1$$

$$= \int_\Gamma \left(\epsilon(r_1)\phi(\vec{r_1}) \frac{dG_\epsilon(\vec{r_1}, \vec{r_2})}{d\vec{n}_{r_1}} - \epsilon(r_1) G_\epsilon(\vec{r_1}, \vec{r_2}) \frac{d\phi(\vec{r_1})}{d\vec{n}_{r_1}} \right) dr_1 \ , \tag{2.79}$$

where dr_1 is a either a volume or boundary differential (according to the type of the integral in (2.75)). Substituting (2.7) into (2.79) and using the definition of the Green's function (2.24),(2.9) gives

$$-\phi(\vec{r_2}) + 4\pi \int_V G_\epsilon(\vec{r_1}, \vec{r_2})\rho(\vec{r_1}) dr_1$$

$$= \int_\Gamma \left(\epsilon(r_1)\phi(\vec{r_1}) \frac{dG_\epsilon(\vec{r_1}, \vec{r_2})}{d\vec{n}_{r_1}} - \epsilon(r_1) G_\epsilon(\vec{r_1}, \vec{r_2}) \frac{d\phi(\vec{r_1})}{d\vec{n}_{r_1}} \right) dr_1 \ . \tag{2.80}$$

2.5 Understanding Integrals in (2.78) and (2.80)

Equation (2.80) is different from (2.78) because, for example, it does not contain ϵ in the volume integral. Instead, the ϵ dependency in (2.80) is included in $G_\epsilon(\vec{r_1}, \vec{r_2})$. Comparing (2.80) and (2.78) one can conclude that (2.80) is simpler. The reason why (2.80) is not widely used for solving electrostatic problems is that $G_\epsilon(\vec{r_1}, \vec{r_2})$ is usually unknown. In this thesis we employ (2.80) to build a DBIM which is an efficient inversion method explained in section 5.2.3. We now explain the meaning of the boundary and volume integrals in (2.78) and (2.80).

Equation (2.78) is a Fredholm integral equation of the second kind provided that $\phi(\vec{r_2})$ is considered as the unknown function. We now consider (2.78) as an expression for $\phi(\vec{r_2})$ given by a sum of integrals. Each of these integrals satisfies the Laplace equation in V. In (2.80) $\phi(\vec{r_2})$ is also given by a sum of integrals however these integrals now satisfy a more general equation (2.7). Despite integrals contributing to $\phi(\vec{r_2})$ in (2.78) and (2.80) being different they have a similar physical interpretation. Therefore we restrict our discussion to the integrals in (2.78).

The first volume integral in (2.78)

$$\phi_1(\vec{r_2}) = 4\pi \int_V G(\vec{r_1}, \vec{r_2})\rho(\vec{r_1})dr_1 \tag{2.81}$$

defines an electrostatic potential in free space caused by a volume charge density $\rho(\vec{r_1})$. We now make an important observation regarding $\rho(\vec{r})$ in (2.81). When we introduced the charge density function $\rho(\vec{r})$ in the governing differential electrostatic equation (2.7) we did not specify the properties of $\rho(\vec{r})$. Very often $\rho(\vec{r_1})$ is considered to be either a continuous function or a sum of Dirac delta functions. The Dirac delta function belongs to a wide class of functions also known as generalised functions which are defined in the form of functionals and very often cannot be represented in a conventional form of $f(x)$. In this thesis we treat $\rho(\vec{r})$ as a generalized function. In particular $\rho(\vec{r})$ can reduce the volume integral (2.81) to a surface integral representing the potential due to a single layer (surface charge distribution) or double layer (surface dipole distribution)

$$4\pi \int_S G(\vec{r_1}, \vec{r_2})\rho_s(\vec{r_1})dr_1 \ , \tag{2.82}$$

$$4\pi \int_S \frac{dG(\vec{r_1}, \vec{r_2})}{d\vec{n}_{r_1}} \sigma_s(\vec{r_1})dr_1 \ , \tag{2.83}$$

where S is any surface in V, with normal $\vec{n}$, $\rho_s(\vec{r})$ and $\sigma_s(\vec{r})$, $\vec{r} \in S$ are the single and double layer densities.

The second volume integral in (2.78)

$$\phi_2(\vec{r_2}) = -\int_V (\epsilon(r_1) - 1)\nabla_{r_1}\phi(\vec{r_1})\nabla_{r_1}G(\vec{r_1}, \vec{r_2})dr_1 \tag{2.84}$$

is a potential field due to a volume dipole distribution and can be represented as follows

$$\phi_2(\vec{r_2}) = 4\pi \int_V \vec{\sigma}_V(\vec{r_1})\nabla_{r_1}G(\vec{r_1}, \vec{r_2})dr_1 \ , \tag{2.85}$$

where the volume dipole density $\vec{\sigma}_V$ is given by

$$\vec{\sigma}_V(\vec{r_1}) = -\frac{(\epsilon(r_1) - 1)\nabla_{r_1}\phi(\vec{r_1})}{4\pi} \ . \tag{2.86}$$

Note that (2.86) represents a fundamental relationship

$$4\pi\vec{P} + \vec{E} = \vec{D} \ , \tag{2.87}$$

where $\vec{E} = -\nabla\phi$ is an electric field intensity, $\vec{D} = \epsilon\vec{E}$ is an electric flux density (2.3) and $\vec{P} = \vec{\sigma}_V$ is a polarization vector.

We now consider the boundary integral in (2.78)

$$\phi_3(\vec{r_2}) = \int_\Gamma \{\epsilon(r_1)G(\vec{r_1},\vec{r_2})\frac{d\phi(\vec{r_1})}{d\vec{n}_{r_1}} - \phi(\vec{r_1})\frac{dG(\vec{r_1},\vec{r_2})}{d\vec{n}_{r_1}}\}dr_1 \ . \tag{2.88}$$

The physical interpretation of (2.88) is not as simple as for the two previous integrals (2.81) and (2.84) and requires additional consideration which we now discuss. To start with we show that (2.88) is a field due to a superposition of both single and double layers. Indeed we can rewrite (2.88) as follows

$$\phi_3(\vec{r_2}) = 4\pi\int_\Gamma \rho_\Gamma(\vec{r_1})G(\vec{r_1},\vec{r_2})dr_1 + 4\pi\int_\Gamma \sigma_\Gamma(\vec{r_1})\frac{dG(\vec{r_1},\vec{r_2})}{d\vec{n}_{r_1}}dr_1 \ , \tag{2.89}$$

where the single and double layer densities $\rho_\Gamma(\vec{r_1})$, $\sigma_\Gamma(\vec{r_1})$ are given by

$$\rho_\Gamma(\vec{r_1}) = \frac{\epsilon(r_1)\frac{d\phi(\vec{r_1})}{d\vec{n}_{r_1}}}{4\pi} \ , \tag{2.90}$$

$$\sigma_\Gamma(\vec{r_1}) = -\frac{\phi(\vec{r_1})}{4\pi} \ . \tag{2.91}$$

It can be shown that (2.90) and (2.91) are not necessarily physically existing field sources. Indeed we can always place Γ in the electric field beyond the actual field sources. In that case (2.90) and (2.91) are nonzero while Γ is free of charges and dipoles. Hence we cannot explain the origin of (2.88) by assuming the presence of actual sources or suggested by (2.90) and (2.91).

Let V be a finite domain in the XY plane and Γ be a boundary of V. We assume that a charge distribution $\rho_V(\vec{r})$ and a dielectric susceptibility $\epsilon(\vec{r}) - 1$ have a finite support in the XY plane such that $\text{supp}\{\rho_V(\vec{r})\} \in V$ and $\text{supp}\{\epsilon(\vec{r}) - 1\} \in V$. The supports for

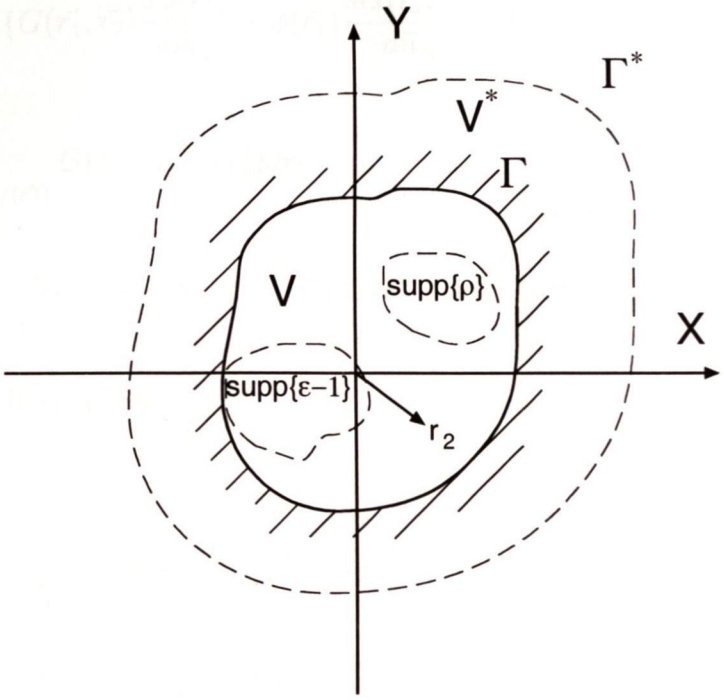

Figure 2.7: Domain V where equation (2.74) holds

$\rho_V(\vec{r})$ and $\epsilon(\vec{r}) - 1$ are shown in figure 2.7. Assuming that $\vec{r_2} \in V$, as shown in figure 2.7, is fixed and then applying (2.78) to V gives

$$-\phi(\vec{r_2}) + \int_\Gamma \{G(\vec{r_1}, \vec{r_2}) \frac{d\phi(\vec{r_1})}{d\vec{n}_{r_1}} - \phi(\vec{r_1}) \frac{dG(\vec{r_1}, \vec{r_2})}{d\vec{n}_{r_1}}\} dr_1$$

$$+4\pi \int_{\text{supp}\{\rho_V(\vec{r})\}} G(\vec{r_1}, \vec{r_2}) \rho_V(\vec{r_1}) dr_1$$

$$- \int_{\text{supp}\{\epsilon(\vec{r})-1\}} (\epsilon(r_1) - 1) \nabla_{r_1} \phi(\vec{r_1}) \nabla_{r_1} G(\vec{r_1}, \vec{r_2}) dr_1 = 0 \ , \ \vec{r_2} \in V \ . \tag{2.92}$$

Without modifying the charge and dielectric susceptibility distributions we now consider another domain V^* (in the same XY plane as V) having boundary Γ^* such that $\text{supp}\{\rho_V(\vec{r})\} \subset V^*$, $\text{supp}\{\epsilon(\vec{r}) - 1\} \subset V^*$. We also assume that $\vec{r_2} \in V \bigcap V^*$ as shown in figure 2.7. Applying (2.78) to V^* gives

$$-\phi(\vec{r_2}) + \int_{\Gamma^*} \{G(\vec{r_1},\vec{r_2})\frac{d\phi(\vec{r_1})}{d\vec{n}_{r_1}} - \phi(\vec{r_1})\frac{dG(\vec{r_1},\vec{r_2})}{d\vec{n}_{r_1}}\}dr_1$$

$$+4\pi \int_{\text{supp}\{\rho_V(\vec{r})\}} G(\vec{r_1},\vec{r_2})\rho_V(\vec{r_1})dr_1$$

$$-\int_{\text{supp}\{\epsilon(\vec{r})-1\}} (\epsilon(r_1)-1)\nabla_{r_1}\phi(\vec{r_1})\nabla_{r_1}G(\vec{r_1},\vec{r_2})dr_1 = 0 \ , \ \vec{r_2} \in V \ . \tag{2.93}$$

Subtracting (2.93) from (2.92) gives

$$\int_{\Gamma} \{G(\vec{r_1},\vec{r_2})\frac{d\phi(\vec{r_1})}{d\vec{n}_{r_1}} - \phi(\vec{r_1})\frac{dG(\vec{r_1},\vec{r_2})}{d\vec{n}_{r_1}}\}dr_1$$

$$-\int_{\Gamma^*} \{G(\vec{r_1},\vec{r_2})\frac{d\phi(\vec{r_1})}{d\vec{n}_{r_1}} - \phi(\vec{r_1})\frac{dG(\vec{r_1},\vec{r_2})}{d\vec{n}_{r_1}}\}dr_1 = 0 \ , \ \vec{r_2} \in V \ . \tag{2.94}$$

Equality (2.94) holds for any Γ^* which means that

$$\int_{\Gamma^*} \{G(\vec{r_1},\vec{r_2})\frac{d\phi(\vec{r_1})}{d\vec{n}_{r_1}} - \phi(\vec{r_1})\frac{dG(\vec{r_1},\vec{r_2})}{d\vec{n}_{r_1}}\}dr_1 = \text{const} \ , \ \vec{r_2} \in V \ . \tag{2.95}$$

We now prove that if the field in the entire 2D space is caused by a dipole distribution having a finite support then the constant in (2.95) is zero. Let ϕ be an electrostatic potential in the 2D due to the volume dipoles. It can be shown that ϕ is asymptotically represented as $\phi = A_1/R + o(1/R)$, $R \to \infty$. Let Γ^* in (2.95) be a circle domain of radius R centred at the origin. Fixing the observation point $\vec{r_2}$ and letting R tend to infinity gives the following asymptotic representation for (2.95)

$$\int_{\Gamma^*} \{G(\vec{r_1},\vec{r_2})\frac{d\phi(\vec{r_1})}{d\vec{n}_{r_1}} - \phi(\vec{r_1})\frac{dG(\vec{r_1},\vec{r_2})}{d\vec{n}_{r_1}}\}dr_1 = \frac{\log(R)}{R}C + o(\frac{\log(R)}{R}) \ , R \to \infty \ , \tag{2.96}$$

where C is a constant. The right hand side in (2.96) tends to zero as R tends to infinity. At the same time the left hand side in (2.96) is constant according to (2.95). This can only hold if the constant in (2.95) is zero.

If we assume that the electrostatic field ϕ is asymptotically represented as a constant $\phi = A_0 + O(1/R)$ then repeating the same analysis one can show that the constant in (2.95) is A_0. Analysis of the non-compensated charge distribution is more complicated. In that case the potential is increasing, at infinity, as a logarithm. In any given direction ϕ is given by the following series

$$\phi = B \log R + A_0 + \sum_{k=1}^{\infty} A_k \frac{1}{R^k} \ . \tag{2.97}$$

Asymptotically representing (2.95) it can be shown that the integral in (2.95) is still given by A_0. In fact coefficient A_0 (2.97) is independent of the radial direction and arbitrary. Since we have not defined the electrostatic potential at infinity we can assume that $A_0 = 0$. The electrostatic governing integral equation for the problem illustrated in figure 2.7 can now be written in the following form

$$-\phi(\vec{r_2}) + 4\pi \int_{\text{supp}\{\rho_V(\vec{r})\}} G(\vec{r_1}, \vec{r_2}) \rho_V(\vec{r_1}) dr_1$$

$$- \int_{\text{supp}\{\epsilon(\vec{r})-1\}} (\epsilon(r_1) - 1) \nabla_{r_1} \phi(\vec{r_1}) \nabla_{r_1} G(\vec{r_1}, \vec{r_2}) dr_1 = 0 \ . \tag{2.98}$$

We now consider another electrostatic problem where the support for the dielectric susceptibility distribution and electric charge density function is outside V having a boundary Γ: $\text{supp}\{\epsilon(\vec{r}) - 1\} \bigcap V = 0$, $\text{supp}\{\rho(\vec{r})\} \bigcap V = 0$. Let the observation point $\vec{r_2}$ be placed in V: $\vec{r_2} \in V$. We also consider another domain V^* having boundary Γ^* such that $V \subset V^*$, $\text{supp}\{\epsilon(\vec{r}) - 1\} \subset V^* \setminus V$ and $\text{supp}\{\rho(\vec{r})\} \subset V^* \setminus V$.

Applying (2.78) to V gives

$$-\phi(\vec{r_2}) + \int_{\Gamma} \{\epsilon(r_1) G(\vec{r_1}, \vec{r_2}) \frac{d\phi(\vec{r_1})}{d\vec{n}_{r_1}} - \phi(\vec{r_1}) \frac{dG(\vec{r_1}, \vec{r_2})}{d\vec{n}_{r_1}}\} dr_1 = 0 \ , \ \vec{r_2} \in V \ . \tag{2.99}$$

Note that (2.99) does not contain volume integrals. We now apply (2.78) to V^*

$$-\phi(\vec{r_2}) + 4\pi \int_{\text{supp}\{\rho_V(\vec{r})\}} G(\vec{r_1}, \vec{r_2}) \rho_V(\vec{r_1}) dr_1$$

$$- \int_{\text{supp}\{\epsilon(\vec{r})-1\}} (\epsilon(r_1) - 1) \nabla_{r_1} \phi(\vec{r_1}) \nabla_{r_1} G(\vec{r_1}, \vec{r_2}) dr_1 = 0 \ . \tag{2.100}$$

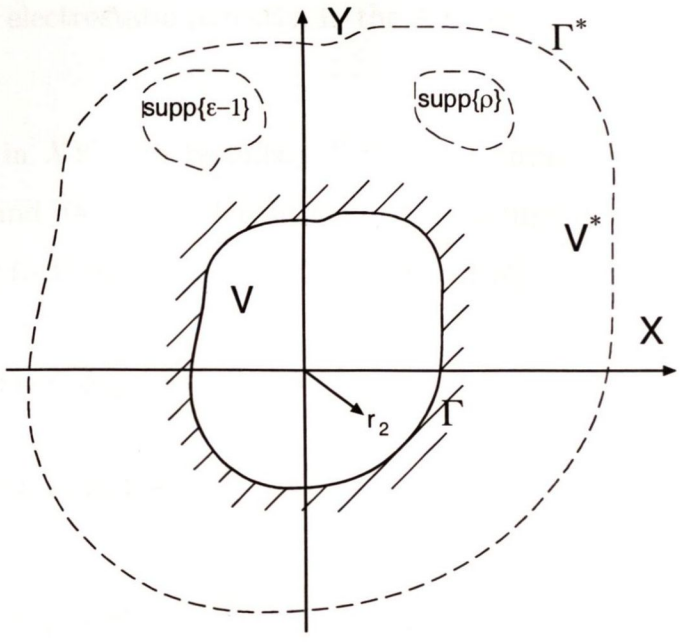

Figure 2.8: Domain V where equation (2.74) holds

The electrostatic potential $\phi(\vec{r_2})$ in (2.99) and (2.100) is the same because it is caused by the same field sources. Hence the boundary integral in (2.99) gives the same values in V as two volume integrals in (2.100) we write

$$\int_\Gamma \{\epsilon(r_1)G(\vec{r_1},\vec{r_2})\frac{d\phi(\vec{r_1})}{d\vec{n}_{r_1}} - \phi(\vec{r_1})\frac{dG(\vec{r_1},\vec{r_2})}{d\vec{n}_{r_1}}\}dr_1$$

$$= 4\pi \int_{\text{supp}\{\rho_V(\vec{r})\}} G(\vec{r_1},\vec{r_2})\rho_V(\vec{r_1})dr_1$$

$$- \int_{\text{supp}\{\epsilon(\vec{r})-1\}} (\epsilon(r_1)-1)\nabla_{r_1}\phi(\vec{r_1})\nabla_{r_1}G(\vec{r_1},\vec{r_2})dr_1 \ . \tag{2.101}$$

We see that the boundary integral (2.101) is no longer zero. It is given by the sum of two volume integrals which have already been explained in this section, one of these integrals defines a potential due to isolated charge $\rho(\vec{r})$ and the other represents a field of the polarized dielectric. Note that the polarized dielectric and the charge distribution are now external to V while the observation point is inside V.

Summarizing the above examples we now consider the meaning of the boundary integral (2.88). Let the dielectric ϵ and charge distribution ρ be known in the whole XY plane.

As a consequence we know the total electrostatic field in XY and the polarization of the dielectric. The total electrostatic potential in the XY plane is given by the sum of (2.81) and (2.84).

Let V be a domain in XY with boundary Γ having a normal $\vec{n}$. Representing the electrostatic potential (and its normal derivative) on Γ as a superposition of two fields due to exterior and interior to V sources ϕ_{ext} and ϕ_{int} respectively gives

$$\phi_3(\vec{r_2}) = \phi_{3_{ext}}(\vec{r_2}) + \phi_{3_{int}}(\vec{r_2}), \quad \vec{r_2} \in V \ , \tag{2.102}$$

$$\phi_{3_{ext}}(\vec{r_2}) = \int_\Gamma \{\epsilon(r_1) G(\vec{r_1}, \vec{r_2}) \frac{d\phi_{ext}(\vec{r_1})}{d\vec{n}_{r_1}} - \phi_{ext}(\vec{r_1}) \frac{dG(\vec{r_1}, \vec{r_2})}{d\vec{n}_{r_1}}\} dr_1 \ , \tag{2.103}$$

$$\phi_{3_{int}}(\vec{r_2}) = \int_\Gamma \{\epsilon(r_1) G(\vec{r_1}, \vec{r_2}) \frac{d\phi_{int}(\vec{r_1})}{d\vec{n}_{r_1}} - \phi_{int}(\vec{r_1}) \frac{dG(\vec{r_1}, \vec{r_2})}{d\vec{n}_{r_1}}\} dr_1 \ . \tag{2.104}$$

As we have demonstrated $\phi_{3_{ext}}(\vec{r_2})$ is zero and $\phi_{3_{int}}(\vec{r_2})$ is an electrostatic potential in V due to external field sources. This accomplishes our analysis of (2.88).

2.6 Formulation of Dirichlet Type and Neumann Type Electrostatic Boundary Value Problem Using Integral Equation Approach.

Equation (2.78) was obtained in a general form. It contains all integrals that appear in the electrostatic problem. In this thesis we study electrostatic problems which are free of volume electric charge ρ. Assuming $\rho = 0$ in (2.78) gives

$$-\phi(\vec{r_2}) + \int_\Gamma \{\epsilon(r_1) G(\vec{r_1}, \vec{r_2}) \frac{d\phi(\vec{r_1})}{d\vec{n}_{r_1}} - \phi(\vec{r_1}) \frac{dG(\vec{r_1}, \vec{r_2})}{d\vec{n}_{r_1}}\} dr_1$$

$$- \int_V (\epsilon(r_1) - 1) \nabla_{r_1} \phi(\vec{r_1}) \nabla_{r_1} G(\vec{r_1}, \vec{r_2}) dr_1 = 0 \ . \tag{2.105}$$

In order to solve an electrostatic problem using an integral equation approach we need well conditioned integral formulations. Usually the Fredholm integral equation of the second kind is more likely to lead to a well conditioned numerical formulation while the Fredholm

integral equation of the first kind would usually result in ill-conditioning. We say "usually" and "normally" because the Fredholm integral equation of the second kind can be rewritten in the form of the integral equations of the first kind with added singularities to the kernel. Indeed the Fredholm integral equation of the second kind

$$f(\vec{r}) + \int K(\vec{r},\vec{r}')f(\vec{r}')dr' = g(\vec{r}) \ , \tag{2.106}$$

where f is the unknown function, K is the continuous kernel of the integral equation and g is the known function, is given by

$$\int K^*(\vec{r},\vec{r}')f(\vec{r}')dr' = g(\vec{r}) \ , \tag{2.107}$$

where $K^*(\vec{r},\vec{r}') = K(\vec{r},\vec{r}') + \delta(\vec{r}-\vec{r}')$ is a new kernel of the integral equation with a singularity at $\vec{r}=\vec{r}'$ given by the Dirac delta function $\delta(\vec{r}-\vec{r}')$. Therefore before claiming that the integral equation is ill/well posed we need to analyse the singularities of the kernel.

The analysis of ill-conditioning of systems of algebraic equations is introduced in section 4.1.2. Since the algebraic equations are directly related to the integral equations we do not provide the same level of detail of the conditioning of integral equations.

We now analyse the problem of posing (2.105) in a well conditioned form. This analysis is split into two cases when equation (2.105) is applied to the boundary $\vec{r_2} \in \Gamma$ and to the volume domain $\vec{r_2} \in V$.

2.6.1 Well conditioned electrostatic integral equations on the boundary

We now consider a boundary electrostatic problem with boundary Γ posed in free space $\epsilon = 1$. The boundary condition on Γ which may be a Dirichlet or mixed (Neumann) condition is specified later. Substituting $\epsilon = 1$ in (2.105) gives

$$-\phi(\vec{r_2}) + \int_\Gamma \{G(\vec{r_1},\vec{r_2})\frac{d\phi(\vec{r_1})}{d\vec{n}_{r_1}} - \phi(\vec{r_1})\frac{dG(\vec{r_1},\vec{r_2})}{d\vec{n}_{r_1}}\}dr_1 = 0 \ . \tag{2.108}$$

The unknowns in the integral in (2.108) are on Γ which forces us to place an observation point $\vec{r_2}$ also on Γ. Doing otherwise we create an additional unknown in domain V where

the electrostatic problem is posed. This does not violate the consistency of the problem but involves redundant computations.

Let the electrostatic problem be a Dirichlet boundary problem with a Dirichlet boundary condition given by

$$\phi(\vec{r}) = a(\vec{r}), \quad \vec{r} \in \Gamma \ , \tag{2.109}$$

where a is an arbitrary function on Γ. Substituting (2.109) into (2.108) gives

$$-a(\vec{r_2}) + \int_\Gamma \{G(\vec{r_1},\vec{r_2})\frac{d\phi(\vec{r_1})}{d\vec{n}_{r_1}} - a(\vec{r_1})\frac{dG(\vec{r_1},\vec{r_2})}{d\vec{n}_{r_1}}\}dr_1 = 0 \ , \quad \vec{r_2} \in \Gamma \ . \tag{2.110}$$

The normal derivative of ϕ on Γ is the only unknown in (2.110). Solving (2.110) for $\frac{d\phi(\vec{r})}{d\vec{n}_r}$, $\vec{r} \in \Gamma$ leads to an ill-conditioned problem since (2.110) is a Fredholm Integral equation of the first kind. One way to eliminate the ill-conditioning is to differentiate (2.108) prior to substituting the boundary condition (2.109)

$$-\frac{d\phi(\vec{r_2})}{d\vec{n}_{r_2}} + \int_\Gamma \{\frac{dG(\vec{r_1},\vec{r_2})}{d\vec{n}_{r_2}}\frac{d\phi(\vec{r_1})}{d\vec{n}_{r_1}} - \phi(\vec{r_1})\frac{d}{d\vec{n}_{r_1}}\frac{dG(\vec{r_1},\vec{r_2})}{d\vec{n}_{r_2}}\}dr_1 = 0 \ . \tag{2.111}$$

Substituting (2.109) into (2.111) gives

$$-\frac{d\phi(\vec{r_2})}{d\vec{n}_{r_2}} + \int_\Gamma \{\frac{dG(\vec{r_1},\vec{r_2})}{d\vec{n}_{r_2}}\frac{d\phi(\vec{r_1})}{d\vec{n}_{r_1}} - a(\vec{r_1})\frac{d}{d\vec{n}_{r_1}}\frac{dG(\vec{r_1},\vec{r_2})}{d\vec{n}_{r_2}}\}dr_1 = 0 \ . \tag{2.112}$$

Equation (2.112) is a Fredholm integral equation of the second kind. To evaluate the condition of (2.112) we need to study the singularities in the boundary integral.

Recall the single and double layers, introduced in section 2.5 (2.82),(2.83)

$$\phi_{single}(\vec{r_2}) = 4\pi \int_S G(\vec{r_1},\vec{r_2})\rho_s(\vec{r_1})dr_1 \ \text{ and} \tag{2.113}$$

$$\phi_{double}(\vec{r_2}) = 4\pi \int_S \frac{dG(\vec{r_1},\vec{r_2})}{d\vec{n}_{r_1}}\sigma_s(\vec{r_1})dr_1 \ . \tag{2.114}$$

The potentials due to the single and double layers have singularities on Γ given by

$$\frac{d\phi^+_{single}(\vec{r})}{d\vec{n}_r} - \frac{d\phi^-_{single}(\vec{r})}{d\vec{n}_r} = -4\pi\rho_s \ , \tag{2.115}$$

$$\phi^{+}_{double}(\vec{r}) - \phi^{-}_{double}(\vec{r}) = 4\pi\sigma_s \ , \tag{2.116}$$

where $\vec{n}_r$ is a normal to Γ, σ_s is a projection of $\vec{\sigma}_s$ on $\vec{n}_r$, ϕ^+ is an electrostatic potential on the side of Γ where the normal $\vec{n}$ is pointing (positive side), ϕ^- is the value of potential on the opposite side of Γ (negative side). The first integral in (2.112)

$$I = \int_\Gamma \frac{dG(\vec{r_1},\vec{r_2})}{d\vec{n}_{r_2}} \frac{d\phi(\vec{r_1})}{d\vec{n}_{r_1}} = \frac{d}{d\vec{n}_{r_2}} \int_\Gamma G(\vec{r_1},\vec{r_2}) \frac{d\phi(\vec{r_1})}{d\vec{n}_{r_1}} \ , \ \vec{r_2} \in \Gamma \tag{2.117}$$

is a normal derivative of the potential due to a single layer given by $\rho_s = \frac{1}{4\pi}\frac{d\phi(\vec{r})}{d\vec{n}_r}$, $\vec{r} \in \Gamma$. According to (2.113) and (2.115) integral (2.117) experiences a jump when we cross Γ

$$I^+ - I^- = \frac{d\phi(\vec{r})}{d\vec{n}_r} \ . \tag{2.118}$$

Removing the singularity from the integral in (2.112) i.e. subtracting the principal value for (2.117) for $\vec{r_1} = \vec{r_2}$ and adding that principal value as an individual term gives

$$-\frac{1}{2}\frac{d\phi(\vec{r_2})}{d\vec{n}_{r_2}}$$

$$+ \int_\Gamma^{\text{removed singularity at } \vec{r_1}=\vec{r_2}} \{\frac{dG(\vec{r_1},\vec{r_2})}{d\vec{n}_{r_2}} \frac{d\phi(\vec{r_1})}{d\vec{n}_{r_1}} - a(\vec{r_1}) \frac{d}{d\vec{n}_{r_1}} \frac{dG(\vec{r_1},\vec{r_2})}{d\vec{n}_{r_2}}\} dr_1 = 0. \tag{2.119}$$

Equation (2.119) is a Fredholm integral equation of the second kind with no singularities in the kernel which means well conditioning.

We now consider a Neumann electrostatic boundary problem. Let the Neumann boundary condition be given by

$$\frac{d\phi(\vec{r})}{d\vec{n}_r} = b(\vec{r}), \ \ \vec{r} \in \Gamma \ , \tag{2.120}$$

where b is an arbitrary function. Substituting (2.120) into (2.108) gives

$$-\phi(\vec{r_2}) + \int_\Gamma \{G(\vec{r_1},\vec{r_2}) b(\vec{r_2}) - \phi(\vec{r_1}) \frac{dG(\vec{r_1},\vec{r_2})}{d\vec{n}_{r_1}}\} dr_1 = 0 \ , \ \vec{r_2} \in \Gamma \ . \tag{2.121}$$

The only unknown in (2.121) is $\phi(\vec{r})$, $\vec{r} \in \Gamma$. Extracting the principal value from $-\int_\Gamma \phi(\vec{r_1}) \frac{dG(\vec{r_1},\vec{r_2})}{d\vec{n}_{r_1}} dr$ in (2.121) and adding it to that equation for consistency gives

$$-\frac{1}{2}\phi(\vec{r_2})$$

$$+\int_{\Gamma}^{\text{removed singularity at } \vec{r_1}=\vec{r_2}} \{G(\vec{r_1},\vec{r_2})b(\vec{r_2}) - \phi(\vec{r_1})\frac{dG(\vec{r_1},\vec{r_2})}{d\vec{n}_{r_1}}\}dr_1 = 0 \ , \ \vec{r_2} \in \Gamma \ . \quad (2.122)$$

Integral equation (2.122) is of the second kind having a smooth kernel. Since (2.122) and (2.121) are the same we admit (2.121) as being well conditioned.

We presented the well posed integral equations for the Dirichlet and Neumann boundary electrostatic problems (2.119), (2.122). These equations are well suited for solving boundary problems, although, there exist more efficient analytical representations of (2.108) which we now introduce.

In section 2.5 we explained the meaning of the boundary integral in (2.108). This integral represents the electrostatic potential due to electrostatic sources external to V. It can be proved that for any electrostatic potential ϕ in V produced by sources external to V there exists a single/double layer on Γ that establishes the same potential in V. We now replace the boundary integral in (2.108) by an unknown single/double layer

$$-\phi(\vec{r_2}) + 4\pi \int_{\Gamma} \rho_s(r_1)G(\vec{r_1},\vec{r_2})dr_1 = 0 \ , \quad (2.123)$$

$$-\phi(\vec{r_2}) + 4\pi \int_{\Gamma} \sigma_s(\vec{r_1})\frac{dG(\vec{r_1},\vec{r_2})}{d\vec{n}_{r_1}}dr_1 = 0 \ . \quad (2.124)$$

Equations (2.123), (2.124) are the Fredholm integral equations of the first kind. We use the derivative of (2.123) to tackle the Neumann electrostatic boundary problem (2.120) while (2.124) can be directly applied to the Dirichlet electrostatic boundary problem (2.109)

$$4\pi\frac{d}{d\vec{n}_{r_2}} \int_{\Gamma} \rho_s(r_1)G(\vec{r_1},\vec{r_2})dr_1 = b(\vec{r_2}) \ , \ \vec{r_2} \in \Gamma \ , \quad (2.125)$$

$$4\pi \int_{\Gamma} \sigma_s(\vec{r_1})\frac{dG(\vec{r_1},\vec{r_2})}{d\vec{n}_{r_1}}dr_1 = a(\vec{r_2}) \ , \ \vec{r_2} \in \Gamma \ . \quad (2.126)$$

Removing singularities from the integrals in (2.125), (2.126) at $\vec{r_1} = \vec{r_2}$ and adding the corresponding principal values to the equation gives

$$2\pi\rho_s(r_2) + 4\pi\frac{d}{d\vec{n}_{r_2}} \int_{\Gamma}^{\text{removed singularity at } \vec{r_1}=\vec{r_2}} \rho_s(r_1)G(\vec{r_1},\vec{r_2})dr_1 = b(\vec{r_2}) \ , \ \vec{r_2} \in \Gamma \ , \quad (2.127)$$

$$2\pi\sigma_s(\vec{r_2}) + 4\pi \int_{\Gamma}^{\text{removed singularity at } \vec{r_1}=\vec{r_2}} \sigma_s(\vec{r_1}) \frac{dG(\vec{r_1},\vec{r_2})}{d\vec{n}_{r_1}} dr_1 = a(\vec{r_2}) \ , \ \vec{r_2} \in \Gamma \ . \quad (2.128)$$

2.6.2 Well Conditioned Electrostatic Volume Integral Equations

In a non-homogeneous dielectric ϵ the volume integral in (2.105) is nonzero. To simplify analysis we replace the boundary integral in (2.105) by a background electrostatic potential ϕ_{inc}. Assuming $\vec{r_2} \in V$ we write

$$\phi(\vec{r_2}) + \int_V (\epsilon(r_1) - 1)\nabla_{r_1}\phi(\vec{r_1})\nabla_{r_1}G(\vec{r_1},\vec{r_2})dr_1 = \phi_{inc}(\vec{r_2}) \ , \ \vec{r_2} \in V \ . \quad (2.129)$$

Note that (2.129) includes both the value of the potential ϕ and its derivatives which complicates practical implementation. Applying a gradient operator to (2.129) does not add higher order derivatives of ϕ

$$\nabla_{r_2}\phi(\vec{r_2}) + \nabla_{r_2} \int_V (\epsilon(r_1) - 1)\nabla_{r_1}\phi(\vec{r_1})\nabla_{r_1}G(\vec{r_1},\vec{r_2})dr_1 = \nabla_{r_2}\phi_{inc}(\vec{r_2}) \ , \ \vec{r_2} \in V \ . \quad (2.130)$$

(2.130) is a Fredholm vector integral equation of the second kind with no singularity in the kernel and yields two scalar well posed equations in 2D

$$\frac{\partial\phi(\vec{r_2})}{\partial x_2} + \int_V (\epsilon(r_1) - 1) \left\{ \frac{\partial \phi(\vec{r_1})}{\partial x_1} \frac{\partial^2 G(\vec{r_1},\vec{r_2})}{\partial x_1 \partial x_2} + \frac{\partial \phi(\vec{r_1})}{\partial y_1} \frac{\partial^2 G(\vec{r_1},\vec{r_2})}{\partial y_1 \partial x_2} \right\} dr_1 = \frac{\partial\phi_{inc}(\vec{r_2})}{\partial x_2} \ , \quad (2.131)$$

$$\frac{\partial\phi(\vec{r_2})}{\partial y_2} + \int_V (\epsilon(r_1) - 1) \left\{ \frac{\partial \phi(\vec{r_1})}{\partial x_1} \frac{\partial^2 G(\vec{r_1},\vec{r_2})}{\partial x_1 \partial y_2} + \frac{\partial \phi(\vec{r_1})}{\partial y_1} \frac{\partial^2 G(\vec{r_1},\vec{r_2})}{\partial y_1 \partial y_2} \right\} dr_1 = \frac{\partial\phi_{inc}(\vec{r_2})}{\partial y_2} \ , \quad (2.132)$$

$$\vec{r_2} \in V \ .$$

2.7 Governing Equations for Capacitive Sensor Array

2.7.1 Metal Electrodes and Boundary Conditions

In order to both measure and establish electrostatic fields we employ an arrangement of metal electrodes of a given physical size. The boundary of these electrodes determines the

boundary of the inverse electrostatic problem that we solve and the corresponding boundary conditions. In this section we relate the boundary conditions to the measurements that can be physically observed using metal electrodes.

We consider a solid electrically conducting electrode of an arbitrary shape which we refer to as the basic electrode. A set of such electrodes is shown in figure 2.9. Using that electrode we have a possibility to both measure and pre-set its electrostatic potential and/or electric charge.

The electrostatic potential does not vary along the surface of the basic electrode. Indeed a non-zero electric field component along the conductor wall would cause an electric current that would violate the static distribution of charges. If the surface of the electrode is Γ_e then a constant Dirichlet boundary condition (2.12) holds $\phi(\vec{r}) = const$, $\vec{r} \in \Gamma_e$.

The charge of the conducting electrode is located on its surface. The surface density of the electrode charge can be obtained using (2.7)

$$\epsilon \frac{d\phi(\vec{r})}{dn} = -4\pi\rho(\vec{r}) \ , \ \vec{r} \in \Gamma_e \tag{2.133}$$

where ϵ is the boundary value of the dielectric permittivity on the electrode surface Γ_e, $\vec{n}$ is a normal to Γ_e and ρ is the surface charge density.

Integrating (2.133) over the electrode's surface Γ_e gives

$$\int_{\Gamma_e} \epsilon \frac{d\phi}{d\vec{n}} d\Gamma = -4\pi Q \ , \tag{2.134}$$

where Q is the total charge accumulated on the electrode. Equation (2.134) relates the Neumann boundary condition to the charge accumulated on the electrode. By measuring an electrostatic charge accumulated on the electrode we collect the average of $\epsilon \frac{d\phi}{d\vec{n}}$ while the exact Neumann condition on Γ_e remains unknown.

2.7.2 Capacitive Array

We now consider N metal electrodes of arbitrary shape and arrangement in space. We assume that the space in between these electrodes is filled with a non-conducting non-

homogeneous dielectric medium (figure 2.9) characterised by dielectric permittivity $\epsilon(\vec{r})$[4].

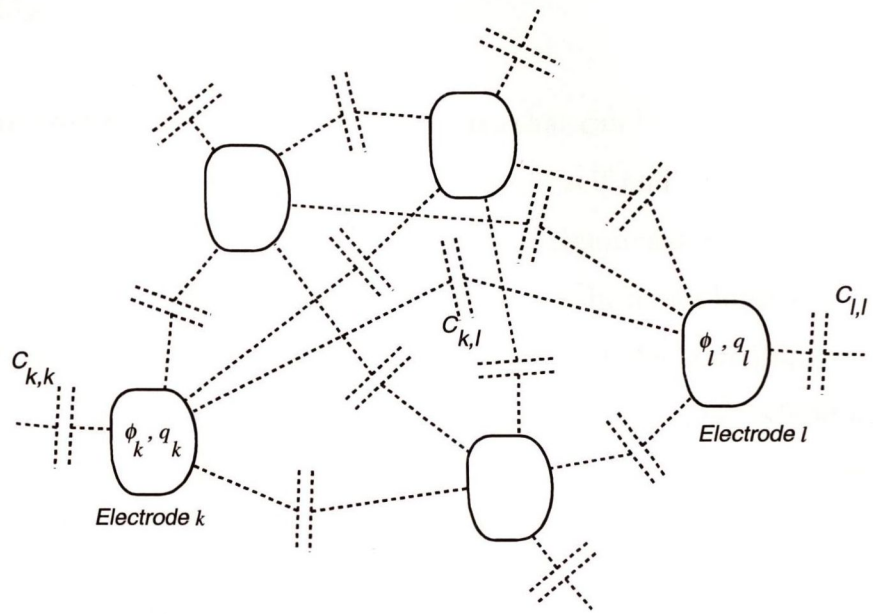

Figure 2.9: Capacitive prototype.

Each electrode is represented by its potential ϕ_n and charge q_n, $n = 1, ..., N$. According to classical electrostatic theory charges q_n and potentials ϕ_n are related through the following set of N equations

$$q_k = \sum_{l=1,...,N} C_{k,l}\phi_l \ , \quad k = 1, \cdots, N \ , \tag{2.135}$$

where $C_{k,l}$, $k \neq l$ are mutual capacitances between the k^{th} and l^{th} electrodes and $C_{i,i}$, $i = 1, ..., N$ are self capacitances. The capacitances in (2.135) are functions of the dielectric permittivity profile and the electrode geometry. The set of equations (2.135) arises from applying a principle of superposition of the electrostatic field and it can be obtained by integrating the normal derivative of the potential over the electrode surfaces taking into account (2.134). According to the reciprocity theorem the mutual capacitances satisfy the

[4]In this project we also refer to the dielectric permittivity $\epsilon(\vec{r})$ as a dielectric profile. The electrostatic inverse imaging problem can be then referred to as a profile reconstruction or profile inversion problem.

following equality

$$C_{k,l} = C_{l,k} \ . \tag{2.136}$$

The mutual and self capacitances are the only data that can be measured using a capacitive sensor array. According to (2.135) we can measure N self and $N(N-1)/2$ mutual capacitances. Reconstruction of simple images requires a significant number of electrodes and consequently a large number of numerical simulations. In many inverse imaging methods such as the Born iterative method (BIM) (section 5.2.3) the contribution of the mutual capacitances $C_{i,j}$, $i \neq j$ into the final dielectric profile image can be individually processed. If there are hardware limitations we can exclude any selected mutual or self capacitances $C_{i,j}$ from the analysis.

A cross-section of the 2D capacitive sensor array that complies with the bed sensor application introduced in section 1.1 is shown in figure 2.10. The sensor array employs N flat electrodes that are used to establish/measure the field, and a Ground plane. The Ground plane electrode is included in (2.135) along with other electrodes. It is also characterized by an electrostatic potential (which is pre-set to zero), an accumulated charge and a mutual capacitance between it and other electrodes. The purpose of the Ground plane electrode is to establish a shield that reduces the sensitivity of the mutual capacitance between the electrodes placed on the top side of the capacitive sensor arrangement to the underneath dielectric medium. This feature is an advantage of the proposed capacitive sensor array.

2.8 Quasi-Electrostatic theory

So far we have considered purely static fields. It is easier to measure dynamic currents and voltages than static charges and potentials and we can significantly simplify the hardware requirements if we use low frequency (LF) electric fields instead of the electrostatic fields. The governing equations (2.135) for the capacitive sensor array operating at the low frequency are valid at any moment in time if the wavelength λ of the electromagnetic wave

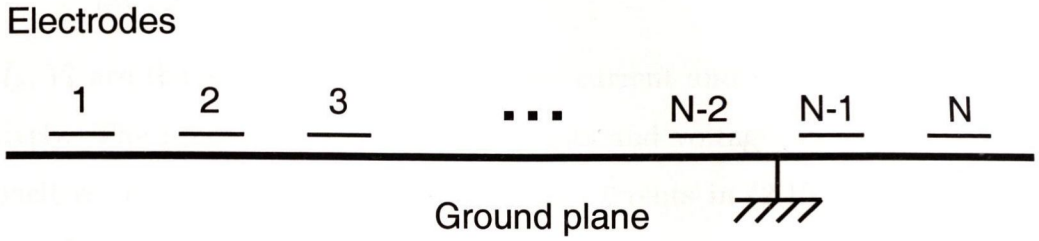

Figure 2.10: A 2D capacitive sensor array.

in free space

$$\lambda = c/\omega \ , \tag{2.137}$$

where c and ω are the speed of the light and the radian frequency, is significantly larger than the maximum linear dimension of the capacitive sensor array. Our hardware prototypes employing capacitive sensor arrays are designed to operate at $\omega = 300 - 500$kHz. The corresponding λ is of the order of 600-1000 meters. The linear size of the capacitive sensor arrays that we design varies in the range from 20cm to 2m which justifies the LF application. The low frequency electric field is called quasi-electrostatic. The amplitude of the quasi-electrostatic field satisfies Laplace's equation.

We now assume that charges q_n and potentials ϕ_n, $n = 1, ..., N$ in (2.135) oscillate at frequency ω_0. We employ complex arithmetic and assume harmonic excitation $e^{j\omega_0 t}$. Differentiating (2.135) and using

$$I = \frac{dq}{dt}$$

and

$$\frac{dV}{dt} = j\omega V \tag{2.138}$$

we obtain

$$I_k = j\omega \sum_{l=1,...,N} C_{k,l} V_l \ , \quad k = 1, ..., N \ , \tag{2.139}$$

where I_k, V_k are the complex amplitudes of the current and voltage for the k^{th} electrode respectively. The procedure of collecting currents and voltages in (2.139) is the basis of the capacitive sensor technique. Recall that all currents in (2.139) lead the voltages by $\pi/2$ phase shift.

We now briefly explain how we measure $C_{k,n}$, where k and n are the indices of the Tx and Rx electrodes respectively. We apply a sinusoidal voltage V_k to the k^{th} Tx electrode, terminate the rest of Tx and Rx electrodes to ground and measure current I_n induced on the n^{th} electrode. The n^{th}equation in (2.139) then becomes

$$I_n = j\omega C_{k,n} V_k \ , \tag{2.140}$$

which immediately gives the following expression for the mutual capacitance

$$C_{k,n} = \left| \frac{I_n}{\omega V_k} \right| \ . \tag{2.141}$$

2.9 Appendix: Conformal Mapping and Helmholtz Operator

In section 2.3.2 we presented a technique for applying conformal mapping to electrostatic problems in a general form. It is a misleading opinion that conformal mapping is conservative in the sense that it is only suitable for mapping an electrostatic field equation. In this section we demonstrate how conformal mapping can be applied to a Helmholtz equation

$$-\nabla_{xy}^T \nabla_{xy} u + \epsilon u = f \ , \tag{2.142}$$

where operator ∇_{xy} is given by (2.46).

We admit that analysis of the Helmholtz equation is beyond the subject of this thesis. Although (2.142) cannot be reduced to an electrostatic equation, many 2D inverse electrodynamic problems are governed by (2.142). Hence (2.142) is relevant to inverse imaging

problem and is indirectly relevant to our study. Being able to apply conformal mapping to (2.142) gives an option to substitute the Helmholtz equation for electrostatic field equation and to apply electrostatic inversion methods to electrodynamics.

Transforming (2.142) into $\tilde{Z}$ domain using a conformal mapping gives

$$-\nabla^T_{\tilde{x}\tilde{y}}\nabla_{\tilde{x}\tilde{y}}u + \frac{\epsilon}{\det|J|}u = \frac{f}{\det|J|}\,, \tag{2.143}$$

where $\det|J|$ is a Jacobian of the conformal mapping (2.40).

According to (2.143) in order to conformally map a Helmholtz operator based problem we scale both the source function f and a dielectric distribution ϵ by $\frac{1}{\det|J|}$. Potential u obtained by a conformal mapping will satisfy the same Helmholtz equation in the new domain as in the original domain.

UNIQUENESS OF THE SOLUTION FOR THE IMAGING PROBLEM

When presented with a problem to solve one must find all of its solutions or prove that the problem does not have a solution. This directly applies to systems of algebraic linear equations and is valid in general. In practical applications it is often required to find the most physical solution. If a problem has a unique solution numerical evaluation is simplified.

In section 3.3 we present several existing uniqueness theorems for the inverse electrostatic problem and, then, in section 3.6 we explain how the application of the capacitive sensor array to an imaging problem complies with the conditions imposed by these theorems. We claim this study to be original.

Along with the analysis of uniqueness of the solution for the inverse electrostatic problem we present examples of the object models (employed in electrostatic problems) that reveal fundamental difficulties arising in the electrostatic inverse problem. Some of our examples such as an electrostatic problem of conducting and dielectric cylinders in the homogeneous field presented in appendices 3.7 and 3.8 and a problem of artificial dielectric explained later come from the author's college background and have never been applied to the analysis of the electrostatic inverse problems. Other examples have already been proposed in electrodynamics yet their electrostatic counterparts are new. In this chapter we aim to develop a practical understanding of possibilities and limitations of the electrostatic inverse imaging techniques.

Is knowledge of the uniqueness theorem required prior to solving the problem? The answer lies, for example, in the inverse electromagnetic problems which have been successfully tackled [48], [51], [90], [49] many years before a relevant uniqueness theorem was discovered [81], [68], [99]. Before the uniqueness theorem emerged researchers were primarily

motivated by their intuition and the success of the existing approaches.

If the data for the inverse problem is obtained experimentally then at least one solution for the inverse electromagnetic or electrostatic problem must exist. However if the problem is ill-conditioned then new difficulties arise. The electrostatic imaging problem as well as other inverse problems in acoustics and electrodynamics is governed by the Fredholm integral equation of the first kind [72] which is ill posed [4], [38], [40]. The noise in the measured data contributes to distortion of the solution and the distortion does not have to become smaller as the noise tends to zero. We now illustrate ill-conditioning for the electrostatic inverse imaging problem on a simple practical example. We consider the problem of the reconstruction of two objects in 2D having the same geometry (fig. 3.1). One object is made of homogeneous dielectric $\epsilon = \epsilon_0$ (fig. 3.1(a)) and the other one is hollow and composed of small metal cylinders of radius r_0 with density d (figure 3.1(b)) such that $r_0^2 d = \frac{\epsilon_0 - 1}{4\pi}$. According to appendix 3.7 these two objects produce nearly identical

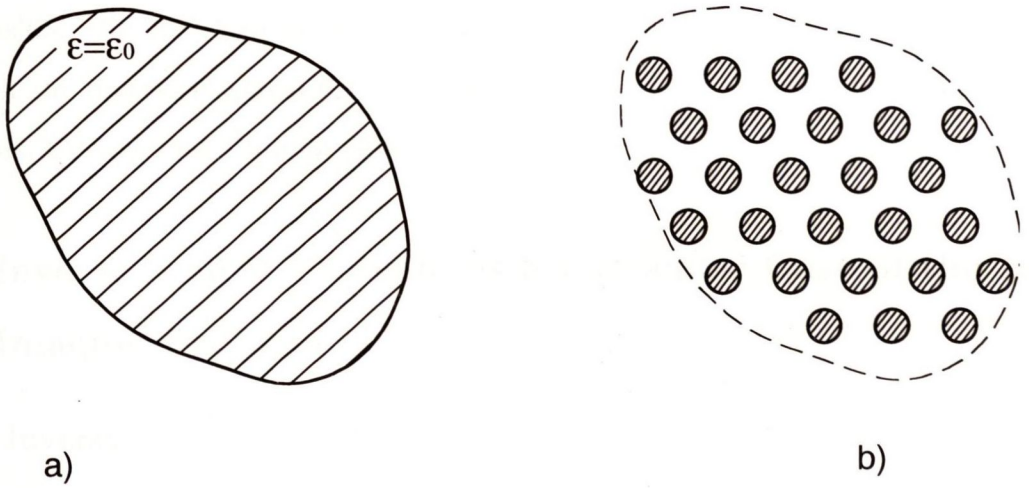

Figure 3.1: A homogeneous dielectric object $\epsilon = \epsilon_0$ (a) and a hollow artificial object (b) having the same geometry as (a) and composed of metal cylinders of radius r_0 and density d

scattered[1] fields. From the inverse electrostatic problem perspective these two objects are indistinguishable in the presence of noise. For any given precision of measurement and for any given level of noise it is possible to find large enough d and small enough r_0

[1]Hereafter for convenience we use the term 'scattered field' for electrostatic problem. This term is originally borrowed from electrodynamics.

(to hold $r_0^2 d = \frac{\epsilon_0 - 1}{4\pi}$) such that the two objects in figure 3.1 will be undistinguishable. We now compare the objects in figure 3.1 in terms of their dielectric distribution. An object in figure 3.1 (a) has a finite homogeneous dielectric distribution $\epsilon = \epsilon_0$. An object in figure 3.1 (b) is constructed so that it always has metal insertions that can be seen as dielectric insertions having an infinitely large dielectric permittivity. Thus while the scattered electrostatic fields caused by these objects can be made close to one another to any precision, a difference in the dielectric properties for these scatterers remains and is , in fact, infinitely large. Thus we have to be careful when talking about the existence of solution for the experimentally implemented electrostatic imaging problem.

The uniqueness theorem for the inverse imaging problem is important because it gives confidence that the problem is consistent and that a numerical solution is unique provided all assumptions of the theorem are satisfied. In particular the uniqueness theorem determines the measurements that have to be made in order to provide a unique solution and consequently improve the inversion. Although in many of the existing inverse imaging problems[65], [40], [33], [66] the corresponding uniqueness theorem is not referred to, in our approach the inverse electrostatic problem complies with a uniqueness theorem obtained by Lassas, Cheney and Uhlman [99].

3.1 Inverse Source Problem as a Particular Case of the Inverse Imaging Problem

3.1.1 Inverse Imaging Problem.

We define the inverse electrostatic problem as the reconstruction of the properties of the surrounding medium, such as a dielectric permittivity distribution, using remote measurements of the electrostatic field. In Chapter 5 we present many successful implementations of the inverse imaging problem which can be grouped under the type of the incident[2] fields used, the location of the points at which the measurements are collected, the *a priori*

[2]To avoid the introduction of new terminology we use some of the well understood electrodynamic terms in electrostatics.

information imposed on the unknown profile and other criteria. Thus there are many ways to formulate an electrostatic imaging problem. We admit the definition of the inverse electrostatic problem as of the reconstruction of the unknown medium until we introduce a uniqueness theorem in section 3.5.

3.1.2 Inverse Source Problem

The electrostatic inverse source problem is similar to the electrostatic inverse imaging problem. Its objective is to reconstruct the locations and intensities of the unknown distribution of electric field sources using electrostatic field measurements. In the older literature both the inverse source and inverse scattering problems have been thought of as a one large class of inverse problems. Even in periodicals these two problems used to appear together [36]. At present the inverse imaging problem is intensively investigated in periodicals while the inverse source problem would rarely be encountered. We now give more insight into the similarity between these two problems.

Let an electrostatic field be established in some domain Ω which we refer to as an incident field $\vec{E} = \vec{E}_{inc}$. If we place a homogeneous dielectric body $\epsilon = \epsilon_0$ of known permittivity in Ω then the dielectric material will become polarized producing another field called the scattered field $\vec{E}_{scat}$. The total field $\vec{E}_{tot}$ in Ω is given by a superposition of the incident and scattered fields $\vec{E}_{tot} = \vec{E}_{inc} + \vec{E}_{scat}$. Polarization of the dielectric results in uncompensated immobile charges on the surface of the dielectric body. The inverse scattering problem is to find the shape of the dielectric body while the inverse source problem is to find charges that produce the scattered field. Thus both problems will have the shape of the unknown body as a solution. Summarizing, if the only incident field is used to employ an inverse imaging problem then that imaging problem can also be seeing as an inverse source problem.

3.2 Nonuniqueness of Solution for Inverse Source Problem

The field ϕ of an arbitrary charge distribution $\rho(\vec{r})$ is given by

$$\phi(\vec{r_1}) = \int G(\vec{r_1}, \vec{r_2})\rho(\vec{r_2})d\vec{r_2} \ , \tag{3.1}$$

where G is the Green's function (2.22),(2.23).

If we know ϕ in some domain Ω then the charge distribution ρ in Ω can be immediately obtained using the following formula

$$\rho = \frac{1}{4\pi}\nabla^2\phi \ . \tag{3.2}$$

Thus the inverse source problem may seem to have a unique solution (3.2) provided we require the knowledge of the potential ϕ in Ω where Ω can be the entire 3D space for example. Thus the ability to measure ϕ at any point of Ω is similar the ability to measure the charge or dielectric constant in Ω. In reality we measure an electrostatic field outside the domain containing the field sources of interest. In that case (3.2) does not establish the uniqueness of the solution for the inverse source problem.

The nonuniqueness of the solution for the inverse source problem in electrodynamics has been proved for example in [35]. Bleisten and Kohen [35] relate the nonuniqueness of the solution to the features of the direct radiation problem namely the existence of the non-radiating sources. We now conduct our own investigation that reveals a nonuniqueness of the solution for the electrostatic inverse source problem in the 2D. Assuming that ρ has a finite support[3] as shown in figure 3.2 and that integral (3.1) is measured on a boundary Γ at N points $\vec{r_k}$, $k = 1, ..., N$ outside the support of ρ we write

$$\phi(\vec{r_k})|_\Gamma = \int_{\text{Supp}(\rho)} G(\vec{r_k}, \vec{r})\rho(\vec{r})d\vec{r} \ , k = 1, ..., N \ , \tag{3.3}$$

where $\text{Supp}(\rho)$ denotes the support of ρ. Note that the Fredholm integral equation (3.3) is of the first kind. We now show that a solutions to (3.3) is not unique i.e we present an electrostatic source distribution which is a null space to the integral operator $\int_{\text{Supp}(\rho)} d\vec{r}G(\vec{r_k}, \vec{r})$ in (3.3).

The 2D cylindrical capacitor shown in figure 3.2 is composed of two cylinders of different radii having the same centre. It is well known that a cylindrical capacitor produces a zero external field. Thus if ρ is a solution to (3.3) then we can add the charge of the cylindrical

[3] A domain where ρ is nonzero

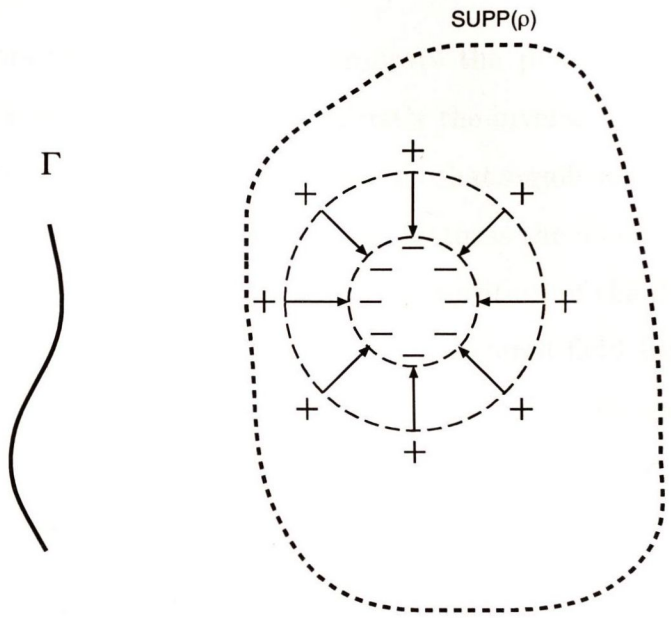

Figure 3.2: The charge of the cylindrical capacitor that gives a null space to the integral in (3.3)

capacitor to ρ to obtain another solution for (3.3). We have proved that if the inverse source problem in electrostatic has a solution then it has infinitely many solutions.

One might expect that since the inverse source problem does not have a unique solution it does not have practical applications. In fact the inverse source problem found its application in the radar, for example. If we impose some stipulations (which is also called *a priori* knowledge) on the function ρ then we can eliminate the non-radiating sources and make the solution unique [73]. We present another application of the inverse source problem in section 5.1.2.

3.3 Preface to Uniqueness Theorem for Electrostatic Inverse Imaging Problem

There are two factors that significantly complicate the proof of the uniqueness of the solution of the inverse electrostatic problem. Firstly the inverse problem is ill-conditioned. In the introduction to this chapter we demonstrated that significantly different objects can produce nearly identical scattered fields. Another factor is the non-linearity of the imaging problem. Non-linearity means that if we have superposition of the dielectric permittivity distributions, for example, then the corresponding scattered field (sensor measurements) is not given by the superposition of the fields due to the presence of these dielectrics individually. We now survey the relevant publications that deal with the uniqueness of various inverse problems.

An enlightening discussion is presented in [36], 1982. This paper relates to a dispute that had occurred just before several important works appeared that convinced people of the existence of a unique solution for the inverse imaging problem in electrostatics, electrodynamics and acoustics [78] 1986,[79] 1987,[80] 1988, [100] 1988, [85] 1993. Note that while the foundation for the uniqueness of the solution for the inverse problems had appeared in the middle of 80-ies, there still exist many modern works that further that research [99] 1998, [68] 1998, [70] 1998, [81] 1999. The above list of references is not complete but does give an insight into how many people are involved in uniqueness analysis of the inverse problem and how complicated the problem is.

We now briefly overview issues important to our study i.e. that relate to the uniqueness of solution for the imaging problem. In [36] Devaney and Sherman claim that neither the inverse source nor the scattering problems possess a unique solution. Firstly they consider an electrodynamic inverse source problem for spherically symmetric distribution of electromagnetic sources located within the sphere of radius R_0. The outer field for these sources satisfies the equation

$$\psi(r) = A\frac{e^{ik_0 r}}{r} \ , \tag{3.4}$$

where A is a constant and is the only parameter that can be extracted from measurements. Obviously knowing one scalar A we cannot reconstruct an arbitrary distribution of sources $\rho(r)$ that relates to A as follows

$$A = \frac{1}{k_0}\int_0^{R_0} r\rho(r)\sin k_0 r dr \ . \tag{3.5}$$

Examples similar to (3.4), (3.5) can be constructed for the electrostatic inverse source problem.

Next Devaney and Sherman consider an inverse scattering problem for a small conducting sphere having radius R_0 and conductivity σ. Because the conducting sphere is small $k_0 R_0 << 1$ it can be seen as being placed in a homogeneous field $E^{(i)}$ that induces current J in it

$$J = \left(\frac{k_0}{k_c}\right)\sigma E^{(i)} \ , \tag{3.6}$$

where $k_c^2 = \omega^2\mu_0\epsilon_0 + i\omega\mu_0\sigma$ is the squared propagation constant inside the sphere. Using (3.6) it is easy to demonstrate that R_0 and σ cannot be simultaneously obtained by measuring the scattered field. The fact that we are not able to determine R_0 and σ does not prove existence of multiple solutions for the inverse scattering problem because we use an assumption that the sphere is placed in the uniform field. Despite (3.6) does not prove or disprove the uniqueness theorem it illustrates that in reality we are not able to determine R_0 and σ due to technical limitations.

We now present the 2D electrostatic analogy for the electrodynamic inverse problem (3.6). Let an incident electrostatic field $\vec{E}_0$ at a given point have a curvature radius r_0 and let a cylindrical dielectric body of radius R_0 and dielectric permittivity ϵ_0 be centred at that point. If $R_0 << r_0$ then the incident field can be seeing as a homogeneous electric field having intensity $\vec{E}_0$. According to appendix 3.8 the scattered field produced by the dielectric cylinder in a homogeneous field is given by the field of dipole with dipole moment $\vec{p}$

$$\vec{p} = \frac{\epsilon_0 - 1}{\epsilon_0 + 1} R_0^2 \vec{E}_0 \ . \tag{3.7}$$

Even if employing many incident fields with a local curvature of the field lines not smaller than r_0 then the only parameter that we can measure from the distorted field is $\frac{\epsilon_0-1}{\epsilon_0+1}R_0^2$. Thus the values of ϵ_0 and R_0 cannot be obtained individually.

An important conclusion to us is that due to ill-conditioning of the inverse problem we cannot reconstruct high contrast images wherever the incident field that we establish is close to homogeneous. If we move away from the sensor array in figure 2.10 then the curvature radius of the electrostatic field lines increases. As a result we must expect that the sharpness of the reconstructed image will deteriorate in the outward direction for the capacitive sensor array in figure 2.10.

Furthermore, in [36], Bojarski rises an objection to Devany and Sherman saying: "*The present unresolved issues in the inverse-scattering inverse source problem are the problems of what scattering information needs to be known (measured) and which, and how much additional* ***a priori*** *known specific information about the source or the scattering potentials needed for the determination of what properties of the source or the scattering potential, and to which accuracy and/or resolution*". Thus in one sentence Bojarski expressed the most critical questions that needed to be answered for the imaging problem. When we first confronted a problem of non-contact sensing and imaging we did not know about the existence of the uniqueness theorem. Indeed uniqueness of the solution for the inverse imaging problem is rarely referred to in periodicals while the earlier publications claim that an imaging problem probably does not posses a unique solution. [35] and [36] were the first publications on the uniqueness problem that we found and we are proud that our opinion was similar to Bojarki's rather then Devaney's and Sherman's.

One of the first successful imaging applications that we developed during our early research was an experimental prototype using a 2D inverse imaging algorithm capable of determining the position of a metal cylinder of known radius using only one incident field (section 5.1.2). As we have mentioned in section 3.2 an inverse scattering problem employing only one incident field is similar to the inverse source problem and does not possess a unique solution. Following Devaney [36] we imposed *a priori* information on the scattering body (we assumed that the scatterer is a metal cylinder having predefined radius) and we have

obtained a unique solution for the inverse problem and stable operation of both the numerical algorithm and the experimental prototype. We employed four measurements of the electrostatic field to extract only two unknowns namely x and y co-ordinates for the metal cylinder. Three measurements were sufficient to determine the position of the cylinder while the fourth measurement was added to achieve robust operation of the prototype and to increase the range of sensitivity for the prototype. Note that due to non-linearity of the imaging problem two measurements are usually not sufficient to uniquely determine the position for the 2D cylindrical scatterer. The prototype array is shown in figure 5.4.

Another important example for our uniqueness study is [48]. In [48] the shape of the arbitrary conducting scatterer is uniquely recovered from the scattered electromagnetic field. The inversion algorithm employs the 3D analytical continuation of the electromagnetic field in the vicinity and inside of the unknown object. Then the extrapolated electromagnetic field is processed in order to find possible location and shape for the unknown object. In the case of the perfectly conducting object the criteria is to find such surface that the tangential component of the electric field intensity $\vec{E}$ and the normal component of the magnetic field $\vec{H}$ vanish. One incident field was sufficient to reconstruct the surface of two perfectly conducting spheres [48].

The method in [48] can be employed in the electrostatic inverse problem of reconstructing the shape of a conducting object. Indeed employing analytical continuation of the electrostatic potential we can extrapolate the field outside of the measurement domain towards the expected unknown object location. Since the object is conducting, its surface must lie on the equi-potential surface. In the case of several incident fields the wall of the conducting object must lie on the equi-potential surface for each incident field. Increasing the number of incident fields we reduce the number of possible solutions to only one.

3.4 Dirichlet-to-Neumann Map as a Complete Set of Data That Can Be Measaured in the Electrostatic Imaging Problem

In this section we introduce a so-called Dirichlet-to-Neumann map. The Dirichlet-to-Neumann map incorporates data of infinitely many incident fields and, in fact, yields complete information that can be collected in the electrostatic inverse imaging problem. If the uniqueness theorem for the electrostatic imaging problem exists then the knowledge of the Dirichlet-to-Neumann map must be sufficient for obtaining a unique solution.

Let an unknown dielectric distribution be placed in Ω and electrostatic field measurements be employed in D. We also assume that Ω and D do not overlap except for the boundary Γ. If Ω does not share its boundary with D then we expand Ω or enlarge the support for the unknown dielectric distribution until the boundaries for Ω and D are merged. In figure 3.3, D and Ω are shown as finite and infinite domains respectively for illustrative purposes only.

For the sake of simplicity we assume that D is free of dielectric ($\epsilon = 1$). Let ρ be a volume charge distribution in D which we use to establish an electrostatic field in Ω. According to (2.105) the electrostatic potential ϕ in D is

$$\phi(\vec{r_2}) = \int_\Gamma \{G(\vec{r_1}, \vec{r_2}) \frac{d\phi(\vec{r_1})}{d\vec{n}_{r_1}} - \phi(\vec{r_1}) \frac{dG(\vec{r_1}, \vec{r_2})}{d\vec{n}_{r_1}}\} dr_1 + 4\pi \int_D G(\vec{r_1}, \vec{r_2}) \rho(\vec{r_1}) dr_1 \quad , \vec{r_2} \in D \tag{3.8}$$

The electrostatic potential in D (3.8) is uniquely determined by the Neumann and Dirichlet boundary condition on Γ. This means that any measurement of the electrostatic field in D is redundant provided ϕ and $\epsilon \frac{d\phi}{d\vec{n}}$ are known on Γ. If there is more than one incident electrostatic field then for each incident field we collect two one-dimensional functions on Γ to constitute the measurement set.

We now consider any selected electrostatic incident field employed in the inverse electrostatic problem. Let the corresponding $\phi(\vec{r}) = a(\vec{r})$ and $\frac{d\phi(\vec{r})}{d\vec{n}} = b(\vec{r})$ be measured on Γ. We remove the incident electrostatic field and consider a boundary electrostatic problem in Ω with a Dirichlet boundary condition $\phi(\vec{r}) = a(\vec{r})$, $\vec{r} \in \Gamma$. Since an electrostatic problem in Ω has a unique solution the measured value for $\frac{d\phi(\vec{r})}{d\vec{n}} = b(\vec{r})$ on Γ is the same as in the

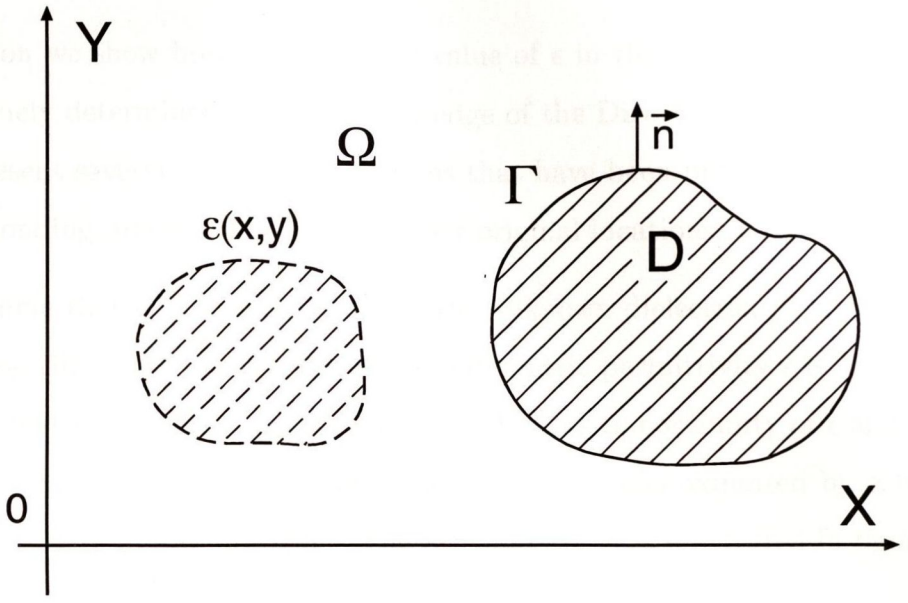

Figure 3.3: Unknown scatterer and boundary Γ where the potential and its normal derivative are measured.

case of the incident electrostatic field excitation. Thus establishing any incident field in Ω and D can be seen as establishing a particular Dirichlet (yet *a priori* unknown) boundary condition on Γ.

If we are able to pre-set any Dirichlet boundary condition on Γ then we are also able to establish an electrostatic field in Ω corresponding to any electrostatic field source in D regardless of the properties of the dielectric in Ω. We now introduce a so called Dirichlet-to-Neumann map Λ_ϵ on Γ [67],[70],[74],[81]

$$\Lambda_\epsilon : \phi \to \epsilon \frac{d\phi}{d\vec{n}}\bigg|_\Gamma \quad , \tag{3.9}$$

where ϵ is the boundary value of the dielectric permittivity in Ω. We have demonstrated that the Dirichlet-to-Neumann map (3.9) includes the entire information that can be measured in the inverse electrostatic problem.

The boundary value of ϵ in (3.9) is defined in Ω and is unknown. It arises in (3.9) due to continuity of the normal component of the electric flux density on the dielectric boundary. We recall that $\epsilon = 1$ in D.

3.5 Various Uniqueness Theorems for Inverse Problem

In this section we show how the boundary value of ϵ in the inverse electrostatic problem can be uniquely determined from the knowledge of the Dirichlet-to-Neumann map[4] (3.9). Then we present several uniqueness theorems that have been proven by different authors. The corresponding proofs are referred to their original locations.

We now assume that (i) Γ is a boundary of the unknown dielectric, (ii) A is a point on Γ, (ii) $\epsilon(A) = \epsilon_0$, (iii) Γ is smooth at A, (iv) the dielectric permittivity ϵ is continuous at A, (v) the Dirichlet-to-Neumann map is known for Γ. Due to continuity of ϵ and smoothness of Γ at A we can choose a vicinity of A such that Γ is approximated by a line and ϵ is approximated by ϵ_0 to any precision. The proximity of A is illustrated in figure 3.4.

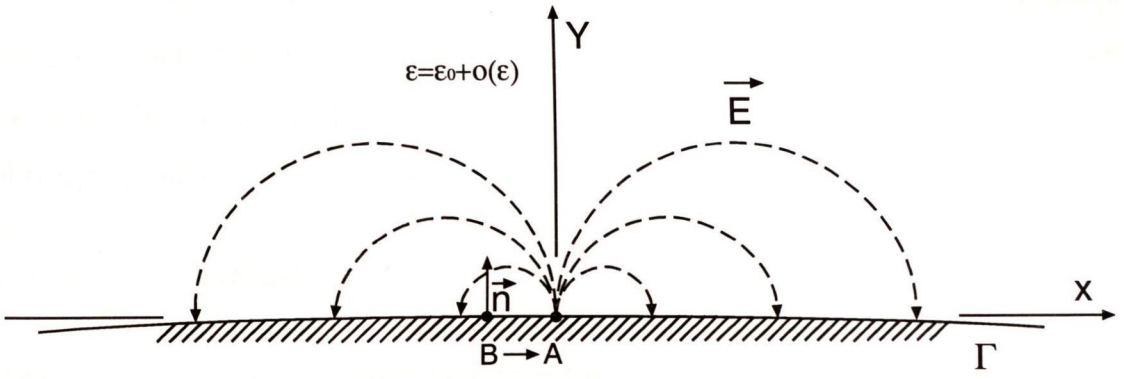

Figure 3.4: A vicinity of point A on a smooth boundary Γ and an electrostatic field $\vec{E}$ due to the Dirichlet boundary condition $\phi(A) = \delta$.

We consider the following Dirichlet boundary condition on Γ in the neighborhood of A

$$\phi(\vec{r})|_\Gamma = \delta(\vec{r} - \vec{r}_A) \quad , \vec{r} \in \Gamma \quad , \tag{3.10}$$

where δ is the Dirac delta function and $\vec{r}_A$ is the position vector for A.

[4]During our early study of the inverse electrostatic problem we discovered that the boundary value of the unknown dielectric can be uniquely reconstructed from the knowledge of the Dirichlet-to-Neumann map. We believed that this result is novel until we found a number of uniqueness theorems having our ideas as a consequence. In particular, the uniqueness theorem presented in [101] says that the boundary value of both the dielectric permittivity and its higher order derivatives are uniquely determined by the Dirichlet-to-Neumann map.

The electrostatic field intensity $\vec{E}_{tot}$ in the vicinity of A is the sum of the dipole field $\vec{E}_d$ (due to (3.10)) and some external field $\vec{E}_{ext}$ which is a function of the boundary shape and dielectric distribution ϵ outside the vicinity of A

$$\vec{E}_{tot} = \vec{E}_{ext} + \vec{E}_d \ . \tag{3.11}$$

Let B be a boundary point in the vicinity of A. The dipole field intencity $\vec{E}_d$ at B can be calculated to give

$$\vec{E}_d\Big|_\Gamma = -2\frac{\vec{n}}{|r|^2} \ , \tag{3.12}$$

where r is a distance between A and B.

The external field $\vec{E}_{ext}$ in (3.11) in the vicinity of A is unknown yet finite. We introduce a constant C such that $|\vec{E}_{ext}| < C$ in the vicinity of A. The dipole field $\vec{E}_d$(3.12) is known in the proximity of A and does not depend on ϵ_0. Using the Dirichlet-to-Neumann map we obtain the value of $\epsilon\frac{d\phi}{d\vec{n}}$ corresponding to (3.10) on Γ

$$b = \epsilon\frac{d\phi}{d\vec{n}} = -\epsilon_0\vec{E}_{tot}\vec{n} \ . \tag{3.13}$$

We now calculate a limit for the following ratio

$$\lim_{r\to 0}\frac{b}{-\vec{E}_{tot}} = \lim_{r\to 0}\frac{\epsilon_0(\vec{E}_{ext}+\vec{E}_d)\vec{n}}{\vec{E}_{ext}+\vec{E}_d} = \epsilon_0 \ . \tag{3.14}$$

The values of b and $\vec{E}_{tot} \approx \vec{E}_d$ are given by (3.12) and (3.13) respectively. Therefore the value of the limit in (3.14) can be directly computed. Thus (3.14) not only illustrates a uniqueness of the boundary value of the dielectric permittivity ϵ_0 but also gives a method according to which ϵ can be obtained on Γ using the Dirichlet-to-Neumann map.

Several uniqueness theorems have been proved in periodicals which we now present.

Let $\Omega \subset \mathbb{R}^n$ $(n \geq 2)$ be a bounded domain with smooth boundary Γ. The Dirichlet integral Q_ϵ for $\hat{L}_\epsilon$ is defined as follows:

$$Q_\epsilon = \int_\Gamma f\epsilon\frac{d\phi}{\vec{n}}d\Gamma \ , \tag{3.15}$$

where operator $\hat{L}_\epsilon$ is introduced in section 2.1 (2.9), $\vec{n}$ is a normal to Γ and ϕ is a unique solution to the Dirichlet boundary problem:

$$\hat{L}_\epsilon = 0, \quad \phi|_\Gamma = f \ . \tag{3.16}$$

In [101] Kohn and Vogelius prove the following theorem:

Theorem 3.5.1 *Suppose that $x \in \Gamma$ and that there exists a neighbourhood B of x relative to Ω such that*

$$Q_{\epsilon_1}(\phi) = Q_{\epsilon_2}(\phi) \text{ for all } \phi \in H^{1/2}(\Gamma) \text{ with supp } \phi \subset B \tag{3.17}$$

then

$$D^k\epsilon_1 = D^k\epsilon_2 \text{ for all } k = (k_1, ..., k_n), \quad k_i > 0 \, . \tag{3.18}$$

In the above theorem function ϕ is in the Sobolev space $H^{1/2}$ defined (in terms of the Fourier transform $\hat{\phi}$) by

$$H^s = \left\{ \phi : \int |\hat{\phi}(\zeta)|^2 (1 + |\zeta|^2)^s d\zeta < \infty \right\} \tag{3.19}$$

Theorem 3.5.1 says that from the knowledge of the Dirichlet integrals we can determine all derivatives of ϵ on Γ. If ϵ is *a priori* known to be real analytic then Q_ϵ determines ϵ.

In [78] Sylvester and Uhlman prove another theorem that establishes the uniqueness of the solution for the inverse electrostatic problem provided we know the Dirichlet integrals Q_ϵ and provided ϵ is *a priori* small.

Theorem 3.5.2 *Let Ω be a bounded domain in $\mathbb{R}^2$ with smooth boundary Γ. Then there exists $\varepsilon(\Omega) > 0$ such that if*

$$||1 - \epsilon||^* < \varepsilon \text{ in } \Omega \ , \tag{3.20}$$

and if

$$Q_{\epsilon_1}(\phi) = Q_{\epsilon_2}(\phi) \text{ for all } \phi \in H^{1/2}(\Gamma) \ , \tag{3.21}$$

then $\epsilon_1 = \epsilon_2$ *in* Ω,

where $||\epsilon||^* = \max_{|k|\leq 3} ||D^k \epsilon||_{L^\infty}$

In theorem 3.5.2 ϵ together with its derivatives are each bounded by 2. In [79] Sylvester and Uhlman prove a theorem similar to theorem 3.5.2 but for any large ϵ. Furthermore Sylvester and Uhlman [80] introduce a novel (different from Kohn's) proof of the uniqueness theorem using the methods of microlocal analysis. In particular Sylvester and Uhlman [80] demonstrate that ϵ can be uniquely reconstructed from the knowledge of the Dirichlet-to-Neumann map. It can be proven that the knowledge of the Dirichlet-to-Neumann map and the knowledge of the Dirichlet integrals are equivalent [100].

It appears that to obtain a unique solution for the inverse electromagnetic problem we do not need to know the Dirichlet-to-Neumann map on the entire Γ. According to Lassas, Cheney and Uhlman [99] ϵ can be uniquely reconstructed from the knowledge of the Dirichlet-to-Neumann map on an open subset of Γ. In the next section we explain the measurement methodology that we employ in our numerical algorithm in chapter 6. That measurement technique complies with the Dirichlet-to-Neumann map.

3.6 Electrostatic Measurements That Satisfy the Criteria of the Uniqueness Theorem.

In previous section we introduced several theorems on uniqueness of solution for the inverse electrostatic problem. The significance of these theorems is that the inverse electrostatic problem has a unique solution if we know the Dirichlet-to-Neumann map on the open subset of the boundary Γ covering the unknown dielectric. In this section we explain how we measure the Dirichlet-to-Neumann map experimentally. This analysis is novel from the electrostatic inverse problem perspective.

The Dirichlet-to-Neumann map can be measured directly by recording the Neumann boundary condition for all possible Dirichlet boundary conditions. If we follow that method we will most probably collect redundant linearly-dependent measurements. We need a practical method for collecting the Dirichlet-to-Neumann map.

Let Γ be a smooth boundary of the domain Ω (fig. 3.5) having an unknown dielectric profile. We also assume that Γ has a length L and is parameterised using an arc length $s \in [0, L)$. The Dirichlet and Neumann boundary conditions are now functions of s and given by

$$\phi|_\Gamma = a(s) \ , \tag{3.22}$$

$$\epsilon \frac{d\phi}{d\vec{n}}\bigg|_\Gamma = b(s) \ , \tag{3.23}$$

where $\vec{n} = \vec{n}(s)$ is the normal to Γ and $\epsilon = \epsilon(s)$ is the boundary value of the dielectric permittivity on Γ. The Dirichlet-to-Neumann map (3.9) is

$$\Lambda_\epsilon : a(s) \to b(s) \ , \ s \in [0, L). \tag{3.24}$$

The linearity of (3.24) is a direct consequence of the linearity of the electrostatic field. For any two functions $a_1(s)$,$a_2(s)$,$s \in [0, L)$ and any constants α_1,α_2 the following relation holds

$$\Lambda_\epsilon : \alpha_1 a_1(s) + \alpha_2 a_2(s) \to \alpha_1 b_1(s) + \alpha_2 b_2(s) \ , \ s \in [0, L) \ . \tag{3.25}$$

Using complete set of base functions $f_n(s)$, $n = 1, ..., \infty$, $s \in [0, L)$ we expand the Dirichlet boundary condition (3.22) in the following series

$$a(s) = \sum_{n=1}^{\infty} \alpha_n f_n(s), \ \ s \in [0, L). \tag{3.26}$$

Applying the Dirichlet-to-Neumann map $\hat{\Lambda}_\epsilon$ to (3.26) and taking into account linearity of $\hat{\Lambda}_\epsilon$ (3.25) gives

$$b(s) = \hat{\Lambda}_\epsilon [a(s)] = \sum_{n=1}^{\infty} \alpha_n \hat{\Lambda}_\epsilon [f_n(s)], \ \ s \in [0, L) \ . \tag{3.27}$$

If the Dirichlet-to-Neumann map operator can be specified for each of the basis functions $f_n(s)$, $n = 1, ..., \infty$, $s \in [0, L)$ then the mapping $a(s) \rightarrow b(s)$ is defined according to (3.26), (3.27) for an arbitrary $a(s)$. Such representation of the Dirichlet-to-Neumann map eliminates linearly dependent pairs $a(s)$,$b(s)$ and optimises the amount of data to be stored.

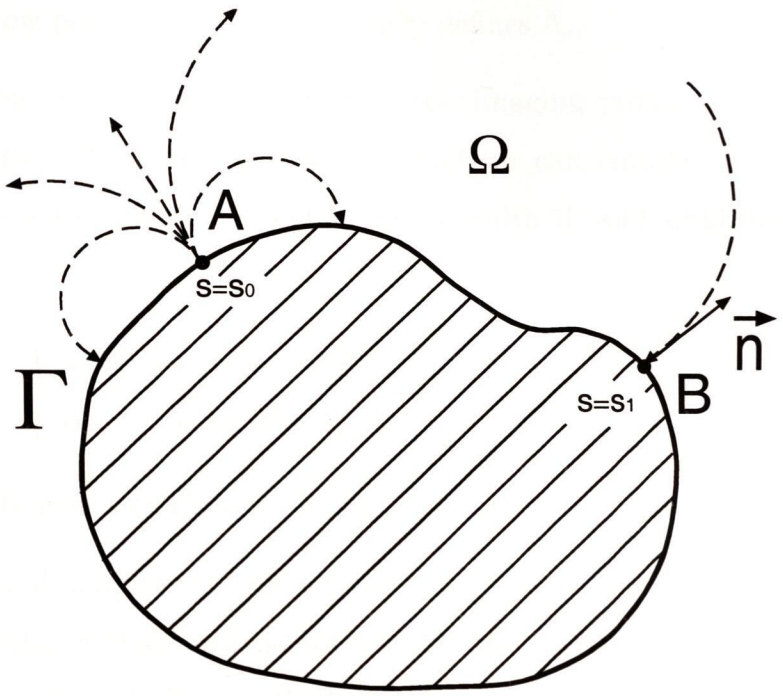

Figure 3.5: A domain Ω with parameterised boundary Γ. The dashed lines represent an electric field due to the Dirichlet boundary condition (3.28)

We consider the Dirichlet boundary condition of the form (figure 3.5)

$$\tilde{a}(s, s_0) = \delta(s - s_0) \ , \ s, s_0 \in [0, L) \ , \tag{3.28}$$

where δ is the Dirac delta function. A corresponding Neumann boundary condition $\tilde{b}(s, s_0)$ follows from the Dirichlet-to-Neumann map (3.24)

$$\Lambda_\epsilon : \tilde{a}(s, s_0) \rightarrow \tilde{b}(s, s_0) \ , s \in [0, L) \ , s_0 \in [0, L) \ . \tag{3.29}$$

Using the linearity of Λ_ϵ (3.25) we multiply both sides of (3.29) by $a(s_0)$ and then integrate the result over Γ using s_0 as an integration variable to give

$$\Lambda_\epsilon : a(s) \rightarrow \int_0^L \tilde{b}(s, s_0) a(s_0) ds_0 \ \ s \in [0, L) \ . \tag{3.30}$$

Comparing (3.30) and (3.24) and noting that Λ_ϵ is a singlevalue mapping, we write

$$b(s) = \int_0^L \tilde{b}(s, s_0) a(s_0) ds_0 \ . \tag{3.31}$$

Thus once we know $\tilde{b}(s, s_0)$ in (3.29) then we can use (3.31) to obtain $b(s)$ for an arbitrary $a(s)$. We have now proved that (3.29) uniquely defines Λ_ϵ.

In practical implementations of the electrostatic imaging problem we cannot employ a boundary condition of the form (3.28). Instead we can employ a Dirichlet boundary condition representing a narrow pulse function of width W and amplitude $1/W$ so that it has a unity area

$$\tilde{a}(s - s_0) = \begin{cases} 1/W & s \in [s_0 - W/2, s_0 + W/2], \\ 0 & \text{elsewhere} \ . \end{cases} \tag{3.32}$$

When W tends to zero this Dirichlet boundary condition reduces to (3.28).

In reality, a normal derivative of the electrostatic potential $\epsilon \frac{d\phi}{d\vec{n}}$ cannot be measured at a point B, $s = s_1$ (figure 3.5). Instead we evaluate the average value of $\epsilon \frac{d\phi}{d\vec{n}}$ in the vicinity of the point B, $s \in [s_1 - W/2, s_1 + W/2]$.

Figure 3.6 represents the same boundary Γ as figure 3.5 but with two physically extended electrodes. These electrodes are placed on Γ and are electrically insulated from it. Fixing the potential at zero and $\phi = 1/W$ on Γ and the first electrode respectively we pre-set Dirichlet boundary condition (3.32). The second electrode in figure 3.6 is used to estimate an electric field or alternatively a Neumann boundary condition at point B. This electrode is kept at the same potential as Γ and consequently does not violate the distribution of the electrostatic field. One can show that when the size of the second electrode tends to zero, the corresponding charge induced (2.134) on the electrode is given by

$$Q = -\frac{1}{4\pi} W \epsilon \frac{d\phi}{d\vec{n}} + o(W) \Big|_{\text{point}B} \ . \tag{3.33}$$

The Neumann boundary condition measured by a small electrode is then given by

$$\epsilon \frac{d\phi}{d\vec{n}} = -\frac{4\pi Q}{W} \ . \tag{3.34}$$

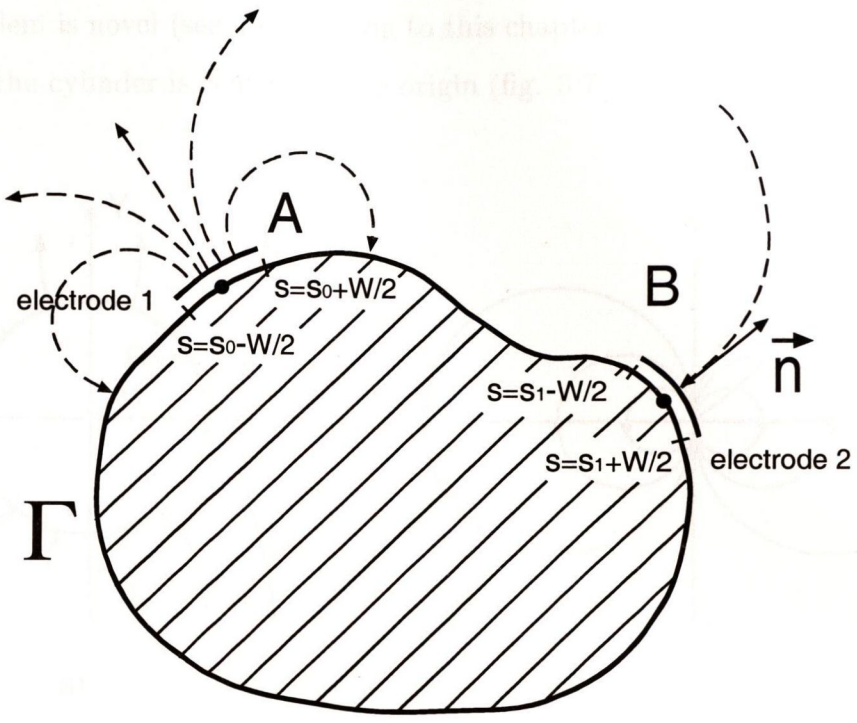

Figure 3.6: A domain Ω with parameterised boundary Γ and two physically implemented electrodes to simulate the Dirichlet boundary condition (3.28)

Charge Q accumulated on the second electrode (3.33) (figure 3.6) can be expressed through the mutual capacitance C_{12} for the first and second electrodes as follows

$$Q = C_{12}V_{12} \ , \tag{3.35}$$

where V_{12} is a potential difference between the two electrodes $V_{12} = 1/W$. An important conclusion that we can make from the above discussion (3.33),(3.35) is that the knowledge of the Dirichlet-to-Neumann map is equivalent to the knowledge of the mutual capacitances between any small segments of Γ.

3.7 Appendix: Conducting Cylinder in a Homogeneous Electrostatic Field and Its Application to Artificial Dielectric.

In this appendix we outline a 2D electrostatic problem for a metal cylinder of radius R_0 in a homogeneous electrostatic field $\vec{E}_0$. This problem is not novel and comes from the college background, yet the application of this problem to the analysis of the electrostatic

imaging problem is novel (see introduction to this chapter). Without loss of generality we assume that the cylinder is centred at the origin (fig. 3.7 (a)).

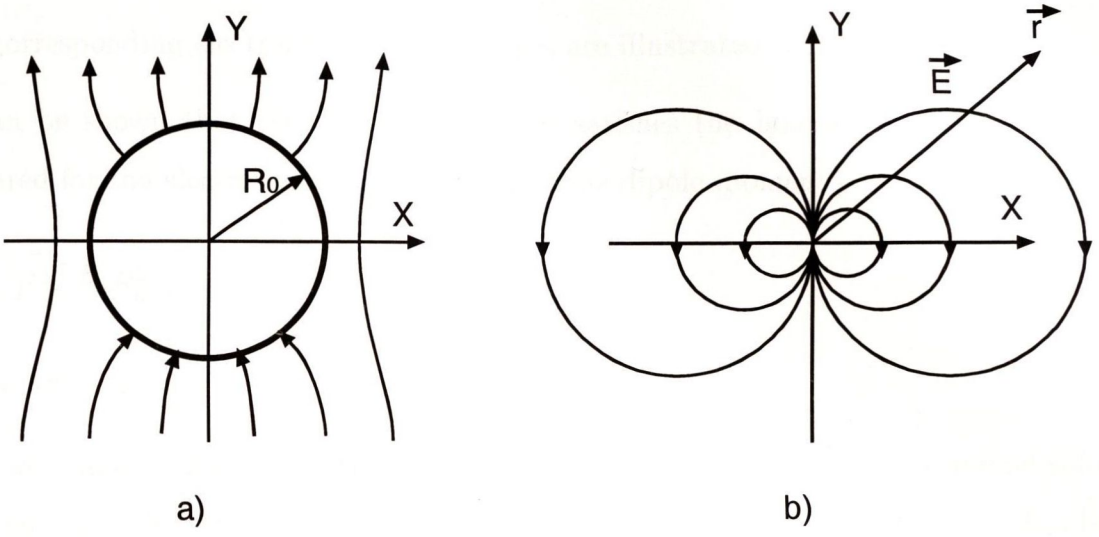

Figure 3.7: a) metal cylinder in the electrostatic field b) dipole field

To solve this problem one first makes an assumption regarding the solution and then proves that this solution satisfies the boundary conditions. The field outside the cylinder can be represented as the sum of the background homogeneous electrostatic field $\vec{E}_0$ and a distorted field $\vec{E}_{dist}$. The problem is to find $\vec{E}_{dist}$ such that the tangential component of the electric field $\vec{E}_0 + \vec{E}_{scat}$ on the boundary of the cylinder Γ is zero. This condition is equivalent to the following Dirichlet boundary condition for the scattered potential ϕ on Γ

$$(\phi_{dist} + \phi_{inc})|_\Gamma = 0 \ . \tag{3.36}$$

The potential ϕ_{inc} due to the homogeneous incident field $\vec{E}_0$ is given by

$$\phi_{inc} = -\vec{E}_0 \vec{r} \ , \tag{3.37}$$

where r is a co-ordinate vector $(\vec{x, y})$. It can be shown that the electrostatic potential for the distorted field $\vec{E}_{dist}$ (3.36), (3.37) must satisfy the following condition

$$\phi_{dist}|_\Gamma = \vec{E}_0 \vec{r} \ . \tag{3.38}$$

An electrostatic potential of the dipole having a dipole moment $\vec{p}$ is given by

$$\phi_{dipole} = \frac{\vec{p}\,\vec{r}}{x^2 + y^2} \ , \tag{3.39}$$

the corresponding electric field intensity lines are illustrated in figure 3.7 (b).

It can be shown that the dipole field (3.39) satisfies the boundary condition (3.38) as required for the electrostatic potential ϕ_{dist} if the dipole moment $\vec{p}$ is given by

$$\vec{p} = \vec{E}_0 R_0^2 \ , \tag{3.40}$$

where $R_0^2 = x^2 + y^2$.

It is well known that an electrostatic Dirichlet boundary problem has a unique solution. Consequently the scattered electrostatic potential given by (3.39),(3.40) solves the electrostatic problem for the cylinder in a homogeneous electrostatic field. It can be shown that a conducting 3D sphere in the homogeneous electrostatic field also establishes a dipole field.

Now we consider a hollow body of an arbitrary shape (figure 3.1 (b)) homogeneously filled with small metal cylinders of the same radius. Let the density and the radius for these cylinders be d and R_0 respectively and let an electrostatic field $\vec{E}$ inside that artificial body polarize each cylinder. Since each cylinder contributes into the overall polarization $\vec{P}$ we can write

$$\vec{P} = \vec{E} d R_0^2 \ . \tag{3.41}$$

On the other hand if we consider an arbitrary dielectric then the polarization vector $\vec{P}$ is given by

$$\vec{P} = \frac{\vec{E}(\epsilon - 1)}{4\pi} \ . \tag{3.42}$$

Comparing (3.41) and (3.41) we conclude that the effective dielectric permittivity for the object composed of metal cylinders is given by

$$\epsilon = 1 + 4\pi d R_0^2 \ . \tag{3.43}$$

3.8 Appendix: Dielectric Cylinder in the Homogeneous Electrostatic Field.

The previous section presented an electrostatic problem of a metal cylinder in a homogeneous field $\vec{E}_0$. We now present a solution to a similar problem where the metal cylinder is replaced by a dielectric cylinder of the same radius R_0. This 2D problem is illustrated in figure 3.8. While this problem is not novel, its application to the uniqueness analysis of the electrostatic inverse problem presented in section 3.3 is original.

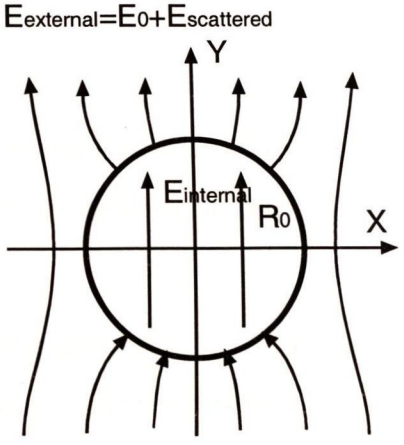

Figure 3.8: Dielectric cylinder of radius R_0 in homogeneous field $\vec{E}_0$.

The electrostatic field in the above problem must satisfy the boundary conditions on the cylinder surface. The tangential component for the electric field intensity $\vec{E}$ and the normal component for the electric field density $\epsilon\vec{E}$ must be continuous on the surface of the cylinder

$$(\vec{E}_{int})_\tau = (\vec{E}_{ext})_\tau \ , \tag{3.44}$$

$$\epsilon(\vec{E}_{int})_n = (\vec{E}_{ext})_n \ . \tag{3.45}$$

We omit the derivation of the solution and present a final result. The total field inside the

dielectric cylinder is a homogeneous electric field given by

$$\vec{E}_{int} = \frac{2}{1+\epsilon}\vec{E}_0 \ . \tag{3.46}$$

The scattered field outside the cylinder is given by a formula for the dipole field

$$\vec{E}_{scat} = -\frac{\vec{p}}{|r|^2} + 2\vec{r}\frac{\vec{p}\vec{r}}{|r|^4} \ , \tag{3.47}$$

where the dipole moment $\vec{p}$ is given by

$$\vec{p} = \frac{\epsilon - 1}{\epsilon + 1} R_0^2 \vec{E}_0 \ . \tag{3.48}$$

One can show that fields (3.46) and (3.47) satisfy the boundary conditions (3.44) and (3.45). Because a solution to the electrostatic problem is unique, (3.46) and (3.47) solve the problem.

One can show that if the dielectric permittivity ϵ tends to infinity then the electrostatic field inside the cylinder (3.46) vanishes while the dipole moment for the dipole field representing the scattered field (3.48) tends to the one that we have already obtained in the previous section for a metal cylinder (3.40). In electrodynamics the dielectric permittivity of the metal is approximately given by $\epsilon \approx j\frac{\sigma}{\omega}$ and has an imaginary part significantly larger than unity. In electrostatics the metal can be seen as a dielectric having infinitely large but purely real dielectric permittivity.

NUMERICAL METHODS IN ELECTROSTATICS

4.1 Ill and well conditioned systems of linear equations.

We consider a system of linear equations

$$A\vec{X} = \vec{Y} \ , \tag{4.1}$$

where A is a matrix, $\vec{Y}$ is a given vector and $\vec{X}$ is to be calculated. In this section we answer the question whether system 4.1 is ill or well conditioned i.e. whether any variations in A or $\vec{Y}$ have a significant impact on the solution $\vec{X}$.

This section is divided into three subsections. In subsection 4.1.1 we present the background linear algebra which is required for understanding the material developed later. In subsection 4.1.2 we derive the criteria for ill-conditioning of (4.1). Finally, in subsection 4.1.3 we present a regularization method which allows to tackle the ill-conditioned problems.

4.1.1 Linear algebra background.

We now briefly outline well known facts of linear algebra that will be used in subsequent subsections and throughout the thesis. A good reference on the material presented in this subsection is 'Twelve lecture notes on numerical mathematics' by V. I. Kosarev [7]. This book includes a regular 12 lecture course on numerical mathematics which is currently arranged for second year students of the Moscow Institute of Physics and Technology. Another reference that we recommend is [8].

If the reader is familiar with the basics of linear algebra then we recommend to skip this section and proceed with the next one.

Definition of vector norm. The norm of vector $\vec{X}$ is defined as a number denoted by $||\vec{X}||$ satisfying the following conditions

1. $||\vec{X}|| \geq 0$, $||\vec{X}|| = 0 \Leftrightarrow \vec{X} = 0$,
2. $||\alpha\vec{X}|| = |\alpha|\ ||\vec{X}||$, α is a scalar,
3. $||\vec{X} + \vec{Y}|| \leq ||\vec{X}|| + ||\vec{Y}||$.

The following are examples of the vector norm

1. $$||\vec{X}||_1 = \sum |x_i|, \tag{4.2}$$
2. $$||\vec{X}||_2 = \sqrt{\sum x_i^2}, \tag{4.3}$$
3. $$||\vec{X}||_\infty = ||\vec{X}||_c = \max_i |x_i|. \tag{4.4}$$

In a finite dimensional space all vector norms are equivalent in the sense that if $\lim_{n\to\infty} ||\vec{X}_n||_\alpha = 0$ then $\lim_{n\to\infty} ||\vec{X}_n||_\beta = 0$, where α and β are used to distinguish different norms.

Definition of matrix norm. The norm of the square matrix A is a number denoted by $||A||$ satisfying the following conditions

1. $||A|| \geq 0$, $||A|| = 0 \Leftrightarrow A = 0$,
2. $||\alpha A|| = |\alpha|\ ||A||$, α is a scalar
3. $||A + B|| \leq ||A|| + ||B||$,
4. $||AB|| \leq ||A||\ ||B||$.

In this thesis we use a matrix norm definition that is based on the definition of the vector norm as follows

$$||A|| = \sup_{\vec{X}\neq 0} \frac{||A\vec{X}||}{||\vec{X}||} = \sup_{||\vec{X}||=1} ||A\vec{X}|| \ , \tag{4.5}$$

where sup is the supremum or least upper bound. In particular, the matrix norms $||\cdot||_1$, $||\cdot||_2$, $||\cdot||_\infty$, (4.2), (4.3), (4.4) are defined as

$$||A||_1 = \sup_{||\vec{X}||_1=1} ||A\vec{X}||_1 \ , \tag{4.6}$$

$$||A||_2 = \sup_{||\vec{X}||_2=1} ||A\vec{X}||_2 \ , \tag{4.7}$$

$$||A||_\infty = ||A||_c = \sup_{||\vec{X}||_\infty=1} ||A\vec{X}||_\infty \ . \tag{4.8}$$

If the matrix norm is introduced as in (4.5) then the fourth property of the matrix norm $||AB|| \leq ||A||\ ||B||$ is valid not only when B is a square matrix but also when B is a vector. Indeed according to (4.5) we can write

$$\frac{||A\vec{X}||}{||\vec{X}||} \leq \sup_{\vec{X}\neq 0} \frac{||A\vec{X}||}{||\vec{X}||} = ||A|| \ . \tag{4.9}$$

Multiplying both parts of the relation (4.9) by $||\vec{X}||$ gives

$$||A\vec{X}|| \leq ||A||\ ||\vec{X}|| \ . \tag{4.10}$$

Matrix norm $||\cdot||_c$. Matrix norm (4.8) is given by

$$||A||_c = \max_i \sum_j |A_{ij}| \ . \tag{4.11}$$

Indeed assuming that (4.1) is satisfied and using $||A|| = \sup_{\vec{X}=1} ||A\vec{X}||$ (4.5) gives

$$||A\vec{X}||_c = ||\vec{Y}||_c = \max_i |y_i| = \max_i |\sum_j A_{ij}x_j| \ , \tag{4.12}$$

then

$$|\sum_j A_{ij}x_j| \leq \sum_j |A_{ij}|\ |x_j| \leq \max_j |x_j| \sum_j |A_{ij}| = ||\vec{X}||_c \sum_j |A_{ij}| \ . \tag{4.13}$$

Substituting (4.13) into (4.12) and taking into account that $||\vec{X}||_c = 1$ gives

$$||A\vec{X}||_c \leq \max_i \sum_j |A_{ij}| \ . \tag{4.14}$$

There exists such $\vec{X}_0$ that the least upper bound in (4.14) is achieved $||A\vec{X}_0||_c = \max_i \sum_j |A_{ij}|$. Assuming that $i = i_0$ is the index when the right hand side in (4.14) is maximum we construct $\vec{X}_0$ as follows

$$\vec{X}_0 = \{\text{sign}A_{i_0 j}, j = 1, 2, \cdots, k\} \ , \tag{4.15}$$

where k is the dimension of A. Note that $||\vec{X}_0||_c = 1$. Substituting (4.15) into (4.14) leads to an equality which also means that $\max_i \sum_j |A_{ij}|$ is the least upper bound or supremum of $||A\vec{X}||_c$

$$\sup_{||\vec{X}||_\infty = 1} ||A\vec{X}||_c = \max_i \sum_j |A_{ij}| \ . \tag{4.16}$$

According to (4.8), (4.16) defines a matrix norm and hence (4.11) is proved.

Eigenvectors and eigenvalues. A vector $\vec{X}_\lambda$ that satisfies

$$A\vec{X}_\lambda = \lambda\vec{X}_\lambda \ , \tag{4.17}$$

where λ is some scalar, is called an eigenvector for matrix A and λ is the corresponding eigenvalue. k-dimensional matrix A has k linearly independent eigenvectors

$$\{\vec{X}_{\lambda_i}, \lambda_i\} \ , \ i = 1, 2, \cdots, k. \tag{4.18}$$

Usually all eigenvectors (4.17) are normalised. This helps avoid confusion due to scaling the eigenvectors. Scaling the eigenvector results in a new (linearly dependent) eigenvector having the same eigenvalue. If $\det|A| \neq 0$ the rank of A equals to the dimension of A and all eigenvalues are nonzero. Different eigenvectors may have equal eigenvalues.

Orthogonality of eigenvectors for symmetric matrix. If A is symmetric i.e $A = A^T$ where A^T is a transposed A then the eigenvectors corresponding to different eigenvalues are

orthogonal. To prove this statement we consider two eigenvectors $\vec{X}_{\lambda_i}$ and $\vec{X}_{\lambda_j}$ such that $\lambda_i \neq \lambda_j$. Using the definition of the eigenvector (4.17) gives

$$\vec{X}_{\lambda_j}^T A \vec{X}_{\lambda_i} = \lambda_i \vec{X}_{\lambda_j}^T \vec{X}_{\lambda_i} \ . \tag{4.19}$$

Transposing the left hand side of (4.19) (which is a scalar) gives

$$\left(\vec{X}_{\lambda_j}^T A \vec{X}_{\lambda_i}\right)^T = \vec{X}_{\lambda_i}^T A^T \vec{X}_{\lambda_j} = \lambda_j \vec{X}_{\lambda_i}^T \vec{X}_{\lambda_j} \ . \tag{4.20}$$

Transposing (4.20) again gives

$$\vec{X}_{\lambda_j}^T A \vec{X}_{\lambda_i} = \lambda_j \vec{X}_{\lambda_j}^T \vec{X}_{\lambda_i} \ . \tag{4.21}$$

Subtracting (4.21) from (4.19) results in the following equation

$$(\lambda_i - \lambda_j)\, \vec{X}_{\lambda_j}^T \vec{X}_{\lambda_i} = 0 \tag{4.22}$$

which is only possible if $\vec{X}_{\lambda_j}^T \vec{X}_{\lambda_i} = 0$.

Let $\vec{X}_{\lambda_i}$ and $\vec{X}_{\lambda_j}$ be two linearly independent eigenvectors with equal eigenvalues $\lambda_i = \lambda_j = \lambda$. Any linear combination of these eigenvectors $\vec{X}_\lambda(\alpha_1, \alpha_2) = \alpha_1 \vec{X}_{\lambda_i} + \alpha_2 \vec{X}_{\lambda_j}$ is also an eigenvector having the same eigenvalue λ. Because $\vec{X}_{\lambda_i}$ and $\vec{X}_{\lambda_j}$ are linearly independent they can be orthogonalized by seeking $\vec{X}_\lambda(\alpha_1, \alpha_2)$ such that $\vec{X}_\lambda(\alpha_1, \alpha_2) \perp \vec{X}_{\lambda_i}$. Replacing $\vec{X}_{\lambda_j}$ by $\vec{X}_\lambda(\alpha_1, \alpha_2)$ one obtains two linearly independent orthogonal eigenvectors for the same eigenvalue. Therefore one can assume that the eigenvectors for a symmetric k dimensional A create a k dimensional orthonormal basis.

Using a basis of eigenvectors for representing a solution to (4.1) having symmetric A. If eigenvectors for A are linearly independent then they can be used as a basis to represent a solution to (4.1)

$$\vec{X} = \sum_{i=1}^{k} a_i \vec{X}_{\lambda_i} \ , \tag{4.23}$$

where a_i are unknown coefficients. If A is symmetric and $\det|A| \neq 0$ then the eigenvectors in (4.23) create an orthonormal basis. Substituting (4.23) into (4.1) and then multiplying the resulting expression by $\vec{X}^T_{\lambda_j}$ on the left gives the following expression for a_i in (4.23)

$$a_i = \frac{\vec{X}^T_{\lambda_i}\vec{Y}}{\lambda_i} \quad , \quad i = 1, 2, \cdots, k \quad , \tag{4.24}$$

where the index is adjusted for (4.23). Thus a solution to (4.1) is given by

$$\vec{X} = \sum_{i=1}^{k} \frac{\vec{X}^T_{\lambda_i}\vec{Y}}{\lambda_i}\vec{X}_{\lambda_i} \quad . \tag{4.25}$$

Matrix norm $||\cdot||_2$. If A is symmetric then the matrix norm (4.7) based on the vector norm (4.3) is given by the maximum absolute value of the eigenvalue for A

$$||A||_2 = \max|\lambda_i|. \tag{4.26}$$

To prove (4.26) one can expand $\vec{X}$ into an orthonormal basis of eigenvectors (4.23). Assuming that $||\vec{X}||_2 = 1$ which is equivalent to $\sqrt{\sum_i a_i^2} = 1$, where a_i are the coefficients in (4.23), gives

$$||A\vec{X}||_2 = ||\sum_i a_i\lambda_i\vec{X}_{\lambda_i}||_2 = \sqrt{\sum_i a_i^2\lambda_i^2} \leq \sqrt{\max\lambda_i^2 \sum_i a_i^2} = \max|\lambda_i| \quad . \tag{4.27}$$

Thus $\max|\lambda_i|$ is the upper bound for $||A\vec{X}||_2$. To demonstrate that $\max|\lambda_i|$ is a supremum for $||A\vec{X}||_2$ one can show that there exists $\vec{X}_0$ such that it results in equality in (4.27). If $i = i_0$ is the index for which $\max|\lambda_i|$ is achieved then choosing $\vec{X}_0 = \vec{X}_{\lambda_{i_0}}$ and substituting $\vec{X}_0$ into (4.27) results in equality. According to (4.7) (4.26) is a norm for A.

Eigenvalues and eigenvectors for inverse matrix. If $\vec{X}_{\lambda_i}$ and λ_i, $i = 1, 2, \cdots, k$ (4.18) are the eigenvectors and eigenvalues for matrix A then

$$\{\vec{X}_{\lambda_i}, \frac{1}{\lambda_i}\} \quad , \quad i = 1, 2, \cdots, k \tag{4.28}$$

are the eigenvectors and eigenvalues for matrix A^{-1}. Here A^{-1} is an inverse matrix to A i.e. $A^{-1}A = E$ where E is a unity diagonal matrix. Indeed multiplying both sides of (4.17) by A^{-1} on the left gives

$$\vec{X}_{\lambda_i} = \lambda_i A^{-1}\vec{X}_{\lambda_i} \ , \ i = 1, 2, \cdots, k \ . \tag{4.29}$$

Dividing (4.29) by λ_i proves (4.28).

Eigenvalues for positive definite matrix. Matrix A is called positive definite if for any $\vec{X} \neq 0$ $\vec{X}^T A\vec{X}$ is positive

$$\vec{X}^T A\vec{X} > 0 \ , \ \forall \vec{X} \neq 0 \ . \tag{4.30}$$

All eigenvalues for a positive definite matrix are positive. Indeed assuming that the eigenvectors are normalized $||\vec{X}_{\lambda_i}||_2 = 1$, $i = 1, 2, \cdots, k$ and substituting $\vec{X}_{\lambda_i}$ into (4.30) gives

$$\vec{X}^T_{\lambda_i} A\vec{X}_{\lambda_i} = \lambda_i \vec{X}^T_{\lambda_i}\vec{X}_{\lambda_i} = \lambda_i \, ||\vec{X}_{\lambda_i}||_2^2 = \lambda_i > 0 \ , \ i = 1, 2, \cdots, k \ . \tag{4.31}$$

4.1.2 Criterion for Ill/Well-Conditioning of a System of Linear Equations.

We now consider a perturbed problem (4.1) i.e. we assume that due to the errors which may have numerical or physical origin the matrix A and the right hand side Y in (4.1) are subject to small variations δA and $\delta\vec{Y}$ respectively [7]. If the reader is familiar with the ill/well conditioning analysis of the algebraic systems of linear equations then we recommend to proceed with the next section.

The solution to the perturbed problem is violated by $\delta\vec{X}$

$$(A + \delta A)(\vec{X} + \delta\vec{X}) = \vec{Y} + \delta\vec{Y} \ . \tag{4.32}$$

Subtracting (4.1) from (4.32) gives

$$A\delta\vec{X} + \delta A\delta\vec{X} + \delta A\vec{X} = \delta Y \ . \tag{4.33}$$

Here we assume that the variations δA, $\delta\vec{Y}$ and $\delta\vec{X}$ are small and that the second-order small parameter $\delta A\delta\vec{X}$ can be neglected. Reordering (4.33) and multiplying by A^{-1} on the left gives

$$\delta\vec{X} = A^{-1}\left(\delta Y - \delta A\vec{X}\right) \ . \tag{4.34}$$

Applying the vector norm to (4.34) and using (4.10) yields

$$||\delta\vec{X}|| = ||A^{-1}\left(\delta\vec{Y} - \delta A\vec{X}\right)|| \leq ||A^{-1}||\ \left(||\delta\vec{Y}|| + ||\delta A||\ ||\vec{X}||\right) \ . \tag{4.35}$$

Representing (4.35) in the form

$$||\delta\vec{X}|| \leq ||A^{-1}||\ \left(||\vec{Y}||\frac{||\delta\vec{Y}||}{||\vec{Y}||} + ||A||\frac{||\delta A||}{||A||}\ ||\vec{X}||\right) \ , \tag{4.36}$$

and using $||\vec{Y}|| \leq ||A||\ ||\vec{X}||$ (4.10) gives

$$||\delta\vec{X}|| \leq ||A||\ ||A^{-1}||\ ||\vec{X}||\ \left(\frac{||\delta\vec{Y}||}{||\vec{Y}||} + \frac{||\delta A||}{||A||}\right) \ . \tag{4.37}$$

Dividing (4.37) by $||\vec{X}||$ gives the following expression for the error $\frac{||\delta\vec{X}||}{||\vec{X}||}$

$$\frac{||\delta\vec{X}||}{||\vec{X}||} \leq K\left(\frac{||\delta\vec{Y}||}{||\vec{Y}||} + \frac{||\delta A||}{||A||}\right) \ , \tag{4.38}$$

where K is the conditioning factor that determines the ill-conditioning of the problem (4.1)

$$K = ||A||\ ||A^{-1}|| \ . \tag{4.39}$$

K is larger than unity $K \geq 1$. Indeed

$$1 = ||E|| = ||A^{-1}A|| \leq ||A^{-1}||\ ||A|| = K \ , \tag{4.40}$$

where E is a unity diagonal matrix.

Problem (4.1) is considered to be well conditioned if K is in the range between 1 and 10 [7]. If K is larger than 1000 then (4.1) is considered to be ill-conditioned.

To simplify further analysis of the perturbed problem (4.32) we assume that $\delta A = 0$. In that case (4.38) becomes

$$\frac{||\delta\vec{X}||}{||\vec{X}||} \leq K\frac{||\delta\vec{Y}||}{||\vec{Y}||} \quad . \tag{4.41}$$

We now prove that the upper bound for the error $\frac{||\delta\vec{X}||}{||\vec{X}||}$ in (4.41) is not overestimated. Indeed to obtain (4.41) we use an inequality (4.10) which in turn is obtained as a result of the supremum based equation which means that the upper bound can be reached. In other words

$$\exists\delta\vec{Y} \quad : \quad \frac{||\delta\vec{X}||}{||\vec{X}||} = K\frac{||\delta\vec{Y}||}{||\vec{Y}||} \quad . \tag{4.42}$$

Expression (4.42) is a fundamental criterion that can be used to estimate the maximum error that may occur when tackling (4.1). We now study (4.42) and its application to the numerical methods implemented in the thesis.

(4.41) is obtained in the most general form. The type of the norm in (4.41) is not specified which is an advantage of (4.41). If we choose the norm to be $||\cdot||_2$ we may use a more specific expression for K (4.39). According to (4.26) $||A||_2 = \max|\lambda_i|$. Applying (4.26) to an inverse matrix A^{-1} and using (4.28) gives

$$||A^{-1}||_2 = \max|\frac{1}{\lambda_i}| = \frac{1}{\min|\lambda_i|} \quad , \tag{4.43}$$

where λ_i, $i = 1, 2, \cdots, k$ are the eigenvalues for A. Ultimately applying (4.43) and (4.26) to (4.39) we obtain

$$K = \frac{\max|\lambda_i|}{\min|\lambda_i|} \quad . \tag{4.44}$$

If matrix A is positive definite then according to previous section all eigenvalues are also positive and we do not need to use the absolute values in (4.44)

$$K = \frac{\max\lambda_i}{\min\lambda_i} \quad . \tag{4.45}$$

We now present an example illustrating a mechanism resulting in problem (4.1) being ill posed. This example is the author's study of the ill-conditioning mechanism, yet we would expect that a similar analysis must have been done by other researchers. In the end of this analysis we come to the same criterion as in (4.38) but with more insight into the ill-conditioning mechanism. Let the right hand side of (4.1) be given by the eigenvector having a maximum absolute value of eigenvalue $|\lambda_{i_{max}}|$, where i_{max} is a corresponding index i.e. $\vec{Y} = \vec{X}_{\lambda_{i_{max}}}$. For simplicity we consider symmetric positive definite A and hence $|\lambda_{i_{max}}| = \lambda_{i_{max}}$. The system of linear equations (4.1) is now given by

$$A\vec{X} = \vec{X}_{\lambda_{i_{max}}} \ . \tag{4.46}$$

According to (4.25) a solution to (4.46) is given by

$$\vec{X} = \frac{\vec{X}_{\lambda_{i_{max}}}}{\lambda_{i_{max}}} \ . \tag{4.47}$$

We now consider a solution to the problem

$$A\vec{X} = \vec{X}_{\lambda_{i_{max}}} + \gamma \vec{X}_{\lambda_{i_{min}}} \ , \tag{4.48}$$

where i_{min} is the index corresponding to the eigenvector having the smallest eigenvalue and γ is a small number. A solution to (4.48) is given by

$$\vec{X} = \frac{\vec{X}_{\lambda_{i_{max}}}}{\lambda_{i_{max}}} + \gamma \frac{\vec{X}_{\lambda_{i_{min}}}}{\lambda_{i_{min}}} \ . \tag{4.49}$$

In this example we treat (4.46) as an original unperturbed problem and (4.48) as a corresponding perturbed problem. Within the context of (4.32) $Y = \vec{X}_{\lambda_{i_{max}}}$, $\delta\vec{Y} = \gamma\vec{X}_{\lambda_{i_{min}}}$, $\vec{X} = \frac{\vec{X}_{\lambda_{i_{max}}}}{\lambda_{i_{max}}}$, $\delta\vec{X} = \delta\frac{\vec{X}_{\lambda_{i_{min}}}}{\lambda_{i_{min}}}$. The error $\frac{||\delta\vec{X}||_2}{||\vec{X}||_2}$ and $\frac{||\delta\vec{Y}||_2}{||\vec{Y}||_2}$ are now given by

$$\frac{||\delta\vec{X}||_2}{||\vec{X}||_2} = \gamma \frac{||\vec{X}_{i_{min}}||_2}{\lambda_{i_{min}}} \frac{\lambda_{i_{max}}}{||\vec{X}_{i_{max}}||_2} \ , \tag{4.50}$$

$$\frac{||\delta\vec{Y}||_2}{||\vec{Y}||_2} = \gamma \frac{||\vec{X}_{i_{min}}||_2}{||\vec{X}_{i_{max}}||_2} \ . \tag{4.51}$$

Combining (4.50) and (4.51) gives

$$\frac{||\delta\vec{X}||_2}{||\vec{X}||_2} = \frac{\lambda_{i_{max}}}{\lambda_{i_{min}}} \frac{||\delta\vec{Y}||_2}{||\vec{Y}||_2} \quad . \tag{4.52}$$

Equation (4.52) is not only in agreement with the previously obtained criteria (4.41) for ill-conditioning of the system of linear equations but also proves the existence of a least upper bound in (4.42) for $||\cdot||_2$ and symmetric positive definite A.

4.1.3 Solving ill-conditioned problems. Regularization method.

An ill conditioned problem is one with a solution which is very sensitive to numerical and physical errors. Small perturbation of the coefficients in the ill posed problem (4.1) may cause significant distortion making the solution useless from the practical point of view. Another disadvantage of the ill conditioned problem is a slow convergence of the numerical methods. In the example of the previous section we studied the mechanism resulting in the problem being ill conditioned. In particular we illustrated that in the case of symmetric positive definite A, a solution to (4.1) can be of the order of $1/\max|\lambda_i|$ while the distortion is $1/\min|\lambda_i|$. In this section we present a regularization method [5] that allows the improvement of the condition of (4.1) i.e. which reduces the condition factor $\max|\lambda_i|/\min|\lambda_i|$.

A variational approach to solving (4.1) is to build a functional such that its minimum is obtained at a solution to (4.1) [13]. In that case the problem of directly solving (4.1) is replaced by the problem of minimization of the functional. A simple way to build such a functional is to present (4.1) in the form of equation where the right hand side is zero

$$A\vec{X} - \vec{Y} = 0 \tag{4.53}$$

and to take a square of that equation

$$(A\vec{X} - \vec{Y})^T(A\vec{X} - \vec{Y}) = 0 \quad . \tag{4.54}$$

The functional in (4.54)

$$F(\vec{X}) = (A\vec{X} - \vec{Y})^2 \tag{4.55}$$

is nonnegative and has an absolute minimum of zero for solutions of (4.1). Thus (4.1) is now replaced by a problem of finding $\vec{X}$ such that $F(\vec{X})$ is minimized

$$\min_{\vec{X}} F(\vec{X}) \ . \tag{4.56}$$

Variational methods [13] are a branch of the mathematical science that deals with (4.56). According to variational theory the necessary (but not sufficient) condition for the minimum to F is

$$\frac{\partial F(\vec{X})}{\partial \vec{X}} = 0 \ . \tag{4.57}$$

For the variational problem (4.56), criterion (4.57) is sufficient when $\det|A| \neq 0$. Indeed differentiating (4.55) gives

$$\frac{\partial F(\vec{X})}{\partial \vec{X}} = 2A^T(A\vec{X} - \vec{Y}) = 0 \ . \tag{4.58}$$

Because $\det|A| \neq 0$ the inverse of A^T exists, and multiplying (4.58) by $(A^T)^{-1}$ gives (4.1). The use of the variational methods does not alleviate the ill conditioning of (4.1). However it gives additional flexibility which we now discuss. An artificial method for improving the condition number of problem (4.56) is to distort (4.55) by adding a small nonnegative functional $\gamma^2 P(\vec{X})$ or a regularizer

$$F_R(\vec{X}) = (A\vec{X} - \vec{Y})^2 + \gamma^2 P(\vec{X}) \ , \tag{4.59}$$

where γ is a small coefficient and $P(\vec{X})$ is referred to as the potential function of the regularization method. The whole term $\gamma^2 P(\vec{X})$ is often referred as the regularization function. Replacing the variational problem (4.56) by a problem of minimization of (4.59) leads to a new perturbed solution. Indeed, substituting (4.59) into (4.57) gives

$$\frac{\partial F(\vec{X})}{\partial \vec{X}} = 2A^T(A\vec{X} - \vec{Y}) + \gamma^2 \frac{\partial P(\vec{X})}{\partial \vec{X}} = 0 \ , \tag{4.60}$$

where $\frac{\partial P(\vec{X})}{\partial \vec{X}}$ is a vector

$$\frac{\partial P(\vec{X})}{\partial \vec{X}} = \begin{pmatrix} \frac{\partial P(\vec{X})}{\partial x_1} \\ \frac{\partial P(\vec{X})}{\partial x_2} \\ \vdots \end{pmatrix} . \tag{4.61}$$

Multiplying both sides of (4.60) by $\frac{1}{2}(A^T)^{-1}$ gives

$$A\vec{X} = \vec{Y} - \frac{\gamma^2}{2}(A^T)^{-1}\frac{\partial P(\vec{X})}{\partial \vec{X}} \tag{4.62}$$

which is now different from (4.1). We now study a solution to the following variational problem

$$\min_{\vec{\tilde{X}}} F_R(\vec{\tilde{X}}) = \min_{\vec{\tilde{X}}} \left((A\vec{\tilde{X}} - \vec{Y})^2 + \gamma^2 P(\vec{\tilde{X}}) \right) , \tag{4.63}$$

where tilde stands for a solution to a perturbed problem (4.62), and how it compares to the solution of the problem of minimization of (4.59). The "R" in the functional in (4.63) stands for "regularization".

The Tikhonov potential function is the square of $\vec{X}$ and was originally proposed by Tikhonov and Arsenin [5]

$$F_R(\vec{X}) = (A\vec{X} - Y)^2 + \gamma^2 \vec{X}^2 . \tag{4.64}$$

We dedicate the rest of this section to the analysis of the Tikhonov regularization method (4.64). Many researchers appear to believe that the Tikhonov regularization method (4.64) works as a spatial filter [38], [95], removing high order oscillations from the solution $\vec{X}$. The researchers claim that due to the Tikhonov regularization method the sharp edges of the original scatterer that normally occur on the boundary of the dielectric bodies, for example, are smoothed in the reconstructed images. Now, although the edges of the reconstructed image are indeed smoothed, the nature of such distortion does not lie in the Tikhonov regularization method but in the properties of A in (4.64), (4.1). We now

conduct our own analysis of the phenomenon of the low pass spatial filtering of the solution that arises when solving ill-posed inverse problems using a regularization technique.

To illustrate that the Tikhonov regularization method does not smooth the edges of the solution we consider a problem where the solution is known in both cases with regularization and without. Let A in (4.1) be a unity diagonal matrix I

$$I\vec{X} = \vec{Y} \ . \tag{4.65}$$

A solution to (4.65) is given by

$$\vec{X} = \vec{Y} \ . \tag{4.66}$$

We now apply a Tikhonov regularization to (4.65). The functional F_R with Tikhonov regularization term (4.64) for (4.65) is given by

$$F_R(\vec{X}) = (\vec{X} - \vec{Y})^2 + \gamma^2 \vec{X}^T \vec{X} \ , \tag{4.67}$$

where we already employed $I\vec{X} = \vec{X}$. The variational problem (4.63) for (4.67) results in the following equation (4.57)

$$\frac{\partial F_R(\vec{X})}{\partial \vec{X}} = 2(\vec{X} - \vec{Y}) + 2\gamma^2 \vec{X} = 0 \ . \tag{4.68}$$

A solution to (4.69) is given by

$$\vec{X} = \frac{1}{1+\gamma^2} \vec{Y} \ . \tag{4.69}$$

Comparing (4.66) and (4.69) we see that the Tikhonov regularization method scales the solution of the unperturbed problem by a factor of $\frac{1}{1+\gamma^2}$. The spectral representation of the solution is also scaled down although no spatial filtering of the higher harmonics is performed which confirms that the Tikhonov regularization method does not necessarily affect the spectrum of the solution.

We now perform analytical analysis of the Tikhonov regularization method in a general form. Applying (4.60) to (4.64) gives

$$A^T A\vec{X} + \gamma^2 \vec{X} = A\vec{Y} \ . \tag{4.70}$$

We rewrite (4.70) to give

$$(A^T A + \gamma^2 E)\vec{X} = A\vec{Y} \ . \tag{4.71}$$

Denoting $A^T A + \gamma^2 E$ by M we formulate the distorted variational problem in matrix form

$$M\vec{X} = A\vec{Y} \ . \tag{4.72}$$

If $\det|A| \neq 0$ then $A^T A$ is positive definite. Indeed

$$\vec{X}^T A^T A\vec{X} = (A\vec{X})^T (A\vec{X}) = ||A\vec{X}||_2^2 \geq 0 \ , \forall \vec{X}. \tag{4.73}$$

$A^T A$ is also a symmetric matrix and, according to section 4.1.1, $A^T A$ has orthogonal eigenvectors. We now prove that if the eigenvectors and eigenvalues for $A^T A$ are given by (4.18) then the eigenvectors and eigenvalues for M are given by

$$\{\vec{X}_{\lambda_i}, \lambda_i + \gamma^2\} \ , \ i = 1, 2, \cdots, k, \tag{4.74}$$

where k is the dimension of A. Indeed multiplying M by any of $\vec{X}_{\lambda_i}$ gives

$$M\vec{X}_{\lambda_i} = (A^T A + \gamma^2 E)\vec{X}_{\lambda_i} = \lambda_i \vec{X}_{\lambda_i} + \gamma^2 \vec{X}_{\lambda_i} = (\lambda_i + \gamma^2)\vec{X}_{\lambda_i} \ . \tag{4.75}$$

Using (4.25) we write a solution for (4.72)

$$\vec{X} = \sum_{i=1}^{k} \frac{\vec{X}_{\lambda_i}^T A^T \vec{Y}}{\lambda_i + \gamma^2} \vec{X}_{\lambda_i} \ . \tag{4.76}$$

If $\gamma = 0$ then the regularization term in F_R vanishes and (4.76) becomes a solution to the non-perturbed problem (4.1). We rewrite (4.76) in the form

$$\vec{X} = \sum_{i=1}^{k} \frac{\vec{X}_{\lambda_i}^T A^T \vec{Y}}{\lambda_i} \vec{X}_{\lambda_i} G(\lambda_i, \gamma^2) \ , \tag{4.77}$$

where G is given by

$$G = \frac{\lambda_i}{\lambda_i + \gamma^2} \quad . \tag{4.78}$$

A solution to the problem without regularization is given by (4.77) with $G = 1$. With regularization, for a given i if $\lambda_i >> \gamma^2$, then $G \approx 1$ and the corresponding term in the sum in (4.77) is only slightly affected by the regularization method. On the other hand if $\lambda_i << \gamma^2$ then $G \approx \lambda_i/\gamma^2 << 1$ and the corresponding term in (4.77) is significantly attenuated by the regularization method. Thus the Tikhonov regularization method scales down those terms in (4.77) that correspond to eigenvalues small relative to γ^2. In the example of section 4.1.2 we demonstrated that the ill conditioned problem is particularly sensitive to the terms in (4.77) having small (compared to the maximum) eigenvalues. This explains how the Tikhonov regularization method improves the conditioning of the problem making it less sensitive to distortions in the right hand side in (4.72) $A^T\vec{Y}$.

If the eigenvectors for A^TA corresponding to small eigenvalues are highly oscillatory then a solution to $A^TA\vec{X} = A^T\vec{Y}$ will also be corrupted by oscillations[1]. That situation occurs in the electrostatic and electrodynamic inverse imaging problems. Applying a regularization method to any of these problems removes the oscillations from the solution making the problem more robust i.e well posed. This explains why many researchers reported that the Tikhonov regularization methods works as a low pass spatial filter. However it is possible to construct A^TA such that the eigenvectors corresponding to small eigenvalues are smooth. In that case the Tikhonov regularization will effectively attenuate these smooth terms in (4.77) leaving oscillating terms. For this contrived problem the Tikhonov regularization method will manifest itself as being a high pass spatial filter. We have already constructed problem (4.65) where all eigenvectors for A^TA have the same unity eigenvalue (the problem is well posed). Applying (4.77) to (4.65) and analysing factors (4.78) gives $G = \frac{1}{1+\gamma^2}$ which is in agreement with (4.69), of course.

We now develop a method for choosing γ^2 in the Tikhonov regularization method which

[1]Here we mean spatial oscillations of the solution to $A\vec{X} = \vec{Y}$ where $\vec{X}$ represents some physical 2D or 3D distribution such as a dielectric distribution in the inverse imaging problem.

we later implement numerically in the inverse electrostatic problem. While the method that we propose is unlikely to be novel, we have not found it being employed in the existing inverse problems (which are ill-conditioned). The condition number for M (4.72) is given by

$$K(\gamma) = \frac{\max_i \lambda_i + \gamma^2}{\min_i \lambda_i + \gamma^2}. \tag{4.79}$$

Recall that $A^T A$ is positive definite and the eigenvalues in (4.79) are also positive. Let K_0 be the condition number for the problem without regularization ($\gamma = 0$)

$$A^T A\vec{X} = A^T\vec{Y} \ . \tag{4.80}$$

Assuming $K_0 = K(0) >> 1$ (or $\min_i \lambda_i << \max_i \lambda_i$) we choose

$$\min_i \lambda_i << \gamma^2 << \max_i \lambda_i \tag{4.81}$$

in (4.79) we attenuate the noisy terms in (4.77) leaving solution critical terms. The condition number (4.79) is approximated by

$$K(\gamma) = \frac{\max_i \lambda_i + \gamma^2}{\min_i \lambda_i + \gamma^2} \approx \frac{\max_i \lambda_i + \gamma^2}{\gamma^2} = \frac{\max_i \lambda_i}{\gamma^2} + 1 \approx \frac{\max_i \lambda_i}{\gamma^2} \ . \tag{4.82}$$

For practical applications we need to be able to estimate $\max_i \lambda_i$ for $A^T A$. Unfortunately $||A^T A||_2$ which is the exact value for $\max_i \lambda_i$ does not have a simple estimation method. At the same time, in order to to choose $\gamma^2 = \max_i \lambda_i / K$, where K is the desired condition number for the problem, we do not need to know the precise value of $\max_i \lambda_i$ because there are no strict directions for choosing the desired K (which has to be in the range of from 10 to 1000). Hence we need a non-precise but simple estimation for $\max_i \lambda_i$ which we now derive.

We prove that if λ_{max} is the maximum eigenvalue for a symmetric positive definite matrix[2]

[2]Note that problem $A\vec{X} = \vec{Y}$ can always be replaced by $A^T A\vec{X} = A^T\vec{Y}$ where $A^T A = B$ is a positive definite symmetric matrix provided $\det|A| \neq 0$. Hence we consider a symmetric positive matrix without loss of generality.

B and $\vec{X}_{\lambda_{max}}$ is the corresponding eigenvector, then any matrix norm $||B||$ introduced by (4.5) is greater than or equal to λ_{max}. Indeed by definition

$$B\vec{X}_{\lambda_{max}} = \lambda_{max}\vec{X}_{\lambda_{max}} \ . \tag{4.83}$$

Applying a vector norm to (4.83) gives

$$||B\vec{X}_{\lambda_{max}}|| = ||\lambda_{max}\vec{X}_{\lambda_{max}}|| = \lambda_{max}||\vec{X}_{\lambda_{max}}|| \ . \tag{4.84}$$

Dividing (4.83) by $||\vec{X}_{\lambda_{max}}||$ and using (4.5) gives

$$\lambda_{max} = \frac{||B\vec{X}_{\lambda_{max}}||}{||\vec{X}_{\lambda_{max}}||} \leq \sup_{\vec{X}} \frac{||B\vec{X}||}{||\vec{X}||} = ||B|| \ . \tag{4.85}$$

We will use $||\cdot||_\infty$ (4.8) as a matrix norm for (4.83). In subsection (4.1.1) we derived an analytical representation for matrix norm $||\cdot||_\infty$ which we now substitute into (4.85) to give

$$\lambda_{max} \leq \max_i \sum_j |B_{ij}| \ . \tag{4.86}$$

We use (4.86) to derive the criterion for choosing γ^2. In our numerical algorithm presented in chapter 6, we want to ensure a condition number being not greater than 100. Denote $B = AA^T$. We use the upper bound for λ_{max} for B given by (4.86) as an estimate of λ_{max} and use (4.82) to give

$$\gamma^2 = \frac{\max_i \sum_j |B_{ij}|}{100} \ . \tag{4.87}$$

To claim that (4.87) is novel we need to conduct a broader survey of literature. In the examples of the inverse problems that we know (4.87) has not been implemented.

4.2 Numerical Implementation of the Forward Electrostatic Problem.

In the introduction part of chapter 2 we mentioned that there are two principal ways of formulating the electrostatic problem. One way is to use a differential governing equation

which is introduced in section 2.1. The other alternative is to employ integral governing equations (sections 2.4, 2.5 and 2.6). Both ways are equivalent from the analytical point of view but the corresponding numerical implementations are different.

In sections 4.2.1 and 4.2.2 we introduce a Finite Difference Method (FDM) and a Finite Elements Method (FEM). These methods cast the differential and integral analytical equations in the form of a system of algebraic equations suitable for computer implementation. Systems of linear algebraic equations are studied in sections 4.1.1, 4.1.2 and some methods of tackling these systems are proposed in sections 4.1.3 and 4.4.

4.2.1 Finite Difference Method

The Finite Difference Method is a method for discretising functions on a grid. Once the discretisation is done the derivatives of the functions are constructed using the values on the grid. The approximations of the functions and their derivatives are then substituted into the differential governing equation. If the finite difference scheme is chosen properly then a stable numerical formulation is obtained. By refining the grid we increase the precision of representation of functions and their derivatives hence obtaining a more precise representation of the original analytical equations.

There are many implementations of the FDM which differ from each other by the grid type and schemes for representing the derivatives [7]. We now consider a classical implementation of the FDM for the electrostatic problem [7] governed by the 2D Laplace's equation

$$\frac{\partial^2 \phi}{\partial x^2} + \frac{\partial^2 \phi}{\partial y^2} = 0 \ . \tag{4.88}$$

We assume that an electrostatic problem (4.88) is posed in a finite domain D with boundary Γ shown in figure 4.1. We also assume that potential ϕ satisfies a Dirichlet boundary condition on Γ

$$\phi|_\Gamma = \phi^{(h)} \ . \tag{4.89}$$

A square grid with step h is probably the simplest grid for representing both the functions

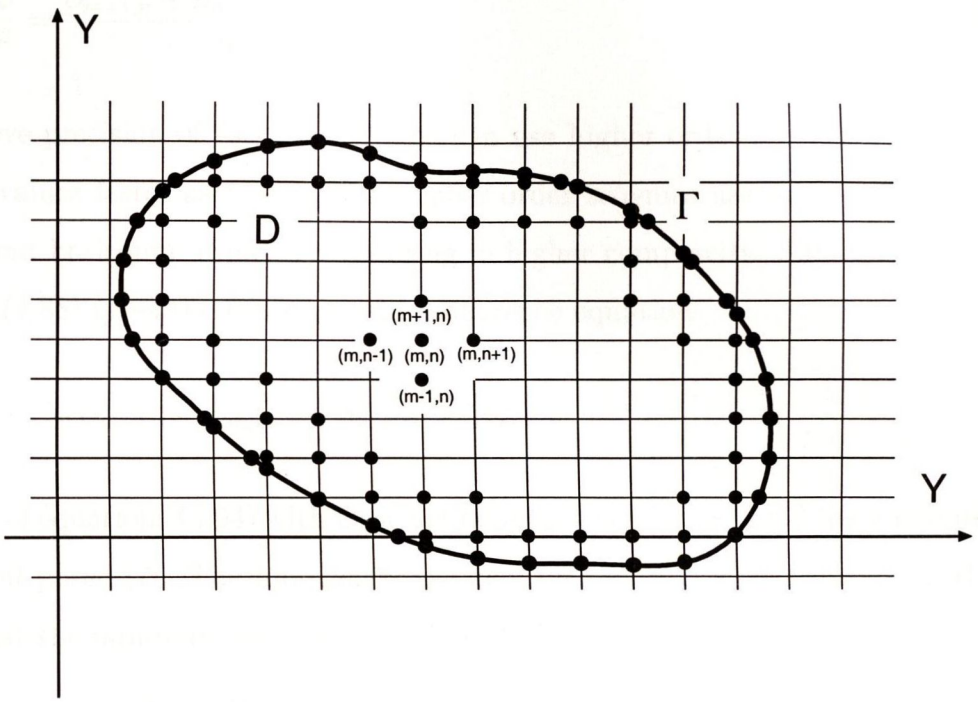

Figure 4.1: Rectangular discretisation grid for domain D with boundary Γ.

and their derivatives. Its implementation in D is shown in figure 4.1. The problem of having an irregular Γ is overcome by placing additional grid nodes at the cross points of the grid lines and Γ.

For simplicity we assume that Γ is aligned with the grid nodes and hence no additional nodes are required. We refer to the grid nodes using two indices (m, n) and denote the corresponding value of the electrostatic potential by $\phi_{m,n}$. A classical finite difference scheme for the first and second order derivatives of ϕ at (m, n) is

$$\frac{\partial \phi}{\partial x} = \frac{\phi_{m,n+1} - \phi_{m,n-1}}{2h} \quad , \tag{4.90}$$

$$\frac{\partial \phi}{\partial y} = \frac{\phi_{m+1,n} - \phi_{m-1,n}}{2h} \quad , \tag{4.91}$$

$$\frac{\partial^2 \phi}{\partial x^2} = \frac{\phi_{m,n+1} + \phi_{m,n-1} - 2\phi_{m,n}}{h^2} \quad , \tag{4.92}$$

$$\frac{\partial^2 \phi}{\partial y^2} = \frac{\phi_{m+1,n} + \phi_{m-1,n} - 2\phi_{m,n}}{h^2} \quad . \tag{4.93}$$

To improve precision of (4.90)-(4.93) one can use higher order schemes that converge to the true values faster as $h \to 0$. The higher order schemes use more points in both the vertical and horizontal directions resulting in higher complexity. Substituting (4.92) and (4.93) in (4.88) gives the following finite difference equation

$$\phi_{m+1,n} + \phi_{m-1,n} + \phi_{m,n+1} + \phi_{m,n-1} - 4\phi_{m,n} = 0 \quad . \tag{4.94}$$

A system of equations (4.94) with Dirichlet boundary condition (4.89) has a unique solution and is well posed [7]. The uniqueness theorem for (4.94) is a consequence of the lemma saying that the minimum and maximum values for $\phi_{m,n}$ are given on the boundary nodes.

We do not employ the FDM to solve our electrostatic inverse imaging problem for several reasons. According to our literature survey none of the existing inverse problems employs the FDM. This raises a question mark on whether we would succeed in adopting the FDM. In contrast the application of the Finite Element Method (section 4.2.2) to the inverse problems has been studied by many researchers for several decades. Of course the motivation to choose the FEM does not diminish the possible, undiscovered potential of the FDM.

However, there are several clear disadvantages of the FDM which we now introduce. The FDM is inefficient (as compared to the FEM) for electrostatic problems employing multiple sparse objects with free space in between them. In the case of the inverse imaging problem this includes the space between the sensor array and the reconstruction domain. The FDM is not well suited for the infinite domains that arise in our inverse imaging problem. Also the high curvature electrostatic fields arising, for example, near the boundary where a step function Dirichlet boundary condition is pre-set as shown in figure 4.2 are difficult to represent accurately on the grid of the FDM.

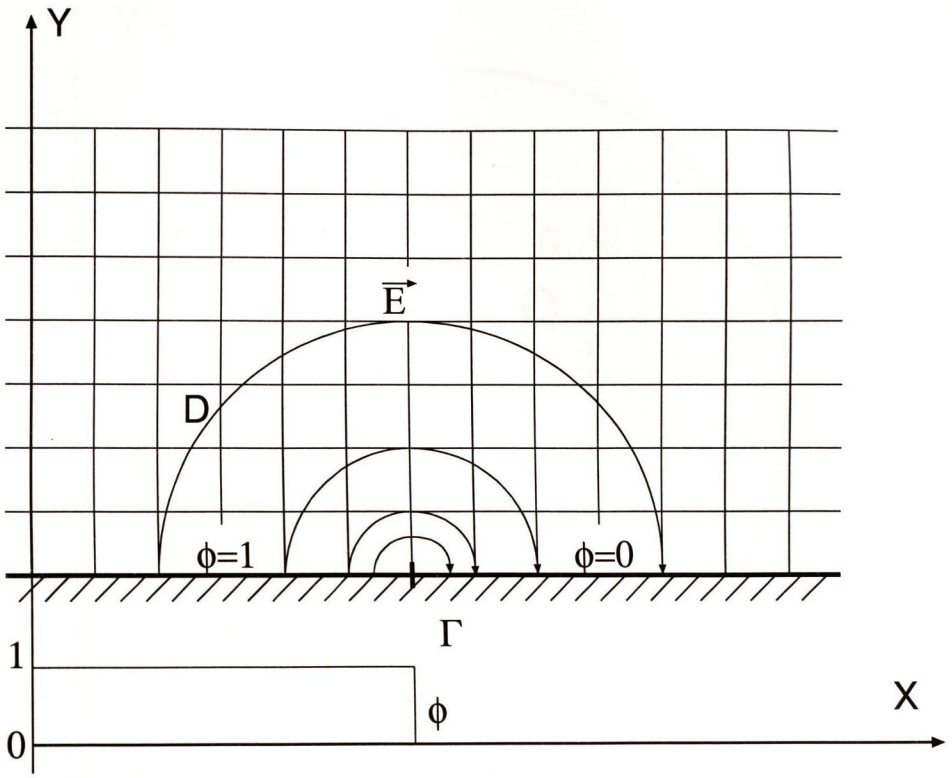

Figure 4.2: A step Dirichlet boundary condition for boundary Γ and the corresponding electric field intensity lines.

4.2.2 Finite Element Method

A Finite Element Method is a method for representing an integral equation in the form of a system of algebraic equations[3]. Almost all electrostatic and electrodynamic problems are now tackled using the FEM [77]. The FEM is also essential to the purpose of this thesis as we use it to solve the inverse electrostatic problem. Instead of a general introduction to the FEM we start this section with a particular implementation of the FEM.

We consider a Dirichlet boundary electrostatic problem in a finite domain D having a single-connected smooth boundary Γ. In figure 4.3 Γ is shown as a circle which is an example of the simply connected boundary. In section 4.3 we will consider a more com-

[3]In the case of the boundary integrals the FEM is called a Boundary Element Method.

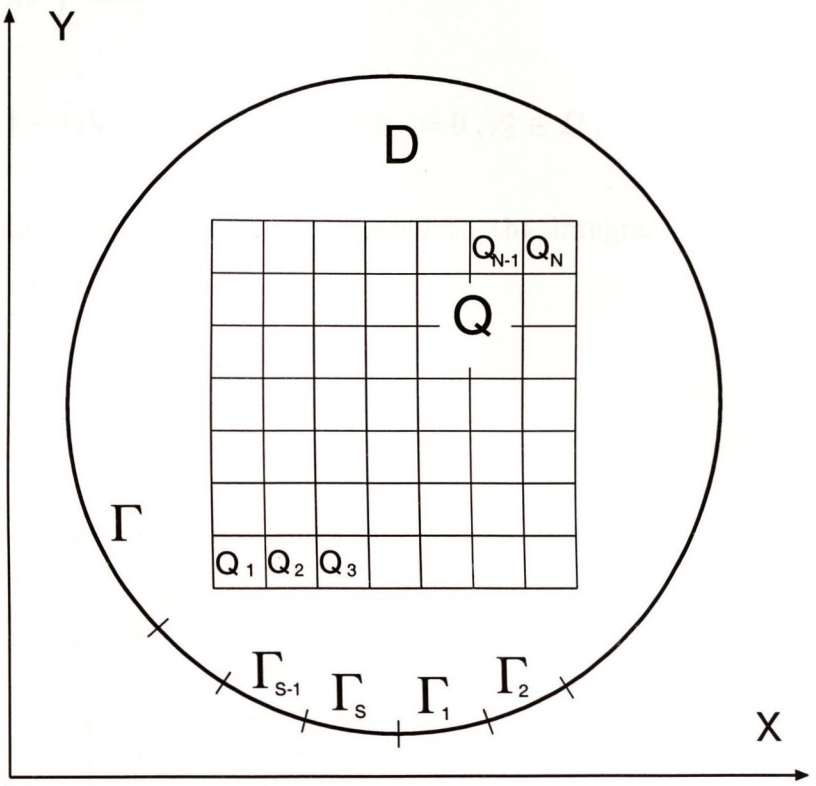

Figure 4.3: A boundary electrostatic problem in the D domain.

plicated case of the electrostatic problem employing a doublesided boundary. Let the Dirichlet boundary condition (2.12) on Γ be

$$\phi|_\Gamma = a \,. \tag{4.95}$$

We also assume that a nonhomogeneous dielectric ϵ is placed in D. For convenience we assume that $\epsilon = 1$ outside the square domain Q as shown in figure 4.3. According to section 2.4 the electrostatic potential ϕ in D satisfies the electrostatic governing integral equations employing a Green's function for either free (2.78) or non-free (2.79) space. To tackle the Dirichlet boundary problem in D we employ a well conditioned electrostatic integral equation as proposed in section 2.6. Placing a double layer on Γ having unknown

density σ gives

$$-\phi(\vec{r_2}) + 4\pi \int_\Gamma \frac{\partial\, G(\vec{r_1},\vec{r_2})}{\partial\, \vec{n}_{r_1}} \sigma(\vec{r_1}) dr_1$$

$$- \int_Q (\epsilon(r_1) - 1) \nabla_{r_1} \phi(\vec{r_1}) \nabla_{r_1} G(\vec{r_1},\vec{r_2}) dr_1 = 0\,, \vec{r_2} \in D\,, \tag{4.96}$$

where the volume integral over D is reduced to the integral over the square Q. The unknowns in (4.96) are

$$\begin{array}{ll} \sigma(\vec{r})\,, & \vec{r} \in \Gamma\,, \\ \frac{\partial\, \phi(\vec{r})}{\partial\, x}\,,\ \frac{\partial\, \phi(\vec{r})}{\partial\, y}\,, & \vec{r} \in Q\,. \end{array} \tag{4.97}$$

Equation (4.96) yields a system of three integral equations

$$-\frac{d\phi(\vec{r_2})}{dx_2} + 4\pi \frac{d}{dx_2} \int_\Gamma \frac{dG(\vec{r_1},\vec{r_2})}{d\vec{n}_{r_1}} \sigma(\vec{r_1}) dr_1$$

$$- \int_Q (\epsilon(r_1) - 1) \left\{ \frac{\partial\, \phi(\vec{r_1})}{\partial\, x_1} \frac{\partial^2\, G(\vec{r_1},\vec{r_2})}{\partial\, x_1 \partial\, x_2} + \frac{\partial\, \phi(\vec{r_1})}{\partial\, y_1} \frac{\partial^2\, G(\vec{r_1},\vec{r_2})}{\partial\, y_1 \partial\, x_2} \right\} dr_1 = 0\,,\ \vec{r_2} \in Q\,, \tag{4.98}$$

$$-\frac{d\phi(\vec{r_2})}{dy_2} + 4\pi \frac{d}{dy_2} \int_\Gamma \frac{dG(\vec{r_1},\vec{r_2})}{d\vec{n}_{r_1}} \sigma(\vec{r_1}) dr_1$$

$$- \int_Q (\epsilon(r_1) - 1) \left\{ \frac{\partial\, \phi(\vec{r_1})}{\partial\, x_1} \frac{\partial^2\, G(\vec{r_1},\vec{r_2})}{\partial\, x_1 \partial\, y_2} + \frac{\partial\, \phi(\vec{r_1})}{\partial\, y_1} \frac{\partial^2\, G(\vec{r_1},\vec{r_2})}{\partial\, y_1 \partial\, y_2} \right\} dr_1 = 0\,,\ \vec{r_2} \in Q\,, \tag{4.99}$$

$$-a(\vec{r_2}) + 4\pi \int_\Gamma \frac{\partial\, G(\vec{r_1},\vec{r_2})}{\partial\, \vec{n}_{r_1}} \sigma(\vec{r_1}) dr_1$$

$$- \int_Q (\epsilon(r_1) - 1) \left\{ \frac{\partial\, \phi(\vec{r_1})}{\partial\, x_1} \frac{\partial\, G(\vec{r_1},\vec{r_2})}{\partial\, x_1} + \frac{\partial\, \phi(\vec{r_1})}{\partial\, y_1} \frac{\partial\, G(\vec{r_1},\vec{r_2})}{\partial\, y_1} \right\} dr_1 = 0\,, \vec{r_2} \in \Gamma\,, \tag{4.100}$$

where (4.98) and (4.99) are the Fredholm integral equations of the second kind giving a solution to the electrostatic problem in Q provided the field of the double layer on Γ is treated as an incident field. The final equation (4.100) is a well posed Fredholm integral equation of the first kind with a singularity in the kernel. This equation employs the

double layer on Γ and electrostatic field intensity in Q to satisfy the Dirichlet boundary condition on Γ.

We now obtain a system of linear algebraic equations based on (4.98), (4.99) and (4.100). In order to do so we approximate the volume and boundary functions by their piecewise constant approximations. Let Q be divided into N rectangular non-overlapping subdomains Q_n, $n = 1, 2, \cdots, N$: $Q = Q_1 \bigcup Q_2 \bigcup \cdots \bigcup Q_N$ and let Γ be approximated by a piecewise linear curve composed of S segments Γ_n, $n = 1, 2, \cdots, S$. We approximate ϵ and the derivatives of the electrostatic potential ϕ in Q as follows

$$\begin{aligned} &\epsilon(\vec{r}) = \epsilon^{(n)} , \\ &\frac{\partial \phi(\vec{r})}{\partial x} = \phi_x'^{(n)} , \\ &\frac{\partial \phi(\vec{r})}{\partial y} = \phi_y'^{(n)} , \quad \vec{r} \in Q_n , \quad n = 1, 2, \cdots, N , \end{aligned} \tag{4.101}$$

where $\phi_x'^{(n)}$, $\phi_y'^{(n)}$ and $\epsilon^{(n)}$ are constants. We also introduce a piecewise constant representation of the double layer σ and the Dirichlet boundary condition (4.95) as follows

$$\begin{aligned} &\sigma(\vec{r}) = \sigma^{(n)} , \\ &a(\vec{r}) = a^{(n)} , \quad \vec{r} \in \Gamma_n , \quad n = 1, 2, \cdots, S , \end{aligned} \tag{4.102}$$

where $\sigma^{(n)}$, $a^{(n)}$ are constants. If we employ a moment method to solve the electrostatic problem in D then a piecewise constant approximation of the Dirichlet boundary condition on Γ is not necessary because the moment method only requires the knowledge of the Dirichlet boundary condition in a finite number of points on Γ.

Substituting piecewise constant approximations (4.101), (4.102) into electrostatic integrals in (4.98), (4.99), (4.100) gives[4]

$$4\pi \frac{d}{dx_2} \int_\Gamma \frac{dG(\vec{r_1}, \vec{r_2})}{d\vec{n}_{r_1}} \sigma(\vec{r_1}) dr_1 = 4\pi \sum_{i=1}^{S} \sigma^{(i)} \int_\Gamma \frac{d}{dx_2} \frac{dG(\vec{r_1}, \vec{r_2})}{d\vec{n}_{r_1}} dr_1 , \tag{4.103}$$

[4]Hereafter we present complete lists of expressions that need to be implemented numerically. We aim to provide comprehensive information on our numerical techniques and to skip the demonstration of the actual computer codes.

$$4\pi \frac{d}{dy_2} \int_\Gamma \frac{dG(\vec{r_1},\vec{r_2})}{d\vec{n}_{r_1}} \sigma(\vec{r_1}) dr_1 = 4\pi \sum_{i=1}^{S} \sigma^{(i)} \int_\Gamma \frac{d}{dy_2} \frac{dG(\vec{r_1},\vec{r_2})}{d\vec{n}_{r_1}} dr_1 \ , \tag{4.104}$$

$$4\pi \int_\Gamma \frac{\partial\, G(\vec{r_1},\vec{r_2})}{\partial\, \vec{n}_{r_1}} \sigma(\vec{r_1}) dr_1 = 4\pi \sum_{i=1}^{S} \sigma^{(i)} \int_{\Gamma_i} \frac{\partial\, G(\vec{r_1},\vec{r_2})}{\partial\, \vec{n}_{r_1}} dr_1 \ , \tag{4.105}$$

$$\int_Q (\epsilon(r_1)-1) \frac{\partial\, \phi(\vec{r_1})}{\partial\, x_1} \frac{\partial^2\, G(\vec{r_1},\vec{r_2})}{\partial\, x_1 \partial\, x_2} dr_1 = \sum_{i=1}^{N} (\epsilon^{(i)}-1) \phi_x'^{(i)} \int_{Q_i} \frac{\partial^2\, G(\vec{r_1},\vec{r_2})}{\partial\, x_1 \partial\, x_2} dr_1 \ , \tag{4.106}$$

$$\int_Q (\epsilon(r_1)-1) \frac{\partial\, \phi(\vec{r_1})}{\partial\, y_1} \frac{\partial^2\, G(\vec{r_1},\vec{r_2})}{\partial\, y_1 \partial\, x_2} dr_1 = \sum_{i=1}^{N} (\epsilon^{(i)}-1) \phi_y'^{(i)} \int_{Q_i} \frac{\partial^2\, G(\vec{r_1},\vec{r_2})}{\partial\, y_1 \partial\, x_2} dr_1 \ , \tag{4.107}$$

$$\int_Q (\epsilon(r_1)-1) \frac{\partial\, \phi(\vec{r_1})}{\partial\, x_1} \frac{\partial^2\, G(\vec{r_1},\vec{r_2})}{\partial\, x_1 \partial\, y_2} dr_1 = \sum_{i=1}^{N} (\epsilon^{(i)}-1) \phi_x'^{(i)} \int_{Q_i} \frac{\partial^2\, G(\vec{r_1},\vec{r_2})}{\partial\, x_1 \partial\, y_2} dr_1 \ , \tag{4.108}$$

$$\int_Q (\epsilon(r_1)-1) \frac{\partial\, \phi(\vec{r_1})}{\partial\, y_1} \frac{\partial^2\, G(\vec{r_1},\vec{r_2})}{\partial\, y_1 \partial\, y_2} dr_1 = \sum_{i=1}^{N} (\epsilon^{(i)}-1) \phi_y'^{(i)} \int_{Q_i} \frac{\partial^2\, G(\vec{r_1},\vec{r_2})}{\partial\, y_1 \partial\, y_2} dr_1 \ , \tag{4.109}$$

$$\int_Q (\epsilon(r_1)-1) \frac{\partial\, \phi(\vec{r_1})}{\partial\, x_1} \frac{\partial\, G(\vec{r_1},\vec{r_2})}{\partial\, x_1} dr_1 = \sum_{i=1}^{N} (\epsilon^{(i)}-1) \phi_x'^{(i)} \int_{Q_i} \frac{\partial\, G(\vec{r_1},\vec{r_2})}{\partial\, x_1} dr_1 \ , \tag{4.110}$$

$$\int_Q (\epsilon(r_1)-1) \frac{\partial\, \phi(\vec{r_1})}{\partial\, y_1} \frac{\partial\, G(\vec{r_1},\vec{r_2})}{\partial\, y_1} dr_1 = \sum_{i=1}^{N} (\epsilon^{(i)}-1) \phi_y'^{(i)} \int_{Q_i} \frac{\partial\, G(\vec{r_1},\vec{r_2})}{\partial\, y_1} dr_1 \ . \tag{4.111}$$

The integrals under the summation operator in (4.103)-(4.111) are the boundary and volume integrals of the Green's function of free space given by (2.22)

$$G(\vec{r_1},\vec{r_2}) = -\frac{1}{2\pi} \log(|\vec{r_1}-\vec{r_2}|) \ . \tag{4.112}$$

These integrals have a simple analytical form for rectangular integration domains. A list of integrals of the Green's function that can be encountered in various 2D formulations of the electrostatic problem is presented in appendix 4.5.

For the sake of simplicity we replace the piecewise constant dielectric permittivity ϵ by a corresponding dielectric susceptibility χ such that: $\chi_n = \epsilon_n - 1$, $n = 1, 2, \cdots, N$. We also denote the integrals in (4.103)-(4.111) as follows[5]

$$BnVx^{(i,j)} = 4\pi \int_{\Gamma_i} \frac{d}{dx_2} \frac{dG(\vec{r_1}, \vec{r_2})}{d\vec{n}_{r_1}} dr_1 \ , \ \vec{r_2} \in Q_j \ , \ 1 \leq i \leq S \ , \ 1 \leq j \leq N \ , \tag{4.113}$$

$$BnVy^{(i,j)} = 4\pi \int_{\Gamma_i} \frac{d}{dy_2} \frac{dG(\vec{r_1}, \vec{r_2})}{d\vec{n}_{r_1}} dr_1 \ , \ \vec{r_2} \in Q_j \ , \ 1 \leq i \leq S \ , \ 1 \leq j \leq N \ , \tag{4.114}$$

$$BnB^{(i,j)} = 4\pi \int_{\Gamma_i} \frac{\partial\, G(\vec{r_1}, \vec{r_2})}{\partial\, \vec{n}_{r_1}} dr_1 \ , \ \vec{r_2} \in \Gamma_j \ , \ 1 \leq i \leq S \ , \ 1 \leq j \leq S \ , \tag{4.115}$$

$$VxVx^{(i,j)} = \int_{Q_i} \frac{\partial^2\, G(\vec{r_1}, \vec{r_2})}{\partial\, x_1 \partial\, x_2} dr_1 \ , \ \vec{r_2} \in Q_j \ , \ 1 \leq i \leq N \ , \ 1 \leq j \leq N \ , \tag{4.116}$$

$$VyVx^{(i,j)} = \int_{Q_i} \frac{\partial^2\, G(\vec{r_1}, \vec{r_2})}{\partial\, y_1 \partial\, x_2} dr_1 \ , \ \vec{r_2} \in Q_j \ , \ 1 \leq i \leq N \ , \ 1 \leq j \leq N \ , \tag{4.117}$$

$$VxVy^{(i,j)} = \int_{Q_i} \frac{\partial^2\, G(\vec{r_1}, \vec{r_2})}{\partial\, x_1 \partial\, y_2} dr_1 \ , \ \vec{r_2} \in Q_j \ , \ 1 \leq i \leq N \ , \ 1 \leq j \leq N \ , \tag{4.118}$$

$$VyVy^{(i,j)} = \int_{Q_i} \frac{\partial^2\, G(\vec{r_1}, \vec{r_2})}{\partial\, y_1 \partial\, y_2} dr_1 \ , \ \vec{r_2} \in Q_j \ , \ 1 \leq i \leq N \ , \ 1 \leq j \leq N \ , \tag{4.119}$$

$$VxB^{(i,j)} = \int_{Q_i} \frac{\partial\, G(\vec{r_1}, \vec{r_2})}{\partial\, x_1} dr_1 \ , \ \vec{r_2} \in \Gamma_j \ , \ 1 \leq i \leq N \ , \ 1 \leq j \leq S \ , \tag{4.120}$$

$$VyB^{(i,j)} = \int_{Q_i} \frac{\partial\, G(\vec{r_1}, \vec{r_2})}{\partial\, y_1} dr_1 \ . \ \vec{r_2} \in \Gamma_j \ , \ 1 \leq i \leq N \ , \ 1 \leq j \leq S \ . \tag{4.121}$$

Using piecewise constant approximations (4.101),(4.102) and (4.113)-(4.121) we now rewrite electrostatic governing equations (4.98), (4.99) and (4.100) in the form of a system of linear algebraic equations

$$-\phi_x'^{(j)} - \sum_{i=1}^{N} VxVx^{(i,j)} \chi^{(i)} \phi_x'^{(i)} - \sum_{i=1}^{N} VyVx^{(i,j)} \chi^{(i)} \phi_y'^{(i)} + \sum_{i=1}^{S} BnVx^{(i,j)} \sigma^{(i)} = 0 \ , \tag{4.122}$$

[5] In our nomenclature B and V stand for "boundary" and "volume" respectively and x and y correspond to x- and y- differentiation of the electrostatic potential. For example $BnVx^{(i,j)}$ is the x-derivative of the electrostatic potential produced by the field sources of the i^{th} boundary mesh in the j^{th} volume mesh.

$$-\phi_y'^{(j)} - \sum_{i=1}^{N} VxVy^{(i,j)}\chi^{(i)}\phi_x'^{(i)} - \sum_{i=1}^{N} VyVy^{(i,j)}\chi^{(i)}\phi_y'^{(i)} + \sum_{i=1}^{S} BnVy^{(i,j)}\sigma^{(i)} = 0 \ , \quad (4.123)$$

$$j = 1, \cdots, N \ ,$$

$$-\sum_{i=1}^{N} VxB^{(i,j)}\chi^{(i)}\phi_x'^{(i)} - \sum_{i=1}^{N} VyB^{(i,j)}\chi^{(i)}\phi_y'^{(i)} + \sum_{i=1}^{S} BnB^{(i,j)}\sigma^{(i)} = a^{(j)} \ , \quad (4.124)$$

$$j = 1, \cdots, S \ .$$

We group (4.122), (4.123) and (4.124) to give a single matrix form equation

$$A\vec{X} = \vec{Y} \ , \quad (4.125)$$

where $\vec{X}$ and $\vec{Y}$ are $2N + S$ dimensional vectors

$$\vec{X} = \begin{pmatrix} \phi_x'^{(1)} \\ \phi_x'^{(2)} \\ \vdots \\ \phi_x'^{(N)} \\ \phi_y'^{(1)} \\ \phi_y'^{(2)} \\ \vdots \\ \phi_y'^{(N)} \\ \sigma^{(1)} \\ \sigma^{(2)} \\ \vdots \\ \sigma^{(S)} \end{pmatrix} \ , \quad \vec{Y} = \begin{pmatrix} 0 \\ 0 \\ \vdots \\ 0 \\ 0 \\ 0 \\ \vdots \\ 0 \\ a^{(1)} \\ a^{(2)} \\ \vdots \\ a^{(S)} \end{pmatrix} \ , \quad (4.126)$$

and A is a square matrix that consists of 9 submatrices

$$A = \begin{pmatrix} A_{1,1} & A_{1,2} & A_{1,3} \\ A_{2,1} & A_{2,2} & A_{2,3} \\ A_{3,1} & A_{3,2} & A_{3,3} \end{pmatrix} \ , \quad (4.127)$$

$$A_{1,1} = \begin{pmatrix} -\chi^{(1)} VxVx^{(1,1)} - 1 & -\chi^{(2)} VxVx^{(1,2)} & \cdots & -\chi^{(N)} VxVx^{(1,N)} \\ -\chi^{(1)} VxVx^{(2,1)} & -\chi^{(2)} VxVx^{(2,2)} - 1 & \cdots & -\chi^{(N)} VxVx^{(2,N)} \\ \vdots & \vdots & \ddots & \vdots \\ -\chi^{(1)} VxVx^{(N,1)} & -\chi^{(2)} VxVx^{(N,2)} & \cdots & -\chi^{(N)} VxVx^{(N,N)} - 1 \end{pmatrix}, \quad (4.128)$$

$$A_{1,2} = \begin{pmatrix} -\chi^{(1)} VyVx^{(1,1)} & -\chi^{(2)} VyVx^{(1,2)} & \cdots & -\chi^{(N)} VyVx^{(1,N)} \\ -\chi^{(1)} VyVx^{(2,1)} & -\chi^{(2)} VyVx^{(2,2)} & \cdots & -\chi^{(N)} VyVx^{(2,N)} \\ \vdots & \vdots & \ddots & \vdots \\ -\chi^{(1)} VyVx^{(N,1)} & -\chi^{(2)} VyVx^{(N,2)} & \cdots & -\chi^{(N)} VyVx^{(N,N)} \end{pmatrix}, \quad (4.129)$$

$$A_{1,3} = \begin{pmatrix} BnVx^{(1,1)} & BnVx^{(1,2)} & \cdots & BnVx^{(1,S)} \\ BnVx^{(2,1)} & BnVx^{(2,2)} & \cdots & BnVx^{(2,S)} \\ \vdots & \vdots & \ddots & \vdots \\ BnVx^{(N,1)} & BnVx^{(N,2)} & \cdots & BnVx^{(N,S)} \end{pmatrix}, \quad (4.130)$$

$$A_{2,1} = \begin{pmatrix} -\chi^{(1)} VxVy^{(1,1)} & -\chi^{(2)} VxVy^{(1,2)} & \cdots & -\chi^{(N)} VxVy^{(1,N)} \\ -\chi^{(1)} VxVy^{(2,1)} & -\chi^{(2)} VxVy^{(2,2)} & \cdots & -\chi^{(N)} VxVy^{(2,N)} \\ \vdots & \vdots & \ddots & \vdots \\ -\chi^{(1)} VxVy^{(N,1)} & -\chi^{(2)} VxVy^{(N,2)} & \cdots & -\chi^{(N)} VxVy^{(N,N)} \end{pmatrix}, \quad (4.131)$$

$$A_{2,2} = \begin{pmatrix} -\chi^{(1)} VyVy^{(1,1)} - 1 & -\chi^{(2)} VyVy^{(1,2)} & \cdots & -\chi^{(N)} VyVy^{(1,N)} \\ -\chi^{(1)} VyVy^{(2,1)} & -\chi^{(2)} VyVy^{(2,2)} - 1 & \cdots & -\chi^{(N)} VyVy^{(2,N)} \\ \vdots & \vdots & \ddots & \vdots \\ -\chi^{(1)} VyVy^{(N,1)} & -\chi^{(2)} VyVy^{(N,2)} & \cdots & -\chi^{(N)} VyVy^{(N,N)} - 1 \end{pmatrix}, \quad (4.132)$$

$$A_{2,3} = \begin{pmatrix} BnVy^{(1,1)} & BnVy^{(1,2)} & \cdots & BnVy^{(1,S)} \\ BnVy^{(2,1)} & BnVy^{(2,2)} & \cdots & BnVy^{(2,S)} \\ \vdots & \vdots & \ddots & \vdots \\ BnVy^{(N,1)} & BnVy^{(N,2)} & \cdots & BnVy^{(N,S)} \end{pmatrix}, \quad (4.133)$$

$$A_{3,1} = \begin{pmatrix} -\chi^{(1)} VxB^{(1,1)} & -\chi^{(2)} VxB^{(1,2)} & \dots & -\chi^{(N)} VxB^{(1,N)} \\ -\chi^{(1)} VxB^{(2,1)} & -\chi^{(2)} VxB^{(2,2)} & \dots & -\chi^{(N)} VxB^{(2,N)} \\ \vdots & \vdots & \ddots & \vdots \\ -\chi^{(1)} VxB^{(S,1)} & -\chi^{(2)} VxB^{(S,2)} & \dots & -\chi^{(N)} VxB^{(S,N)} \end{pmatrix}, \tag{4.134}$$

$$A_{3,2} = \begin{pmatrix} -\chi^{(1)} VyB^{(1,1)} & -\chi^{(2)} VyB^{(1,2)} & \dots & -\chi^{(N)} VyB^{(1,N)} \\ -\chi^{(1)} VyB^{(2,1)} & -\chi^{(2)} VyB^{(2,2)} & \dots & -\chi^{(N)} VyB^{(2,N)} \\ \vdots & \vdots & \ddots & \vdots \\ -\chi^{(1)} VyB^{(S,1)} & -\chi^{(2)} VyB^{(S,2)} & \dots & -\chi^{(N)} VyB^{(S,N)} \end{pmatrix}, \tag{4.135}$$

$$A_{3,3} = \begin{pmatrix} BnB^{(1,1)} & BnB^{(1,2)} & \dots & BnB^{(1,S)} \\ BnB^{(2,1)} & BnB^{(2,2)} & \dots & BnB^{(2,S)} \\ \vdots & \vdots & \ddots & \vdots \\ BnB^{(S,1)} & BnB^{(S,2)} & \dots & BnB^{(S,S)} \end{pmatrix}, \tag{4.136}$$

The condition number K for (4.125) can be calculated using (4.39). K depends on many parameters and, in particular, on the shape of boundary Γ. A common practice is to skip the condition number analysis for those problems that are expected to be well conditioned. We do not test (4.125) for ill/well conditioning directly. Instead we check the speed of convergence of our numerical solver. If the numerical algorithm converges rapidly then we conclude that we deal with a well posed formulation.

The system of liner equations (4.125) for the electrostatic problem shown in figure 4.3 can be tackled using a conjugate gradient method explained in appendix 4.4. According to our numerical experiments the cg-method applied to (4.125) converges to a precision of 10^{-4} in about 10-20 iterations regardless of the dimension of A. This suggests that (4.125) is well-conditioned. We also observed that in the case of ill-posed algebraic equations the cg-method may not converge even after the number of iterations equal to the dimension of A. It is well known that in the absence of the round-off errors the cg-method converges to the exact solution of $A\vec{X} = \vec{Y}$ after N iterations where is the dimension of A (appendix 4.4).

4.3 Electrostatic Problem Employing a Doublesided Boundary

In the 2D physical implementation of the electrostatic imaging problem that we investigate the flat metal electrodes are placed just above a ground plane as shown in figure 4.4 (a). Let a nonzero potential ϕ_k be applied to the k-th electrode. If we now approach the capacitive sensor array in the directions A and B as shown in figure 4.4 (a), the electrostatic potential tends to ϕ_k and zero respectively. We model a capacitive sensor array by introducing a line segment boundary with a doublesided Dirichlet boundary conditions on it (figure 4.4 (b)). In this analytical model we force the electrostatic potential to tend to the same values as in the real physical implementation as we approach the boundary i.e. to the values ϕ_k and zero in the directions A and B respectively as shown in figure 4.4 (b). We denote the upper and lower sides of the line segment boundary by $\Gamma^{(+)}$ and $\Gamma^{(-)}$ respectively.

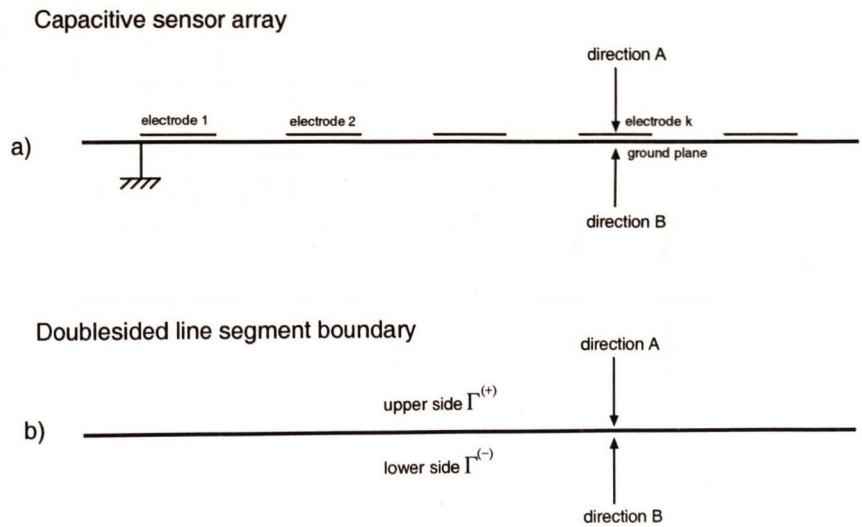

Figure 4.4: A 2D capacitive sensor array and its analytical model.

The ill/well conditioning considerations significantly change when the doublesided bound-

ary is added to the electrostatic problem. First we demonstrate that in contrast to the electrostatic problem with a simply connected boundary the doublesided boundary electrostatic problem cannot be efficiently solved by employing either a single or double unknown layer; using both layers leads to an ill-conditioned integral equation. Then we show that there is a method employing a conformal mapping that allows us to obtain a well posed problem. Finally we explain the numerical implementation of the double sided Dirichlet electrostatic problem and the advantages of the method.

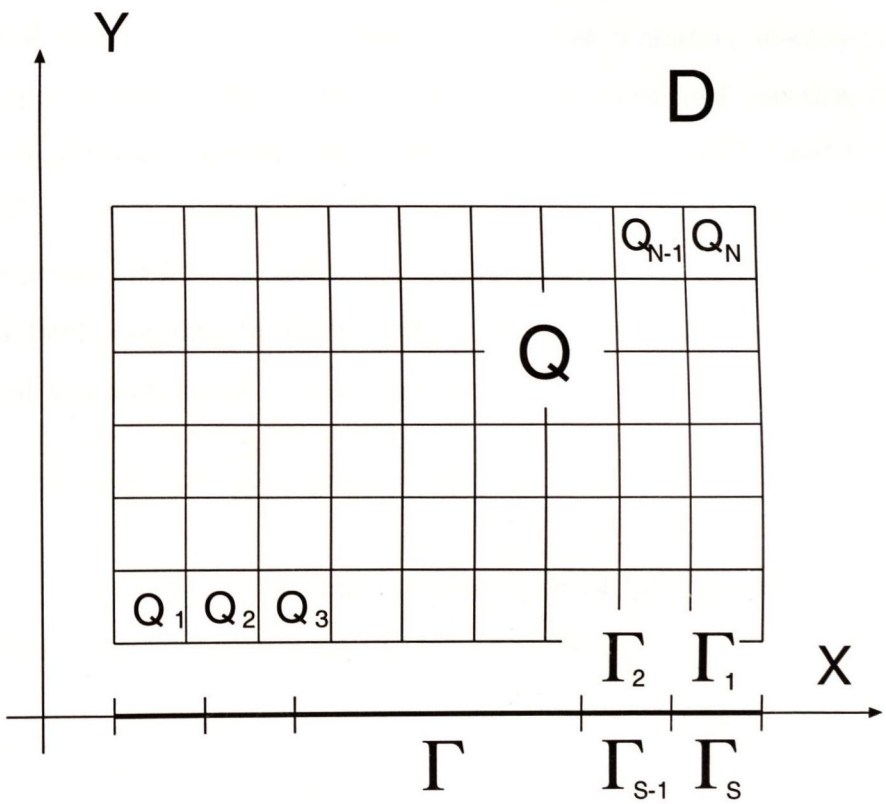

Figure 4.5: D domain with a doublesided boundary Γ.

A Dirichlet boundary electrostatic problem with a line segment boundary Γ is shown in figure 4.5. Without loss of generality we assume that the left and right ends of Γ are given by $x = -1$ and $x = +1$. The Dirichlet boundary condition is prescribed on $\Gamma^{(+)}$ and $\Gamma^{(-)}$.

We rewrite boundary condition (4.95) for the doublesided boundary Γ as follows

$$\phi^{(+)}|_{\Gamma^{(+)}} = a^{(+)}(x) \,, \tag{4.137}$$

$$\phi^{(-)}|_{\Gamma}^{(-)} = a^{(-)}(x) \,, \; x \in (-1,1) \,, \tag{4.138}$$

where the superscripts $(+)$ and $(-)$ denote the upper and the lower sides $\Gamma^{(+)}$ and $\Gamma^{(-)}$ of Γ. Recall that $a^{(+)}(x) \neq a^{(-)}(x)$. We now show that approaches to deriving the integral equation for electrostatic problem in figure 4.5 that use a single or double layer on Γ do not possess a well conditioned form. Indeed the Dirichlet boundary electrostatic problem is commonly approached by placing an unknown double layer on Γ (section 2.6). Since Γ in figure 4.5 is doublesided placing double layers $\sigma^{(+)}$ and $\sigma^{(-)}$ on $\Gamma^{(+)}$ and $\Gamma^{(-)}$ is equivalent to placing $\sigma^{(+)} - \sigma^{(-)}$ on segment $(-1,1)$, where sign '-' arises because of the rotated by 180 degrees normal $\vec{n}$ for $\Gamma^{(+)}$ and $\Gamma^{(-)}$. This statement can be proved by considering an electrostatic field produced by the boundary integrals in (4.98), (4.99) and (4.100). Thus it is sufficient to place $\sigma = \sigma^{(+)} - \sigma^{(-)}$ on $(-1,1)$ to include both $\sigma^{(+)}$ and $\sigma^{(-)}$

$$\sigma(x) = \sigma^{(+)}(x) - \sigma^{(-)}(x) \,, \; x \in (-1,1) \,. \tag{4.139}$$

We now show that the Dirichlet boundary condition (4.137), (4.138) determines σ (4.139) uniquely. According to section 2.6.1 (2.116) we write

$$\sigma = \frac{a^{(+)}(x) - a^{(-)}(x)}{2\pi} \,. \tag{4.140}$$

If we now apply the FEM to (4.98), (4.99) and (4.100) then we obtain a numerical formulation where the number of unknowns is less then the number of algebraic equations. To obtain a consistent numerical formulation for the electrostatic problem in figure 4.5 we place additional electrostatic field sources on Γ i.e an unknown single layer ρ

$$\rho(x) = \rho^{(+)}(x) - \rho^{(-)}(x) \,, \; x \in (-1,1) \,, \tag{4.141}$$

where $\rho^{(+)}$ and $\rho^{(-)}$ are surface charge densities on the upper and lower sides of Γ respectively. It can be shown that now we have sufficient number of unknowns to solve an

electrostatic problem. While the double layer is given by (4.140) a single layer (4.141) still has to be resolved. The unknown single layer on Γ in the Dirichlet boundary electrostatic problem leads to a Fredholm integral equation of the first kind with a smooth kernel which is ill posed. Summarizing, the Dirichlet boundary electrostatic problem cannot be efficiently solved using traditional approaches employing unknown single and double layers without preconditioning.

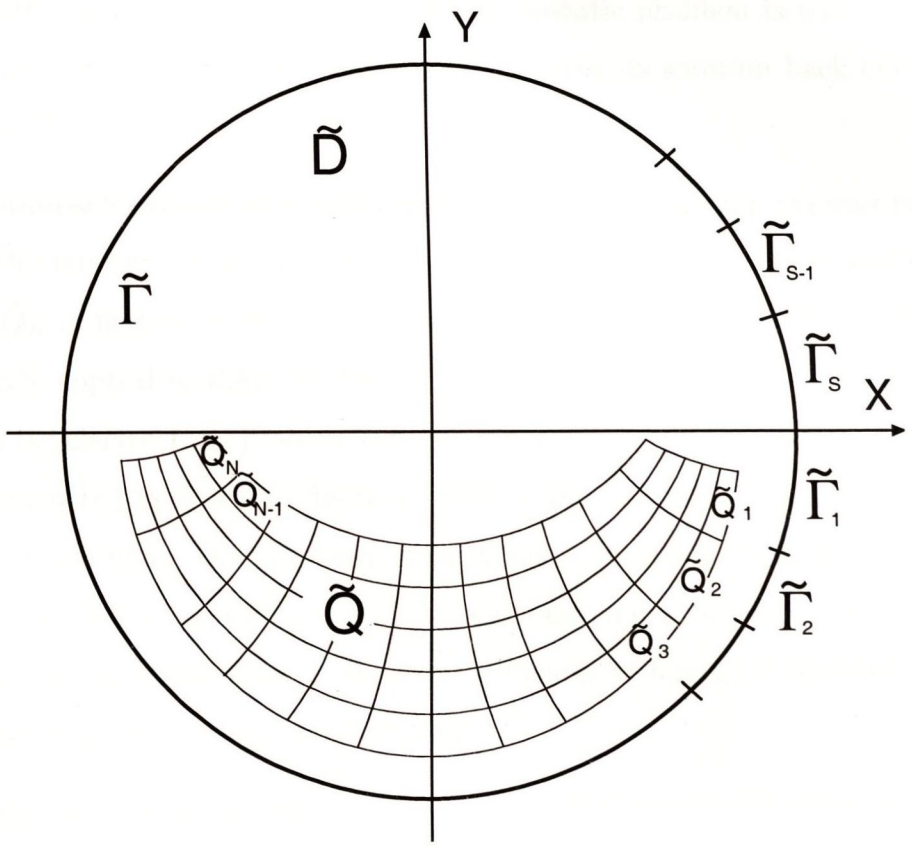

Figure 4.6: $\tilde{D}$ domain with a simply connected boundary $\tilde{\Gamma}$.

One of the methods to obtain a well posed formulation for the electrostatic boundary problem in figure 4.5 is to map domain D onto another domain $\tilde{D}$ with a simply connected boundary Γ. Conformal mapping introduced in section 2.3.1 preserves the electrostatic equation and therefore is particularly suited for that method. Figure 4.6 illustrates domain $\tilde{D}$ having boundary $\tilde{\Gamma}$ obtained from D and Γ in figure 4.5 according to the conformal

mapping example presented in section 2.3.4.

The electrostatic problem in figure 4.6 is now posed in the same type of domain as the electrostatic problem presented in section 4.2.2 (figure 4.3). Thus we can directly employ equations (4.98), (4.99) and (4.100) in $\tilde{D}$ with a circle boundary $\tilde{\Gamma}$ and a non-regular $\tilde{Q}$ shown in figure 4.6. The fact that $\tilde{Q}$ is not a square domain as compared to figure 4.3 is not essential for the analytical formulation of the electrostatic problem. Equations (4.98), (4.99) and (4.100) in $\tilde{D}$ are the Fredholm integral equations of the second kind with a smooth kernel which means that the electrostatic problem is well posed. Solving an electrostatic problem in $\tilde{D}$ and conformally mapping its solution back onto D obtains a solution in D.

The above approach employing a conformal mapping of the domain exterior to a line segment onto the interior circle domain has several disadvantages. Firstly the new meshes $\tilde{Q}_1, \tilde{Q}_2, \cdots, \tilde{Q}_N$ in figure 4.6 are not rectangular and hence formulae in appendix 4.5 cannot be directly applied to these meshes. A second disadvantage is that if the doublesided boundary in the electrostatic problem consists of several segments which are not necessarily aligned or connected as shown in figure 4.7 then a simple form for the conformal mapping does not exist and hence the proposed method has a limited applicability. Indeed implementing a conformal mapping for one of the segments maps the remaining segments onto the doublesided curves resulting in the same difficulty of having a doublesided Dirichlet boundary condition as in the original problem.

In this thesis we develop a method for solving a doublesided Dirichlet boundary electrostatic problem free of the above mentioned disadvantages. Instead of mapping the electrostatic problem in figure 4.5 (i.e. ϵ and ϕ) onto $\tilde{D}$ we formulate it in D as if the electrostatic problem did not have a doublesided Γ. The innovation is to use $\tilde{D}$ to place a double layer $\tilde{\sigma}$ on $\tilde{\Gamma}$ as if an electrostatic problem was mapped onto $\tilde{D}$. The electrostatic integral equation (4.96) in our approach becomes a hybrid integral equation given by

$$-\phi(\vec{r_2}) + \hat{\mathrm{CF}}[\tilde{D} \rightarrow D] \left\{ 4\pi \int_{\tilde{\Gamma}} \frac{\partial\, G(\vec{r_1}, \vec{r_2})}{\partial\, \vec{n}_{r_1}} \tilde{\sigma}(\vec{r_1}) dr_1 \right\}$$

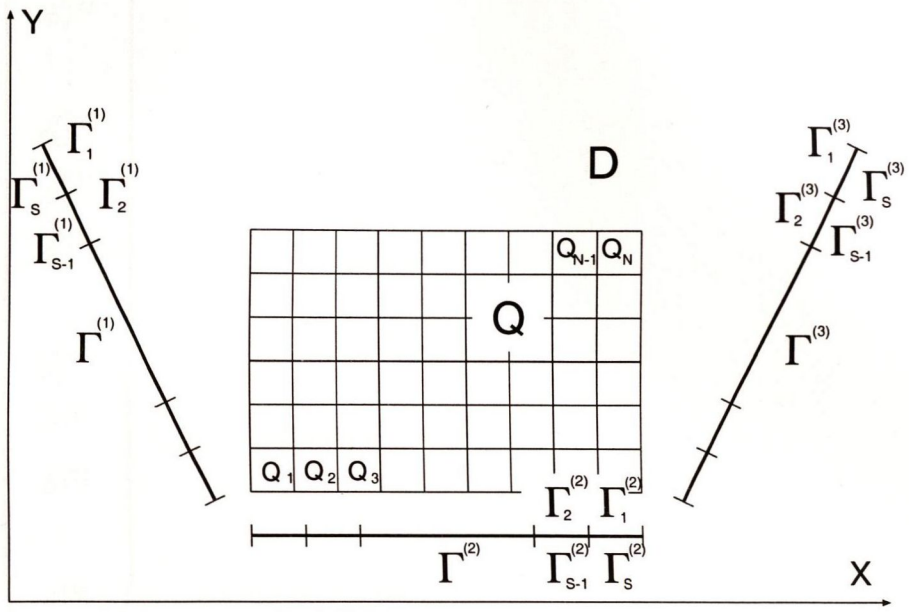

Figure 4.7: Boundary electrostatic problem with $\tilde{\Gamma}$ composed of three segments $\tilde{\Gamma}^{(1)}$, $\tilde{\Gamma}^{(2)}$ and $\tilde{\Gamma}^{(3)}$.

$$-\int_Q (\epsilon(r_1)-1)\nabla_{r_1}\phi(\vec{r_1})\nabla_{r_1}G(\vec{r_1},\vec{r_2})dr_1 = 0\,,\vec{r_2}\in D\,,\ \vec{\tilde{r}_2}\in\tilde{D}\,, \tag{4.142}$$

where $\hat{\mathrm{CF}}[\tilde{D}\rightarrow D]$ is an operator that conformally maps $\tilde{D}$ onto D and $\tilde{\sigma}$ is a double layer density on $\tilde{\Gamma}$ in $\tilde{D}$. Note that Γ is not included in (4.142). Instead it is implicitly referred to in the conformal mapping operator $\hat{\mathrm{CF}}[\tilde{D}\rightarrow D]\left\{\tilde{\Gamma}\right\}$. The unknowns of the electrostatic problem (4.142) are given by $\frac{\partial\,\phi}{\partial\,x}$, $\frac{\partial\,\phi}{\partial\,y}$ in Q and $\tilde{\sigma}$ on $\tilde{\Gamma}$.

Employing piecewise constant approximations for $\frac{\partial\,\phi}{\partial\,x}$, $\frac{\partial\,\phi}{\partial\,y}$ in Q and $\tilde{\sigma}$ on $\tilde{\Gamma}$ in (4.142) in the same way as (4.101), (4.102) are introduced we reduce (4.142) to a system of linear

algebraic equations (4.125) where $\vec{Y}$ is given in (4.125) and $\vec{X}$ is defined as follows

$$\vec{X} = \begin{pmatrix} \phi_x'^{(1)} \\ \phi_x'^{(2)} \\ \vdots \\ \phi_x'^{(N)} \\ \phi_y'^{(1)} \\ \phi_y'^{(2)} \\ \vdots \\ \phi_y'^{(N)} \\ \tilde{\sigma}^{(1)} \\ \tilde{\sigma}^{(2)} \\ \vdots \\ \tilde{\sigma}^{(S)} \end{pmatrix} . \tag{4.143}$$

Matrix A can still be represented in the form of 9 submatrices (4.127) where $A_{1,1}$, $A_{1,2}$, $A_{2,1}$, $A_{2,2}$, $A_{3,1}$, $A_{3,2}$, are given by (4.128),(4.129),(4.131),(4.132),(4.134),(4.135) and $A_{1,3}$, $A_{2,3}$, $A_{3,3}$ are defined as follows

$$A_{1,3} = \begin{pmatrix} \tilde{B}nVx^{(1,1)} & \tilde{B}nVx^{(1,2)} & \cdots & \tilde{B}nVx^{(1,S)} \\ \tilde{B}nVx^{(2,1)} & \tilde{B}nVx^{(2,2)} & \cdots & \tilde{B}nVx^{(2,S)} \\ \vdots & \vdots & \ddots & \vdots \\ \tilde{B}nVx^{(N,1)} & \tilde{B}nVx^{(N,2)} & \cdots & \tilde{B}nVx^{(N,S)} \end{pmatrix} , \tag{4.144}$$

$$A_{2,3} = \begin{pmatrix} \tilde{B}nVy^{(1,1)} & \tilde{B}nVy^{(1,2)} & \cdots & \tilde{B}nVy^{(1,S)} \\ \tilde{B}nVy^{(2,1)} & \tilde{B}nVy^{(2,2)} & \cdots & \tilde{B}nVy^{(2,S)} \\ \vdots & \vdots & \ddots & \vdots \\ \tilde{B}nVy^{(N,1)} & \tilde{B}nVy^{(N,2)} & \cdots & \tilde{B}nVy^{(N,S)} \end{pmatrix} , \tag{4.145}$$

$$A_{3,3} = \begin{pmatrix} \tilde{B}nB^{(1,1)} & \tilde{B}nB^{(1,2)} & \dots & \tilde{B}nB^{(1,S)} \\ \tilde{B}nB^{(2,1)} & \tilde{B}nB^{(2,2)} & \dots & \tilde{B}nB^{(2,S)} \\ \vdots & \vdots & \ddots & \vdots \\ \tilde{B}nB^{(S,1)} & \tilde{B}nB^{(S,2)} & \dots & \tilde{B}nB^{(S,S)} \end{pmatrix} , \tag{4.146}$$

where coefficients $\tilde{B}nVx$, $\tilde{B}nVx$ and $\tilde{B}nB$ are given by

$$\tilde{B}nVx^{(i,j)} = 4\pi \frac{d}{dx_2} \hat{\mathrm{CF}}[\tilde{D} \to D] \int_{\vec{\Gamma}_i} \frac{dG(\vec{r_1}, \vec{\tilde{r}_2})}{d\vec{n}_{r_1}} dr_1 \ , \ \vec{r}_2 \in Q_j \ , \ 1 \le i \le S \ , \ 1 \le j \le N \ , \tag{4.147}$$

$$\tilde{B}nVy^{(i,j)} = 4\pi \frac{d}{dy_2} \hat{\mathrm{CF}}[\tilde{D} \to D] \int_{\vec{\Gamma}_i} \frac{dG(\vec{r_1}, \vec{\tilde{r}_2})}{d\vec{n}_{r_1}} dr_1 \ , \ \vec{r}_2 \in Q_j \ , \ 1 \le i \le S \ , \ 1 \le j \le N \ , \tag{4.148}$$

$$\tilde{B}nB^{(i,j)} = 4\pi \hat{\mathrm{CF}}[\tilde{D} \to D] \int_{\vec{\Gamma}_i} \frac{\partial \, G(\vec{r_1}, \vec{\tilde{r}_2})}{\partial \, \vec{n}_{r_1}} dr_1 \ , \ \vec{r}_2 \in \Gamma_j \ , \ 1 \le i \le S \ , \ 1 \le j \le S \ . \tag{4.149}$$

In the above equations $\vec{\tilde{r}_2} \in \tilde{D}$ is an image of $\vec{r} \in D$. Formulae (4.147) and (4.148) are the x and y projections for the Laplace operator placed in front of the conformal mapping operator $\hat{CF}$

$$(\tilde{B}nVx^{(i,j)}, \tilde{B}nVy^{(i,j)}) = 4\pi \nabla_{\vec{r}_2} \hat{\mathrm{CF}}[\tilde{D} \to D] \int_{\vec{\Gamma}_i} \frac{dG(\vec{r_1}, \vec{\tilde{r}_2})}{d\vec{n}_{r_1}} dr_1 \ , \tag{4.150}$$

where $\vec{r}_2 \in Q_j$, $1 \le i \le S$, $1 \le j \le N$. From the computational point of view the order of the operators in (4.150) is not desirable. Indeed the conformal mapping operator $\hat{CF}$ maps the value of the integral at a particular point, further differentiation requires the knowledge the value of the integral in the vicinity of that point which is numerically inefficient. In section 2.3.2 (2.48) it was shown how the Laplace operator can be moved inside the conformal mapping operator

$$(\tilde{B}nVx^{(i,j)}, \tilde{B}nVy^{(i,j)}) = 4\pi \hat{\mathrm{CF}}[\tilde{D} \to D] J_{\tilde{D} \to D}(\vec{\tilde{r}_2}) \int_{\vec{\Gamma}_i} \nabla_{\vec{\tilde{r}}_2} \frac{dG(\vec{r_1}, \vec{\tilde{r}_2})}{d\vec{n}_{r_1}} dr_1 \ , \tag{4.151}$$

where $J_{\tilde{D} \to D}(\vec{\tilde{r}_2})$ is the Jacobi matrix of the conformal mapping. Representation (4.151) is now symbolic: the conformal mapping operator in (4.151) does not scale or rotate the

vector on its right, this operation is done by the Jacobi matrix. $\hat{\mathrm{CF}}[\tilde{D} \to D]$ in (4.151) performs only a mapping function establishing correspondence between $\tilde{D}$ and D.

We now present a consequence of our approach that explains the efficiency of the presented method and proposes an approach to a general (including 3D) electrostatic problem having a doublesided boundary. We recall that we solve the electrostatic problem in the D domain with a doublesided boundary Γ (given by segment $(-1, 1)$). We use a conformal mapping to represent the electrostatic field in D due to the boundary sources represented in $\tilde{D}$

$$\phi(\vec{r_2}) = 4\pi \hat{\mathrm{CF}}[\tilde{D} \to D] \left\{ \int_{\tilde{\Gamma}} \frac{\partial\, G(\vec{r_1}, \vec{\tilde{r}_2})}{\partial\, \vec{n}_{r_1}} \tilde{\sigma}(\vec{r_1}) dr_1 \right\} \quad , \vec{r}_2 \in D \; , \; \vec{\tilde{r}}_2 \in \tilde{D} \; . \tag{4.152}$$

Using a piecewise constant representation of $\tilde{\sigma}$

$$\tilde{\sigma}(\vec{r}) = \tilde{\sigma}^{(i)} \; , \; \vec{r} \in \tilde{\Gamma}_i \; , \; 1 \leq i \leq S \tag{4.153}$$

and linearity of the conformal mapping operator we rewrite (4.152) as follows

$$\phi(\vec{r_2}) = 4\pi \sum_{i=1}^{S} \tilde{\sigma}^{(i)} \hat{\mathrm{CF}}[\tilde{D} \to D] \left\{ \int_{\tilde{\Gamma}_i} \frac{\partial\, G(\vec{r_1}, \vec{\tilde{r}_2})}{\partial\, \vec{n}_{r_1}} dr_1 \right\} \quad , \vec{r}_2 \in D \; , \; \vec{\tilde{r}}_2 \in \tilde{D} \; . \tag{4.154}$$

Note that the partial electrostatic potential

$$\phi_i(\vec{r_2}) = 4\pi \hat{\mathrm{CF}}[\tilde{D} \to D] \left\{ \int_{\tilde{\Gamma}_i} \frac{\partial\, G(\vec{r_1}, \vec{\tilde{r}_2})}{\partial\, \vec{n}_{r_1}} dr_1 \right\} \quad , \vec{r}_2 \in D \; , \; \vec{\tilde{r}}_2 \in \tilde{D} \tag{4.155}$$

is fixed in D and there exist corresponding single and double layers $\rho_i(\vec{r})$ and $\sigma_i(\vec{r})$, $\vec{r} \in \Gamma$ such that they establish ϕ_i in D (4.155)

$$\phi_i(\vec{r_2}) = 4\pi \int_{\Gamma} \sigma_i(\vec{r_1}) \frac{\partial\, G(\vec{r_1}, \vec{r_2})}{\partial\, \vec{n}_{r_1}} dr_1 + 4\pi \int_{\Gamma} \rho_i(\vec{r_1}) G(\vec{r_1}, \vec{r_2}) dr_1 \; , \; \forall \vec{r}_2 \in D \; . \tag{4.156}$$

These single and double layer densities $\rho_i(\vec{r})$ and $\sigma_i(\vec{r})$ are uniquely given by the following formulae

$$\rho_i(\vec{r}) = 2\pi \frac{\partial\, \phi_i(\vec{r})^{+}}{\partial\, \vec{n}} - 2\pi \frac{\partial\, \phi_i(\vec{r})^{-}}{\partial\, \vec{n}} \quad , \tag{4.157}$$

$$\sigma_i(\vec{r}) = 2\pi\phi_i(\vec{r})^+ - 2\pi\phi_i(\vec{r})^- \ . \tag{4.158}$$

Equations (4.156), (4.157) and (4.158) can be validated using a uniqueness of the solution of the boundary electrostatic problem. We rewrite (4.154) in the form

$$\phi(\vec{r_2}) = \sum_{i=1}^{S} \tilde{\sigma}^{(i)}\phi_i(\vec{r_2}) = \sum_{i=1}^{S} \tilde{\sigma}^{(i)} 4\pi \int_\Gamma \left\{ \sigma_i(\vec{r_1}) \frac{\partial\, G(\vec{r_1},\vec{r_2})}{\partial\, \vec{n}_{r_1}} + \rho_i(\vec{r_1}) G(\vec{r_1},\vec{r_2}) \right\} dr_1 \ , \ \vec{r_2} \in D \ , \tag{4.159}$$

and substitute into (4.142) to give

$$-\phi(\vec{r_2}) + \sum_{i=1}^{S} \tilde{\sigma}^{(i)} 4\pi \int_\Gamma \left\{ \sigma_i(\vec{r_1}) \frac{\partial\, G(\vec{r_1},\vec{r_2})}{\partial\, \vec{n}_{r_1}} + \rho_i(\vec{r_1}) G(\vec{r_1},\vec{r_2}) \right\} dr_1$$

$$- \int_Q (\epsilon(r_1) - 1) \nabla_{r_1}\phi(\vec{r_1}) \nabla_{r_1} G(\vec{r_1},\vec{r_2}) dr_1 = 0 \ , \vec{r_2} \in D \ . \tag{4.160}$$

Note that now (4.160) is entirely formulated in D and is well posed because it is an alternative form of another well posed problem. This shows that the method employing a conformal mapping is not the only efficient method to tackle a boundary electrostatic problem having a doublesided boundary. An alternative way is to find and use such $\rho_i(\vec{r})$ and $\sigma_i(\vec{r})$, $\vec{r} \in D$ and to represent an electrostatic potential in the form of series (4.159) such that the electrostatic integral equation (4.96) becomes well conditioned. In order to derive (4.160) we first employed the FEM with a piecewise constant approximation of the boundary sources. A similar analysis can be done analytically.

Functions $\rho_i(\vec{r})$ and $\sigma_i(\vec{r})$, $\vec{r} \in D$ obtained above can be developed for a wide range of types of the doublesided boundaries including 3D. This suggests methods avoiding the use of conformal mapping.

4.4 Appendix: Conjugate Gradient Algorithm for Solving Systems of Linear Equations.

The conjugate gradient method (cg-method) [43] is an elegant iterative method for solving a system of k linear equations (4.1)

$$A\vec{X} = \vec{Y} \ , \tag{4.161}$$

which is guaranteed to converge after k iterations in the absence of the round-off errors which is an advantage. The cg-method is originally proposed by Hestenes and Stiefel [43]. In this section we briefly outline the main operations involved into the cg-method.

The conjugate directions method or cd-method for solving (4.161) is to find conjugate vectors $\vec{p}_i$, $i = 1, 2, \cdots, k$ for A i.e vectors that satisfy

$$(\vec{p}_i, A\vec{p}_j) = \vec{p}_i^T A\vec{p}_j = 0 \ , \ \ i \neq j. \tag{4.162}$$

Note that the conjugate directions are linearly independent. Indeed if we assume that one of the conjugate directions $\vec{p}_{i_0} \neq 0$ is a linear superposition of the others then a direct consequence of (4.162) is $(\vec{p}_{i_0}, A\vec{p}_{i_0}) = 0$. Since A is positive definite we obtain $\vec{p}_{i_0} = 0$ which contradicts our original assumption. A solution to (4.161) is then given by

$$\vec{X} = \sum_{i=1}^{k} \frac{\vec{p}_i^T \vec{Y}}{\vec{p}_i^T A\vec{p}_i} \vec{p}_i \ . \tag{4.163}$$

Note that the eigenvectors for symmetric A is a particular case of the conjugate directions. Formulae (4.163) is similar to (4.25) where the eigenvalues are replaced by $\vec{p}_i^T A\vec{p}_i$.

The cg-method is a particular type of the cd-method (4.163). On each iteration of the cg-method a new conjugate direction $\vec{p}$ and new value of residual $\vec{r}$ are calculated. We now assume that A (4.161) is symmetric and positive definite. The choice of initial values for $\vec{p}$ and $\vec{r}$ is based on the initial guess of solution $\vec{X}_0$ for (4.161) which is arbitrary

$$\vec{p}_0 = \vec{r}_0 = \vec{Y} - A\vec{X}_0 \ . \tag{4.164}$$

The general routine for the cg-method is the following

$$a_i = \frac{(\vec{r}_i, \vec{p}_i)}{(\vec{p}_i, A\vec{p}_i)} \ , \tag{4.165}$$

$$\vec{X}_{i+1} = \vec{X}_i + a_i\vec{p}_i \ , \tag{4.166}$$

$$\vec{r}_{i+1} = \vec{r}_i - a_i A\vec{p}_i \ , \tag{4.167}$$

$$b_i = -\frac{(\vec{r}_{i+1}, A\vec{p}_i)}{(\vec{p}_i, A\vec{p}_i)} \ , \tag{4.168}$$

$$\vec{p}_{i+1} = \vec{r}_{i+1} + b_i\vec{p}_i \ . \tag{4.169}$$

Repeating (4.165), (4.166), (4.167), (4.168), (4.169) one monotonically decreases the error $|\vec{X}_i - \vec{X}_k|^2$, $i < k$ at each iteration and, in the absence of round-off errors, one obtains a solution after k iterations. In reality we cannot calculate the error because the final solution is unknown. Instead we use the square of the residual $\vec{r}_i$, $i = 1, 2, \cdots, k$ as a measure of the error. Note that that measure of the error is not absolutely reliable since it is possible to construct such cases where $|\vec{r}_i|^2$ increases after each iteration but after the final iteration becomes zero. We now present a conjugate gradient method [43] that allows to solve (4.161) where A is general non-symmetric and non-singular $\det|A| \neq 0$. The first iteration of the cg-method employs an initial guess of the solution $\vec{X}_0$ and is given by

$$\vec{r}_0 = \vec{Y} - A\vec{X}_0, \ \ \vec{p}_0 = A^T\vec{r}_0 \ . \tag{4.170}$$

The main iteration routine is given by

$$a_i = \frac{|A^T\vec{r}_i|^2}{|A\vec{p}_i|^2} \ , \tag{4.171}$$

$$\vec{X}_{i+1} = \vec{X}_i + \vec{p}_i \ , \tag{4.172}$$

$$\vec{r}_{i+1} = \vec{r}_i - a_i A\vec{p}_i \ , \tag{4.173}$$

$$b_i = \frac{|A^T \vec{R}_{i+1}|^2}{|A^T \vec{R}_i|^2} \ , \tag{4.174}$$

$$\vec{p}_{i+1} = A^T \vec{r}_{i+1} + b_i \vec{p}_i \ . \tag{4.175}$$

Because the algorithm (4.171)-(4.175) is suitable for any non-singular matrix it can also be used in the case of a symmetric matrix. However, from the numerical point of view algorithm (4.165)-(4.169) employs only one matrix-vector multiplication which is the most computationally intensive operation in the algorithm while (4.171)-(4.175) requires two matrix-vector multiplications per iteration. Thus (4.171)-(4.175) is about half speed compared to (4.165)-(4.169). Note that a larger number of matrix-vector multiplications also increases the round-off errors in the cg-method.

It is of interest to mention that the Gaussian elimination method of solving a nonsingular system (4.161) can also be seen as a particular implementation of the cd-method. From the cd-method perspective, the difference between the Gaussian elimination method and the cg-method is that the cg-method is building the conjugate directions using the orthogonal set of residual vectors $\vec{r}_i$, $i = 1, 2, \cdots, k$ while the Gaussian elimination method is building the conjugate gradients using a set of mutually orthogonal vectors $(1, 0, \cdots, 0)$, $(0, 1, \cdots, 0)$, $\cdots$, $(0, 0, \cdots, 1)$.

The cg-method is well suited to solving linear systems of algebraic equations arising in electrodynamic, electrostatic and other problems. A super linear convergence of the cg-method implemented in electromagnetic and other problems has been reported in [44], [45], [46], [47]. The cg-method is also employed in many inverse imaging problems [16], [17] [33].

4.5 Appendix: Analytical representation of the electrostatic integrals.

This section presents a list of boundary and volume integrals that can be encountered when applying the FEM to an electrostatic problem. These integrals allow calculation of

electrostatic field (both an electrostatic potential and an electrostatic field intensity) due to a uniform distribution of charge and dipole (single and double layer) on the segment boundary and in the rectangular domain. We obtained these integrals and verified their applicability to the electrostatic problem. The Green's Function which we integrate is a function of two arguments and is given by

$$G(\vec{r_1}, \vec{r_2}) = -\frac{1}{4\pi} \log[(x_1 - x_2)^2 + (y_1 - y_2)^2] \tag{4.176}$$

where $\vec{r_1}$ and $\vec{r_2}$ are the locations of the source and the observation point respectively.

4.5.1 Potential of volume charge

$$\int\int G dx_1 dy_1 = \frac{1}{4\pi}\left\{3(x_1 - x_2)(y_1 - y_2) - (x_1 - x_2)^2 \arctan\left[\frac{y_1 - y_2}{x_1 - x_2}\right] - \right.$$

$$\left. -(y_1 - y_2)^2 \arctan\left[\frac{x_1 - x_2}{y_1 - y_2}\right] - (x_1 - x_2)(y_1 - y_2) \log[(x_1 - x_2)^2 + (y_1 - y_2)^2]\right\} \tag{4.177}$$

4.5.2 Electric field of volume charge

$$\frac{d}{dx_2}\int\int G dx_1 dy_1 = \frac{1}{2\pi}\left\{(x_1 - x_2) \arctan\left[\frac{y_1 - y_2}{x_1 - x_2}\right] + \frac{1}{2}[y_1 - y_2] \log[(x_1 - x_2)^2 + (y_1 - y_2)^2]\right\} \tag{4.178}$$

$$\frac{d}{dy_2}\int\int G dx_1 dy_1 = \frac{1}{2\pi}\left\{(y_1 - y_2) \arctan\left[\frac{x_1 - x_2}{y_1 - y_2}\right] + \frac{1}{2}[x_1 - x_2] \log[(x_1 - x_2)^2 + (y_1 - y_2)^2]\right\} \tag{4.179}$$

4.5.3 Electric potential of volume dipole

$$\int\int \frac{d}{dy_1} G dx_1 dy_1 = -\frac{1}{2\pi}\left\{(y_1 - y_2) \arctan\left[\frac{x_1 - x_2}{y_1 - y_2}\right] + \frac{1}{2}[x_1 - x_2] \log[(x_1 - x_2)^2 + (y_1 - y_2)^2]\right\} \tag{4.180}$$

$$\int\int \frac{d}{dx_1} G dx_1 dy_1 = -\frac{1}{2\pi}\left\{(x_1 - x_2) \arctan\left[\frac{y_1 - y_2}{x_1 - x_2}\right] + \frac{1}{2}[y_1 - y_2] \log[(x_1 - x_2)^2 + (y_1 - y_2)^2]\right\} \tag{4.181}$$

4.5.4 Electric field of volume dipole

$$\frac{d}{dy_2}\int\int \frac{d}{dy_1} G dx_1 dy_1 = \frac{1}{2\pi} \arctan\left[\frac{x_1 - x_2}{y_1 - y_2}\right] \tag{4.182}$$

$$\frac{d}{dy_2}\int\int \frac{d}{dx_1} G dx_1 dy_1 = \frac{1}{4\pi} \log[(x_1 - x_2)^2 + (y_1 - y_2)^2] \tag{4.183}$$

$$\frac{d}{dx_2}\int\int \frac{d}{dy_1} G dx_1 dy_1 = \frac{1}{4\pi}\log[(x_1-x_2)^2+(y_1-y_2)^2] \tag{4.184}$$

$$\frac{d}{dx_2}\int\int \frac{d}{dx_1} G dx_1 dy_1 = \frac{1}{2\pi}\arctan\left[\frac{y_1-y_2}{x_1-x_2}\right] \tag{4.185}$$

4.5.5 Electric potential of boundary charge (single layer)

$$\int G dx_1 = -\frac{1}{2\pi}\left\{(y1-y2)\arctan\left[\frac{x_1-x_2}{y_1-y_2}\right]+(x1-x2)(-1+\frac{1}{2}\log[(x_1-x_2)^2+(y_1-y_2)^2])\right\} \tag{4.186}$$

4.5.6 Electric field of boundary charge

$$\frac{d}{dx_2}\int G dx_1 = \frac{1}{4\pi}\log[(x_1-x_2)^2+(y_1-y_2)^2] \tag{4.187}$$

$$\frac{d}{dy_2}\int G dx_1 = \frac{1}{2\pi}\arctan\left[\frac{x_1-x_2}{y_1-y_2}\right] \tag{4.188}$$

4.5.7 Electric potential of boundary dipoles (double layer)

$$\int \frac{dG}{dy_1} dx_1 = -\frac{1}{2\pi}\arctan\left[\frac{x_1-x_2}{y_1-y_2}\right] \tag{4.189}$$

4.5.8 Electric field of the boundary dipole (double layer)

$$\frac{d}{dx_2}\int \frac{dG}{dy_1} dx_1 = \frac{1}{2\pi}\frac{y_1-y_2}{(x_1-x_2)^2+(y1-y_2)^2} \tag{4.190}$$

$$\frac{d}{dy_2}\int \frac{dG}{dy_1} dx_1 = -\frac{1}{2\pi}\frac{x_1-x_2}{(x_1-x_2)^2+(y1-y_2)^2} \tag{4.191}$$

EXISTING IMAGING METHODS

The inverse electrostatic problem is to reconstruct the original medium using remote electrostatic field measurements. Another definition of the inverse electrostatic problem is to reconstruct the medium whose resultant electrostatic field in the observation points matches the measured data. The second definition does not require that the reconstructed medium matches the original one. Practical inverse algorithms are based on the second definition. If the inverse problem is properly set up then the reconstructed medium resembles the original one which justifies the imaging application. An important observation for us is that most inverse algorithms are based on the moment method [4], [39]. An exception would be the layer stripping method explained in section 5.2.8 [83], [84] and a method of reconstruction of a metal surface based on the analytical continuation of the field [48].

The governing equations for the electrostatic and inverse electrostatic problems are the same. They are presented in chapter 2. A principal difference between the electrostatic and inverse electrostatic problems is linearity. The electrostatic problem is linear. The inverse electrostatic problem, as we will see, is strongly non-linear: a distorted field due to multiple objects is not given by a superposition of the partial distorted fields and, in fact, is obstructed by the object-to-object interactions [38], [49].

At present there is no universal robust technique that can solve a non-linear inverse electrostatic problem for an arbitrary unknown medium. The Newton algorithm is, perhaps, the most common technique employed in various non-linear problems including the electrostatic inverse problem. Modifications of the Newton method lead to numerous implementations of the inverse problem such as a Born approximation [98], [18] or algorithms employing the source type integral equations [55], [65].

Since the inverse electrostatic problem is non-linear there is no analysis tool that would guarantee convergence of the inverse problem, unless the unknown object is restricted

to provide one. The non-linear problem is often approached as a black box where the researcher relies upon the previous experience and intuition.

Classification of inverse electrodynamic and electrostatic problems is a challenging task. The efficiency of the inverse problem depends on many factors such as what type of governing equation is used and how it is implemented numerically [50]. The type and number of the incident fields[1], position and number of the sensors also influence the speed and precision of the inverse method [41], [89], [65], [33]. Finally the *a priori* information imposed on the scattering object and the way the object is modelled [49] are also important and are surveyed in section 5.1. Popular inverse methods are presented in section 5.2.

5.1 Various scatterer models employed in the imaging algorithms

We have stated in previous chapters that an imaging problem has many formulations. Even when we limit our discussion to the inverse electrostatic problem and require the knowledge of the Dirichlet-to-Neumann map in order to obtain a unique solution, the imaging problem may be formulated in various ways which can be classified, for example, according to the *a priori* information known about the scatterer. Very often these *a priori* constraints relating to the scatterer are employed in the scatterer model. In this section we introduce various models for the scattering object that have been widely used in the imaging problem. Due to the similarity of the inverse problems based on different physical effects we do not limit ourselves to the electrostatic case alone.

5.1.1 Conducting Scatterers.

There are several reasons why conductive scatterers have attracted researchers during the study of the imaging problem in the 1970s and early 1980s. First of all, the uniqueness of the solution for the perfectly conductive scatterers is easier to prove and can even be established intuitively (section 3.3). Another reason is, for example, that the 2D or 3D

[1] In electrodynamics the illuminating fields and measurements are more versatile than in electrostatics. An incomplete list involves near and far field measurements, including and excluding the phase from the data, multifrequency illumination, plane/non-plane incident waves etc. [54]

conducting scatterer can be often represented using 1D or 2D functions respectively giving the profile (boundary) of the scatterer. The low frequency electric field does not penetrate deeply into the conductive scatterer which allows one to reduce the analysis of interaction between the scatterer and the electric field to boundary effects. Even in electrodynamics the Leontovich boundary condition on the surface of a lossy metal accurately describes interaction of the electromagnetic field and the scatterer without involving interior field analysis of the skin effect. An imaging method that seeks to reconstruct the shape of the unknown homogeneous scatterer is referred to as a profile inversion problem [48], [92]. The possibility of using a lower dimensional model for the scatterer reduces computation time and memory demand making the imaging problem more suitable for practical applications.

Multiple connectivity for the conducting scatterer

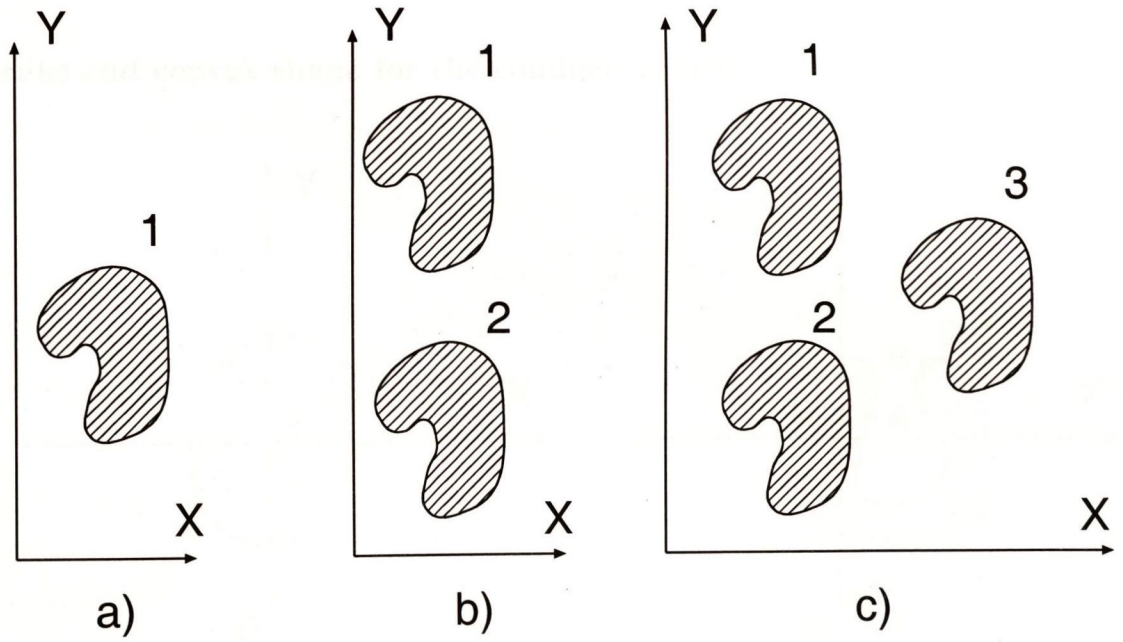

Figure 5.1: The 2D conducting scatterers with different connectivity property.

One of the ways to define the surface of the metal scatterer is to parameterise it analytically which can be done in different ways. We consider 2D representations for the metal scatterers or alternatively a cross-section of infinitely long cylinders. A difficulty encoun-

tered while representing the surface of the conducting scatterer is multiple connectivity of the scatterer. Usually assuming that the scatterer is composed of multiple individual parts one employs a scatterer model that

1. simulates the object of a given degree of connectivity,
2. makes an assumption regarding the approximate location of the individual simply connected parts of the scatterer.

Figure 5.1 illustrates the simply connected, 2-connected and 3-connected cross-sections for the 2D metal scatterer. The model of the simply connected 2D scatterer shown in figure 5.1 (a) is employed in the inverse problem, for example, in [51], [37]. In more complicated cases the surface of the conducting scatterer can be 2-connected or 3-connected (fig. 5.1 (b),(c)). Analysis of the imaging problem employing both the simply connected and 2-connected scatterers is presented in [48], [38]. The 3-connected model for the metal scatterer is rarely encountered in periodicals and is studied, for example, in [40].

Starlike and convex shape for the conducting scatterer

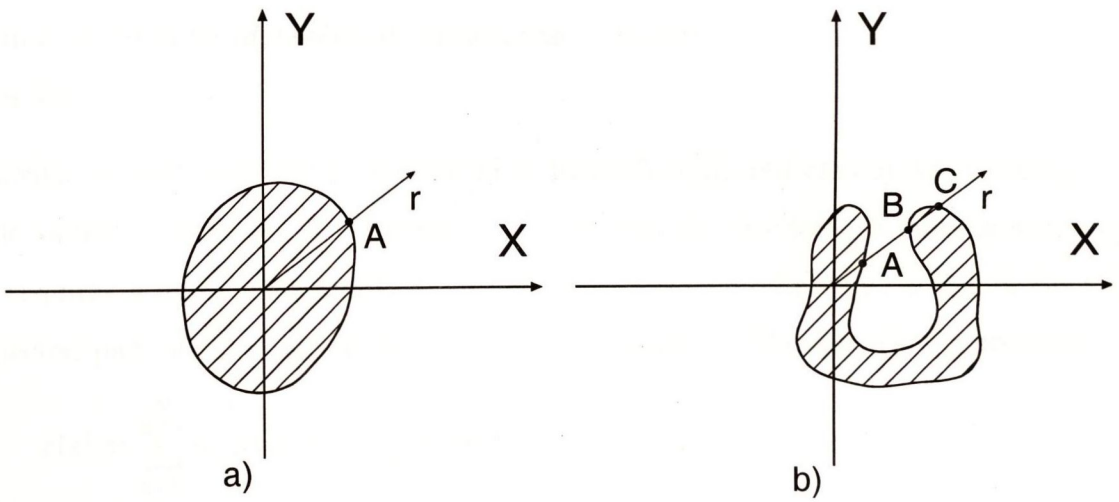

Figure 5.2: Non-starlike shaped (a) and star-like shaped (b) boundary for the conducting scatterer.

Representation of the boundary for the simply connected parts of the multi-connected metal scatterers can be further classified according to complexity. We now explain the terms of the starlike and non-starlike (convex) shapes for the simply connected boundary.

We reduce our discussion to 2D space and consider the shape of the simply connected scatterer in the polar co-ordinates. Let the origin of the polar co-ordinates be placed inside the scatterer and let Θ be a polar angle indicating a direction in the 2D space. If the shape of the scatterer can be given by a real single-valued function of Θ then the shape is non-starlike. If the shape of the scatterer cannot be expressed as a single-valued function of Θ then the shape is referred to as a starlike shape.

The scatterer having a non-starlike shape [38], [37] is shown in figure 5.2 (a). One can see that any vector r starting an the origin will cross the boundary of the object in only one point A which allows to parameterise the boundary in the form $(F(\Theta), \Theta)$. $F(\Theta)$ is a real single-valued function of Θ given, for example, by the truncated Fourier expansion as follows [38]

$$F_i(\Theta_i) = \sum_{n=0}^{N} a_{in} \cos(n\Theta_i) + \sum_{n=1}^{N} b_{in} \sin(n\Theta_i) \ , \tag{5.1}$$

where i is the index of the simply connected part of the conducting object. The locations of the simply-connected parts for the multiple scatterer are usually assumed to be known and may be given by $(d_1 \cos(\psi), d_1 \sin(\psi))$ and $(-d_2 \cos(\psi), -d_2 \sin(\psi))$ in the xy Cartesian plane [38].

A starlike shaped scatterer is illustrated in figure 5.2 (b) and cannot be represented as a single valued function of Θ. Obviously that type of the scatterer is more general and in fact requires a more complicated analytical representation. Let the surface of the simply connected part of the scatterer be parameterised using s. The following expressions

$$x(s) = \sum_{n=0}^{N} a_n \cos(ns) + \sum_{n=1}^{N} b_n \sin(ns) \tag{5.2}$$

$$y(s) = \sum_{n=0}^{N} a'_n \cos(ns) + \sum_{n=1}^{N} b'_n \sin(ns) \tag{5.3}$$

are chosen to represent the boundary in [40]. Cartesian co-ordinate system in (5.2) allows to overcome the difficulty associated with having a multi-valued function $F(\Theta)$ that arises in polar co-ordinates.

5.1.2 Low Dimensional Inverse Imaging Applications

We have considered several examples of the inverse problem defined as of reconstruction of the boundary of the unknown conducting scatterer. These examples deal with various ways of the boundary parameterisation. In the problem of determination of the position of the human hand in the 3D [2] the human hand is modelled as a conducting scatterer of a known shape. Since the shape and connectivity properties are *a priori* known, only the location of the human hand or, alternatively, three Cartesian co-ordinates are subject to reconstruction. We refer to this inverse problem as a positioning inverse problem which is a very low dimensional inverse imaging problem.

Uniqueness of the solution for the low dimensional imaging problem

The uniqueness of the solution of the positioning inverse problem is studied in [2]. [2] also presents a probabilistic approach to the stability analysis of the positioning techniques in the noisy environment. We now explain how the uniqueness of the solution is approached in [2].

Consider the problem of the determination of the co-ordinates of a small conducting sphere of radius r using electrostatic field measurements. In particular we assume that r is small compared to the curvature of the incident field so that the sphere can be seen as being placed in a quasi-homogeneous field. In that case, the distorted field produced by the sphere is given by a dipole field (see appendix 3.7). Let several capacitive sensors (each being composed of one transmit and one receive electrodes) be used to establish and measure the field. We refer to each capacitive sensor as a TxRx sensor. We also assume that the response $S(d, \Theta)$ of the TxRx sensor, where d is the distance between the sensor and the sphere and Θ is the polar angle, is known and monotonic in d.

Figure 5.3 shows two TxRx sensors and a metal sphere. The dashed lines in figure 5.3 show the locus of equal sensor response for a given metal sphere. If the response of two sensors in figure 5.3 is experimentally measured to be S_1^0 and S_2^0 then the conducting sphere must be located on the equi-response curves $S_1 = S_1^0$ and $S_2 = S_2^0$. Intersection of these

curves gives the location for the sphere of known radius that solves the inverse positioning problem. The analysis of uniqueness of solution for the positioning inverse electrostatic problem is reduced to the analysis of whether or not there is a single intersection point for the corresponding equi-response curves. Properly arranged sensors can allow the avoidance of ambiguous or multiple solutions for the scatterer.

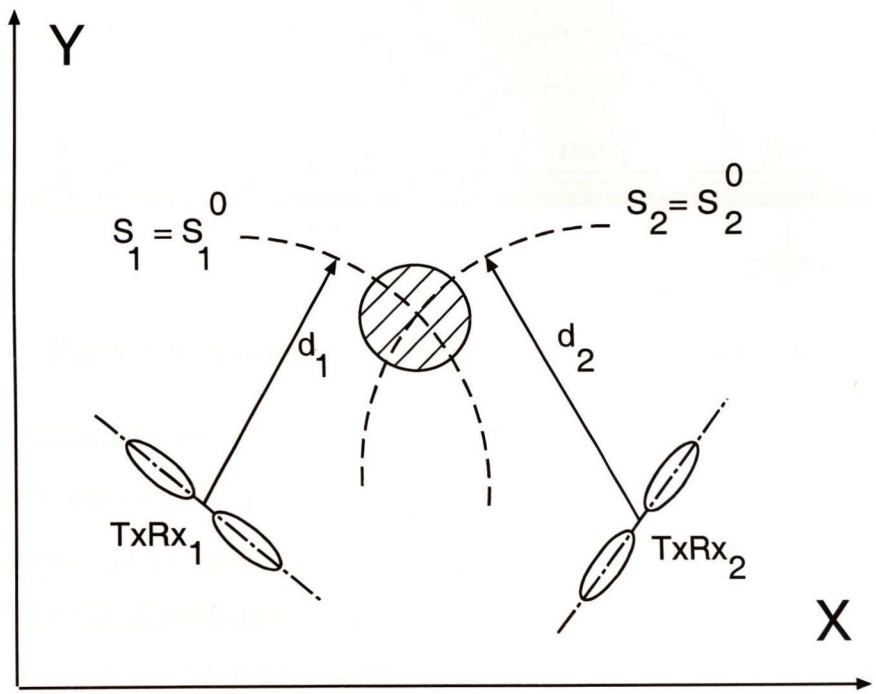

Figure 5.3: Two TxRx sensors and a metal sphere.

One of the important applications of the low dimensional imaging problem is human-computer interface. A novel mouse for 3D virtual navigation has been designed and assembled in the Media Laboratory, Massachusetts Institute of Technology [2]. In [2] the transmit and receive electrodes with the ground plane underneath are approximated by the dipole antennas. The human hand in the quasi-electrostatic field of the dipole antennas is approximated by a metal sphere such that when polarized also produces a dipole field (section 3.7). Using three sensor readings the location of the hand is calculated without solving Laplace's equation. The capacitive low dimensional imaging techniques are referred to as the Electric Field Sensing (EFS) [1], [2], [3].

The first hardware prototype that was designed in the course of this project was capable of collecting data for a low dimensional 2D inverse electrostatic problem and is shown in

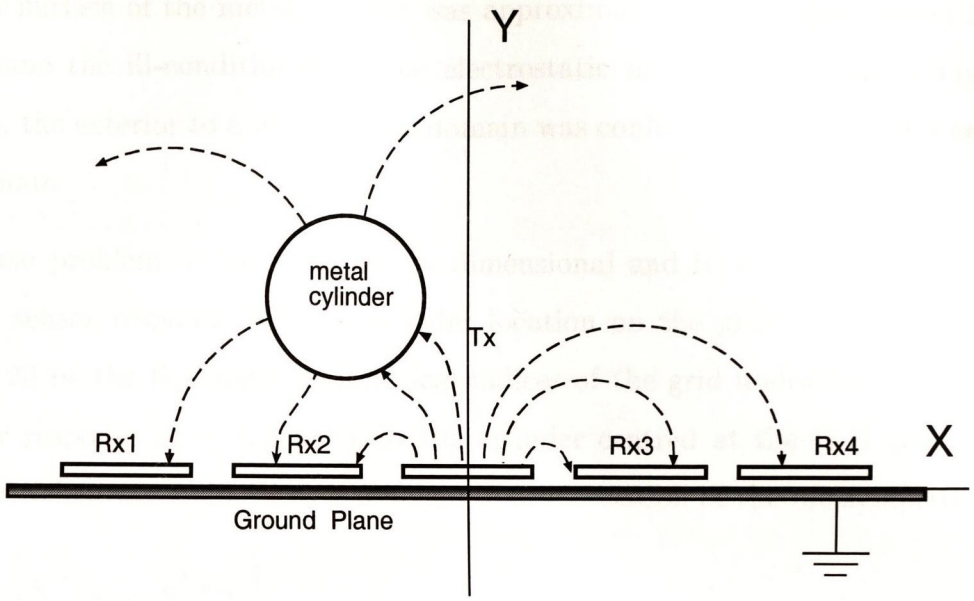

Figure 5.4: A cross-section of the 2D capacitive sensor array.

figure 5.4. In this experiment the sensor data was collected and processed using a numerical algorithm which was estimating the x and y co-ordinates of the scatterer and displaying them in real time. The purpose of that prototype was to demonstrate the advantages and limitations of the low dimensional imaging techniques to our sponsor the Hotron Company Ltd. and to gain experience in EFS techniques.

We now discuss the experiment in more detail. The sensor array that we implemented (figure 5.4) consisted of one transmit (Tx), four receive (Rx) and one ground electrodes. We employed only one incident field and hence the imaging problem was similar to the inverse source problem introduced in section 3.1. We measured mutual capacitance between Tx and Rx electrodes sequentially for each Rx using a method presented in section 2.8. In particular a low frequency oscillating potential was applied to the Tx electrode (1V pk-pk, 300kHz) and the current induced in each of the Rx electrodes was rectified, digitised and collected by the PC. The 2D scatterer was chosen to be a metal cylinder of a fixed large radius such that the corresponding distorted field is no longer given by a dipole field.

In order to simplify the imaging problem the cylinder was assumed to be located inside a rectangular domain above the sensor array. The centre of the cylinder was constrained to be on a grid of 20x40 nodes. In order to calculate the sensor response we employed the BEM

where the surface of the metal cylinder was approximated by a polygon having 20 edges. To overcome the ill-conditioning of the electrostatic problem employing a doublesided boundary, the exterior to a line segment domain was conformally mapped onto an interior circle domain.

The inverse problem in figure 5.4 is low dimensional and it is feasible to simulate and store the sensor response for each cylinder location on the grid. Let $i = 1, ..., 40$ and $j = 1, ..., 20$ be the horizontal and vertical indices of the grid nodes and let $S_k^{(i,j)}$ be the k^{th} sensor response ($k = 1, 2, 3, 4.$) for the cylinder centred at the (i,j) grid node. The imaging problem was reduced to a problem of minimisation of the mean squared error

$$\min_{i,j} \left[\sum_{k=1}^{4} (S_k - S_k^{(i,j)})^2 \right] , \tag{5.4}$$

where S_k, $k = 1, 2, 3, 4$ are the experimental measurements. The algorithm minimising (5.4) estimated $\sum_{k=1}^{4} (S_k - S_k^{(i,j)})^2$ for each of the 800 nodes using the pre-stored values of $S_k^{(i,j)}$. The minimum was then obtained by a direct comparison of the error.

The inverse positioning technique that we implemented reconstructs only the co-ordinates of the metal cylinder. The list of parameters parameterising the cylindrical object can be extended to the radius, dielectric permittivity, elongation and spatial orientation (for the ellipse). Adding extra variables to the scatterer's model increases the complexity of the imaging problem making it impossible to pre-store the sensor response. The stability of the inverse method based on minimisation of (5.4) is then determined by whether or not (5.4) has local minimum(s) as opposed to an absolute minimum. When there are local minima, the numerical solution to the inverse problem largely depends on the initial guess.

5.1.3 Representation of the scatterer based on the representation of the field

A unique approach to the inverse problem of reconstruction of the metal scatterer is proposed in [48]. This approach does not suggest any particular representation of the lossy conducting body. Unlike many other inverse methods, the final representation of the scatterer in [48] is determined by the representation of the electrodynamic field. In order to reconstruct the scatterer analytical continuation of the electrodynamic field is

employed. The electrodynamic field is further analysed by seeking such a surface where the Leontovich boundary condition [6] might be satisfied. Once such a boundary is found it is admitted as the surface of the unknown metal lossy scatterer.

5.1.4 Multi-wire representation of the 2D conducting scatterer

The unknown conducting scatterer in the inverse electrodynamic or electrostatic problem does not have to be restricted to having a smooth boundary (5.1), (5.2) because the inverse problem is ill-posed in such way that small perturbations of the surface of the unknown conducting scatterer are hidden in the measured noise.

This suggested a method of representing the unknown conducting object without parameterisation of its boundary [96]. Instead, a decomposition into smaller metal scatterers is used. The advantage of this method is that an approximate location of the scatterer is not required *a priori*. Let Ω be a 2D reconstruction domain i.e. a domain where the unknown scatterer has to be reconstructed. According to [96] we discretise Ω on a regular grid with grid locations r_i, $i = 1, 2, ..., N$. In figure 5.5 Ω is shown as a rectangular domain. Let the unknown conducting scatterer be approximately decomposed into smaller conducting cylinders (or subscatterers) on this grid and its shape be given by the binary local shape function γ

$$\gamma_i = \begin{cases} 1, & r_i \text{ belongs to the scatterer} \\ 0, & r_i \text{ elsewhere,} \end{cases}, \tag{5.5}$$

where i is the index on the grid where the wire (subscatterer) is placed. The local shape function (5.5) of the original scatterer is *a priori* binary. In the reconstructed image the local shape function does not need to be binary and may vary from 0 to 1 representing the cross-section of the wire relative to the size of the corresponding cell.

If we use sufficiently thin wires such that they cover only small part of the corresponding cells then according to section 3.7 the model in figure 5.5 will behave as a dielectric. If we constrain the imaging algorithm to having a binary representation of the local shape function then, obviously, the recovered image will always be high-contrast. A binary local

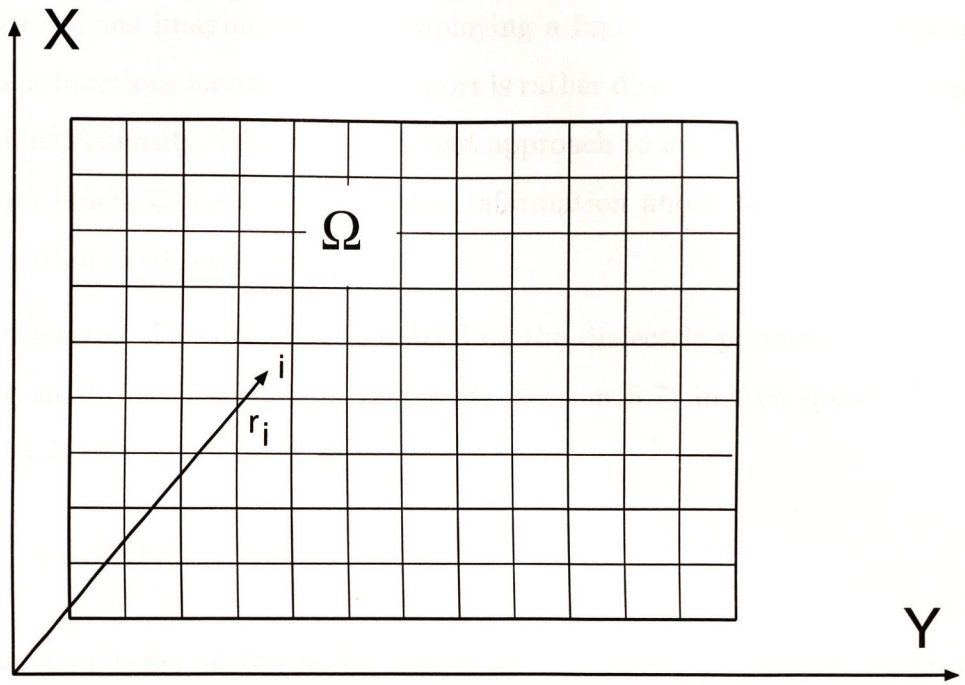

Figure 5.5: The Ω domain discretised on a regular greed.

shape function may significantly complicate the convergence of the Born Iterative Method (section 5.2.3) and is not a good choice.

The type of the local shape function (5.5) is not reported in [96], yet the presented reconstructed images of the metal scatterer are smooth. Hence we conclude that a continuous local shape function has been employed in [96].

Stable operation of an inverse algorithm employing a similar multiwire model is presented in [32]. In particular, the multiwire model has been applied to the problem of reconstruction of a large metal cylinder. The corresponding reconstructed image has a sharp boundary aligned with the surface of the original scatterer while the interior area of the reconstructed image is almost hollow which we attribute to the regularization method.

5.1.5 Modelling dielectric scatterers

The inverse electrostatic and electrodynamic problems employing low contrast dielectrics are quasi-linear. Such inverse problems can benefit from analytical methods and basis

functions having a large support such as Fourier series, for example. Due to the strong non-linearity of the imaging problem employing a high contrast dielectric the use of the general basis functions having a large support is rather disadvantageous due to a redundant computational intensity. Instead, an efficient approach to modelling the dielectric medium is to choose functions containing *a priori* information about the object or to use basis functions with a small support.

We have discussed the possibility of modelling the dielectric permittivity of the medium by placing small metal spheres of radius R_0 (section 3.7) in free space. The dielectric permittivity is then given by (3.43)

$$\epsilon = 1 + 4\pi d R_0^2 \ , \tag{5.6}$$

where d is the density of the metal insertions. This model is similar to the previously introduced multiwire representation of the conducting objects and it has not been applied to the problem of reconstruction of the dielectric medium.

Image representation for Earth exploration problems

A particular case of the piecewise constant distribution of the dielectric permittivity when the subdomains containing an unknown homogeneous dielectric are assumed to be very large is illustrated in figure 5.6. An electrostatic problem for that type of the dielectric distribution can be split into several boundary problems each defined for a given subdomain. The model in figure 5.6 is particularly suited for the Earth exploration and representation of the stratified medium [23], [20]. There is a special method for solving electrostatic and electrodynamic problems in such a medium. This method is called a Numerical Mode Matching method or just a NMM method [53], [52], [21], [22],[25].

Piecewise constant distribution of dielectrics

The piecewise constant representation of the dielectric permittivity is suitable for almost all imaging applications where no *a priori* information is imposed on the scatterer [41],

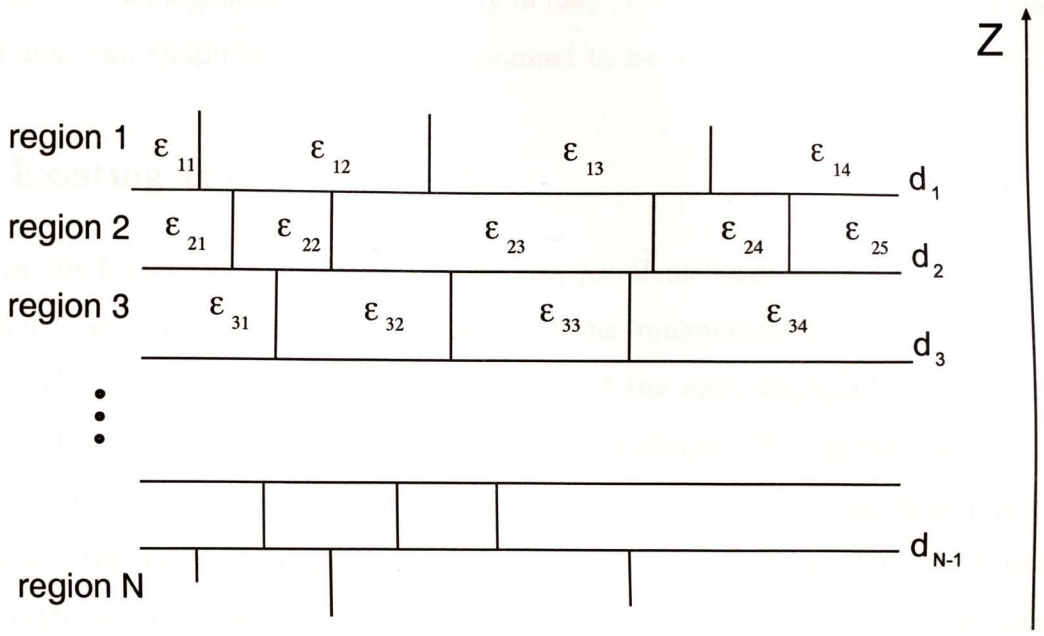

Figure 5.6: A cross-section of the stratified media.

[65], [18], [19], [30], [31], [73], [16]. This model has many advantages. Firstly, it is well suited for the Finite Element Method. Secondly this model can be efficiently employed in the powerful inversion algorithms such as the Born Iterative Method (BIM) and the distorted BIM.

5.1.6 Modelling the hybrid metal-dielectric scatterers

A combination of the piecewise constant representation of the unknown dielectric and a known metal insertion has been successfully employed in the inverse electrodynamic problem [89], [4]. The dielectric permittivity ϵ in [89] is complex. Using electrodynamic measurements both the real and imaginary parts of ϵ are reconstructed. In [4] the 3D dielectric tensor permittivity is successfully recovered. Note that the orientation of the axis for the dielectric tensor permittivity in [4] is predetermined *a priori* which reduces the generality of the inverse problem formulation.

In section 5.1.1 we have discussed electrodynamic inverse problems where the unknown

surface of the conducting scatterer is parameterised. A similar parameterisation technique is applied to a homogeneous dielectric body in [39]. The dielectric and magnetic constants for the unknown shape body in [39] are assumed to be known.

5.2 Existing Inverse Methods

We have not found any examples of the inverse problems employing electrostatic fields[2]. We found few examples of implementation of the magnetostatic[3] [23] and resistivity[4] [17],[52],[53] inverse problems while the number of the electrodynamic inverse problems that have been published in various journals is substantial. The electrodynamic inverse problems are similar to the electrostatic inverse problems and are therefore important to us. Some of the methods employed in the electrodynamic inverse problem such as a Born Iterative Method presented in section 5.2.3 can be employed in electrostatics without modification. There are many electrodynamic inverse methods that do not and, in fact, cannot have analogies in electrostatics. To mention a few, these are the problem of reconstruction of an unknown object in a waveguide [91], an inverse problem employing multi-frequency illumination [94] and X-ray tomography. In this section we present those inverse methods that are useful (can be employed) or potentially useful (requiring additional study) to the electrostatic problem that we study. In order to avoid multiple definitions of the electrostatic inverse problem in later sections we formulate it now.

[2]Here we do not consider low dimensional quasi-electrostatic problems presented in [1], [2], [3] because these problems are not based on the study of the electrostatic equations and are rather empirical.

[3]The magnetostatic and electrostatic problems are governed by the same equations. In magnetostatics the magnetic field is established and measured using current loops or magnetic dipole antennas as opposed to capacitive arrays in electrostatics.

[4]The resistivity inversion problem and electrostatic inverse problem are governed by the same equations. In the resistivity inversion problem the static potentials and currents are applied, injected and measured on the boundary of the unknown object in order to reconstruct its resistivity distribution.

5.2.1 Electrostatic Inverse Imaging Problem

We consider the 2D inverse electrostatic problem of the reconstruction of an unknown dielectric susceptibility $\chi = \epsilon - 1$ having a support in a finite domain Q. It is common to bound the support for χ in the inverse problem [96], [65] i.e. to assume that ϵ is unity outside Q. For convenience let Q be a bounding rectangle of the support of χ. Usually Q is chosen within the sensor range to ensure good quality of the reconstructed image. We call Q the reconstruction domain. Note that the shape of Q does not constrain ϵ in the sense that ϵ can be represented in the form of multiple parts having arbitrary position, location, shape and local dielectric distribution.

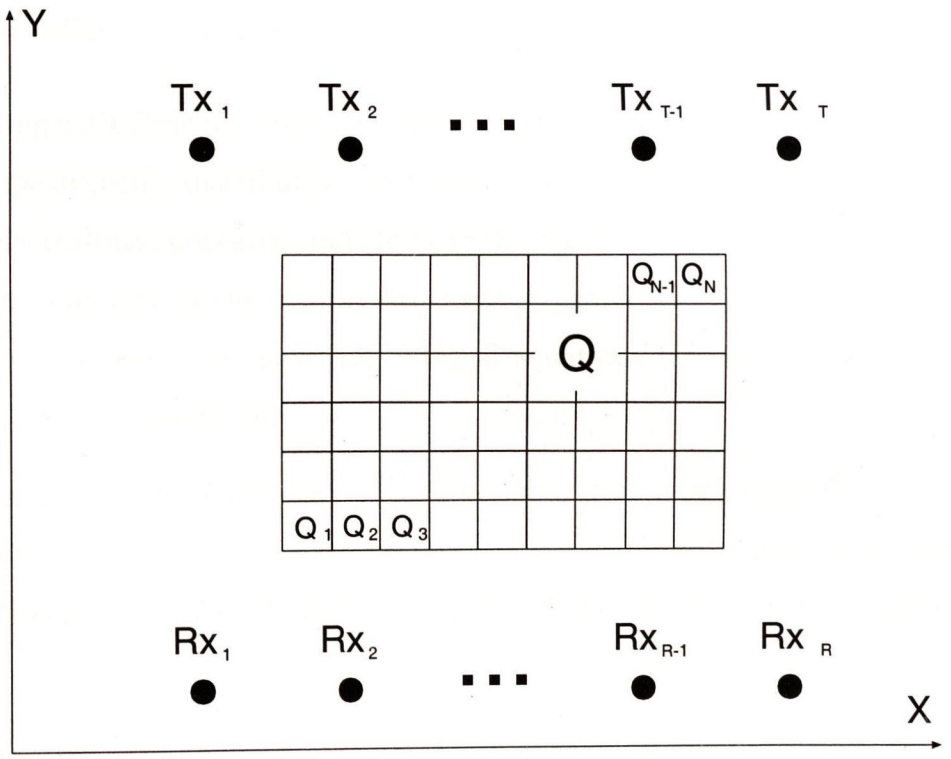

Figure 5.7: Domain of reconstruction with transmit (Tx) and receive (Rx) electrodes.

We assume that ϵ in Q is sequentially placed in T electrostatic fields which we call incident fields. Here for convenience we inherit the terminology such as incident or distorted field

from electrodynamics. For illustrative purpose we assume that the incident electrostatic fields are produced by charges $Tx_1, Tx_2, \cdots, Tx_n$ as shown in figure 5.7. The total electrostatic potential ϕ_{tot} inside and outside Q is given as a superposition of the incident ϕ_{inc} and distorted ϕ_{dist} potentials

$$\phi_{tot}^{(i)}(\vec{r}) = \phi_{inc}^{(i)}(\vec{r}) + \phi_{dist}^{(i)}(\vec{r}) \ , \ i = 1, 2, \cdots, T \ , \tag{5.7}$$

where i is the index for the incident field. The corresponding electric field intensity $\vec{E}_{tot}$ is given by

$$\vec{E}_{tot}^{(i)}(\vec{r}) = \vec{E}_{inc}^{(i)}(\vec{r}) + \vec{E}_{dist}^{(i)}(\vec{r}) \ , \ i = 1, 2, \cdots, T \tag{5.8}$$

and is related to ϕ_{tot} through

$$\vec{E}^{(i)} = -\nabla\phi^{(i)} \ , \ i = 1, 2, \cdots, T \ . \tag{5.9}$$

When dealing with Dirichlet boundary inverse electrostatic problems having a nonhomogeneous volume dielectric distribution the corresponding governing integral equations employ both the electrostatic potential and electrostatic field intensity. In this section we do not introduce a boundary in the inverse electrostatic problem (figure 5.7) which gives us an opportunity to express the governing integral equations for that problem employing an electrostatic field intensity only.

Let the electrostatic field intensity $\vec{E}_{tot}^{(i)}(\vec{r})$ be measured at R points $\vec{r}^{(j)}$, $j = 1, 2, \cdots, R$ using sensors $Rx_1, Rx_2, \cdots, Rx_R$ as shown in figure 5.7. The total number of measurements of $\vec{E}_{tot}^{(i)}(\vec{r}^{(j)})$ is given by TR 2D vectors or $2TR$ scalars. We denote the vector sensor data by

$$\vec{S}_{orig}^{(i,j)} = \vec{E}_{tot}^{(i)}(\vec{r}^{(j)}) \ , \ i = 1, 2, \cdots, T \ , \ j = 1, 2, \cdots, R \ . \tag{5.10}$$

The knowledge of $\vec{E}_{tot}$ and $\vec{E}_{dist}$ is equivalent because $\vec{E}_{tot}$ and $\vec{E}_{dist}$ are related through (5.8) and $\vec{E}_{inc}$ in (5.8) is known. Thus we can use an alternative to (5.10) data representation

$$\vec{S}_{orig}^{*(i,j)} = \vec{E}_{dist}^{(i)}(\vec{r}^{(j)}) \ , \ i = 1, 2, \cdots, T \ , \ j = 1, 2, \cdots, R \ . \tag{5.11}$$

The inverse electrostatic problem is to find a dielectric permittivity distribution ϵ (or χ) that makes the corresponding sensor readings equal to the original (measured) ones (5.10). If the inverse problem is properly set up in terms of the type and position of Tx and Rx then the reconstructed ϵ is likely to resemble or closely coincide with the true one. We now present analytical governing equations for the inverse problem in figure 5.7 and then postulate them in a numerical form by means of the FEM.

Applying the governing electrostatic integral equation (2.78) to the problem in figure 5.7 gives

$$\phi_{tot}^{(i)}(\vec{r}) = \phi_{inc}^{(i)}(\vec{r}) - \int_Q \chi(\vec{r}')\nabla_{r'}\phi_{tot}^{(i)}(\vec{r}')\nabla_{r'}G(\vec{r}',\vec{r})d\vec{r}' \ , \ \forall\vec{r} \ , \ , \tag{5.12}$$

$$i = 1, 2, \cdots, T \ ,$$

where the boundary integral is omitted (zero), the volume integral representing the field due to the volume charge ρ_V is replaced by ϕ_{inc}, i is the index of the incident field and χ is an arbitrary dielectric susceptibility distribution in the reconstruction domain Q. Applying operator $-\nabla_r$ to (5.12) gives an integral equation that does not contain electrostatic potential ϕ

$$\vec{E}_{tot}^{(i)}(\vec{r}) = \vec{E}_{inc}^{(i)}(\vec{r}) - \int_Q \chi(\vec{r}')\vec{E}_{tot}^{(i)}(\vec{r}')\nabla_{r'}\nabla_r G(\vec{r}',\vec{r})d\vec{r}' \ , \tag{5.13}$$

$$i = 1, 2, \cdots, T \ ,$$

where i is the incident field index. We call (5.13) a state equation. Substituting (5.13) in (5.10) gives

$$\vec{S}^{(i,j)} = \vec{E}_{inc}^{(i)}(\vec{r}^{(j)}) - \int_Q \chi(\vec{r}')\vec{E}_{tot}^{(i)}(\vec{r}')\nabla_{r'}\nabla_r G(\vec{r}',\vec{r}^{(j)})d\vec{r}' \ , \tag{5.14}$$

$$i = 1, 2, \cdots, T \ , \ j = 1, 2, \cdots, R$$

which we refer to as an inversion equation. The names "state" and "inversion" equations are justified by the following concept employed in many inverse methods such as the BIM

[18]: the dielectric susceptibility is given as a solution to (5.14) while the electrostatic field $\vec{E}_{tot}$ in (5.14) is uniquely related to χ according to (5.13). Substituting $\chi = 0$ in (5.14) gives $\vec{E}_{tot}^{(i)} = \vec{E}_{inc}^{(i)}$ which results in sensor readings $\vec{S}_0^{(i,j)} = \vec{E}_{inc}^{(i)}(\vec{r}^{(j)})$, $i = 1, 2, \cdots, T$, $j = 1, 2, \cdots, R$ (5.10). Substituting $\vec{S}_0^{(i,j)}$ in (5.14) gives

$$\vec{S}^{(i,j)} = \vec{S}_0^{(i,j)} - \int_Q \chi(\vec{r}')\vec{E}_{tot}^{(i)}(\vec{r}')\nabla_{r'}\nabla_r G(\vec{r}', \vec{r}^{(j)})d\vec{r}' \ , \tag{5.15}$$

$$i = 1, 2, \cdots, T \ , \ j = 1, 2, \cdots, R \ .$$

Note that $\vec{S}_*^{(i,j)} = \vec{S}^{(i,j)} - \vec{S}_0^{(i,j)}$, $i = 1, 2, \cdots, T$, $j = 1, 2, \cdots, R$ and (5.15) has an alternative form

$$\vec{S}_*^{(i,j)} = -\int_Q \chi(\vec{r}')\vec{E}_{tot}^{(i)}(\vec{r}')\nabla_{r'}\nabla_r G(\vec{r}', \vec{r}^{(j)})d\vec{r}' \ , \tag{5.16}$$

$$i = 1, 2, \cdots, T \ , \ j = 1, 2, \cdots, R \ .$$

We now use the FEM in the form explained in section 4.2.2 to put (5.13), (5.15) and (5.16) in a numerical form. Dividing Q into N subdomains ΔQ_i, $i = 1, 2, \cdots, N$, representing the electrostatic fields $\vec{E}$ and dielectric distribution χ by a constant for each ΔQ_i, $i = 1, 2, \cdots, N$ and employing a point matching technique we rewrite (5.13), (5.15) and (5.16) in the form of the algebraic equations

$$[\vec{E}_{tot}^{(i)}] = [\vec{E}_{inc}^{(i)}] + [H_{int}][\chi][\vec{E}_{tot}^{(i)}] \ , \tag{5.17}$$

$$[\vec{S}^{(i)}] = [\vec{S}_0] + [H_{ext}][\chi][\vec{E}_{tot}^{(i)}] \ , \tag{5.18}$$

where $i = 1, 2, \cdots, T$ is an incident electrostatic field index and

$[\chi]$ is an NxN diagonal matrix composed of the local susceptibility values;

$[\vec{E}_{tot}^{(i)}]$ and $[\vec{E}_{inc}^{(i)}]$ are N dimensional vectors composed of local values of $\vec{E}_{tot}^{(i)}$ and $\vec{E}_{inc}^{(i)}$ in Q;

$[\vec{S}^{(i)}]$ and $[\vec{S}_0]$ are R dimensional vectors;

$[H_{int}]$ is a NxN dimensional matrix having components

$$h_{int\ i,j} = -\int_{\Delta Q_j} \nabla_{r'}\nabla_r G(\vec{r}', \vec{r})d\vec{r}' \ , \ \vec{r} \in \Delta Q_i \ , \ 1 \leq i, j \leq N \ ; \tag{5.19}$$

$[H_{ext}]$ is an RxN dimensional matrix having components

$$h_{ext\ i,j} = -\int_{\Delta Q_j} \nabla_{r'}\nabla_r G(\vec{r}', \vec{r}) d\vec{r}' \ , \ \vec{r} = \vec{r}^{(i)} \ , \ 1 \leq i \leq R \ , \ 1 \leq j \leq N \ , \tag{5.20}$$

where $\vec{r}^{(i)}$, $i = 1, 2, \cdots, R$ are sensor locations and $j = 1, 2, \cdots, N$ is the incident field index.

Note that in this section we use advanced linear algebra structures. Each component of the N dimensional vector $[\vec{E}]$ is a 2D vector representing an electric field intencity $(E_{x_i}, E_{y_i})^T$, $i = 1, 2, \cdots, N$ for the corresponding cell in Q. This allows us to avoid the use of the conventional bulky $2N$ dimensional vectors given by $(E_{x_1}, E_{x_2}, \cdots, E_{x_N}, E_{y_1}, E_{y_2}, \cdots, E_{y_N})$. In our nomenclature operator $\nabla_{r'}\nabla_r$ in (5.19),(5.20) acts upon a scalar resulting in a 2x2 matrix given by

$$\nabla_{r'}\nabla_r = \begin{pmatrix} \frac{\partial^2}{\partial x \partial x'} & \frac{\partial^2}{\partial x \partial y'} \\ \frac{\partial^2}{\partial y \partial x'} & \frac{\partial^2}{\partial y \partial y'} \end{pmatrix} \tag{5.21}$$

Thus $[H_{int}]$ and $[H_{int}]$ define matrices, the components of which are 2x2 matrices.

We now present source type integral equations which are an alternative representation of the state and inversion equations (5.13), (5.14). Despite the fact that the source type integral equations are analytically equivalent to (5.13), (5.14), they lead to different numerical implementations of the inverse problem. The electrostatic field $\vec{E}^{(i)}_{tot}$, $i = 1, 2, \cdots, T$ polarizes dielectric χ in Q. The polarization vector $\vec{P}^{(i)}$ is then given by

$$\vec{P}^{(i)} = \frac{\chi \vec{E}^{(i)}_{tot}}{4\pi} \ , \tag{5.22}$$

where $i = 1, 2, \cdots, T$ is the index of the incident field. To obtain source type integral equations we substitute (5.22) in (5.13), (5.14) to give

$$\vec{E}^{(i)}_{tot}(\vec{r}) = \vec{E}^{(i)}_{inc}(\vec{r}) - 4\pi \int_Q \vec{P}^{(i)}(\vec{r}')\nabla_{r'}\nabla_r G(\vec{r}', \vec{r}) d\vec{r}' \ , \tag{5.23}$$

$$i = 1, 2, \cdots, T \ .$$

Substituting (5.13) in (5.10) gives

$$\vec{S}^{(i,j)} = \vec{E}^{(i)}_{inc}(\vec{r}^{(j)}) - 4\pi \int_Q \vec{P}^{(i)}(\vec{r}')\nabla_{r'}\nabla_r G(\vec{r}', \vec{r}^{(j)})d\vec{r}' \ , \tag{5.24}$$

$$i = 1, 2, \cdots, T \ .$$

Note that (5.24) does not include the electrostatic field intensity or dielectric susceptibility in Q. Instead (5.24) defines an inverse source problem which is according to section 3.1.2 does not have a unique solution. The null space to (5.24) is given by sources which produce a zero field outside their support[5] [35]. Using the FEM (5.23), (5.24) yields the following algebraic equations

$$[\vec{E}^{(i)}_{tot}] = [\vec{E}^{(i)}_{inc}] + 4\pi[H_{int}][\vec{P}^{(i)}] \ , \tag{5.25}$$

$$[\vec{S}^{(i)}] = [\vec{S}_0] + 4\pi[H_{ext}][\vec{P}^{(i)}] \tag{5.26}$$

where $[\vec{P}^{(i)}]$ is an N dimensional vector and $i = 1, 2, \cdots, T$ is the index of incident field. Equation (5.22) in the algebraic form is given by

$$[\vec{P}^{(i)}] = \frac{1}{4\pi}[\chi][\vec{E}^{(i)}_{tot}] \ , \ i = 1, 2, \cdots, T \ , \tag{5.27}$$

where $[\chi]$ is a matrix and $[\vec{E}^{(i)}_{tot}]$ is a vector.

5.2.2 Resolution of ϵ

The question of what ϵ resolution the inverse method returns does not have a simple answer. The total number of the scalar data that can be collected using the measurement setup in figure 5.7 is given by $2TR$. In the electrostatic inverse problem we treat $K = 2TR$ as a measure of the effective dimensionality for ϵ that can be achieved by processing the sensor data. We refer to that type of resolution constraint as a TR-resolution.

[5] Non-radiating sources in electrodynamics.

According to figure 5.7 the FEM employs N subdomains of Q to model a piecewise constant ϵ. Thus a piecewise model for ϵ is obviously another resolution limiting factor which we call an FEM-resolution. Usually the FEM-resolution is chosen to be higher than the TR-resolution. This is done from the practical point of view to avoid domination of the FEM-resolution. However if the incident fields are "similar" then $K = 2TR$ may overestimate the effective number of the linearly independent input data $\vec{S}^{(i,j)}_{orig}$ for the inversion algorithm. In that case the FEM-resolution is made smaller than $K = 2TR$.

Numerical Estimate of Error for Inverse Electrostatic Imaging Problem

The quality of the inverse method is usually judged using a Mean Squared Error (MSE) function [18]. However depending on the function that the MSE takes as an argument we obtain different criteria for the inverse method precision. We now discuss two ways of defining the error of the inverse method.

Applying the relative MSE function to ϵ gives

$$MSE_{\epsilon} = \sqrt{\frac{(\vec{\epsilon}_{orig} - \vec{\epsilon}_{approx})^2}{\vec{\epsilon}_{orig}{}^2}} \ , \tag{5.28}$$

where $\vec{\epsilon}_{orig}$ and $\vec{\epsilon}_{approx}$ are the vectors representing the original and reconstructed dielectric distributions respectively. Error (5.28) is useful for theoretical analysis of the quality of the inverse method when $\vec{\epsilon}_{orig}$ is known. However in practical applications $\vec{\epsilon}_{orig}$ has to be found and hence is unknown. The MSE for ϵ (5.28) is not suited for control of the iterative inverse routines presented in later sections.

The use of the MSE_{ϵ} as a quality measure for the inverse problem has other disadvantages particularly relevant to the electrostatic inverse problems that we solve. In electrodynamic inverse problems where the unknown scatterer is, for example, illuminated by sufficiently many plane electromagnetic waves approaching from various directions the quality of the reconstructed ϵ is relatively homogeneous over the reconstruction domain [89], [95] and hence the MSE_{ϵ} (5.28) gives good measure of the error. Analysing numerical results of chapter 6 we find that the absolute error $|\vec{\epsilon}_{orig} - \vec{\epsilon}_{approx}|$ of the reconstructed image in the

electrostatic inverse problem that we solve is strongly inhomogeneous: the resolution of the inverse method particularly deteriorates as we move away from the boundary Γ containing electrodes. The discrepancy between $\vec{\epsilon}_{orig}$ and $\vec{\epsilon}_{approx}$ dominates in the far from Γ area and hence the MSE_ϵ is primarily determined by the distortion in that area. While the ϵ resolution is high in the area near Γ (which is also of practical importance) the MSE_ϵ gives an inadequate estimate.

An alternative method to evaluate the error is to apply the MSE function to the sensor readings $\vec{S}$

$$MSE_\phi = \sqrt{\sum_{i,j} \frac{(\vec{S}^{(i,j)}_{orig} - \vec{S}^{(i,j)}_{approx})^2}{\vec{S}^{(i,j)\ 2}_{orig}}} \ , \tag{5.29}$$

where $\vec{S}_{orig}$ and $\vec{S}_{approx}$ are the vectors representing the original and obtained in the reconstruction routine sensor measurements respectively. Note that the problem of minimisation of the MSE_ϕ (5.29) leads to the moment method.

The MSE_ϵ as a measure of the error of inversion problem has been used, for example, in [17], [18], [50] and [65]. Both the MSE_ϵ and MSE_ϕ have been implemented in [33], [19], where the MSE_ϕ is referred to as a relative residual error (RRE). Only the MSE_ϕ is employed in [94]. The MSE_ϵ and MSE_ϕ are omitted and only plots of the reconstructed dielectric are presented for visual analysis in [16], [23], [96]. Thus the choice of the error analysis is left to the researcher's discretion. We solve the inverse electrostatic problem implementing the moment method; because the MSE_ϕ is intrinsic to this method it is also fundamental to our algorithms.

The inverse problem is strongly ill-posed in such way that information regarding the high order spatial oscillations of ϵ is hidden in the noise of the sensor data [19]. In the example in figure 3.1 of chapter 3 we present two dielectric objects producing identical distorted fields. These two objects can be seeing as being identical from the imaging perspective as they contain identical information about the shape and local average of ϵ. Considering objects a and b in figure 3.1 as the original and approximate ones and substituting their

ϵ and produced sensor data into the formulae for MSE_ϵ and MSE_ϕ respectively gives

$$\lim_{d\to 0} MSE_\epsilon = \infty \ . \tag{5.30}$$

$$\lim_{d\to 0} MSE_\phi = 0 \ . \tag{5.31}$$

5.2.3 Born Approximation, Born Iterative Method and Distorted Born Iterative Method

The Born Iterative Method [18], [33] is a well tested algorithm for electrodynamic problems. The first iteration of the Born Iterative Method is given by a first order Born approximation or just a Born approximation. The Distorted Born iterative Method [19] is a variation of the Born Iterative Method and its first iteration is also given by the Born approximation. Fast and reliable convergence of the BIM/DBIM based methods is reported for electrodynamic inverse problem [33], resistivity inversion problem [17] and inversion of induction problem [23]. We employ the DBIM to solve an inverse electrostatic problem in chapter 6. Therefore we present the BIM based methods in detail.

Born approximation.

We consider an inverse electrostatic problem in figure 5.7 governed by the state equation (5.13) and inversion equation (5.14). The unknown dielectric χ_{orig} is illuminated by T incident waves and the corresponding total electrostatic field intensity is measured in R locations (5.10).

Applying the FEM to (5.13) and (5.14) casts these equations into a system of algebraic equations (5.17) and (5.18)

$$[\vec{E}^{(i)}_{tot}] = [\vec{E}^{(i)}_{inc}] + [H_{int}][\chi][\vec{E}^{(i)}_{tot}] \ , \tag{5.32}$$

$$[\vec{S}^{(i)}_{orig}] = [\vec{S}_0] + [H_{ext}][\chi][\vec{E}^{(i)}_{tot}] \ . \tag{5.33}$$

where $i = 1, 2, \cdots, T$ is the index of the incident electrostatic field.

Under the Born approximation the dielectric susceptibility χ_{upd} is assumed to be sufficiently small [50] so that we can neglect the second term in (5.32) to give

$$[\vec{E}^{(i)}_{tot}] = [\vec{E}^{(i)}_{inc}] \ , \ i = 1, 2, \cdots, T \ . \tag{5.34}$$

Substituting (5.34) into (5.33) gives

$$[\vec{S}^{(i)}_{orig}] = [\vec{S}_0] + [H_{ext}][\chi_{upd}][\vec{E}^{(i)}_{inc}] \ , \ i = 1, 2, \cdots, T \ . \tag{5.35}$$

Algebraic equations (5.35) are solved for χ by minimising the squared error

$$\min_{\chi} \sum_{i=1}^{T} \left\{ [\vec{S}^{(i)}_{orig}] - [\vec{S}_0] - [H_{ext}][\chi_{upd}][\vec{E}^{(i)}_{inc}] \right\}^2 \ . \tag{5.36}$$

Matrix $[H_{ext}]$ in (5.35) is smooth which indicates at ill-conditioning of the system of algebraic equations (5.35). Instability of (5.35) becomes worse if matrix $[H_{ext}]$ is rectangular [65], [42]; its dimension is given by RxN. If $R < 2N$ which is common for inverse problems a solution to (5.35) has a null space and if $R > 2N$ then a solution to (5.36) generally does not exist. Note that a solution to (5.36) always exists even when (5.35) does not have a solution. The ill-conditioning in (5.36) is usually circumvented by employing a regularization technique [98]. We replace problem (5.36) by the following problem of minimisation of the cost function

$$\min_{\chi} \left(\sum_{i=1}^{T} \left\{ [\vec{S}^{(i)}_{orig}] - [\vec{S}_0] - [H_{ext}][\chi_{upd}][\vec{E}^{(i)}_{inc}] \right\}^2 + \gamma^2 [\chi_{upd}]^2 \right) \ , \tag{5.37}$$

where γ is a regularization parameter. On how to choose γ the reader is referred to section 4.1.3. A solution to (5.36) or, in practical applications, (5.37) gives a Born approximation for the inverse electrostatic problem.

The Born approximation does not update the values of the sensor readings $\vec{S}_{upd} = \vec{S}_{approx}$ required for the MSE_ϕ (5.29). In order to find $\vec{S}_{upd}$ we first substitute $[\chi_{upd}]$ (obtained from (5.37)) into (5.32) and solve (5.32) to find an update (a first order approximation)

of the total electrostatic field intensity in Q $[\vec{E}^{(i)}_{tot\ upd}]$, $i = 1, 2, \cdots, T$. Substituting $[\chi_{upd}]$ and $[\vec{E}^{(i)}_{tot\ upd}]$ in (5.33) gives $[\vec{S}^{(i)}_{upd}]$ for the MSE_ϕ

$$[\vec{S}^{(i)}_{upd}] = [\vec{S}_0] + [H_{ext}][\vec{E}^{(i)}_{tot\ upd}][\chi_{upd}] \ , \ i = 1, 2, \cdots, T \ . \tag{5.38}$$

Born Iterative Method

Although the Born approximation is among the oldest inverse methods the Born Iterative Method has only relatively recently been proposed by Wang and Chew [18]. The BIM starts by making an initial guess for $\epsilon = \epsilon_{ini}$. Once the guess is made we calculate the initial electric field intensity for each of the illuminating fields in Q solving (5.17)

$$[\vec{E}^{(i)}_{tot\ ini}] = [\vec{E}^{(i)}_{inc}] + [H_{int}][\chi_{ini}][\vec{E}^{(i)}_{tot\ ini}] \ , \tag{5.39}$$

where $i = 1, 2, \cdots, T$ is the index of the incident electrostatic field and $\chi_{ini} = \epsilon_{ini} - 1$. Then we calculate the sensor response (5.18) for the initial distribution χ_{ini}

$$[\vec{S}^{(i)}_{ini}] = [\vec{S}_0] + [H_{ext}][\chi_{ini}][\vec{E}^{(i)}_{tot\ ini}] \ , \ i = 1, 2, \cdots, T \ . \tag{5.40}$$

We need to know the sensor readings (5.40) in order to estimate the MSE_ϕ. If the MSE_ϕ is below a given level (for example 0.01) then the BIM is terminated.

To find the next approximation $[\chi_{upd}]$ for the dielectric susceptibility one linearises equation (5.18) assuming that the total electrostatic field intensity in Q is given by a solution to (5.39)

$$[\vec{S}^{(i)}_{orig}] = [\vec{S}_0] + [H_{ext}][\chi_{upd}][\vec{E}^{(i)}_{tot\ ini}] \ , \ i = 1, 2, \cdots, T \ . \tag{5.41}$$

For convenience we subtract (5.40) from (5.41) to give

$$[\vec{S}^{(i)}_{orig}] - [\vec{S}^{(i)}_{ini}] = [H_{ext}]\delta[\chi_{upd}][\vec{E}^{(i)}_{tot\ ini}] \ , \ i = 1, 2, \cdots, T \ , \tag{5.42}$$

where

$$\delta\chi_{upd} = \chi_{upd} - \chi_{ini} \ . \tag{5.43}$$

Problem (5.42) is solved by minimising a cost function and circumventing the ill-conditioning by using a regularization technique

$$\min_{\chi} \left(\sum_{i=1}^{T} \left\{ [\vec{S}_{orig}^{(i)}] - [\vec{S}_{ini}] - [H_{ext}]\delta[\chi_{upd}][\vec{E}_{ini}^{(i)}] \right\}^2 + \gamma^2 \delta[\chi_{upd}]^2 \right) , \tag{5.44}$$

where γ is a regularization parameter. The updated value of the dielectric susceptibility χ_{upd} in then given by (5.43). This accomplishes the Born iteration. The next Born iteration takes the updated value of χ as an initial guess and repeats the same steps starting from (5.39). A series of the reconstructed dielectric distributions in the BIM $\epsilon_{ini}, \epsilon_1, \epsilon_2, \cdots$ is called a Born series.

As we have already mentioned the first iteration in the BIM is a Born approximation. This is true if the initial guess for the unknown dielectric permittivity ϵ_{ini} in Q is unity. We choose $\epsilon_{ini} = 1$ when there is no *a priori* information for the initial guess. The unity initial value for the dielectric permittivity is beneficial from the computational time perspective because avoids solving T electrostatic problems (5.39) in the first BIM iteration by recording the incident electrostatic field (which is a field in a free space) in the memory of the computer.

Distorted Born Iterative Method

The Distorted BIM [19] is similar to the BIM. It starts with an initial guess of ϵ_{ini} and then the total electrostatic field intensity $\vec{E}_{tot}^{(i)}$, $i = 1, 2, \cdots, T$ is calculated using (5.39) for each incident field i. The sensor response is then updated using (5.40). The MSE_{ϕ} is then calculated and a decision is made whether to continue the algorithm.

The next step in the DBIM is different from the one in the BIM. Before we formulate the subsequent step in the DBIM we develop a physical interpretation for the linearised inversion equation (5.42). Once we have fixed the total electrostatic field intensity as a background field in (5.42) the knowledge of $\delta[\chi_{upd}]$ which we aim to find is equivalent to the knowledge of the polarization vector $\delta\vec{P}^{(i)}$ given by

$$\delta[\vec{P}^{(i)}] = \frac{1}{4\pi}[\chi_{upd}][\vec{E}_{tot\,ini}^{(i)}] \ , \quad i = 1, 2, \cdots, T \tag{5.45}$$

Substituting (5.45) in (5.42) gives equivalent to (5.45) algebraic equations

$$[\vec{S}^{(i)}_{orig}] - [\vec{S}^{(i)}_{ini}] = 4\pi[H_{ext}]\delta[\vec{P}^{(i)}] \ , \ i = 1, 2, \cdots, T \ . \tag{5.46}$$

The right hand side in (5.46) represents an electric field intensity $\delta[\vec{E}^{(i)}_{tot}]$

$$\delta[\vec{E}^{(i)}_{tot}] = 4\pi[H_{ext}]\delta[\vec{P}^{(i)}] \ , \ i = 1, 2, \cdots, T \tag{5.47}$$

produced by a volume dipole (given by a volume polarization vector) in a free space. The left hand side in (5.46) represents the current sensor reading mismatch which is zero in the ideal case. This mismatch is compensated by the field produced by $\delta[\vec{P}^{(i)}]$ (5.47)

$$[\vec{S}^{(i)}_{orig}] - [\vec{S}^{(i)}_{ini}] = \delta[\vec{E}^{(i)}_{tot}] \ , \ i = 1, 2, \cdots, T. \tag{5.48}$$

While (5.47) gives an electrostatic field intensity $\delta[\vec{E}^{(i)}_{tot}]$ due to $\delta\vec{P}^{(i)}$ in free space, an improved technique would be to use a field in (5.48) established in ϵ_{ini} which is the latest approximation of ϵ_{orig} at this stage. The DBIM replaces (5.46) by

$$[\vec{S}^{(i)}_{orig}] - [\vec{S}^{(i)}_{ini}] = 4\pi[H^*_{ext}]\delta[\vec{P}^{(i)}] \ , \ i = 1, 2, \cdots, T \ . \tag{5.49}$$

where matrix $[H^*_{ext}]$ is presented later in (5.52).

Let $G_\epsilon(\vec{r}_1, \vec{r}_2)$ be the Green's function for a dielectric $\epsilon = \epsilon_{ini}$. The governing electrostatic integral equation employing $G_\epsilon(\vec{r}_1, \vec{r}_2)$ is derived in section 2.4 (2.80). Applying (2.80) to an electrostatic problem in figure 5.7 where the incident electrostatic field is zero and the volume dipole $\delta\vec{P}^{(i)}$ is placed in a background dielectric $\epsilon = \epsilon_{ini}$ yields

$$\delta\vec{E}^{(i)}_{tot}(\vec{r}) = -4\pi \int_S \nabla_r \nabla_{r'} G_\epsilon(\vec{r}', \vec{r}) \delta\vec{P}^{(i)}(\vec{r}') dr' \ , \ i = 1, 2, \cdots, T \ . \tag{5.50}$$

The corresponding numerical form for (5.50) within the context of the FEM is given by

$$\delta[\vec{E}^{(i)}_{tot}] = 4\pi[H^*_{ext}]\delta[\vec{P}^{(i)}] \ , \ i = 1, 2, \cdots, T \ , \tag{5.51}$$

where components for $[H^*_{ext}]$ are defined as

$$h^*_{ext\ i,j} = -\int_{\Delta Q_j} \nabla_{r'} \nabla_r G_\epsilon(\vec{r}', \vec{r}^{(i)}) d\vec{r}' \ , \ 1 \le i \le R \ , \ 1 \le j \le N \ , \tag{5.52}$$

where $\vec{r}^{(i)}$ are sensor locations and index j is the index of incident field.

Substituting (5.51) in (5.48) gives (5.49). We now present an efficient method for calculating coefficients (5.52) in (5.49) [19]. According to the reciprocity theorem (2.28) we can swap the arguments for the Greens's function in (5.52) to give

$$h^*_{ext\ i,j} = -\int_{\Delta Q_j} \nabla_{r'}\nabla_r G_\epsilon(\vec{r}^{(i)}, \vec{r}')d\vec{r}' \ , \ 1 \le i \le R \ , \ 1 \le j \le N \ , \tag{5.53}$$

The Green's function $G_\epsilon(\vec{r}^{(i)}, \vec{r})$, $\vec{r} \in Q$ in (5.53), where $\vec{r}^{(i)}$ is fixed at the ith sensor electrode location $i = 1, 2, \cdots, R$, is an electrostatic potential $\phi^{(i)}_{aux}$ of $\frac{1}{4\pi}$ charge in $\vec{r}^{(i)}$ measured in Q. Thus $G_\epsilon(\vec{r}^{(i)}, \vec{r}')$, $i = 1, 2, \cdots, R$ can be obtained by solving R electrostatic problems in Q. This can be accomplished by representing $\phi^{(i)}_{aux}$ in piecewise constant form in Q and further using the FEM. The operator $\nabla_{r'}\nabla_r$ (5.21) can be calculated employing a three point perturbation for $\vec{r}^{(i)}$ and two point finite difference scheme for $\vec{r} \in Q$ for example. This increases the number of auxiliary (additional) electrostatic problems to $3R$ and is not a preferred way of calculating $h^*_{ext\ i,j}$.

We now present a method for calculating $h^*_{ext\ i,j}$ employing only $2R$ auxiliary electrostatic problems [19]. We consider vector $\nabla_r G_\epsilon(\vec{r}^{(i)}, \vec{r}')$, $\vec{r}' \in Q$. The x and y components of this vector are the electrostatic potentials of the x- and y-oriented dipoles with dipole moment $\frac{1}{4\pi}$ located in $\vec{r}^{(i)}$. Applying $-\nabla_{r'}$ to these potentials gives the corresponding electrostatic field intensities. Thus in order to calculate $-\nabla_{r'}\nabla_r G_\epsilon(\vec{r}^{(i)}, \vec{r}')$ we need to find electrostatic field intensities $\vec{E}^{x(i)}_{aux}(\vec{r}')$ and $\vec{E}^{y(i)}_{aux}(\vec{r}')$, $\vec{r}' \in Q$ due to the x- and y-oriented $\frac{1}{4\pi}$ dipoles placed in the ith sensor location $\vec{r}^{(i)}$. Matrix $\nabla_{r'}\nabla_r G_\epsilon(\vec{r}^{(i)}, \vec{r}')$ is then given by

$$-\nabla_{r'}\nabla_r G_\epsilon(\vec{r}^{(i)}, \vec{r}') = \begin{pmatrix} \vec{E}^{x(i)}_{aux\ x}(\vec{r}') & \vec{E}^{x(i)}_{aux\ y}(\vec{r}') \\ \vec{E}^{y(i)}_{aux\ x}(\vec{r}') & \vec{E}^{y(i)}_{aux\ y}(\vec{r}') \end{pmatrix} \ . \tag{5.54}$$

Substituting (5.54) in (5.53) gives coefficients for $[H^*_{ext}]$ in (5.49)

$$h^*_{ext\ i,j} = \begin{pmatrix} \vec{E}^{x(i)}_{aux\ x}(\vec{r}') & \vec{E}^{x(i)}_{aux\ y}(\vec{r}') \\ \vec{E}^{y(i)}_{aux\ x}(\vec{r}') & \vec{E}^{y(i)}_{aux\ y}(\vec{r}') \end{pmatrix} \cdot ||\Delta Q_j|| \ , \ \vec{r}' \in \Delta Q_j \ , \tag{5.55}$$

$1 \le i \le R$, $1 \le j \le N$, where $||\Delta Q_j||$ is a metric measure of ΔQ_j.

We now proceed with the DBIM algorithm. Similarly to the BIM (5.49)

$$[\vec{S}^{(i)}_{orig}] - [\vec{S}^{(i)}_{ini}] = [H^*_{ext}]\delta[\chi_{upd}][\vec{E}^{(i)}_{tot\ ini}] \ , \ i = 1, 2, \cdots, T \tag{5.56}$$

are solved for $\delta[\chi_{upd}]$ by minimising a cost function employing a regularization method

$$\min_{\chi} \left(\sum_{i=1}^{T} \left\{ [\vec{S}^{(i)}_{orig}] - [\vec{S}_{ini}] - [H^*_{ext}]\delta[\chi_{upd}][\vec{E}^{(i)}_{ini}] \right\}^2 + \gamma^2 \delta[\chi_{upd}]^2 \right) \ . \tag{5.57}$$

The updated dielectric susceptibility χ_{upd} is then given by

$$\chi_{upd} = \chi_{ini} + \delta\chi_{upd} \tag{5.58}$$

and is taken as an initial guess for the next DBIM iteration.

Each iteration of the DBIM employs $T+2R$ electrostatic problems while the BIM iteration employs only T electrostatic problems. Despite of the higher computational intensity of each iteration, the DBIM has strategic advantages over the BIM. The DBIM method converges in fewer iterations than the BIM to a significantly higher precision (more than one order of magnitude of improvement) [33]. The BIM is more robust to noise while the DBIM reconstructs sharper images [19]. The laboratory experiments conducted within the course of this project demonstrated that the hardware noise is significantly below the level critical for practical imaging applications. At the same time high precision and sharp reconstructed images make the DBIM ideal for our applications.

5.2.4 Inverse Electrostatic Problem Employing Newton-Kantorovich (NK) Method

In this section we present a Newton-Kantorovich algorithm applied to electrostatic problem. This algorithm proved to be efficient in electrodynamic inverse problems [95], [39], [38] while, to the best of our knowledge, the electrostatic inverse problem has not been tackled using this method.

The unknown object in [39] and [38] is modelled by parametrising the boundary of the homogeneous dielectric and metal respectively. The *a priori* rough locations of the unknown

objects are also assumed in [39] and [38]. Parametrising the boundary is not the preferred way of modelling a dielectric object in our electrostatic inverse imaging application because our goal is to solve the inverse problem with the minimum of *a priori* constraints. Contrary to [39], [38] Joaschimovicz *et al* [95] employ a piecewise constant representation of an arbitrary dielectric in the given reconstruction domain. The FEM is then employed in [95] to solve integral electromagnetic equations which makes [95] particularly valuable for our study. We now re-formulate the method proposed in [95] for an electrostatic case.

Consider an inverse imaging problem in figure 5.7. The unknown dielectric susceptibility χ has its support in Q and is illuminated by T electrostatic fields $\vec{E}^{(i)}_{inc}$, $i = 1, 2, \cdots, T$. The corresponding scattered fields $\vec{E}^{(i)}_{dist}$, $i = 1, 2, \cdots, T$ are measured in R points. After the FEM is employed the electrostatic inverse problem (5.13), (5.13) is reduced to algebraic equations (5.17), (5.18)

$$[\vec{E}^{(i)}_{tot}] = [\vec{E}^{(i)}_{inc}] + [H_{int}][\chi][\vec{E}^{(i)}_{tot}] \ , \tag{5.59}$$

$$[\vec{S^*}^{(i)}] = [H_{ext}][\chi][\vec{E}^{(i)}_{tot}] \ , \tag{5.60}$$

where $[\vec{S^*}^{(i)}] = [\vec{S}^{(i)}] - [\vec{S}^{(i)}_0]$ and $i = 1, 2, \cdots, T$ is the index of illuminating field. Applying small variations of the fields in (5.59), (5.60) gives

$$\delta[\vec{E}^{(i)}_{tot}] = [H_{int}]\delta([\chi][\vec{E}^{(i)}_{tot}]) \ , \tag{5.61}$$

$$\delta[\vec{S^*}^{(i)}] = [H_{ext}]\delta([\chi][\vec{E}^{(i)}_{tot}]) \ , \ i = 1, 2, \cdots, T \ . \tag{5.62}$$

The first order approximation of $\delta([\chi][\vec{E}^{(i)}_{tot}])$ is given by

$$\delta([\chi][\vec{E}^{(i)}_{tot}]) = \delta([\chi])[\vec{E}^{(i)}_{tot}] + [\chi]\delta([\vec{E}^{(i)}_{tot}]) \ , \ i = 1, 2, \cdots, T \ . \tag{5.63}$$

Substituting (5.61) in (5.63) gives

$$\delta([\chi][\vec{E}^{(i)}_{tot}]) = ([I] - [\chi][H_{ext}])^{-1}\delta[\chi][\vec{E}^{(i)}_{tot}] \ , \ i = 1, 2, \cdots, T \ , \tag{5.64}$$

where I is a diagonal NxN dimensional matrix with diagonal components given by $\begin{pmatrix} 1 & 0 \\ 0 & 1 \end{pmatrix}$.

Substituting (5.64) into (5.62) gives a non-linear inversion equation

$$\delta[\vec{S^*}^{(i)}] = [H_{ext}]([I] - [\chi][H_{ext}])^{-1}\delta[\chi][\vec{E}_{tot}^{(i)}] \ , \ i = 1, 2, \cdots, T \ . \tag{5.65}$$

Linearizing (5.65) gives

$$\delta[\vec{S^*}^{(i)}] = [D^{(i)}]\delta[\chi][\vec{E}_{tot}^{(i)}] \ , \ i = 1, 2, \cdots, T \ , \ i = 1, 2, \cdots, T \ . \tag{5.66}$$

Equations (5.66) are ill-conditioned and can be solved for a least square solution employing a regularization approach.

The NK inversion algorithm is given by the following steps

1. Computation of $[\vec{E}_{tot}^{(i)}]$ using (5.59);
2. Estimation of the sensor readings using (5.60);
3. Computation of the MSE_{ϕ}, if the error is satisfactory then quit;
4. Solving (5.66), updating $[\chi]$ and proceeding with step 1.

5.2.5 Pseudoinverse Transformation Method

The pseudoinverse transformation method proposed by Ney, Smith and Stuchly [28] can be seeing as an alternative to using Tikhonov regularization [4]. The pseudoinverse transformation method is applied in [28] to an inverse 2D electrodynamic problem employing TM illumination. We found that the pseudoinverse transformation method is rarely employed in the inverse problems although the method itself is widely referred to in the literature [18], [41], [65]. According to our survey the application of the pseudoinverse transformation to the electrostatic inverse problem has not been investigated. We now present the pseudoinverse transformation method in the electrostatic case.

We approach the inverse problem in figure 5.7 using the same algebraic equations as in the previous section (5.59), (5.60)

$$[\vec{E}_{tot}^{(i)}] = [\vec{E}_{inc}^{(i)}] + [H_{int}][\chi][\vec{E}_{tot}^{(i)}] \ , \tag{5.67}$$

$$[\vec{S_*}^{(i)}] = [H_{ext}][\chi][\vec{E}^{(i)}_{tot}] \ , \tag{5.68}$$

where $[\vec{S_*}^{(i)}] = [\vec{S}^{(i)}] - [\vec{S}^{(i)}_0]$ and $i = 1, 2, \cdots, T$ is the index of illuminating field. Substituting

$$[\vec{P}^{(i)}] = \frac{1}{4\pi}[\chi][\vec{E}^{(i)}_{tot}] \tag{5.69}$$

in (5.67), (5.68) gives

$$[\vec{E}^{(i)}_{tot}] = [\vec{E}^{(i)}_{inc}] + 4\pi[H_{int}][\vec{P}^{(i)}] \ , \tag{5.70}$$

$$[\vec{S_*}^{(i)}] = 4\pi[H_{ext}][\vec{P}^{(i)}] \ , \ i = 1, 2, \cdots, T \ . \tag{5.71}$$

If the resolution of χ in the FEM and the locations of the sensor electrodes are chosen such that matrix $[H_{ext}]$ is invertable then a solution to (5.71) is given by

$$[\vec{P}^{(i)}] = \frac{1}{4\pi}[H_{ext}]^{-1}[\vec{S_*}^{(i)}] \ , \ i = 1, 2, \cdots, T \ . \tag{5.72}$$

First substituting (5.72) in (5.70) gives the total electrostatic field intensity in Q

$$[\vec{E}^{(i)}_{tot}] = [\vec{E}^{(i)}_{inc}] - [H_{int}][H_{ext}]^{-1}[\vec{S_*}^{(i)}] \ , \ i = 1, 2, \cdots, T \ . \tag{5.73}$$

and then substituting (5.73) and (5.72) in (5.69) gives

$$[H_{ext}]^{-1}[\vec{S_*}^{(i)}] = [\chi]\left\{[\vec{E}^{(i)}_{inc}] - [H_{int}][H_{ext}]^{-1}[\vec{S_*}^{(i)}]\right\} \ . \tag{5.74}$$

Equations (5.74) can then be resolved for a least square solution for $[\chi]$.

The problem of obtaining an invertable matrix $[H_{ext}]$ (5.71) is not practical [28]. Instead of solving (5.71) directly Ney, Smith and Stuchley proposed an alternative approach of finding a solution to the following minimisation problem

$$\min_{[\vec{P}^{(i)}]} ||[\vec{S_*}^{(i)}] - [H_{ext}][\vec{P}^{(i)}]|| \ , \ i = 1, 2, \cdots, T \ , \tag{5.75}$$

with an additional condition

$$\min ||[\vec{P}^{(i)}]|| \ . \tag{5.76}$$

The procedure of solving (5.75), (5.76) is called a pseudoinverse transformation. The unknown dielectric is then obtained using (5.69), (5.70).

5.2.6 Modified Gradient Method

The modified gradient method is a powerful iterative algorithm for solving non-linear problems. Application of the modified gradient method to the inverse electrodynamic problems is slow but robust and results in high quality reconstructed images [30], [31], [66].

We now formulate the modified gradient method for the electrostatic inverse problem introduced in section 5.2.1 as of reconstruction of the unknown dielectric in Q using T incident fields and R sensors. After the governing integral equations are employed for this problem they cast by means of the FEM into the following system of algebraic equations (5.17), (5.18)

$$[\vec{E}^{(i)}_{tot}] = [\vec{E}^{(i)}_{inc}] + [H_{int}][\chi][\vec{E}^{(i)}_{tot}] \ , \tag{5.77}$$

$$[\vec{S^*}^{(i)}] = [H_{ext}][\chi][\vec{E}^{(i)}_{tot}] \ , \ i = 1, 2, \cdots, T. \tag{5.78}$$

The total electrostatic field and dielectric susceptibility in the modified gradient method are reconstructed simultaneously at each iteration according to the following formulae

$$[\vec{E}^{(i)}_{tot,n}] = [\vec{E}^{(i)}_{tot,n-1}] + \alpha_n[\vec{v}^{(i)}_n] \ , \tag{5.79}$$

$$[\chi_n] = [\chi_{n-1}] + \beta_n[\vec{d}^{(i)}_n] \ , \ i = 1, 2, \cdots, T \ , \tag{5.80}$$

where $[\vec{v}^{(i)}_n]$ and $[\vec{d}^{(i)}_n]$ are the update directions and α_n and β_n are constants to be obtained at each iteration. The residual error vectors are defined as

$$[r_{i,n}] = [\vec{E}^{(i)}_{inc}] - [\vec{E}^{(i)}_{tot}] + [H_{int}][\chi][\vec{E}^{(i)}_{tot,n}] \ , \tag{5.81}$$

$$[\rho_{i,n}] = [\vec{S^*}^{(i)}] - [H_{ext}][\chi][\vec{E}^{(i)}_{tot,n}] \ . \tag{5.82}$$

The modified gradient iterative algorithm is constructed to minimise the cost function

$$F_n = \frac{\sum_{i=1}^{T} |||[r_{i,n}]|||^2}{\sum_{i=1}^{T} |||[\vec{E}^{(i)}_{inc}]|||^2} + \frac{\sum_{i=1}^{T} |||[\rho_{i,n}]|||^2}{\sum_{i=1}^{T} |||[\vec{S^*}^{(i)}]|||^2} \ . \tag{5.83}$$

The two residual error terms in (5.83) are normalized in such way that they are equal to one for $[\vec{E}^{(i)}_{tot}] = 0, i = 1, 2, \cdots, T$.

In [30] $[\vec{v}^{(i)}_n]$ and α_n are chosen to be

$$[\vec{v}^{(i)}_n] = [r_{i,n-1}] \ , \ \alpha_n = \frac{\sum_{i=1}^{T} [r_{i,n-1}]^t [H_{int}][\chi] - [I])[r_{i,n-1}]}{\sum_{i=1}^{T} |||[H_{int}][\chi] - [I])[r_{i,n-1}]|||^2} \tag{5.84}$$

and β_n and $[\vec{d}^{(i)}_n]$ are obtained using the Fletcher-Reeves-Polak-Ribiere conjugate gradient method [63].

In [31] and [66] both $[\vec{v}^{(i)}_n]$, α_n and $[\vec{d}^{(i)}_n]$, β_n are obtained using the Fletcher-Reeves-Polak-Ribiere conjugate gradient method [63].

5.2.7 Inverse Scattering Method Based on Reconstruction of Nonmeasurable Equivalent Current Density

In section 5.2.5 we presented an inverse method proposed by Ney *et al.* [28]. In [28] the inverse source problem governed by (5.24) is solved prior to calculating the dielectric susceptibility. This is an example of the algorithm that belongs to a larger class of inverse methods based on the source type integral equation [55], [40]. The problem of ill-conditioning and non-uniqueness of the solution of the inverse source problem is overcome in [28] by using a pseudoinverse transformation. In this section we present another inverse method based on the source type integral equation [65]. This method is not only more efficient than a pseudoinverse transformation method but also gives an insight into the fundamental difficulties associated with inverse problems. The method that we now discuss is originally formulated for the electrodynamic inverse problem and we state it in electrostatics.

We consider the electrostatic inverse problem in figure 5.7. An unknown dielectric medium with a support in Q is placed in T linearly independent electrostatic fields and has to be reconstructed to match the distorted field measured at R locations. Using the FEM the governing source type integral equations (5.22) (5.23), (5.24) are replaced by the system of algebraic equations (5.25), (5.26), (5.27)

$$[\vec{P}^{(i)}] = \frac{1}{4\pi}[\chi][\vec{E}^{(i)}_{tot}] \ , \tag{5.85}$$

$$[\vec{E}^{(i)}_{tot}] = [\vec{E}^{(i)}_{inc}] + 4\pi[H_{int}][\vec{P}^{(i)}] \ , \tag{5.86}$$

$$[\vec{S^*}^{(i)}] = 4\pi[H_{ext}][\vec{P}^{(i)}] \ , \ i = 1, 2, \cdots, T \ , \tag{5.87}$$

where $[\vec{P}^{(i)}]$ is an N dimensional vector, $i = 1, 2, \cdots, T$ is the index of incident field and $[\vec{S^*}^{(i)}]$ is given by $[\vec{S}^{(i)}] - [\vec{S_0}^{(i)}]$. According to [65] the inverse problem (5.87) is not only complicated by the existence of the sources which produce a zero field outside their support but also by the existence of the sources that create a non-zero field undetectable at the sensor locations. A large redundancy in the number of the sensors is impractical since they produce data carrying almost the same information, which means ill-conditioning and instability [65]. A rigorous study of these complications is done by performing a singular value decomposition (SVD) [14], [15] of matrix $[H_{ext}]$. It is now assumed that $R < N$ (we recall that $[H_{ext}]$ (5.87) is an RxN matrix) and that $[H_{ext}]$ has rank R which means that all measurements are linearly independent. In that case matrix $[H_{ext}]$ can be decomposed [15] as follows

$$[H_{ext}] = [U][\Sigma][V]^T \ , \tag{5.88}$$

where

$$[U] = [u_1|u_2|\cdots|u_M|0]_{MxN} \ , \tag{5.89}$$

$$[V] = [v_1|v_2|\cdots|v_N]_{NxN} \tag{5.90}$$

and vectors $[u_j]$ and $[v_j]$ create two orthonormal sets; a diagonal matrix $[\Sigma]$ has a diagonal form

$$[\Sigma] = \begin{pmatrix} \sigma_1 & \cdots & 0 \\ \vdots & \ddots & \vdots \\ 0 & \cdots & \sigma_N \end{pmatrix}_{N \times N} , \tag{5.91}$$

where the numbers $\sigma_1 \geq \sigma_2 \geq ... \geq \sigma_R > \sigma_{R+1} = \cdots \sigma_N = 0$ are called the singular values of matrix $[H_{ext}]$. We now show the existence of the sources in (5.87) producing a zero field at the sensor locations. For convenience the polarization vector $[\vec{P}^{(i)}]$ is represented in the form

$$[\vec{P}^{(i)}] = [V][\gamma] \ , \ [\gamma^{(i)}] = \begin{bmatrix} \gamma_1^{(i)} \\ \gamma_2^{(i)} \\ \vdots \\ \gamma_N^{(i)} \end{bmatrix} \ , \ i = 1, 2, \cdots, T \ . \tag{5.92}$$

Substituting (5.92) in (5.87) gives

$$\gamma_j^{(i)} \sigma_j [u_j] = 4\pi \gamma_j^{(i)} [H_{ext}][v_j] \ , \ j = 1, 2, \cdots, N \ , \ i = 1, 2, \cdots, T \ , \tag{5.93}$$

and

$$\sum_{j=1}^{N} \gamma_j^{(i)} \sigma_j [u_j] = [\vec{S^*}^{(i)}] \ , \ i = 1, 2, \cdots, T \ . \tag{5.94}$$

Since

$$\sigma_j [u_j] = 0 \ , \ \forall j > R \ , \tag{5.95}$$

only the first R components of $[\vec{P}^{(i)}]$ (in terms of $[\gamma^{(i)}]$) are mapped into the sensor data. For these components coefficients γ are given by

$$\gamma_j^{(i)} = \frac{1}{\sigma_j} \left\{ [u_j]^T [\vec{S^*}^{(i)}] \right\} \ , \ j = 1, 2, \cdots, R \ , \ i = 1, 2, \cdots, T \tag{5.96}$$

and hence $[\vec{P}^{(i)}]$ can be obtained by substituting (5.96) in (5.92)

$$[\vec{P}^{(i)}] = \sum_{j=1}^{R} \frac{1}{\sigma_j} \left\{ [u_j]^T [\vec{S^*}^{(i)}] \right\} [v_j] \ , \quad i = 1, 2, \cdots, T \ . \tag{5.97}$$

Equation (5.97) gives the minimum-norm solution to (5.87). Note that in the inverse problem employing a pseudoinverse transformation (section 5.2.5) solution (5.97) was obtained using a function minimisation approach (5.75), (5.76).

In practice the terms in $[\vec{P}^{(i)}]$ (5.97) corresponding to a small eigenvalues σ_j cannot be reconstructed for $[H_{ext}]$ due to the ill-conditioning of the inverse problem. Assuming that only M largest eigenvalues (of R nonzero terms) are calculated we represent $[\gamma^{(i)}]$ (which is used to parametrise $[\vec{P}^{(i)}]$ (5.92)) in the form

$$[\gamma^{(i)}] = [\gamma_M^{(i)}] + [\gamma_{N-M}^{(i)}] = \begin{bmatrix} \frac{1}{\sigma_1}[u_1]^T[\vec{S^*}^{(i)}] \\ \vdots \\ \frac{1}{\sigma_M}[u_M]^T[\vec{S^*}^{(i)}] \\ 0 \\ \vdots \\ 0 \end{bmatrix} + \begin{bmatrix} 0 \\ \vdots \\ 0 \\ \gamma_{M+1} \\ \vdots \\ \gamma_N \end{bmatrix} \ , \quad i = 1, 2, \cdots, T \ . \tag{5.98}$$

Multiplying (5.86) by $[\chi]$ and substituting $[\vec{P}^{(i)}] = [V]([\gamma_M^{(i)}] + [\gamma_{N-M}^{(i)}])$ (5.98), and using (5.85) gives

$$([I] - [\chi][H_{int}])[V]([\gamma_M^{(i)}] + [\gamma_{N-M}^{(i)}]) = [\chi][\vec{E}_{inc}^{(i)}] \ , \quad i = 1, 2, \cdots, T \ . \tag{5.99}$$

Equations (5.99) is solved for $[\chi]$ and $[\gamma_{N-M}^{(i)}]$ by minimising a functional

$$F([\chi], [\gamma_{N-M}^{(i)}]) = \sum_{i=1}^{T} ||([I] - [\chi][H_{int}])[V]([\gamma_M^{(i)}] + [\gamma_{N-M}^{(i)}]) - [\chi][\vec{E}_{inc}^{(i)}]||^2 \ , \tag{5.100}$$

which accomplishes the method.

5.2.8 Layer Stripping Algorithm for Profile Inversion

In sections 5.2.3-5.2.7 we presented several inverse methods based on the integral equation approach. The FEM was applied to integral equations and the inverse problems were reduced to the systems of algebraic equations. These approaches are similar in the sense that they calculate or update ϵ simultaneously for the whole reconstruction domain Q. In this section we introduce the idea of the layer stripping method which is different from the previous examples.

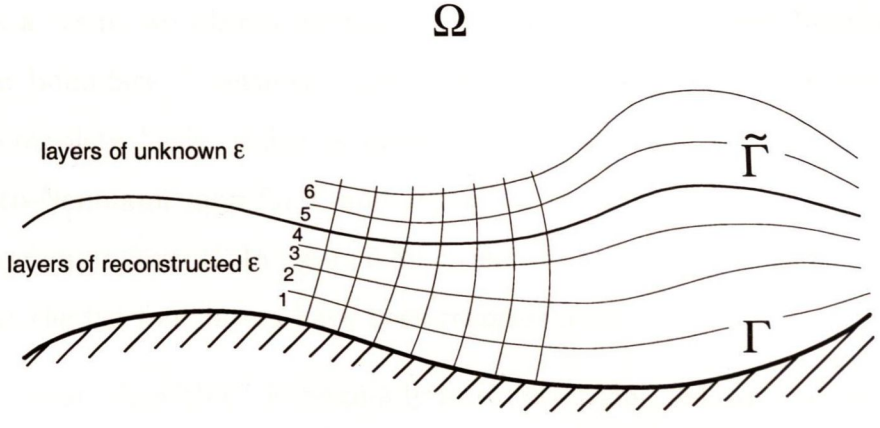

Figure 5.8: A layer stripping approach to the inverse electrostatic problem.

Let the inverse electrostatic problem be posed in a reconstruction domain Ω with boundary Γ and the Dirichlet-to-Neumann map be known on Γ (figure 5.8). The boundary value of the dielectric permittivity is uniquely determined by the Dirichlet-to-Neumann map [101]. In section 3.5 we presented a method of calculation of the boundary value of ϵ. In particular, we have shown that if ϵ is continuous at some point A on Γ then employing

a Dirichlet boundary condition given by the Dirac delta function at A (see figure 3.4) we establish a local high intensity electrostatic field that tends to infinity as we approach A. This field, established in the vicinity of A, is independent of ϵ. According to the Dirichlet-to-Neumann map we know the value of $S = \epsilon\frac{d\phi}{d\vec{n}}$ at any point B on Γ, where ϕ is the electrostatic potential and $\vec{n}$ is the normal at B. The boundary value of the dielectric permittivity at B is then given by $\epsilon = S/\frac{d\phi}{d\vec{n}}$, where $\frac{d\phi}{d\vec{n}}$ is known in the vicinity of A. Letting B tend to A gives ϵ at A.

The layer stripping algorithm consists of the following steps. Approximating ϵ by a piecewise constant function in Q we reconstruct ϵ in some layer 1 adjacent to Γ as shown in figure 5.8. Next we reconstruct the electrostatic fields in layer 1 for each Dirichlet boundary condition of the Dirichlet-to-Neumann map on Γ using, for example, a finite difference scheme. As a result we obtain another map of the Dirichlet onto Neumann boundary condition on boundary $\tilde{\Gamma}$ between layers 1 and 2. If the arising potential functions on $\tilde{\Gamma}$ create a complete basis, which is subject to investigation, then the obtained map is a Dirichlet-to-Neumann map for $\tilde{\Gamma}$ and repeating the same iteration we reconstruct the dielectric medium in layer 2. In figure 5.8 $\tilde{\Gamma}$ is shown to be in between layers 4 and 5 which assumes that the fist four layers have been reconstructed.

A "layer stripping algorithm" is originally introduced [83], [84] for the inverse electrodynamic problem where each new layer is reconstructed using the Fourier transform of the Dirichlet-to-Neumann map on $\tilde{\Gamma}$.

In practical implementations of the layer stripping algorithm the Dirichlet-to-Neumann map has to be measured to a high resolution. This imposes challenging yet feasible requirements on the hardware. We expect an accumulation of the error in the layer stripping algorithm when proceeding from reconstruction of one dielectric layer to another. Even when the dielectric object does not occupy the area close to Γ the error is still accumulated when analytically continuing the electrostatic field in free space. The methods presented in sections 5.2.3-5.2.7 do not have such a disadvantage because the integral equations take into account field interactions for the distant points.

5.3 Comparison and Discussion of Imaging Methods

An important part of the inverse problem is the object model. Usually the object model is chosen to represent either a dielectric or metal scatterer. In chapter 1 we presented the bed sensor application which motivated our study. In the bed sensor application the physical object under reconstruction is a human body. We experimentally observed that the human body behaves as a conductor in the low frequency electric fields. During our early study of the bed sensor application we believed that the best approach to modelling the human body was to introduce an unknown metal object with a parameterised surface. A detailed analysis of this approach revealed fundamental difficulties. The human body is too complex to be parameterised, which increases the possibility that the inverse algorithm minimising the error function might be trapped in a local minimum. We observed multiple minima in the example of the simplest inverse problem employing a 2D metal cylinder of a given radius. Another difficulty in implementing the metal object model is multiple connectivity. The maximum connectivity of the metal object model that we found in the existing inverse problems is 3 for an object represented in 2D. The existing inverse problems parametrising the surface of the metal scatterer make the following assumptions [40],[38]: (i) the connectivity of the object is predetermined and cannot be changed during the inversion, (ii) a position of the centre of each simply connected part of the multiply connected object is fixed, (iii) the initial guess of the shape of the simply connected part is chosen close to the original one in order to achieve stability. From our point of view such constraints are impractical.

The piecewise constant representation of the dielectric is suited to many general purpose inverse problem applications. The metal can be seen as an extreme case of the dielectric medium and hence is included in the model. Also, bearing in mind the bed sensor application, we should expect many dielectric objects surrounding the human body such as mattress, pillows, clothes and casual gadgets. We decided to employ a piecewise constant representation of the dielectric in our inverse methods.

We presented several integral equation based inverse methods namely the BIM and DBIM, Newton-Kantorovich method, pseudoinverse transformation method, modified gradient

method and a method based on the reconstruction of the equivalent current density. These methods have originally been applied to the electrodynamic inverse problem but can be formulated in electrostatics. We also found that these methods have been applied to different types of scatterer using different types of the incident fields and different number and position of measurement antennas. It is difficult to compare the efficiency of these methods because they have not been tested for the same inverse electrodynamic problem. For example, it has been reported that the modified gradient method converges after 128 iterations for the dielectric scatterer having contrast 1.5 [31], the Newton-Kantorovich method converged after 15 iterations for the dielectric scatterer having contrast 1.6 [95], the inverse method based on the reconstruction of a nonmeasurable equivalent current density which is a non-iterative method demonstrated a good quality of the reconstructed image [65] yet the computational intensity of the SVD (singular value decomposition) is not reported. It is even more difficult to predict the efficiency of these methods in electrostatics. Unfortunately we were not able to test all of these methods in electrostatics within the given time/manpower constraint.

Analysing the simulation results presented in the original papers employing inverse algorithms we may note general trends in the performance of the inversion algorithms. Higher contrast distributions of the dielectric permittivity are more difficult to reconstruct. We can account for this trend by the increased non-linearity of the higher contrast inverse problem; as the problem becomes more non-linear the linearisation errors increase resulting in slower convergence of the iterative methods. Sharp edges in the unknown dielectric scatterers tend to be smoothed, the convergence of the inverse methods in the presence of the sharp edges in the original dielectric distribution is also slowed down.

In general the BIM and DBIM, Newton-Kantorovich method, pseudoinverse transformation method, modified gradient method and the method based on the reconstruction of the equivalent current density lead to methods which suit the bed sensor application. In our approach to the electrostatic imaging problem the preference was given to the distorted BIM since this method had already demonstrated good results in the inversion of induction [23] and inversion of resistivity [17] tool problems which are similar to the inverse

electrostatic problem.

The 2D inversion of resistivity tool problem [17] is solved by means of the DBIM and NMM (numerical mode matching method). In the case of two small conductive insertions of (0.01S/m) in a homogeneous background profile (0.2S/m), the MSE_ϕ in [17] is reported to be 1% and 0.25% after the 5-th and 15-th DBIM iterations. The reconstruction domain for this particular profile was chosen to be 15x12 cells each containing medium with unknown constant conductivity.

The 2D inversion of induction tool problem [23] is solved using a combination of the DBIM and CG-FFHT (conjugate gradient-fast Fourier-Hankel transform) [24] which allows a reduction of the computational intensity of each DBIM iteration to $N \log N$. Due to efficient use of the memory resources in [23] a high resolution 64x200 cell reconstruction domain is implemented in the inverse algorithm. The errors of the inversion method are not reported in [23].

By comparing results presented in the literature we found that the quality of the reconstructed images in the layer stripping algorithm [83], [84] is significantly degraded as compared to the integral equation approaches such as the BIM and DBIM. The layer stripping algorithm requires high resolution measurements of the Dirichlet-to-Neumann map while the BIM and DBIM benefit from each individual measurement in the inverse problem. This discouraged us from adopting layer stripping method ideas.

SIMULATION OF INVERSE ELECTROSTATIC PROBLEM

6.1 Analytical and Numerical Formulation of the Inverse Boundary Electrostatic Problem

We now define the inverse boundary electrostatic problem. Let Q be a rectangular reconstruction domain where we seek an unknown dielectric distribution ϵ_{orig}. Let Γ be a

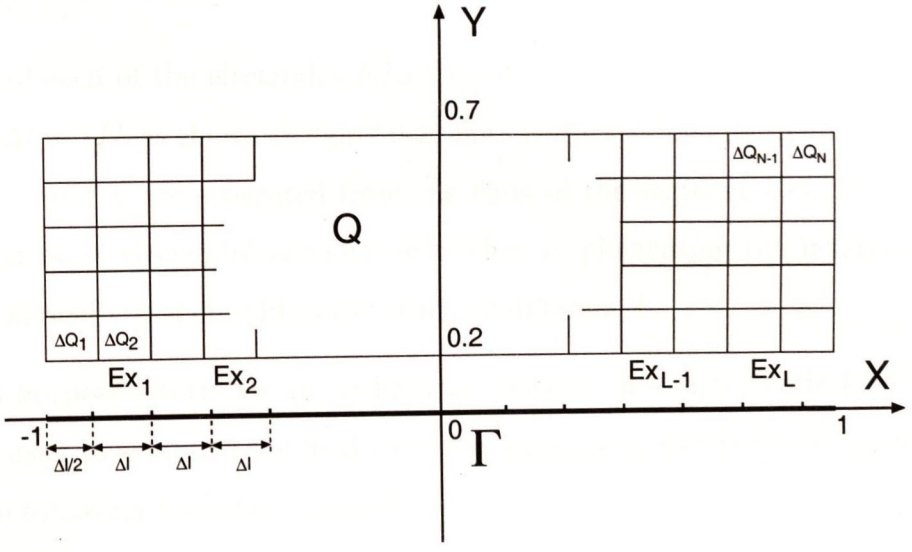

Figure 6.1: Reconstruction domain Q and boundary Γ containing electrodes for inverse electrostatic problem.

segment domain $(-1,1)$ where the Dirichlet boundary condition is preset. Both Q and Γ are shown in figure 6.1. Note that Γ is a doublesided boundary and hence we refer to the electrostatic potentials on its upper and lower sides using subscripts "+" and "-" respectively.

We generate L electrostatic fields by applying unity electrostatic potential to L general purpose electrodes located on the upper side of Γ. Each of the general purpose electrodes can be either a transmit electrode Tx or a receive electrode Rx at a time and hence the name. We consider these electrodes as subdomains of Γ. To distinguish the general purpose electrodes from dedicated Tx or Rx electrodes we denote them by $ELx_1, ELx_2, \cdots, ELx_L$. The Dirichlet boundary condition for the i-th illuminating field is given by

$$\phi_+^{(i)}(\vec{r}) = \begin{cases} 1, & \vec{r} \in ELx_i, \\ 0, & \vec{r} \in \Gamma \setminus ELx_i. \end{cases} \tag{6.1}$$

$$\phi_-^{(i)}(\vec{r}) = 0 \ , \ \vec{r} \in \Gamma \ , \ i = 1, 2, \cdots, L \ .$$

Let the size of each of the electrodes ELx_i, $i = 1, 2, \cdots, L$ and the spacing between them be given by $\Delta l = 1/L$ as shown in figure 6.1. For symmetry the first and the last electrodes with indices 1 and L are separated from the ends of the segment $(-1,1)$ by $\Delta l/2$. This parameterisation of electrodes is convenient when implementing the inverse electrostatic problem numerically and simplifies the study of different L.

The general purpose electrodes are utilized to measure the electrostatic field. If the i_0-th electrode is used to establish the field then the response of the j_0-th electrode ($i_0 \neq j_0$) is given by the following boundary integral

$$S^{(i_0,j_0)} = \int_{ELx_{j_0}} \epsilon(\vec{r}') \frac{d\phi_+^{(i_0)}(\vec{r}')}{d\vec{n}} d\vec{r}' \ , \tag{6.2}$$

where $\epsilon(\vec{r}')$ is the boundary value of the dielectric permittivity and $\vec{n}$ is the outward normal to Γ. In particular, for the problem in figure 6.1, the boundary normal in (6.2) is chosen to be $(0,-1)$. Without loss of generality hereafter we assume that the boundary value for ϵ in (6.2) is unity.

$S^{(i_0,j_0)}$ in (6.2) is proportional to the mutual capacitance between the i_0-th and j_0-th electrodes $C_{i_0,j_0} = \frac{1}{4\pi} S^{(i_0,j_0)}$. We now exclude linearly dependent data in (6.2). According to (2.136) we write

$$S^{(i,j)} = S^{(j,i)} \ , \ 1 \leq i \neq j \leq L \ . \tag{6.3}$$

The total number of linearly independent scalar measurements D available in the inverse problem employing L general purpose electrodes is given by

$$D = \frac{L(L-1)}{2} \ . \tag{6.4}$$

Note that in (6.4) we excluded the self-capacitance data which, if measured, increases D to $\frac{L(L+1)}{2}$. The measurement of the self-capacitance is related to hardware difficulties caused by large mutual capacitance to the ground plane which we do not dwell upon in this section. Even if a more sophisticated electrode is designed capable of shielding itself from the ground plane the unnecessarily large capacitive link to the ground plane over the array significantly shadows the useful data.

The inverse electrostatic problem is to record the sensor data $S^{(i,j)}_{orig}$, $i,j = 1,2,\cdots,L$, $i \neq j$ for the unknown dielectric ϵ_{orig} and to find ϵ in Q such that

$$S^{(i,j)}_{\epsilon} = S^{(i,j)}_{orig} \ , \ i,j = 1,2,\cdots,L \ , \ i \neq j \ . \tag{6.5}$$

6.2 Distorted Born Iterative Method and Physically Extended Electrodes.

The DBIM algorithm is presented in section 5.2.3. For convenience each DBIM iteration is split into two parts namely the forward and inverse path. The forward path includes all electrostatic problems that arise in the DBIM iteration and hence the name. Usually the state electrostatic integral equation (5.13) is employed in the forward path. After the electrostatic problems are solved the electrostatic fields are fixed until the end of the DBIM iteration to linearise in inversion and then the inversion integral equation (5.14) is

employed. This part of the DBIM iteration is called the inverse path. We now present the forward and inverse path of the DBIM.

6.2.1 Forward Path in the DBIM

The DBIM iteration starts with calculation of the electrostatic fields in the background dielectric ϵ_{ini}. The background dielectric is either a guess or an updated approximation for ϵ_{orig} in Q (obtained from the previous iteration) in the first and subsequent iterations respectively. In the first iteration we use $\epsilon_{ini} = 1$ in Q. L electrostatic problems in the forward path of the DBIM are governed by (4.98), (4.99), (4.100)

$$E^{(i)}_{tot\,x}(\vec{r}) + 4\pi \frac{d}{dx}\hat{\mathrm{CF}}[\tilde{D} \to D]\left\{\int_{\tilde{\Gamma}} \frac{\partial\, G(\vec{r}', \vec{\tilde{r}})}{\partial\, \vec{n}_{r'}} \tilde{\sigma}^{(i)}(\vec{r}')dr'\right\}$$

$$+ \int_Q \chi_{ini}(\vec{r}')\left\{E^{(i)}_{tot\,x}(\vec{r}')\frac{\partial^2\, G(\vec{r}', \vec{r})}{\partial\, x' \partial\, x} + E^{(i)}_{tot\,y}(\vec{r}')\frac{\partial^2\, G(\vec{r}', \vec{r})}{\partial\, y' \partial\, x}\right\} dr' = 0\ ,\ \vec{r} \in Q\ , \qquad (6.6)$$

$$E^{(i)}_{tot\,y}(\vec{r}) + 4\pi \frac{d}{dy}\hat{\mathrm{CF}}[\tilde{D} \to D]\left\{\int_{\tilde{\Gamma}} \frac{\partial\, G(\vec{r}', \vec{\tilde{r}})}{\partial\, \vec{n}_{r'}} \tilde{\sigma}^{(i)}(\vec{r}')dr'\right\}$$

$$+ \int_Q \chi_{ini}(\vec{r}')\left\{E^{(i)}_{tot\,x}(\vec{r}')\frac{\partial^2\, G(\vec{r}', \vec{r})}{\partial\, x' \partial\, y} + E^{(i)}_{tot\,y}(\vec{r}')\frac{\partial^2\, G(\vec{r}', \vec{r})}{\partial\, y' \partial\, y}\right\} dr' = 0\ ,\ \vec{r} \in Q\ , \qquad (6.7)$$

$$-\phi^{(i)}(\vec{r}) + 4\pi\hat{\mathrm{CF}}[\tilde{D} \to D]\left\{\int_{\tilde{\Gamma}} \frac{\partial\, G(\vec{r}', \vec{\tilde{r}})}{\partial\, \vec{n}_{r'}} \tilde{\sigma}^{(i)}(\vec{r}')dr'\right\}$$

$$+ \int_Q \chi_{ini}(\vec{r}')\left\{E^{(i)}_{tot\,x}(\vec{r}')\frac{\partial\, G(\vec{r}', \vec{r})}{\partial\, x'} + E^{(i)}_{tot\,y}(\vec{r}')\frac{\partial\, G(\vec{r}', \vec{r})}{\partial\, y'}\right\} dr' = 0\ , \vec{r} \in \Gamma\ , \qquad (6.8)$$

$$i = 1, 2, \cdots, L\ ,$$

where $\chi = \epsilon - 1$ is the dielectric susceptibility, $\phi^{(i)}(\vec{r})$ in (6.8) is given by (6.1), i is the index of the incident field and $4\pi\hat{\mathrm{CF}}[\tilde{D} \to D]\left\{\int_{\tilde{\Gamma}} \frac{\partial\, G(\vec{r}_1, \vec{\tilde{r}}_2)}{\partial\, \vec{n}_{r_1}} \tilde{\sigma}(\vec{r}_1)dr_1\right\}$ is a term explained in section 4.3. We recall that the conventional techniques (section 2.6.1) applied to the

Dirichlet boundary electrostatic problem with a doublesided boundary lead to ill-posed equations.

The governing integral equations (6.6), (6.7), (6.8) are solved using the FEM and a conformal mapping technique explained in sections 4.2.2 and 4.3. We now proceed with inversion path of the DBIM iteration.

6.2.2 Inverse Path in the DBIM

We employ spatially elongated electrodes ELx which is a novel technique (to the best of our knowledge) for both electrostatic and electrodynamic inverse imaging problems[1]. We recall that in the existing definitions of the electrostatic problem presented in section 6.1 the infinitely small radiating and sensing antennas (5.10) are such that their geometries are excluded from consideration.

We now incorporate (6.2) into the DBIM. To calculate sensor readings $S_{ini}^{(i,j)}$ for the background dielectric χ_{ini} in Q we substitute $\phi(\vec{r})$ (6.8)[2] in (6.2) to give

$$S_{ini}^{(i,j)} = 4\pi \int_{ELx_j} \frac{d}{d\vec{n}} \left[\hat{\mathrm{CF}}[\tilde{D} \to D] \left\{ \int_{\tilde{\Gamma}} \frac{\partial\, G(\vec{r}', \vec{\tilde{r}})}{\partial\, \vec{n}_{r'}} \tilde{\sigma}^{(i)}(\vec{r}') dr' \right\} \right] d\vec{r} \tag{6.9}$$

$$+ \int_{ELx_j} \frac{d}{d\vec{n}} \left[\int_{Q} \chi_{ini}(\vec{r}') \left\{ E_{tot\,x}^{(i)}(\vec{r}') \frac{\partial\, G(\vec{r}', \vec{r})}{\partial\, x'} + E_{tot\,y}^{(i)}(\vec{r}') \frac{\partial\, G(\vec{r}', \vec{r})}{\partial\, y'} \right\} dr' \right] d\vec{r} \ ,$$

$$i, j = 1, 2, \cdots, L \ , \ i \neq j \ .$$

For convenience we first present the inversion path for the BIM and then formulate it for the DBIM. In the BIM (section 5.2.3) we linearise (6.9) by freezing $\tilde{\sigma}^{(i)}$ and $\vec{E}_{tot}^{(i)}$, substitute $S_{ini}^{(i,j)}$ by $S_{orig}^{(i,j)}$ and solve it for $\chi = \chi_{upd}$

$$S_{orig}^{(i,j)} = 4\pi \int_{ELx_j} \frac{d}{d\vec{n}} \left[\hat{\mathrm{CF}}[\tilde{D} \to D] \left\{ \int_{\tilde{\Gamma}} \frac{\partial\, G(\vec{r}', \vec{\tilde{r}})}{\partial\, \vec{n}_{r'}} \tilde{\sigma}^{(i)}(\vec{r}') dr' \right\} \right] d\vec{r} \tag{6.10}$$

[1] The imaging problems are those of reconstruction of complex distributions of metal and dielectric.

[2] Provided the total electrostatic field $\vec{E}_{tot}$ is known (6.8) is suitable for calculating an electrostatic potential (which is differentiable) at any given point in Q and its application is not limited to Γ.

$$+\int_{ELx_j}\frac{d}{d\vec{n}}\left[\int_Q \chi_{upd}(\vec{r}')\left\{E^{(i)}_{tot\,x}(\vec{r}')\frac{\partial\, G(\vec{r}',\vec{r})}{\partial\, x'}+E^{(i)}_{tot\,y}(\vec{r}')\frac{\partial\, G(\vec{r}',\vec{r})}{\partial\, y'}\right\}dr'\right]d\vec{r}\ ,$$

$$i,j=1,2,\cdots,L\ ,\quad i\neq j\ .$$

Subtracting (6.9) from (6.10) gives

$$S^{(i,j)}_{orig}-S^{(i,j)}_{ini}=\int_{ELx_j}\frac{d}{d\vec{n}}\left[\int_Q \delta\chi_{upd}(\vec{r}')\vec{E}^{(i)}_{tot}(\vec{r}')\nabla_{r'}G(\vec{r}',\vec{r})dr'\right]d\vec{r} \tag{6.11}$$

$$i,j=1,2,\cdots,L\ ,\quad i\neq j\ .$$

After (6.11) is solved for $\delta\chi_{upd}$ the updated value for the dielectric susceptibility in the inverse path of the BIM is obtained using

$$\chi_{upd}=\chi_{ini}+\delta\chi_{upd}\ . \tag{6.12}$$

To derive the governing equation for the inverse path in the DBIM we rewrite (6.11) in the form

$$S^{(i,j)}_{orig}-S^{(i,j)}_{ini}=4\pi\int_{ELx_j}\frac{d}{d\vec{n}}\left[\int_Q \delta\vec{P}^{(i)}\nabla_{r'}G(\vec{r}',\vec{r})dr'\right]d\vec{r}\ , \tag{6.13}$$

$$i,j=1,2,\cdots,L\ ,\quad i\neq j\ ,$$

where polarization vector $\delta\vec{P}^{(i)}$ is given by

$$\delta\vec{P}^{(i)}=\frac{1}{4\pi}\delta\chi_{upd}(\vec{r}')\vec{E}^{(i)}_{tot}\ . \tag{6.14}$$

According to (6.13) the physical meaning of the BIM is to find a volume dipole distribution (given by polarization vector $\delta\vec{P}^{(i)}$ (6.14)) such that its field in free space compensates for the residual error $S^{(i,j)}_{orig}-S^{(i,j)}_{ini}$. In order to improve (6.13) we take into account that an electrostatic field is established in dielectric χ_{ini} in the presence of boundary Γ with a homogeneous Dirichlet condition on it. Replacing $G(\vec{r}_1,\vec{r}_2)$ in (6.13) by $G_{\epsilon_{ini}}(\vec{r}_1,\vec{r}_2)$,

changing the order of integrals in (6.13) and applying a reciprocity theorem to $G_{\epsilon_{ini}}(\vec{r}_1, \vec{r}_2)$ (see section 2.2) gives an inversion equation for the DBIM

$$S_{orig}^{(i,j)} - S_{ini}^{(i,j)} = \int_Q \delta\chi_{upd}(\vec{r}')\vec{E}_{tot}^{(i)}\nabla_{r'}\int_{ELx_j}\frac{d}{d\vec{n}}G_{\epsilon_{ini}}(\vec{r},\vec{r}')d\vec{r}d\vec{r}' \ , \tag{6.15}$$

$$i,j = 1,2,\cdots,L \ , \ i \neq j \ .$$

We recall that the Green's function in (6.15) satisfies a homogeneous Dirichlet boundary condition on Γ. The inner integral in (6.15) can be seen as an electrostatic field $\vec{E}_{\sigma_0}$ due to a double layer density $\sigma_0 = \frac{1}{4\pi}$ preset on ELx_j

$$\vec{E}_{\sigma_0}^{(j)}(\vec{r}') = 4\pi\nabla_{r'}\int_{ELx_j}\sigma_0\frac{d}{d\vec{n}}G_{\epsilon_{ini}}(\vec{r},\vec{r}')d\vec{r} \ , \ \vec{r}' \in Q \ . \tag{6.16}$$

According to (2.116) the electrostatic potential due to the double layer σ has a step of $4\pi\sigma$ when crossing the surface. We now consider electrode ELx_j in (6.16) as a segment (with a double layer σ_0 on it) electrically isolated from Γ. The electrostatic potential changes by 1 when crossing ELx_j and is zero on Γ. Since ELx_j lies on Γ the total electrostatic field intensity is given by (6.16) and the corresponding Dirichlet boundary condition on Γ yields

$$\phi_+^{(j)}(\vec{r}) = \begin{cases} 1, & \vec{r} \in ELx_i, \\ 0, & \vec{r} \in \Gamma \setminus ELx_i. \end{cases} \tag{6.17}$$

$$\phi_-^{(j)} = 0 \ , \ \vec{r} \in \Gamma \ , \ j = 1,2,\cdots,L \ .$$

The Dirichlet boundary condition (6.1) and (6.17) are the same. Consequently electrostatic field $\vec{E}_{\sigma_0}^{(j)}(\vec{r}')$ (6.16) is given by a solution to (6.6), (6.7), (6.8)

$$\vec{E}_{\sigma_0}^{(j)}(\vec{r}) = \vec{E}_{tot}^{(j)}(\vec{r}) \ , \ \vec{r} \in Q \ . \tag{6.18}$$

Substituting (6.16), (6.18) in (6.15) yields

$$S_{orig}^{(i,j)} - S_{ini}^{(i,j)} = \int_Q \delta\chi_{upd}(\vec{r}')\vec{E}_{tot}^{(i)}\vec{E}_{tot}^{(j)}(\vec{r}')d\vec{r}' \ , \tag{6.19}$$

$$i, j = 1, 2, \cdots, L \ , \ i \neq j \ .$$

Note that (6.19) has the same form as when point measurements are employed in the inverse problem. Applying the FEM to (6.19), resolving it for $\delta\chi_{upd}$ and updating the dielectric susceptibility in Q using (6.12) accomplishes the DBIM iteration. Since (6.19) is a Fredholm integral equation of the first kind it yields an ill-posed numerical formulation. The ill-conditioning is overcome by using an optimised Tikhonov regularization method which has been developed in the course if this thesis and is presented in the next section.

6.2.3 Optimisation of Tikhonov Regularisation Method

The Tikhonov regularization method [5] is an efficient technique for improving the condition number of an ill-conditioned system of algebraic equations (section 4.1.3). Since the Tikhonov regularization method can be seen as a perturbation of the system of algebraic equations it adds an error to the solution. In this section we present an example of a simple electrostatic inverse problem having one transmit electrode Tx, one receive electrode Rx and a reconstruction domain such that the dielectric is represented (within the approximation of the FEM) as a piecewise constant function in only two cells and then study the influence of the Tikhonov regularization method on the solution to this inverse problem.

The inverse electrostatic problem is illustrated in figure 6.2. Without loss of generality we assume that the transmit electrode Tx establishes a dipole field and the receive electrode is a dipole antenna capable of measuring electrostatic field intensity projected in a given direction $S = E$. Both Tx and Rx electrodes are small so that their geometries are excluded from the problem analysis. The reconstruction domain is composed of two cells namely cell 1 and cell 2. The dielectric permittivity within each of these cells is constant and denoted by ϵ_1 and ϵ_2 according to the index of the cell. We now reconstruct ϵ_1 and ϵ_2 such that the original sensor reading S_{orig} is matched.

We reconstruct ϵ_1 and ϵ_2 using the DBIM (section 5.2.3). Without loss of generality we assume that several DBIM iterations elapsed, the dielectric has been updated to $\epsilon_{ini\,1}$ and $\epsilon_{ini\,2}$, the total electrostatic field is updated for both cells and the corresponding sensor

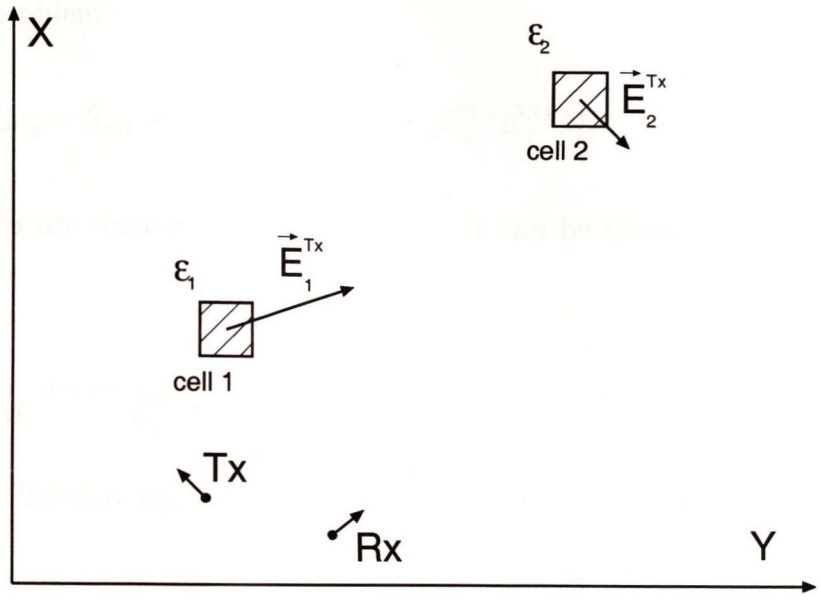

Figure 6.2: Inverse electrostatic problem with one Tx, one Rx and a reconstruction domain composed of two cells.

reading S_{ini} is computed so that we proceed with the inversion path of the DBIM iteration (6.19). The inversion algebraic equation is given by

$$S_{orig} - S_{ini} = \delta\epsilon_1 \vec{E}_1^{Tx} \vec{E}_1^{Rx} M_1 + \delta\epsilon_2 \vec{E}_2^{Tx} \vec{E}_2^{Rx} M_1 \ , \tag{6.20}$$

where $\vec{E}_1^{Tx}$ and $\vec{E}_2^{Tx}$ is the electrostatic field intensity in cells 1 and 2 established by Tx, $\vec{E}_1^{Rx}$ and $\vec{E}_2^{Rx}$ is the electrostatic field intensity in cells 1 and 2 established by a unit dipole having the same location and orientation as Rx (section 5.2.3) and M_1 and M_2 are the metric sizes of cells 1 and 2 respectively. Equation (6.20) has two unknowns and hence cannot be resolved uniquely. Since we reconstruct a general distribution of ϵ_1 and ϵ_2 the preference is given to a condition $\delta\epsilon_1 = \delta\epsilon_2$. Assuming that $\delta\epsilon_1 = \delta\epsilon_2$ in (6.20) gives

$$\delta\epsilon_1 = \delta\epsilon_2 = \frac{S_{orig} - S_{ini}}{\vec{E}_1^{Tx} \vec{E}_1^{Rx} M_1 + \vec{E}_2^{Tx} \vec{E}_2^{Rx} M_1} \ . \tag{6.21}$$

Equation (6.20) also yields a unique solution if we assume either $\delta\epsilon_1 = 0$ or $\delta\epsilon_2 = 0$.

Applying a regularization method in a general form to (6.20) yields the following function minimisation problem

$$\min_{\delta\epsilon_1,\delta\epsilon_2} \left[(S_{orig} - S_{ini} - \delta\epsilon_1 \vec{E}_1^{Tx} \vec{E}_1^{Rx} M_1 - \delta\epsilon_2 \vec{E}_2^{Tx} \vec{E}_2^{Rx} M_2)^2 + \gamma_1^2 \delta\epsilon_1^2 + \gamma_2^2 \delta\epsilon_2^2 \right] , \qquad (6.22)$$

where γ_1 and γ_2 are regularization parameters. It can be shown that (6.22) is minimum when

$$\frac{\gamma_1^2}{\vec{E}_1^{Tx} \vec{E}_1^{Rx} M_1} \delta\epsilon_1 = \frac{\gamma_2^2}{\vec{E}_2^{Tx} \vec{E}_2^{Rx} M_2} \delta\epsilon_2 \ . \qquad (6.23)$$

In the case of Tikhonov regularization method $\gamma_1 = \gamma_2$ and (6.23) yields

$$\frac{1}{\vec{E}_1^{Tx} \vec{E}_1^{Rx} M_1} \delta\epsilon_1 = \frac{1}{\vec{E}_2^{Tx} \vec{E}_2^{Rx} M_2} \delta\epsilon_2 \ . \qquad (6.24)$$

The Tikhonov regularization method ($\gamma_1 = \gamma_2$) tacitly imposes an *a priori* condition that distorts the preferred $\delta\epsilon_1 = \delta\epsilon_2$ in (6.20) and rescales $\delta\epsilon_1$ and $\delta\epsilon_2$ according to the product of the field intensities and a cell size $\vec{E}^{Tx} \vec{E}^{Rx} M$. Summarizing, the Tikhonov regularization method reallocates the dielectric from the areas of weaker electrostatic field intensity and smaller cell size to the areas of higher electrostatic field intensity and larger cell size. To compensate for this type of distortion we rescale the regularization parameter γ for each cell in Q as follows

$$\gamma_1 = \frac{\gamma_0}{\sqrt{\vec{E}_1^{Tx} \vec{E}_1^{Rx} M_1}} \ , \qquad (6.25)$$

$$\gamma_2 = \frac{\gamma_0}{\sqrt{\vec{E}_2^{Tx} \vec{E}_2^{Rx} M_2}} \ ,$$

where γ_0 is a propotionality coefficient. Substituting (6.25) in (6.23) gives $\delta\epsilon_1 = \delta\epsilon_2$.

We now optimise the Tikhonov regularization method for the electrostatic inverse problem in figure 6.1. The FEM cells in the reconstruction domain Q in figure 6.1 have the

same size. Therefore we exclude the cell size from consideration (6.23). If the unmodified Tikhonov regularization method is employed in the inverse problem in figure 6.1 the dielectric distribution will be perturbed in the area near Γ because the electrostatic field intensity significantly increases as we approach the upper side of Γ.

Assuming that the average of the electrostatic field intensity in the reconstruction domain Q over all DBIM illuminating fields can be approximated by the dipole $1/d$ law, where d is a distance between the cell in Q and Γ, we scale the regularization parameter according to

$$\gamma(d) = \frac{\gamma_0}{d^2} \ . \tag{6.26}$$

A further improvement of (6.26) would be an adaptive update of the regularization parameters according to the electrostatic field intensity in Q for each iteration of the DBIM. In the course of these thesis we implement (6.26).

6.3 Numerical Results

We now briefly outline the approaches implemented in the 2D inversion numerical algorithm. We solve the inverse electrostatic problem formulated in section 6.1 using the DBIM [19]. A conformal mapping (section 2.3) is employed in the forward path of the DBIM to overcome difficulties associated with the double sided boundary Γ (figure 6.1) with a Dirichlet boundary condition (6.1) (see also section 4.3). The Dirichlet boundary condition on Γ models the elongated physical electrodes placed on a ground plane (see also a configuration of the inverse problem with four Rx and one Tx electrodes in figure 5.4). The inverse path of the DBIM is derived for spatially elongated electrodes (section 6.2.2) and employs a novel regularization technique obtained by optimising the Tikhonov regularization method (section 6.2.3). The FEM (section 4.2.2) and moment method are employed to put integral electrostatic equations in numerical form. We employ a conjugate gradient algorithm (section 4.4) to solve algebraic equations arising in the forward and inverse paths of the DBIM. The regularization parameter γ is updated for each iteration of the DBIM as proposed in section 4.1.3.

The rectangular reconstruction domain Q in figure 6.1 is divided into 10x40 square cells to represent an arbitrary piecewise constant dielectric distribution. Boundary Γ is divided into 600 cells with a variable cell size. The boundary cells are smaller at the ends of the segment $(-1, 1)$ and gradually increase towards the centre of the segment. This is done primarily to improve the representation of the electrostatic field at the end points of Γ where the boundary values of the electrostatic field intensity tend to infinity. The number of the general purpose electrodes L is 15 (6.1). According to (6.4) the number of independent scalar data measurements representing the input to the inverse algorithm is $D = 105$. Summarizing, the number of unknowns in each of 15 electrostatic problems in the forward path of the DBIM iteration is 1400 and the number of unknowns in the inverse path is 400. The number of unknowns in the inverse path is nearly four times as large as the dimension of the input data $400 > 105$. We use redundant number of the dielectric cells to improve the quality of representation of the electrostatic field in Q. The uniqueness of solution for the inverse problem and well conditioning are achieved by using a regularization approach. To demonstrate the efficiency of the implemented numerical algorithm we now test it for different types of dielectric distributions.

6.3.1 Smooth Edge Dielectric

An original smooth distribution of the dielectric susceptibility is presented in figure 6.3 (a). A Born approximation for this distribution is obtained as a result of the first iteration in the DBIM and is shown in figure 6.3 (b). The DBIM converges after 5 iterations, the reconstructed dielectric susceptibility distributions after the 5-th and 15-th iterations are presented in figures 6.4 (a) and 6.4 (b). Visually the quality of the reconstructed images does not significantly change from iteration to iteration except for the contrast

$$\text{contrast} = \frac{\epsilon_{max}}{\epsilon_{min}} \tag{6.27}$$

which improves towards the contrast of the original distribution which equals to two for this example. The mean squared error MSE_ϕ [3] as a function of 14 iterations of the

[3]Hereafter we use a stricter criteria for MSE_ϕ presented in section 5.2.2. We employ S^* instead of S in (5.29) which is obtained from S by subtracting the sensor response for a free space in Q. This does

DBIM is shown in figure 6.5. According to this plot the DBIM converges to a precision of $MSE_\phi \approx 0.05\%$. We use this plot for comparison in the following numerical experiments.

6.3.2 Low Contrast Dielectric

In a manner similar to the previous experiment the original susceptibility distribution, the corresponding Born approximation and the output of the DBIM after the 5-th and 15-th iterations for the dielectric medium with low contrast=1.15 are presented in figures 6.6 (a),(b) and 6.7 (a),(b) respectively. Visually the quality of the Born approximation is similar to the quality of the DBIM after the 5-th and 15-th iterations. However analysing the convergence of the DBIM using the MSE_ϕ plot in figure 6.8 we see that several subsequent iterations following the Born approximation of the DBIM significantly improve the MSE_ϕ. Comparative analysis of convergence of the DBIM shows nearly identical performance for the DBIM for both low contrast and smooth original susceptibility distributions.

6.3.3 High Contrast Sharp Edge Dielectric

The high contrast sharp edge original dielectric distribution is particularly difficult to reconstruct since the non-linearity of the inverse problem is higher. The DBIM method successfully converges for this type of susceptibility distribution as shown in figures 6.9 (a),(b) and 6.10 (a),(b). Despite the contrast of the original dielectric distribution is $\epsilon_{max}/\epsilon_{min} = 4$ ($\chi_{max} = 3$) the contrast of the reconstructed image is only 2.1 which is approximately 50% less. Analysis of the MSE_ϕ (figure 6.11) shows that the mean squared error for this example converges to a value of 0.25%. This precision is high compared to the inverse problem analysis of other investigators. For example in [77] the sm0oth dielectric with contrast 2 is reconstructed to a precision of $MSE_\phi \approx 2\%$. In [33] a sharp dielectric distribution with contrast 2 is reconstructed to a precision $MSE_\phi \approx 10\%$.

not affect the numerator in (5.29) but significantly reduces the denominator increasing the MSE_ϕ by approximately an order of magnitude depending on the original susceptibility distribution in the inverse problem.

6.3.4 Multi-Part Dielectric

The case of multiple cylinders is particularly interesting from practical application point of view. It demonstrates the advantage of the piecewise constant representation of an arbitrary dielectric distribution as compared to various techniques of parameterising the boundary of the scatterer (section 5.1). The implemented multiple scatterer composed of three dielectric cylinders and the corresponding reconstructed images are presented in figures 6.12 (a),(b) and 6.13 (a),(b). Note that the cylinders in the reconstructed image are well resolved so that the value of the dielectric susceptibility in between the cylinders is close to zero. The DBIM converges to a precision of $MSE_\phi \approx 0.15\%$ as compared to the case of a single smooth cylinder in figure 6.3 (a) when $MSE_\phi \approx 0.05\%$.

6.3.5 Nonsymmetric Dielectric

We now present the DBIM for the problem of reconstruction of a relatively high contrast nonsymmetric dielectric distribution with contrast 3. As shown in figure 6.15 (a) the original object is composed of two adjacent square cross-section cylinders with contrasts 2 and 3. The corresponding Born approximation in figure 6.15 (b) hardly resembles the original profile and is highly oscillating. The profile improves for the 5-th and 15-th DBIM iterations as shown in figure 6.16 (a),(b). Analysis of the MSE_ϕ in figure 6.17 shows a slower yet monotonic convergence of the DBIM as compared to the smooth original distribution in figure 6.3 (a). The final precision after 14 iterations is 0.09%.

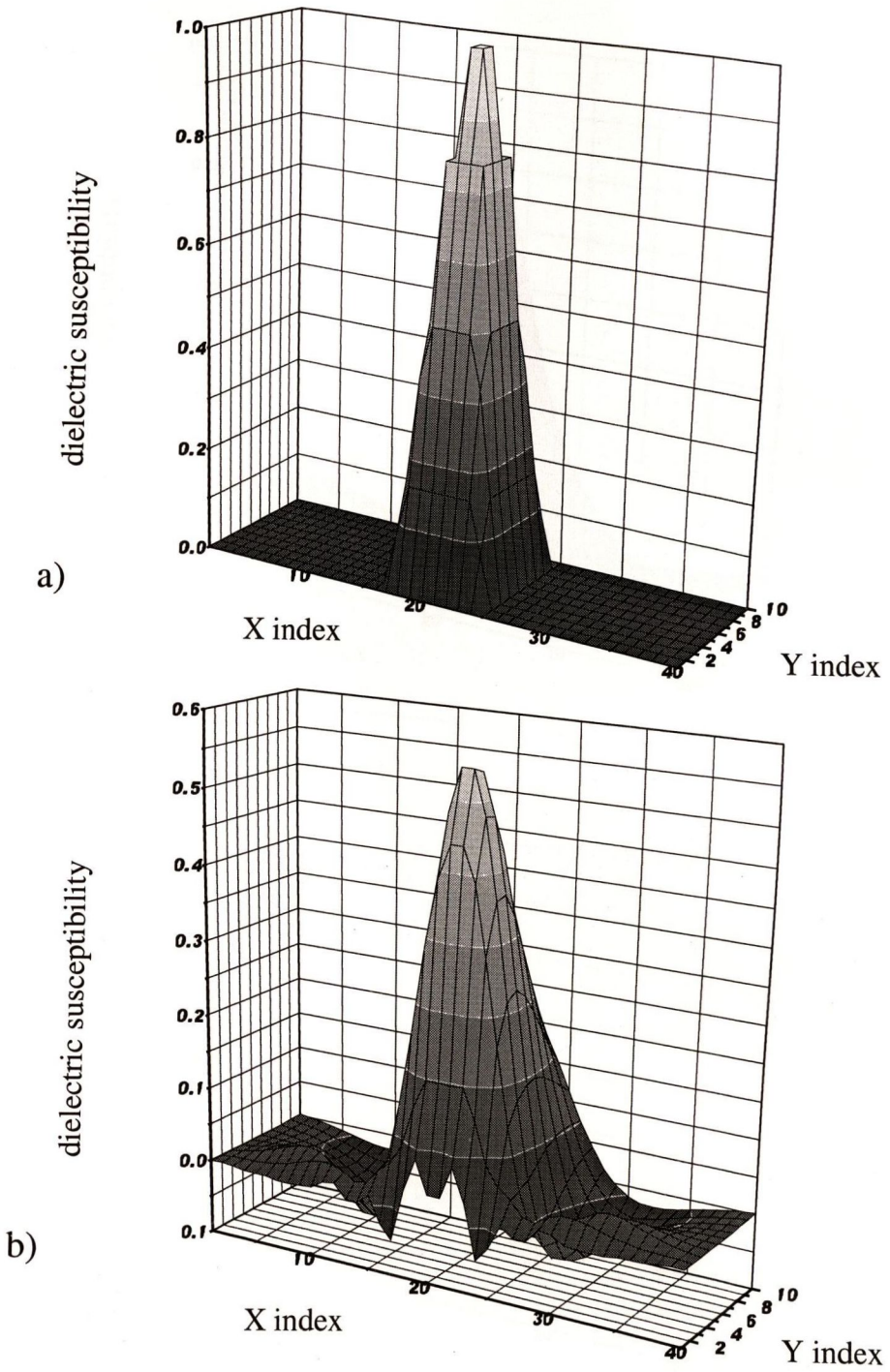

Figure 6.3: Original dielectric susceptibility distribution (a) and a corresponding Born approximation (b).

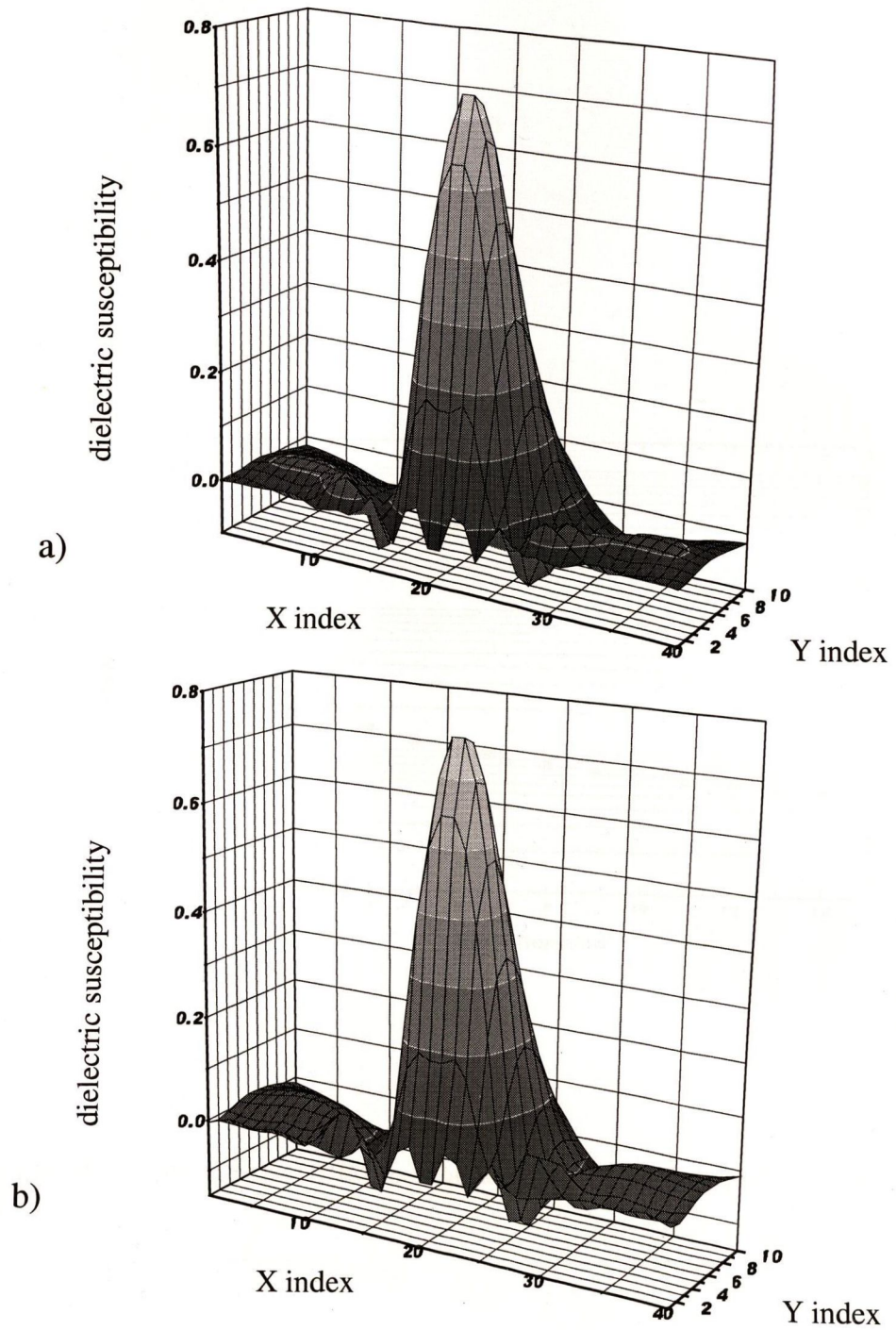

Figure 6.4: Reconstructed dielectric susceptibility distribution after the 5-th (a) and 15-th (b) DBIM iteration for the original profile in figure 6.3 (a).

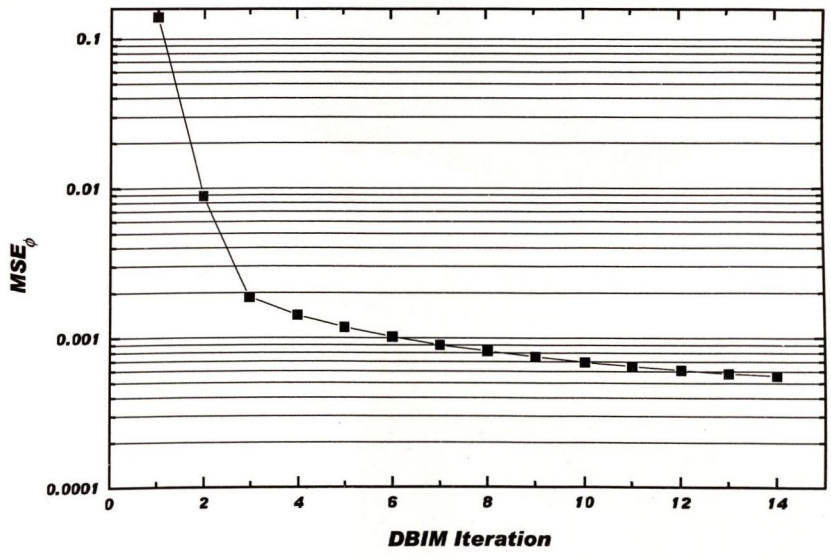

Figure 6.5: MSE_ϕ plot for the DBIM method for the original susceptibility distribution in figure 6.3 (a).

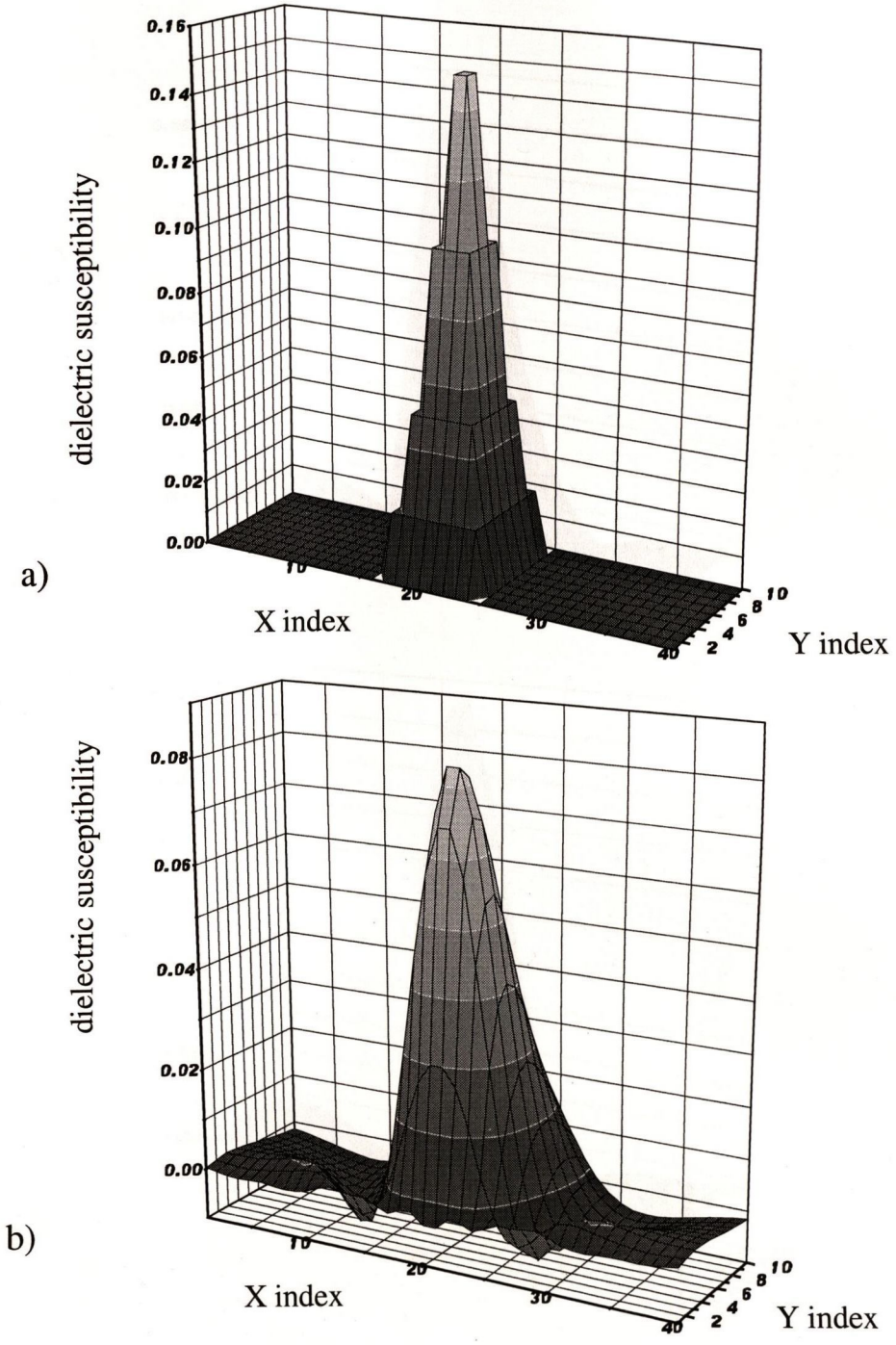

Figure 6.6: Original dielectric susceptibility distribution (a) and a corresponding Born approximation (b).

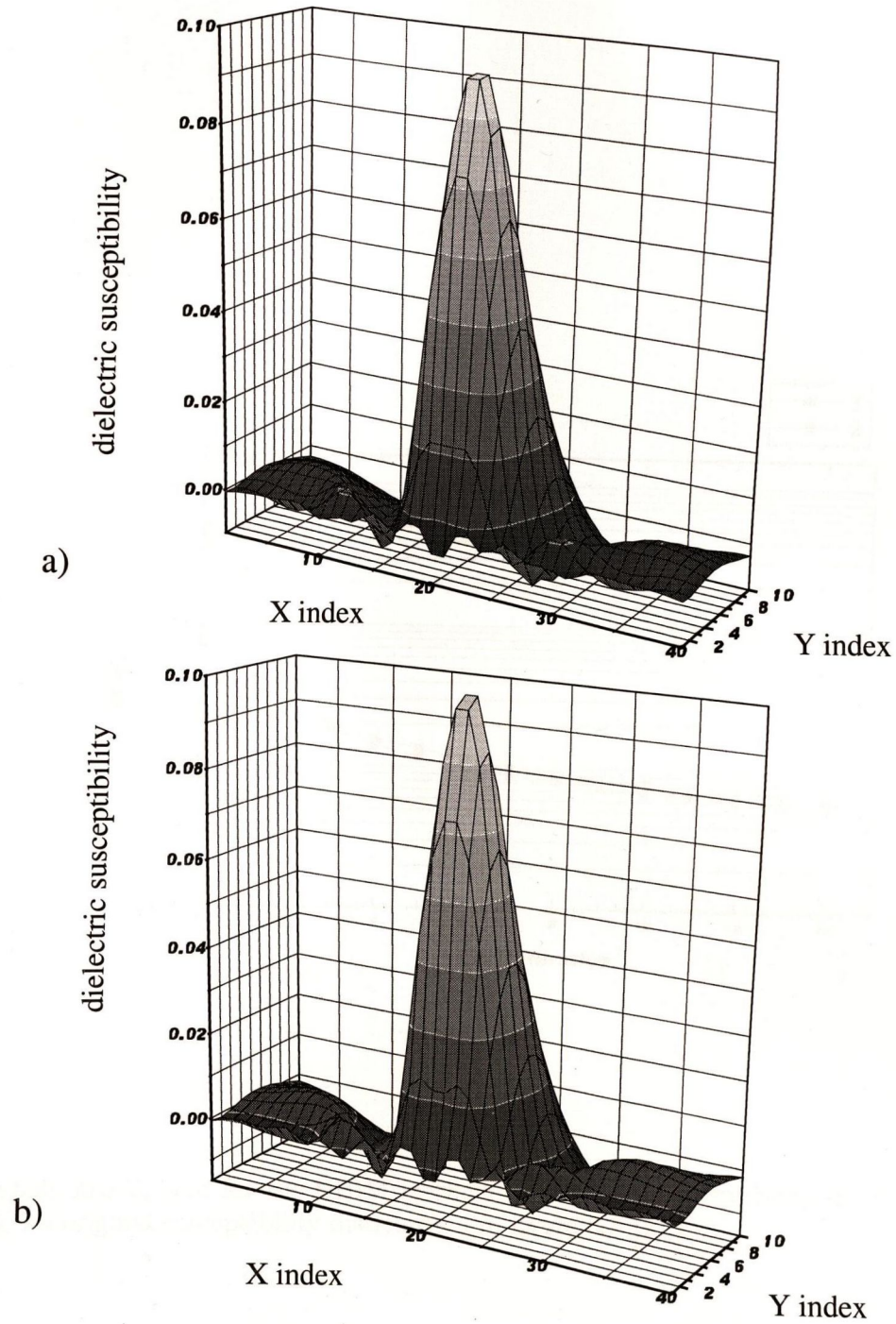

Figure 6.7: Reconstructed dielectric susceptibility distribution after the 5-th (a) and 15-th (b) DBIM iteration for the original profile in figure 6.6 (a).

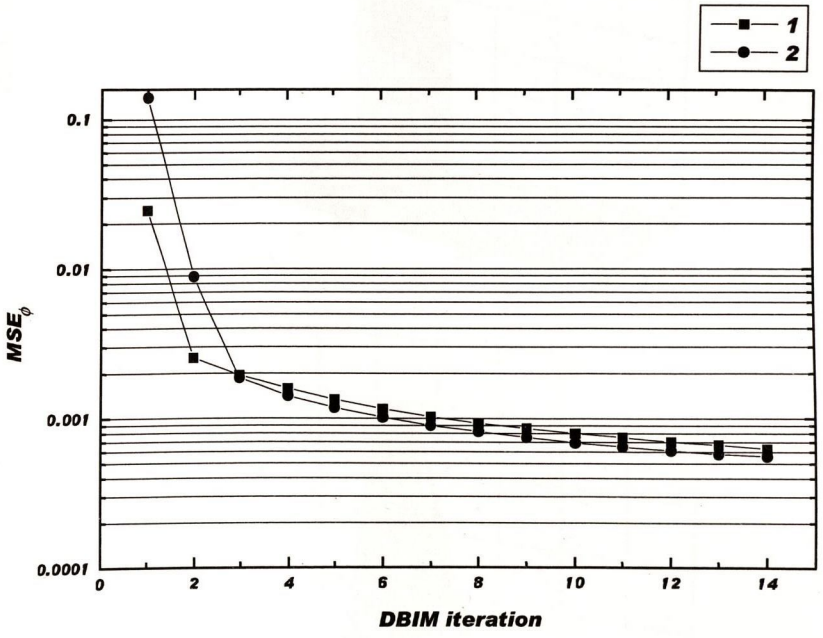

Figure 6.8: MSE_ϕ plot for the DBIM method. 1 - original susceptibility distribution in figure 6.6 (a), 2 - original susceptibility distribution in figure 6.3 (a).

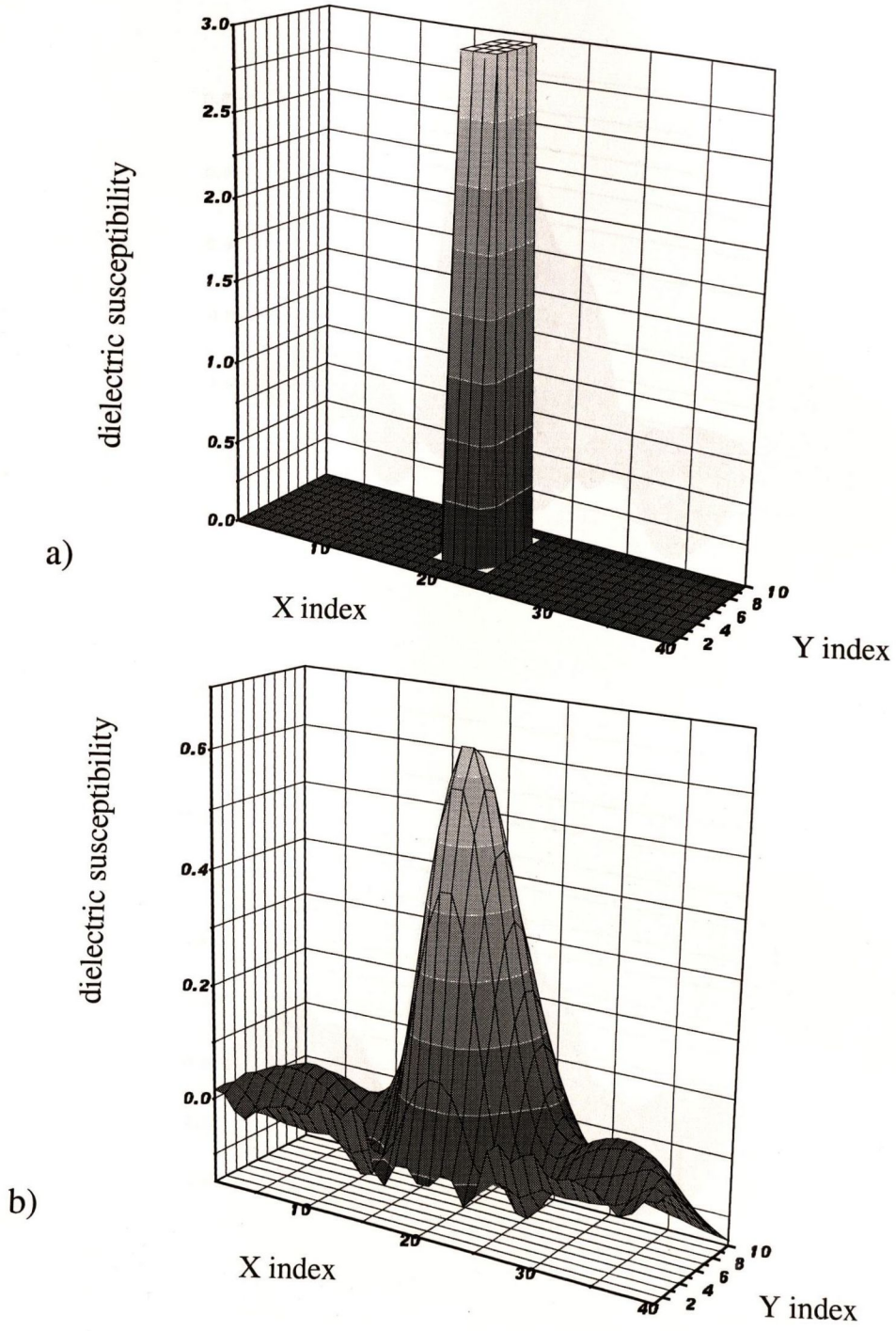

Figure 6.9: Original dielectric susceptibility distribution (a) and a corresponding Born approximation (b).

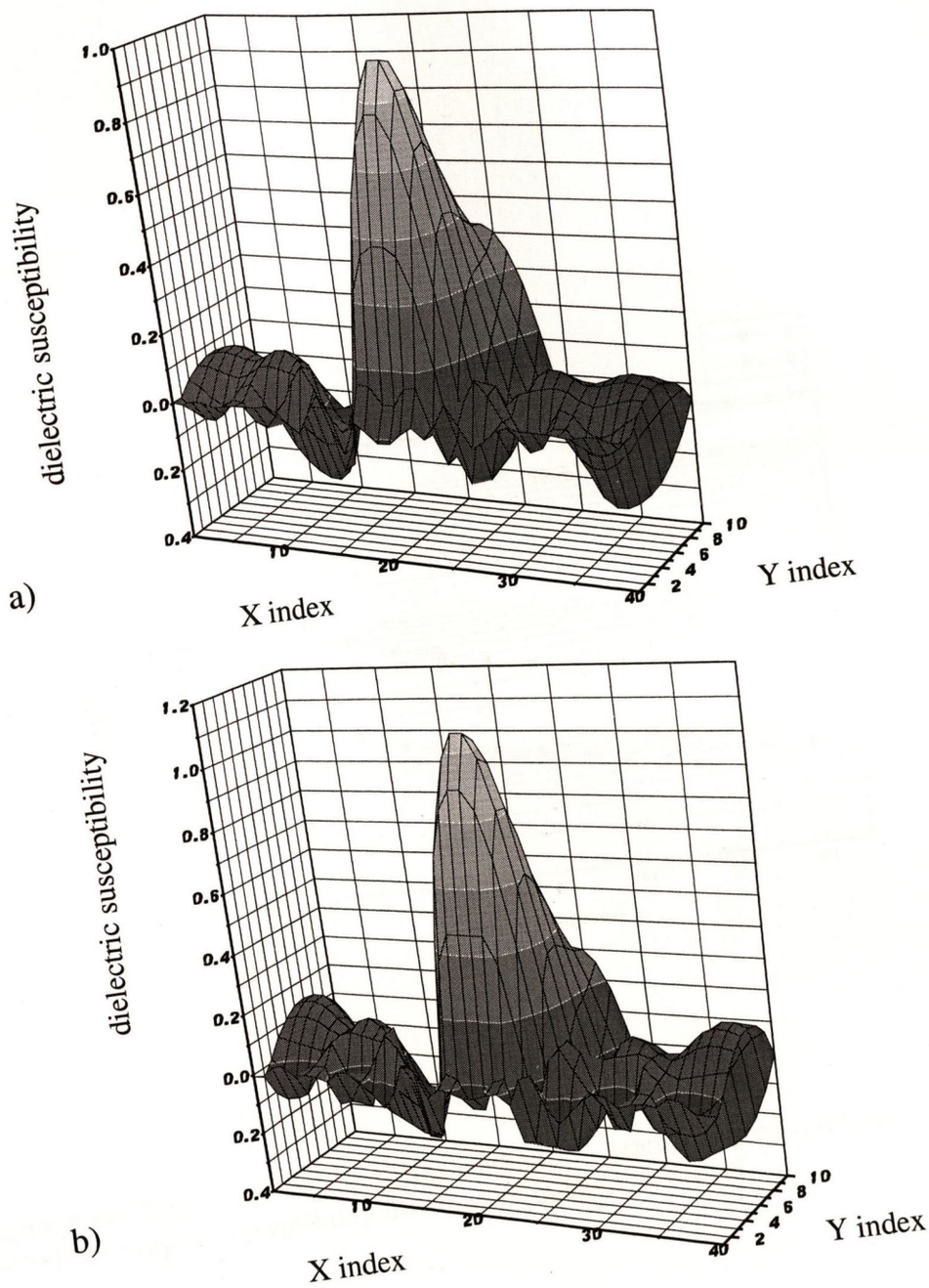

Figure 6.10: Reconstructed dielectric susceptibility distribution after the 5-th (a) and 15-th (b) DBIM iteration for the original profile in figure 6.9 (a).

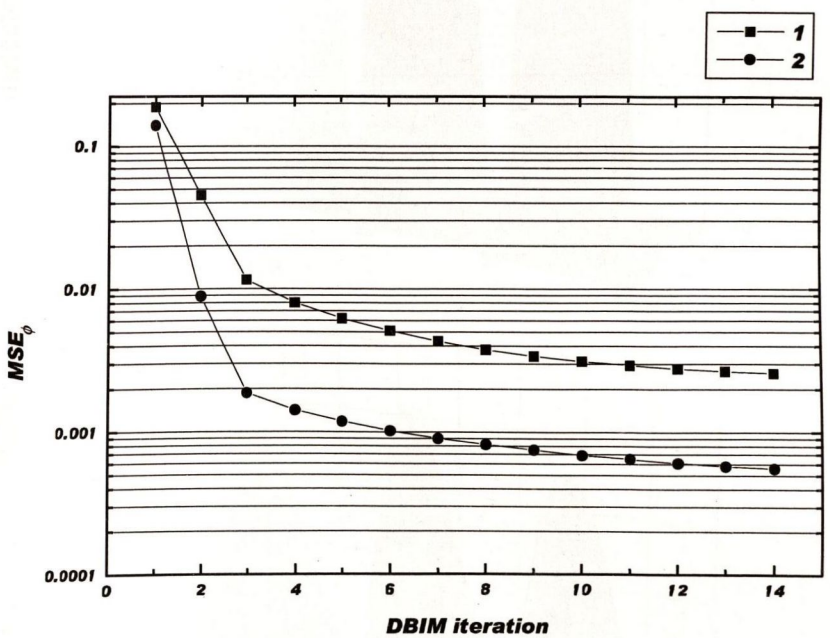

Figure 6.11: MSE_ϕ plot for the DBIM method. 1 - original susceptibility distribution in figure 6.9 (a), 2 - original susceptibility distribution in figure 6.3 (a).

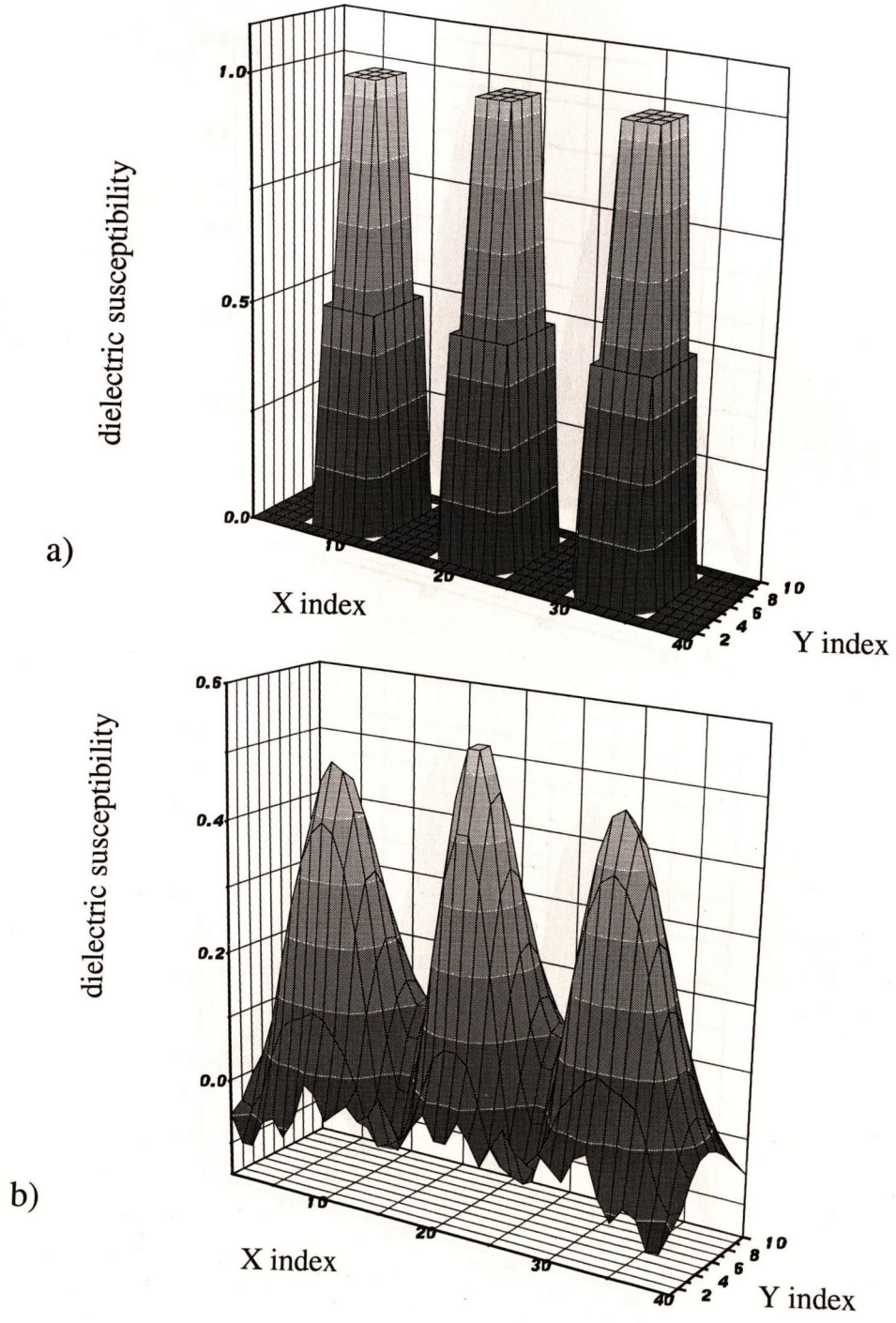

Figure 6.12: Original dielectric susceptibility distribution (a) and a corresponding Born approximation (b).

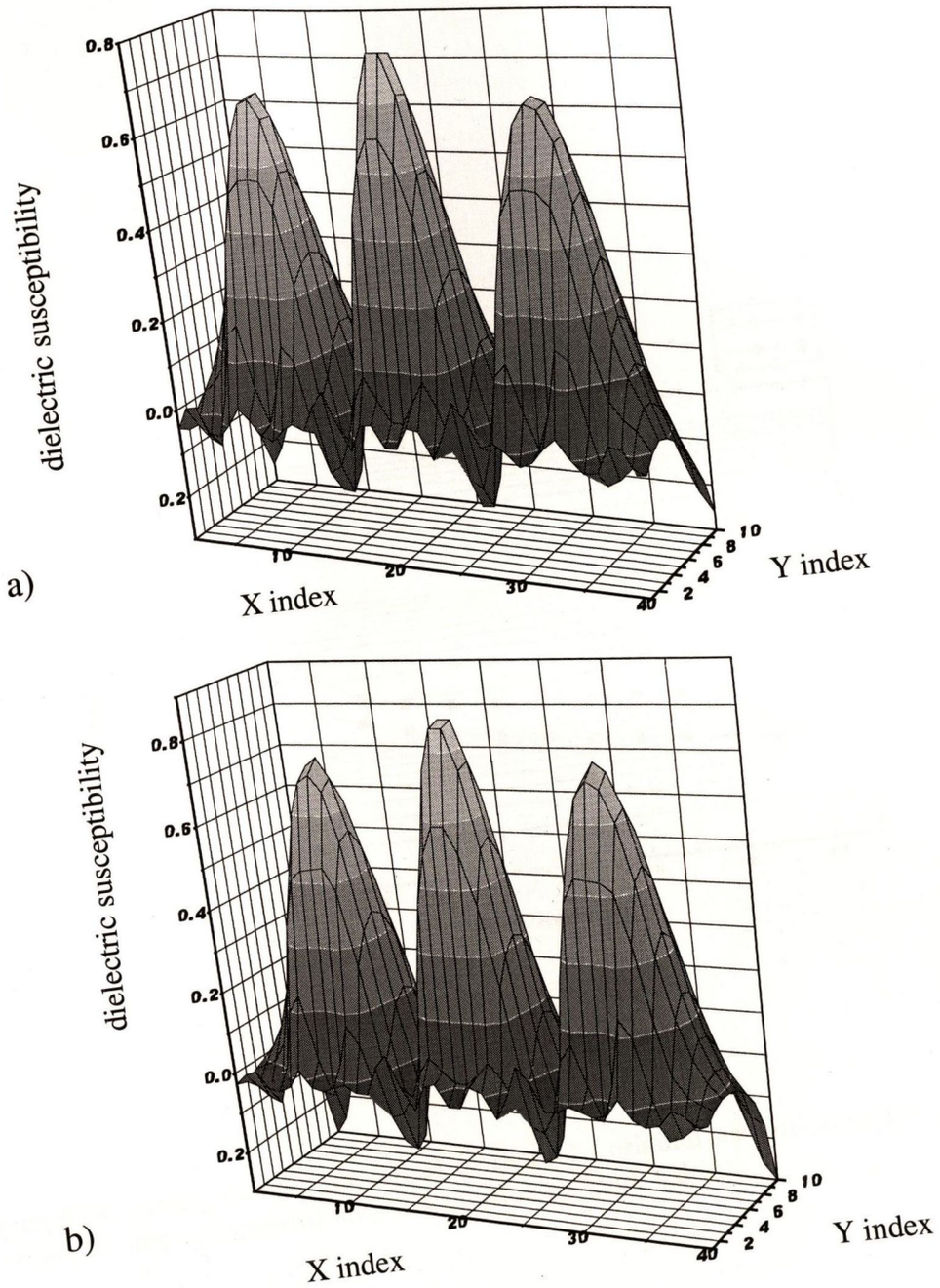

Figure 6.13: Reconstructed dielectric susceptibility distribution after the 5-th (a) and 15-th (b) DBIM iteration for the original profile in figure 6.12 (a).

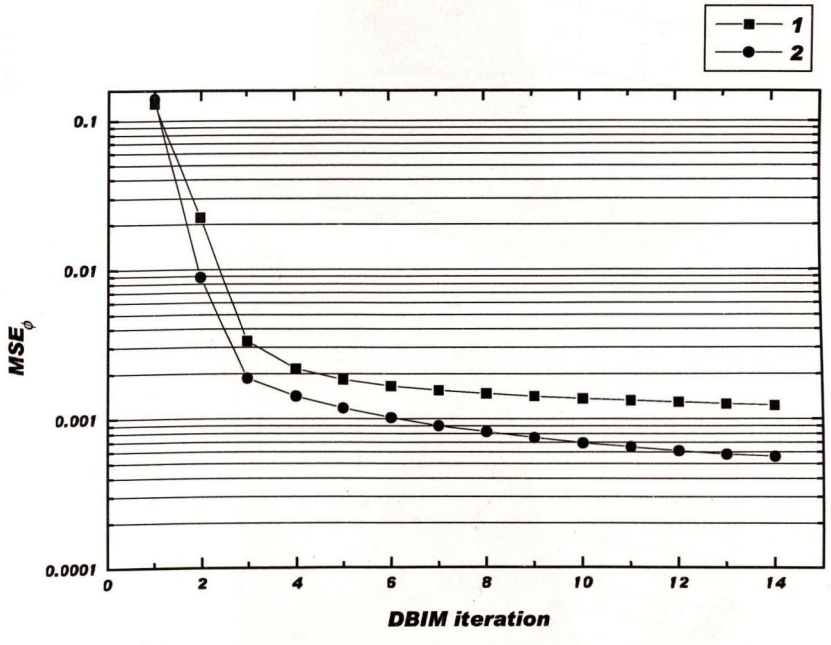

Figure 6.14: MSE_ϕ plot for the DBIM method. 1 - original susceptibility distribution in figure 6.12 (a), 2 - original susceptibility distribution in figure 6.3 (a).

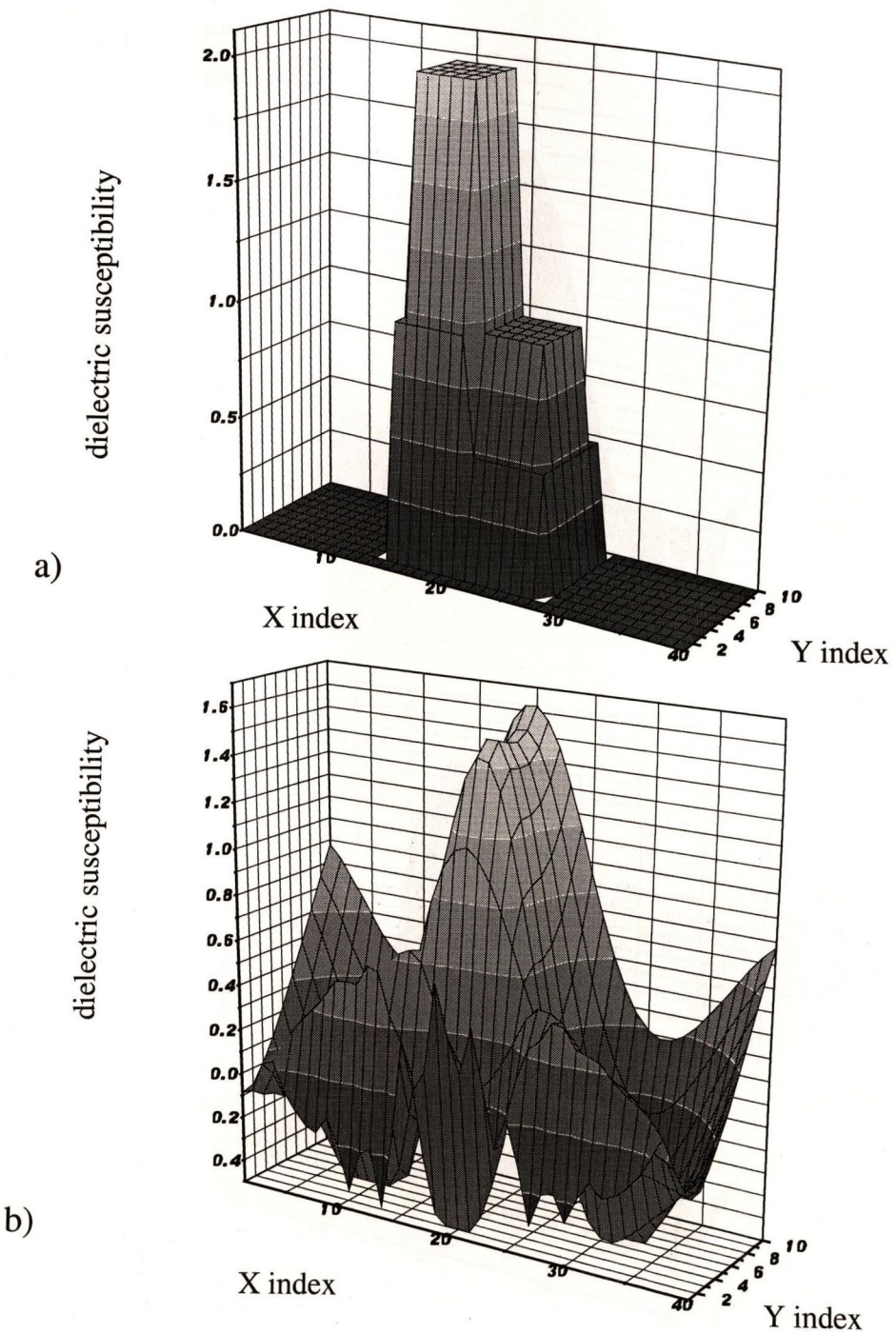

Figure 6.15: Original dielectric susceptibility distribution (a) and a corresponding Born approximation (b).

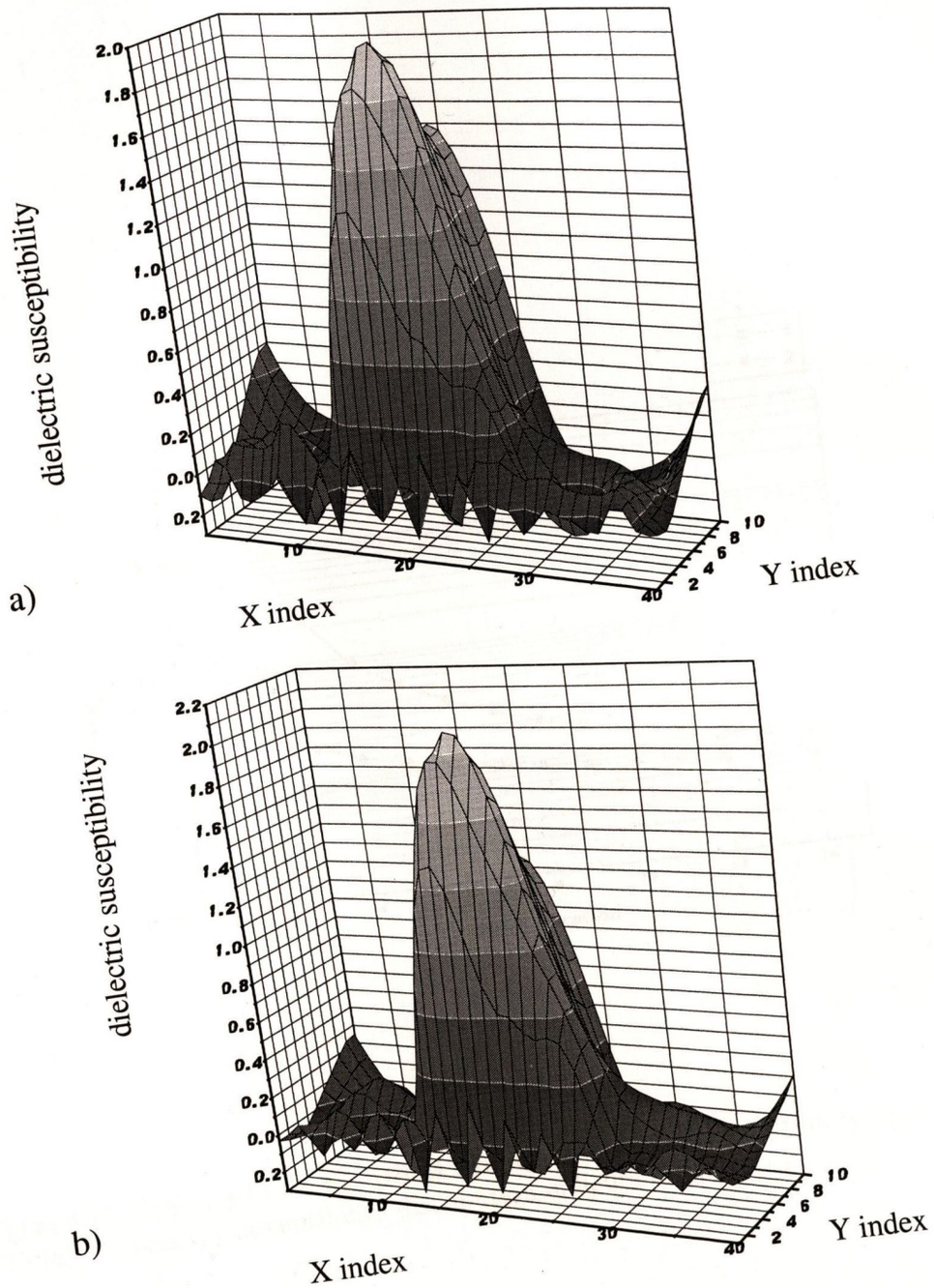

Figure 6.16: Reconstructed dielectric susceptibility distribution after the 5-th (a) and 15-th (b) DBIM iteration for the original profile in figure 6.15 (a).

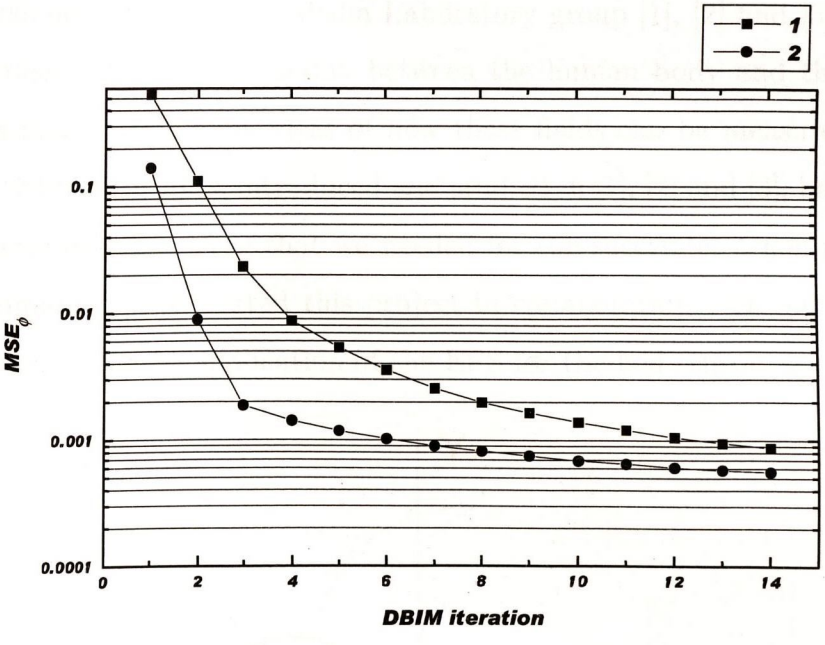

Figure 6.17: MSE_ϕ plot for the DBIM method. 1 - original susceptibility distribution in figure 6.15 (a), 2 - original susceptibility distribution in figure 6.3 (a).

OVERVIEW AND CONCLUSIONS

In this project we explored a novel application of capacitive sensor techniques to the inverse imaging problem. It is worth mentioning that in the beginning of this project we had a very basic understanding of the techniques available to us and our ideas were primarily based on a few works done by the MIT Media Laboratory group [1], [2] and [3]. These articles discuss empirical results of interaction between the human body and the low frequency electric fields and present some ideas of how these fields can be measured. The electric field sensing (EFS) principles, introduced and studied in [1], [2] and [3], have not linked us to wider sources of information that we needed for the successful accomplishment of the project. Summarizing, we started this project in collaboration with our sponsor Hotron Co. Ltd. investigating the application of the EFS for the bed sensor.

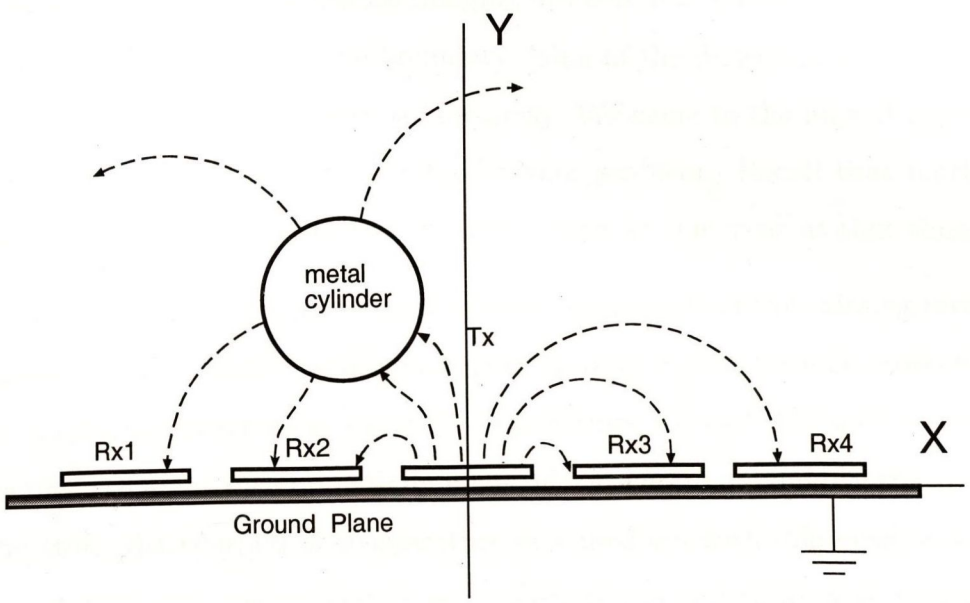

Figure 7.1: A cross-section of the 2D capacitive sensor array.

During the first year of the project we designed and assembled a computer controlled hardware prototype capable of operating the simplest 2D capacitive sensor array having

only one transmit electrode as shown in figure 7.1 (see also section 5.1.2). During that period we also implemented an efficient direct solver for the quasi-electrostatic problem employing the BEM. This algorithm was capable of calculating the response of each of the sensing electrodes Rx in figure 7.1 in the presence of the conducting cylinder. Furthermore, fixing the radius of the cylinder, we implemented a simple yet efficient inverse algorithm explained in section 5.1.2 capable of uniquely determining the position of the cylinder by minimising the MSE_{ϕ} (section 5.2.2). Our inverse method was far more advanced being based on the exact electrostatic problem formulation as opposed to the empirical and intuitive analysis reported in [1], [2] and [3].

Based on the gained experience, we realized that future capacitive sensor arrays must have many transmit and sensing electrodes and be capable of collecting a large amount of scalar data. Also we understood that the unknown object model should not be limited to parameterisation of the co-ordinates of the centre for predetermined shapes. We decided to confront the problem of reconstruction of the shape of the unknown object and to replace the inverse positioning problem by an inverse imaging problem. A fundamental question for us was whether the inverse imaging problem has a unique solution. Analysing this question we discovered that the boundary value of the dielectric permittivity can be uniquely measured using a capacitive sensor array. We came to the idea of measuring the Dirichlet-to-Neumann map for the inverse imaging problem. Recall that neither of the existing inverse methods or uniqueness theorems were known to us at that time.

Searching through periodicals we found a versatile framework of the existing inverse problems in various areas of physics with new keywords to us such as 'inverse problem', 'profile inversion', 'profile reconstruction' etc. with no reference to the 'EFS' and 'electrostatics'. One of the physical areas with potentially many advantages to us could be thermal conductivity. The static distribution of temperature in a medium with inhomogeneous thermal conductivity satisfies the same equation as an electrostatic potential in an inhomogeneous dielectric medium. Also thermal heat flow is similar to electric flux density. Unfortunately, each example of the inverse thermal conductivity problem that we found dealt with dynamic temperature distributions (the corresponding boundary conditions on the surface

of the object with unknown thermal conductivity were dynamic pulses injecting heat into the object). Electrodynamic inverse problems, despite wide use of the Helmholtz operator, appeared to be particularly beneficial to our study (chapter 5).

During the study of the uniqueness of the solution for the inverse electrostatic problem we found that the relevant uniqueness theorems already exist. In particular we found that the knowledge of the Dirichlet-to-Neumann map uniquely determines the dielectric distribution in the inverse electrostatic problem [80], [99]. We also found that in many existing implementations of the inverse problem the corresponding uniqueness theorems are not referred to [65], [40], [33], [66]. The uniqueness theorems for the inverse problems appear to be not widely known among the researchers. Dobson and Kaup [73],1999, for example, believe that the question of uniqueness of the solution for the low frequency electromagnetic inverse problem that they solve is open, yet we found a relevant uniqueness theorem in [85],1993. In our analysis of the uniqueness of the solution for the inverse electrostatic problem in chapter 3 we presented examples of the dielectric/metal objects in electrostatic fields which reveal the practical limitations of the inverse electrostatic techniques. This analysis is original and important to our imaging applications.

We found many existing inverse methods namely the Born iterative methods (BIM) and distorted BIM (DBIM) [18], [19], [33], Newton-Kantorovich method [95], [39], [38], pseudoinverse transformation method [28], modified gradient method [30], [31], [66] and the method based on the reconstruction of the equivalent current density [55], [40] which can be employed in electrostatics. These methods are originally employed in the inverse electrodynamic problems and we found that only the DBIM has been later applied to the resistivity and induction inversion tool problems [23], [17] which are similar to ours. We formulated the inverse electrodynamic methods in electrostatics, which is novel, yet the numerical implementation and comparison of the performance of these methods requires additional study. Implementing the DBIM, which is an advanced version of the BIM, for the capacitive sensor array we met several difficulties. In the existing implementations of the DBIM in electrodynamics and resistivity and induction inversion tools the transmit and receive antennas are assumed to be small so that their physical dimension is excluded

from the interaction with the object under reconstruction. In practical implementations of the capacitive sensor array such an assumption is not justified. We incorporated spatially elongated electrodes into the DBIM without making any approximations. This achievement is novel, to the best of our knowledge. In order to model a flat capacitive sensor array with a ground electrode (figure 7.1) we introduced a double sided boundary Γ such that the electrostatic potential tends to different values on Γ when approaching Γ from the opposite sides (section 4.3). Because the doublesided boundary is rarely encountered it is likely to lead to improper use of its concept [34]. We incorporated the double sided boundary into the inverse problem, which is novel. The Dirichlet boundary electrostatic problems (that arise in the DBIM) employing a doublesided boundary Γ appear to be ill-posed in such way that placing single and double layers on Γ does not improve the stability. Employing conformal mapping we overcome that difficulty and suggested a novel technique which can be seen as a preconditioner.

The inverse problems in electrodynamics and consequently electrostatics are ill posed [72], [4], [38], [40]. A popular technique to overcome the ill-conditioning is to employ a Tikhonov regularization method [5], [16], [77], [55]. Regularization is also essential to the DBIM [19]. We performed comprehensive analysis of the Tikhonov regularization and its application to inverse problems in section 4.1.3. In particular, we demonstrated how the Tikhonov regularization method affects the solution of the ill-conditioned problem and explained the mechanism of low pass spatial filtering of the solution in the inverse problems. We also discovered that in the case of redundancy in dimensionality of the representation of the solution of the inverse electrostatic problem the Tikhonov regularization method tends to distort the solution increasing and decreasing the dielectric constant in strong and weak electrostatic fields respectively. We proposed a novel optimised Tikhonov regularization method that compensates for such distortion (section 6.2.3).

We implemented a 2D electrostatic inverse imaging problem by means of the FEM, BEM, DBIM and a moment method. The inversion algorithm appeared to be robust for various distributions of the dielectric. Thus we demonstrated that the application of the capacitive sensor techniques to the imaging problem is feasible and practical. We observed that the

inverse electrostatic problem is computationally intensive. We see our future goals in incorporating fast forward solvers in the implemented DBIM such as a fast multi-pole method (FMM) [57], exploration of other inverse methods (modified gradient method, source type integral equation based methods etc.) that have not been employed in electrostatics and developing real-time imaging applications employing a preconditioner for the doublesided boundary in 3D.

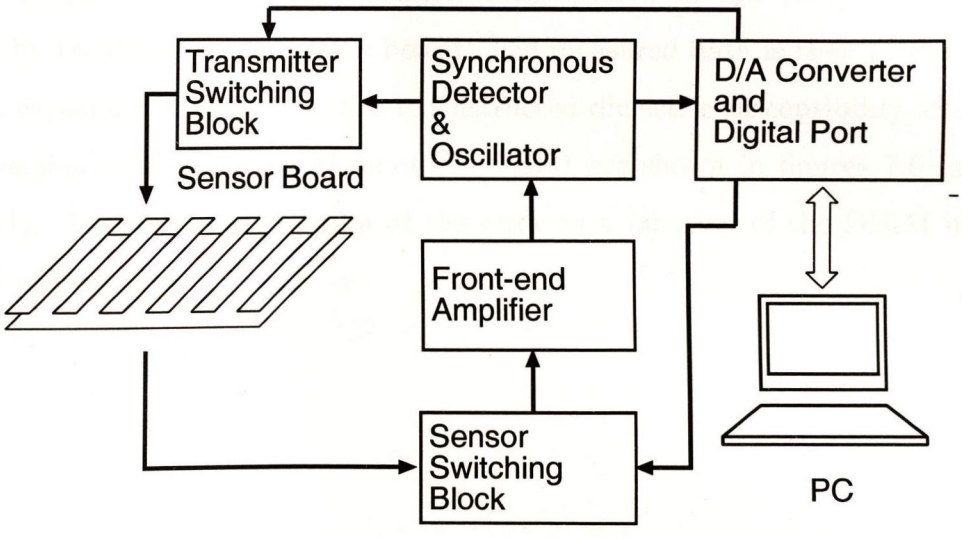

Figure 7.2: Block diagram of the hardware for the 2D electrostatic imaging problem.

To verify our inverse methods we now present the experimental capacitive sensor array employing the idea of the 2D electrostatic inverse imaging problem. The block diagram of the experimental hardware is shown in figure 7.2. An oscillator is connected to the transmitter switching block operated by the PC so that a low voltage low frequency signal (1V pk-pk, 500kHz) can be applied to any pre-selected transmit electrode located on the sensor board. A sensor switching block connects any pre-selected sensor electrode to the front-end amplifier. The signal is then rectified using a synchronous detection technique, digitised in the D/A converter and sent to the PC where the imaging algorithm is executed. Figure 7.3 (a) shows a photograph of the proof-of-concept prototype (designed in the course of this project) connected to the PC. Figure 7.3 (b) is a photograph of the experimental

sensor array. The physical dimension of this sensor array is outlined in figure 7.4. 15 metal electrodes are located on a dielectric substrate above a wider ground plane. The experimental prototype is capable of applying a sinusoidal signal to any of 7 Tx electrodes as marked in figure 7.4. The remaining 8 electrodes are dedicated Rx electrodes used to measure the induced signal. The experiment is arranged in such way that the mutual capacitance between any selected Tx_i and Rx_j, $i = 1, 2, \cdots, 7$, $j = 1, 2, \cdots, 8$ electrodes is collected and stored on the PC resulting in 56 independent scalar data. Figure 7.5 is a photograph of two dielectric cylinders being placed in the quasi-electrostatic field produced by the experimental sensor board. The measured data is then processed by the algorithm explained in chapter 6. The reconstructed dielectric susceptibility after the first (Born inversion) and 15-th iterations of the DBIM are shown in figures 7.6 (a) and (b) respectively. The corresponding plot of the error as a function of the DBIM iteration is presented in figure 7.7.

a)

b)

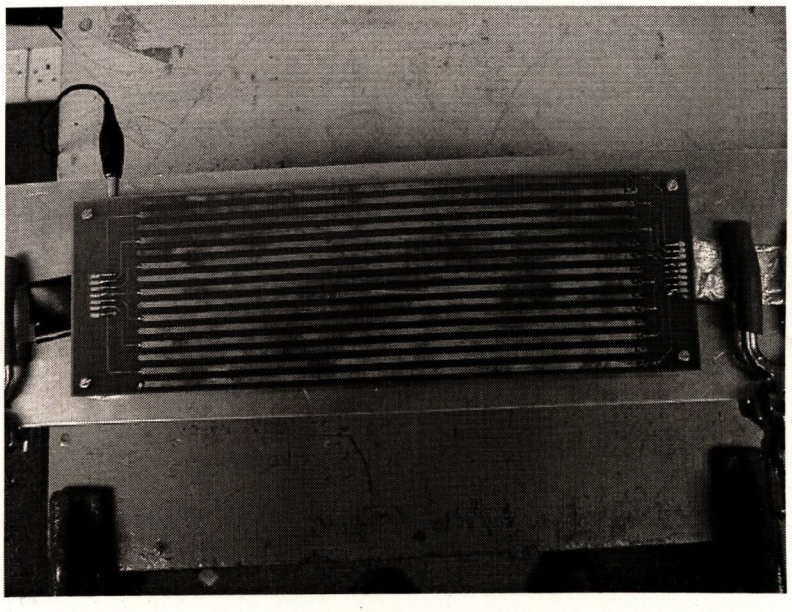

Figure 7.3: Photographs of the mobile experiment setup (a) and a 15 electrode sensor workbench (b).

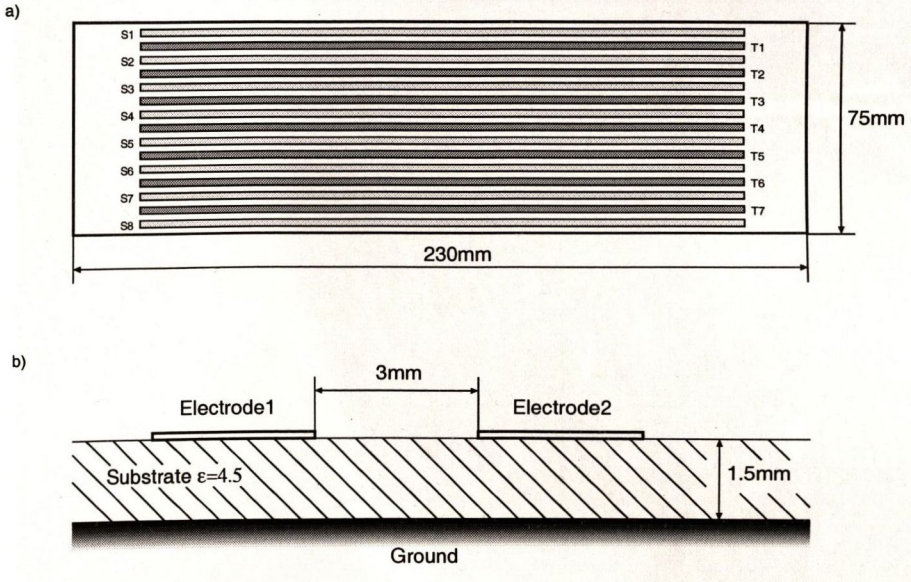

Figure 7.4: Implementation of the sensor workbench with 15 electrodes.

Figure 7.5: Two dielectric cylinders of radius 2cm and dielectric permittivity $\epsilon = 3.7$ in electrostatic field.

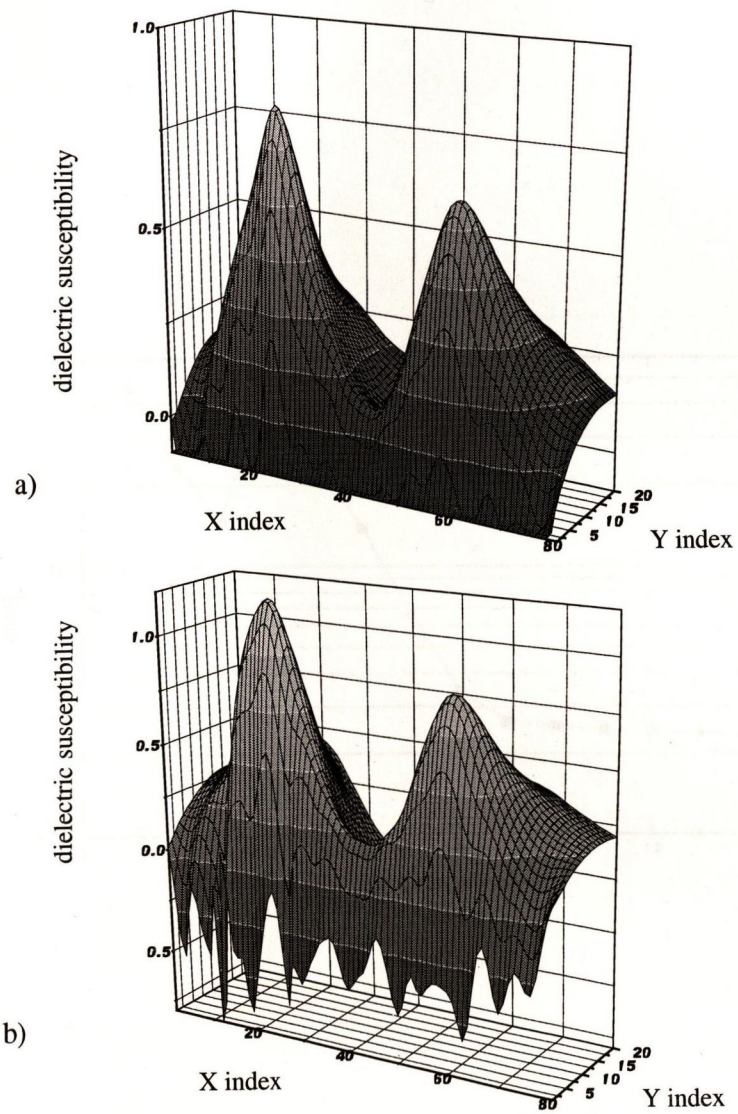

Figure 7.6: Reconstructed image of the two dielectric cylinders (figure 7.5) after the first (a) and 15-s (b) iterations of the DBIM.

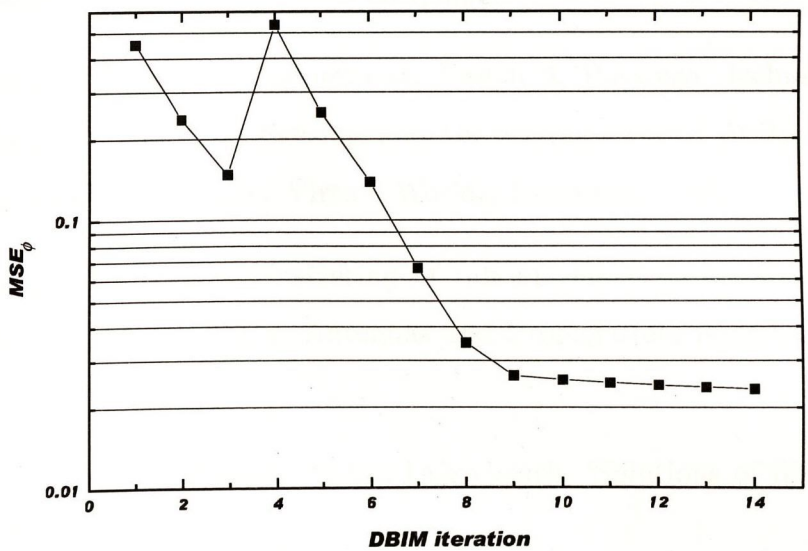

Figure 7.7: Error plot as a function of the iteration.

BIBLIOGRAPHY

[1] Joshua Smith, Tom White, Christopher Dodge,David Allport, Joseph Paradiso, Neil Gershenfeld 'Electric field sensing for graphical Interphases' IEEE Computer Graphics and Applications, Vol. 18, No. 3, May-June 1998, pp. 54-60.

[2] J. R. Smith 'Field mice: Extracting hand geometry from electric field measurements' IBM Systems Journal, Vol 35, NOS 3&4,1996.

[3] David Allport, Thomas G. Zimmerman, Joseph A. Paradiso, Joshua R. Smith, Neil Gershenfeld 'Electric Field Sensing and the"Flying Fish" ' ACM special issue on Multimedia and Multisensory Virtual Worlds, December, 1995

[4] Chein-Ching Chiu 'Inverse Scattering of Inhomogeneous Biaxial Materials Coated on a Conductor ' IEEE Trans. Antennas and Propagation, pp.218-225 Vol.46, No.2, February 1998.

[5] Tikhonov, Andrei N., Arsenin, Vasilii IAkovlevich, 'Solutions of ill posed problems' Wiley, 1977.

[6] B. Kazenelenbaum"High frequency electrodynamics" Nauka, 1966.

[7] Kosarev Vitaliy Ivanovich, '12 lecturenotes on numerical mathematics' ('12 lekciy po vychislitel'noy matematike'), Moscow, MFTI, 1995.

[8] Gene H. Golub, Charles F. van Loan 'Matrix Computations' Oxford Press, 1983.

[9] Brown, James Ward, Churchil, Ruel V., "Complex variables and applications." 1996.

[10] Thomas Ransford,"Potential theory in the complex plane.", Cambridge University Press, 1995.

[11] Olivier Kellog,"Foundations of potential theory.",Dover Publications, 1953.

[12] Weng Cho Chew 'Waves and Fields in Inhomogeneous Media' IEEE Press.

[13] S. G. Mikhlin 'Variational Methods in Mathematical Physics' Pergamon press, 1964.

[14] Bertero,M.,C. De Mol, and E. R. Pike, "Linear Inverse Problems with Discrette Data,I,General Formulation and singular system analysis.", Inverse Probl.,1,301-330, 1985.

[15] Natterer, F., "Numerical treatment of ill-posed problems", Inverse Problems, edited by G. Talenti, Lect. Notes math., 1225,142-167, 1996.

[16] Qing-Huo Liu 'Reconstruction of Two-Dimensional Axisymmetric Inhomogeneous Media' IEEE Transactions on Geoscience and Remote Sensing, Vol.31, No.3, pp.587-594, May 1993.

[17] Qing-Huo Liu 'Nonlinear inversion of Electrode-Type Resistivity Measurements' IEEE Transactions on Geoscience and Remote Sensing, Vol.32, No.3, pp.499-507,May 1994.

[18] Y.M. Wang, W.C. Chew 'An iterative Solution of the Two-Dimentional Electromagnetic Inverse Scattering Problem' International Journal of Imaging Systems and Technology, Vol.1, pp.100-108, 1989.

[19] W.C. Chew, Y.M. Wang 'Reconstruction of Two-Dimentional Permittivity Distribution Using the Distorted Born Iterative Method' IEEE Transactions on Medical Imaging, Vol.9, No.2, pp.218-225, June 1990.

[20] H.Q. Liu, W.C. Chew, M.R. Taherian, K.A. Safinya 'A Modelling Study of Electromagnetic Propagation Tool in Complicated Borehole Environments' Log Analyst, Vol.30, pp.424-435, 1989.

[21] Weng Cho Chew, Zaiping Nie, Qing-Huo Liu, Barbara Anderson 'An Efficient Solution for the Responce of Electrical Well logging Tools in a Complex Environment' IEEE Transactions on Geoscience and Remote Sensing, Vol.29, no.2, pp.308-313, March 1991.

[22] Qing-Huo Liu and Weng Cho Chew 'Numerical Mode-Matching Method for the Multi-region Vertically Stratified Media' IEEE Transactions on Antennas and Propagation, Vol.38, No.4, pp.498-506, April 1990.

[23] Weng Cho Chew, Quing-Huo Liu 'Inversion of Induction Tool Measurements using the Distorted Born Iterative Method and CG-FFHT' IEEE Transactions on Geoscience and Remote Sensing, Vol.32, No.4, pp.878-884, July 1994.

[24] Weng Cho Chew, Quing-Huo Liu 'A CG-FFHT Method for the Scattering Solution of Axisymmetric Inhomogeneous Media.' Micro. Opt. Tech. Lett., vol.6, no.2, p. 101-104, 1993.

[25] W.C.Chew and B. Anderson 'Propagation of electromagnetic waves through geological beds in a geophysical probing environment' Radio Science, V.20, No.3, pp.611-621, May-June, 1985.

[26] Weng Cho Chew, Jian-Ming Jin, Cai-Cheng Lu, Eric Michielssen, Jiming M. Song 'Fast Solution Methods in Electromagnetics' IEEE Transcations on Antennas and Propogation, Vol.45, No.3, pp.533-543, March 1997.

[27] Mark Frank and Constantine A. Balanis, 'Methods for Improving the Stability of Electromagnetic Geophysical Inversions' IEEE Transactions on Geoscience and Remote Sensing, Vol.27, No.3, pp.339-343, May 1989.

[28] M.M. Ney, A.M. Smith, S.S. Stuchly 'A solution of Electromagnetic Imaging Using Pseudoinverse Transformation' IEEE Transcations on Medical Imaging, Vol. MI-3, No.4, pp.152-165, December 1984.

[29] R.E. Kleinman, P.M. van den Berg 'Nonlinearized Approach to Profile Inversion' International Journal of Imaging Systems and Technology, Vol.2, 119-126, 1990.

[30] R.E. Kleinman, P.M. van den Berg 'A modified gradient method for two-dimensional problem in tomography' Journal of Computational and Applied Mathematics, 42 (1992) pp.17-35

[31] R.E. Kleinman, P.M. van den Berg 'An extended range-modified gradient technique for profile inversion' Radio Science, Volume28, Number5, Pages887-884, September-October 1993.

[32] R.E. Kleinman, P.M. van den Berg 'Two-dimensional location and shape reconstruction' Radio Science, Volume29, Number4, pages1157-1169, July-August 1994.

[33] Nie Zaiping, Zhang Yerong 'Hybrid Born Iterative Method in Low-Frequency Inverse Scattering Problem' IEEE Transactions on Geoscience and remote sensing, Vol36, No3, pp.749-753, May 1998.

[34] R.C. Ertekin, C.A. Brebbia, M. Tanaka, R. Shaw 'A new boundary element method for elastostatic problem with unclosed surface' Eleventh International Conference on Boundary Element Technology, BETECH 96.

[35] Norman Bleistein and Jack K. Cohen 'Nonuniqueness in the inverse source problem in acoustics and electromagnetics' Journal of Mathematical Physics, Vol. 18, No.2, pp.194-201, February 1977.

[36] A.J. Devaney and George C. Sherman 'Nonuniqueness in Inverse Source and Scattering Problems' IEEE Transactions on Antennas and Propagation, Vol AP-30, No.5, pp.1034-1042, September 1982.

[37] Andre Roger 'Newton-Kantorovich Algorithm Applied to an Electromagnetic Inverse Problem' IEEE Transactions on Antennas and Propagation, Vol AP-29, No.2, pp.232-238, 1981

[38] Chien-Ching Chiu and Yean-Woei Kiang, 'Microwave Imaging of Multiple Conducting Cylinders' IEEE Transactions on Antennas and Propagation, Vol. 40, No.8, pp.933-941, August 1992.

[39] Huang-Tien Lin and Yean-Woei Kiang, 'Microwave imaging for Dielectric Cylinder' IEEE Transactions on Microwave Theory and Techniques, Vol. 42, No.8, pp.1572-1579, August 1994.

[40] Chai-Yu Lin and Yean-Woei Kiang 'Inverse Scattering for Conductors by the Equavalent Source Method' IEEE Transactions on Antennas and Propagation, Vol.44, No.3, March 1996.

[41] Wang Weiyan and Zhang Shourong 'Unrelated illumination method for Electromagnetic Inverse Scattering of Inhomogeneous Lossy Dielectric Bodies' IEEE Transactions on Antennas and Propagation, Vol.40, No.11, pp.1292-1296, November 1992.

[42] S. Caorsi, G.L. Gragnani 'Redundant Electromagnetic Data for Microwave imaging of Three-Dimensional Dielectric Objects' IEEE Transactions on Antennas and Propagation, Vol.42, No.5, pp.581-589, May 1994.

[43] Magnus R. Hestenes and Eduard Stiefel 'Methods of Conjugate Gradients for Solving Linear Systems' Journal of Research of the National Bureau of Standarts, vol.49, No.6, pp.409-436, December 1952.

[44] Arthur I. Kohen 'Rate of Convergence of Several Conjugate Gradient Algorithms' Siam J. Numer. Anal., Vol.9, No.2, pp.248-259, June 1972.

[45] Ragnar Winther 'Some Superlinear Convergence Results for the Conjugate Gradient Method' SIAM J. Numer. Anal., Vol.17, No.1, pp.14-17, February 1980.

[46] Andrew F. Peterson and Raj Mittra 'Convergence of the Conjugate Gradient Method when Applied to Matrix Equations Representing Electromagnetic Scattering Problems' IEEE Transactions on Antennas and Propogation, Vol.AP-24, No.12, pp.1447-1454, December 1986.

[47] R. Fletcher and C.M. Reeves 'Function minimization by conjugate gradients' Comput. J. Vol.7, No.4, pp149-153, 1964.

[48] Harrinder P. S. Ahluwallia and Wolfgang-Martin Boerner 'Application of Electromagnetic Inverse Boundary Conditions to Profile Characteristics Inversion of Conducting Spherical Shapes' IEEE Transactions on Antennas and Propagation, Vol AP-22, No.5, pp.673-682, September 1974.

[49] Mani Azimi, A. C. Kak 'Distortion in Diffraction Tomography Caused by Multiple Scattering' IEEE Transactions on Medical Imaging, Vol. MI-2, No.4, pp. 176-195, December 1983.

[50] Malcolm Slaney, Avinash C. Kak, Lawrence E. Larcen 'Limitations of Imaging with First-Order Diffraction Tomography' IEEE Transactions on Microwave Theory and Techniques, Vil. MTT-32, No.8, pp.860-874, August 1984.

[51] V.H. Weston and W.M. Boerner 'An Inverse Scattering Technique for electromagnetic bistatic scattering' Canadian Journal of Physics, Vol.47, pp. 1177-1184, 1969.

[52] Leung Tsang, Andrew K. Chan, Stanley Gianzero 'Solution of the fundamental problem in resistivity logging with a hybrid method' Geophysics, Vol.49, No.10, pp.1596-1604, October 1984.

[53] V.L. Druskin and L.A. Knizhnerman 'A method of Solution of Forward Problems of Electric Well Logging and Electric Exploration with Direct Current' Izvestia, Earth Physics, Vol.23, No.4, pp.317-323, 1987.

[54] T.M.Habashy and R.Mittra 'On some inverse methods in electromagnetics' Journal of Electromagnetic Waves and Applications, Vol.1, No.1, pp.25-58, 1987.

[55] Tarek M. Habashy, Edward Y. Chow, Donald G. Dudley 'Profile Inversion Using the Renormalized Source-Type Integral Equation Approach' IEEE transactions on Antennas and Propagation, Vol.38, No.5,pp.668-682, May 1990.

[56] V. Rokhlin 'Rapid Solution of Integral Equations of Scattering Theory in two Dimensions' Research report YALEU/DCS/RR-440 (Yale University, Department of Computer Science) November 1985.

[57] V. Rokhlin 'Rapid Solution of Integral Equations of Classical Potential Theory' Journal of Computational Physics 60, 187-207,1983.

[58] A. Dutt, M. Gu, V Rokhlin 'Fast Algorithms for Polynomial Interpolation, Integration, and Differentiation' SIAM Journal on Numerical Analysis, Vol.33, No.5, pp.1689-1711, October 1996.

[59] Sharad Kapur and Vladimir Rokhlin 'High-Order Corrected Trapezoidal Quadrature Rules for Singular Functions' SIAM Journal on Numerical Analysis, Vol.34, No.4, pp.1331-1356, August 1997.

[60] Lesie Greengard and Vladimir Rokhlin 'A new version of the Fast Multipole Method for the Laplace equation in three dimensions' Acta Numerica, pp.229-269, 1997.

[61] Tomasz Hrycak and Vladimir Rokhlin 'An improved Fast Multipole Algorithm For Potential Fields' SIAM J. Sci. Comput., Vol.19, No.6, pp.1804-1826, November 1998.

[62] Norman Yarvin and Vladimir Rokhlin 'An improved Fast multipole Algorithm for potential fields on the line' SIAM Journal on Numerical Analysis, Vol.36, No.2, pp.629-666, 1999.

[63] W.H.Press, B.P. Flannery, S.A. Teukolsky and W.T. Vetterling "Numerical Recipies, The art of Scientific Computing" Cambridge Univ. Press, New York, 1986

[64] Paul Concus, Gene H. Golub, Dianne P. O'Learly 'A Generalised Conjugate Gradient method For The Numerical Solution Of Elliptical Partial Differential Equations'

[65] Salvatore Gaorsi and Gian Luigi Gragnani 'Inverse-Scattering Method for dielectric objects based on the reconstruction of the nonmeasurable equivalent current density' Radio Science, Volume 34, Number 1, pp.1-8, January-February 1999.

[66] M Lambert, D. Lesseiler, B.J. Kooij 'The retrieval of a buried cylindrical obstacle by a Constrained modified gradient method in the H-polarisation case and for Maxwellian metrials' Inverse problems 14, pp.1265-1283, 1998.

[67] Ian Knowles 'A variational algorithm for electrical impedance tomography' Inverse Problems 14, pp.1513-1525, 1998

[68] M. Piana 'On uniqueness for anisotropic inhomogeneous inverse scattering problems' Inverse Problems 14, pp.1565-1579, 1998.

[69] G.A. Latham 'Best L^2 Tikhonov analogue for Landweber iteration' Inverse Problems 14, pp.1527-1537, 1998.

[70] Shin-ichi Nakamura 'A remark on the global uniqueness theorem for a semilinear elliptic inverse problem' Inverse Problem 14, pp. 1311-1314, 1998.

[71] Karl Kunich and Jun Zou 'Iterative choices of regularisation parameters in linear inverse problems' Inverse problems 14, pp.1247-1264, 1998.

[72] G.D. de Villiers, B. McNally, E.R. Pike 'Positive solution to linear inverse problems' Inverse Problems 15, pp. 615-635, 1999.

[73] David C. Dobson and Peter G. Kaup 'Monitoring underground flows with electromagnetic methods' Inverse Problems 15, pp.597-613, 1999.

[74] Masaru Ikehata 'Recinstruction of source domain from the Cauchy data' Inverse Problems 15, pp.637-645, 1999.

[75] J.L. Ma, W.C. Chew, C.C. Lu, J.M. Song 'Image reconstruction from TE Scattering Data Using Strong Permittivity Fluctuation Theory' IEEE Antennas and Propogation Int Symposium, Vol.2, No.2, pp.702-705, 1998.

[76] A.K. Louis 'A unified approach to regularisation methods for linear ill-posed problems' Inverse Problems 15, pp.489-498, 1999.

[77] Ioannis T. Rekanos, Traianos V. Yioultsis, Thoudoros D. Tsiboukis 'Inverse Scattering Using the Finite-Element method and a Nonlinear optimization Technique' IEEE Transactions on Microwave Theory and Techniques, Vol.47, No.3, pp.336-344, march 1999.

[78] John Sylvester and Gunther Uhlmann 'A Uniqueness Theorem for an Inverse Boundary Value Problem in Electrical Prospection' Communications on Pure and Applied Mathematics, Vol. XXXIX, pp.91-112, 1986.

[79] John Sylvester and Gunther Uhlman 'A global uniqueness theorem for an inverse boundary value problem' Annals of Mathematics, 125, pp.153-169, 1987,

[80] John Sylvester and Gunther Uhlman 'Inverse Boundary Value Problems at the Boundary-Continuous Dependence' Communications on Pure and Applied Mathematics, Vol. XLI, pp.197-219, 1988.

[81] J. Liukkonen 'Uniqueness of electromagnetic inversion by local surface measurements' Inverse Problems 15, pp.265-280, 1999.

[82] Frank Natterer and Frank Wubbeling 'A propagation-backpropagation method for ultrasound tomography' Inverse Problems 11, pp.1225-1232, 1995.

[83] Erkki Somersalo 'Layer stripping for time harmonic Maxwell's equations with high frequency' Inverse problems 10, pp.449-466, 1994.

[84] Erkki Somersalo, Margaret Cheney, David Isaacson and Eli Isaacson 'Layer stripping:a direct numerical method for impedance imaging' Inverse Problems 7, pp.889-926, 1991.

[85] Petri Ola, Lassi Paivarinta, Erkki Somersalo 'An inverse boundary value problem in electrodynamics' Duke Mathematical Journal, Vol 70, No. 3, pp.617-653, 1993

[86] John M. Vranish, Robert L. McConnel, W.Va 'Driven Shielding Capacitive Proximity Sensor' US Paten 5,166,679 Nov. 24,1992.

[87] V. Mathews 'Three Dimentional Baton and Gesture Sensor' US Patent 4,980,519 Dec. 25, 1990

[88] Neil A. Gershenfeld 'Method and Apparatus for electromagnetic non-contact position measurement with respect to one or more axes' US Patent 5,247,261 Sep. 21, 1993.

[89] Chien-Ching Chiu and Po-Tsun Liu 'Image Reconstruction of a Complex Cylinder Illuminated by TE Waves' IEEE Transactions on Microwave Theary and Techniques, Vol.44, No.10, Actober, pp.1921-1927, 1996

[90] Deepak K. Ghodgaonkar, Om P. Gandhi, Mark J. Hagmann 'Estimation of complex Permottivities of Three-Dimensional Inhomogeneous Biological bodies' IEEE Trans-

actions on Microwave theory and Techniques, Vol. MTT-31, No.6, pp.442-446, June 1983

[91] Valeti A. Mikhnev, Ebbe Nyfos, Terrti Vainikainen 'Reconstruction of the Permittivity Profile Using a Nonlinear Guided Wave Technique' IEEE Transactions on Antennas and Propagation, Vol.45, No.9, pp.1405-1410, September 1997

[92] D. Lesselier 'Optimization Techniques and Inverse Problem: Reconstruction of Conductivity Profiles in the Time Domain' IEEE Transactions on Entennas and Propogation, Vol. AP-30, No.1, pp.59-65, January 1982

[93] A. J. Devaney 'A Computer Simulation Study of Diffaraction Tomography' IEEE TRansactions on Biomedical Imaging, Vol. BME-30, No.7, pp.377-386, July 1983.

[94] Kamal Belkebil, Ralph E. Kleinman, Christian Pichot 'Microwave Imaging - Location and Shape Reconstruction from Multifrequency Scattering Data' IEEE Transactions on Microwave Theory and Techniques, Vol.45, No.4, pp.469-476, April 1997.

[95] Nadine Joachimovicz, Christian Pichot, Jean-Paul Hugonin 'Inverse Imaging: An Iterative Numerical Method for Electromagnetic Imaging' Vol.39, No.12, pp.1742-1752, December 1991.

[96] Weng Cho Chew and Gregory P. Otto 'Microwave Imaging of Multiple Conducting Cylinders Using Local Shape Functions' IEEE Microwave and Guided Wave Letters, Vol.2, No.7, pp.284-286, July 1992

[97] Anton G. Tijhuis and Cor van der Worm 'Iterative Approach to the Frequency-Domain Solution of the Inverse-Scattering Problem for an Inhomogeneous Lossless Dielectric Slab' IEEE Transactions on Antennas and Propogation, Vol. Ap-32, No.7, pp.711-716, July 1984.

[98] Mithat Idemen and Ibrahim Akduman 'One-Dimensional Profile Inversion of a Half-Space Over a Two-Part Impedance Ground' IEEE Transactions on Antennas and propogation, Vol.44, No.7, pp.933-942, July 1996.

[99] Matti Lassas, Margaret Cheney, Gunther Uhlman 'Uniqueness for a wave propogation inverse problem in a half-space' Inverse Problems 14, 1998, pp. 679-684.

[100] Adrian I. Nachman 'Reconstruction from boundary measurements' Annals of Mathematics, 128 (1988), pp. 531-576.

[101] Kohn R. and Vogelius M. "Determining conductivity by boundry measurements" Comm. Pure Appl. Math. 37, 1984, pp. 289-298.

[102] Kohn R. and Vogelius M. "Determining conductivity by boundry measurements II. Interior Results" Comm. Pure Appl. Math. 38, 1985, pp. 643-667.